A STUDY OF POSTSTENOTIC SHEAR LAYER INSTABILITIES

Jobst Treiber

A thesis submitted for the
Degree of Doctor of Philosophy of the University of London
and the
Diploma of Membership of Imperial College

September 1988

Electrical Engineering Department
Imperial College of Science and Technology
University of London

ABSTRACT

Laminar shear layer instabilities in poststenotic flows are among the first flow disturbances to indicate arterial narrowing by atherosclerotic lesions. This makes these disturbances particularly useful for the noninvasive diagnosis of extracranial occlusive disease by blood velocity measurements. However, the diagnostic value of flow disturbances depends crucially on their structural stability in the presence of ambient perturbations such as arterial wall vibrations. This *caveat* applies notably to separated shear layers that are by nature excited flows.

The question of structural stability is addressed in a susceptibility study of poststenotic flow instabilities in model experiments. Flow velocities are measured non-intrusively with a laser Doppler velocimeter, the accuracy of which is assessed both experimentally and theoretically by analysis and stochastic modelling of the Doppler demodulation process. Separated flow downstream of model stenoses is subjected to artificially generated periodic flow perturbations of variable frequency and amplitude. Thus the poststenotic flow mechanics are decoupled from the solid mechanics of possible wall motion.

The results show that steady flow is highly susceptible. The separated flow instability locks-on to the perturbations over a wide range of frequencies. Pulsatile flow, in contrast, is significantly less susceptible to flow perturbations, suggesting that quasi-steady analysis is of limited applicability. This finding is substantiated by starting flow experiments. Flow visualisation gives further insight into the poststenotic flow and a vortex wave, thought to be due to a low Reynolds number instability, is observed in pulsatile flow.

The second part of this study concentrates on the separated shear layer instability. A phenomenological model is proposed that interprets the broadband shear layer velocity fluctuations as functionally composite self-sustained oscillations. Self- and forced synchronisation of a population of nonlinear oscillators serve to model latent order and flow regularisation in the (forced) free shear layer. Nonlinear oscillator concepts have not been applied before to extrinsic flows whilst intrinsic flows such as wakes or impinging free shear layers, characterised by a discrete frequency of flow oscillation, lend themselves readily to this approach.

The phenomenological model suffers from a conceptual difficulty in that it gives an Eulerian description of flow oscillations, thus not accounting for the spatial development of the instability. This has prompted an investigation of the Ginzburg-Landau equation which provides a small-amplitude description of spatially developing weakly nonlinear hydrodynamic instability waves. This model open flow system is investigated in respect to its applicability to the free shear layer. A modification of the Ginzburg-Landau equation is shown to give rise to a subharmonic cascade, typically associated with free shear layer growth. The implications and limitations are discussed.

Preliminary findings of this research were reported at the First IFAC Symposium on Modelling and Control in Biomedical Systems, Venice, Italy[1]. Results of the theoretical and experimental analysis of frequency tracking noise in laser Doppler velocimeters have been published[2] and are included in Chapter III (§ 8). Summaries of the phenomenological model of flow synchronisation in the forced free shear layer[3], and of a proposed model system of subharmonic evolution[4] have been accepted for publication.

---

[1]Treiber J and Kitney R I (1988). Nonlinear modelling of vortex phenomena downstream of a stenosis. *IFAC Symp Modelling Contr in Biomed Syst, Venice, Italy.*

[2]Treiber J and Kitney R I (1987). Influence of dropouts on flow velocity measurements with an LDV frequency tracking system. *J Phys E: Sci Instrum* 20 pp 1404.

[3]Treiber J and Kitney R I (1988). Cooperative dynamics of a coupled oscillator system and the forced free shear layer. *Phys Let A* (accepted for publication).

[4]Treiber J and Kitney R I (1988). Evolution of subharmonics in a modified Ginzburg-Landau equation. *Phys Let A* (accepted for publication).

CONTENTS

ACKNOWLEDGEMENTS

My foremost thanks to Dr R I Kitney for introducing me to arterial flow dynamics and for procuring financial support from the Lord Dowding Fund, London Hospital. I am indebted to Dr J M R Graham for his continuous advice throughout the course of this research, and for his patience in guiding my hermeneutic attempts at fluid dynamics. The experimental flow facility was kindly provided by Dr K H Parker. It is a pleasure to acknowledge the stimulating and fruitful co-operation of Dr Marc Thiriet in the flow visualisation experiments.

Thanks are due to Mr B Adams for technical assistance, and to Messrs J O'Leary and R Packer for photographic advice.

Finally, I should like to thank my *commilitones* in the Biomedical Systems Group for providing a worthwhile atmosphere. Special mention must be made of Guan Ong, King Yu Liu, and Fernando Infantosi, who saw the politics behind it all.

PROLOGUE

Cocooned in a Mood of Self-Esteem ?

Technology and values — a seemingly controversial issue[1]. Biomedical engineering, however, would appear to be exempt from such controversy. Judging by what are presumably widely held beliefs, biomedical engineers do not consider their activities a form of instrumental reason. The ends become the means for establishing a moral hierarchy. Medical computer graphics is held to be a highly altruistic undertaking[2] and claimed to benefit patients directly[3]. The concept of beneficience serves to demarcate against other engineering specialities[4] [5]. An IEEE Harris poll[6] conducted some years ago reflects these attitudes fittingly. Biomedical electronics was found to rate amongst the most glamorous and highest valued of the electrical engineering specialities.

Were it not for more enlightened approaches to the value question on the part of professional bodies such as the IFMBE[7], the above views could be doing discredit to the biomedical engineering profession. For they display a profound lack of critical and contextual

---

[1] R J Whelchel. *Is technology neutral?* IEEE Techn Society Vol 5 No 4 (1986).

[2] M L Rhodes, Guest Editor. "*Special altruistic awards are evident when applying computer graphics techniques to medical images. In addition to the visual information delivered to our specialty, computer graphics scientists working in medicine have the added pleasure of knowing their efforts are targeted for health care - patients will benefit directly.*" IEEE Comp Graph Appl (Dec 1985).

[3] L-S Chen, G T Herman, R A Reynolds and J K Udupa . *Surface shading in the cuberille environment. Computed tomography and the cuberille model — an effort to better serve the medical profession and its patients.* IEEE Comp Graph Appl (Dec 1985).

[4] A Wald, Editor. "*But most of all, I believe the one additional factor which differentiates biomedical engineers from all other engineers is that biomedical engineers truly want to dedicate themselves to an activity that they know to be truly humanitarian.*" IEEE Eng Med Biol Vol 4 No 2 (1985).

[5] R W Mann. "*What distinguishes biomedical engineering from traditional engineering fields (civil, mechanical, electrical etc), and from other application areas (transport, computers, sanitary) is that "biomedical" denotes the application of engineering research and/or design practice to questions intrinsically humane. It thus exacts the best in engineering, while being motivated by the highest of human aspirations.*" Biomedical engineering, a cornucopia of challenging engineering tasks — all of direct human significance, *IEEE Eng Med Biol Mag* pp 43 (1985).

[6] Spectrum Harris poll: *EE specialties.* IEEE Spectrum (1984) Vol 21 pp 49.

[7] (1) J Hutton. *IFMBE and ISTAHC proposed joint working group on the implications and assessment of biomedical innovation.* in: Third Annual Meeting Int Soc Tech Assessment Health Care, Rotterdam, The Netherlands (May 1987). (2) MBEC News No 6 Nov 1987.

thinking. Hardly borne out by the realities of today's medical technologies, attributes like 'altruism' and 'benefit' are wishful thinking. With health expenditure absorbing growing percentages of the gross national product — 12% in the United States, 10% in Sweden and West Germany — the value of medical technologies is increasingly being questioned. Notions of the 'medical-industrial complex'[8] are difficult to reconcile with humanitarian activities. Indeed, there is justified concern over impending public policy changes that will lead to indiscriminate cuts in health expenditure, enacted by "technologically ignorant barbarians"[9].

This calls for a comprehensive technology assessment of new medical technologies that not only considers safety and efficacy[10], but cost-benefit analysis (quality of life included) and, most importantly, the definition of macro-alternatives[11]. Notably in less developed countries there is urgent need for problem- rather than technology-oriented technology assessment[12].

However, even on a technology-oriented level of assessment, technologies often fail to demonstrate forms of benefit. For example, comparative studies of acute heart attack treatment in a hospital coronary care unit and a domiciliary setting found no difference in outcome[13]. Other technologies have been linked to iatrogenic illnesses[14], and serious psycho-social side effects. Renal dialysis patients, for instance, were associated with an unusually high occurrence of suicidal behaviour[15]. The CT scanner, a technology "*that epitomises an era of American medicine, in which technological triumphs are confronted with critical questions about their worth*"[16], was criticised strongly by the technology assessment agency of the U.S.

---

[8](1) A Relman. *The new medical industrial complex.* New Engl J Med 303 pp 963 (1980). (2) L C Thurow. *Can we afford the new medical technologies?.* IEEE Eng Med Biol (June 1988).

[9](1) J D Bronzino. *Health care policy: a role for the engineering professional.* IEEE Eng Med Biol (June 1988). (2) L C Thurow. *op. cit.*

[10]Attinger is very critical of assessments based on efficacy and relative safety. He contends that such assessments are often nothing more than a public-relation release (*Transferability of health care technology assessment, with particular emphasis on the third world.* in: 3rd Ann Meeting ISTAHC, see (7)).

[11]E O Attinger and D R Ajuha. *Health and socio-economic change.* Trans IEEE Syst Man Cybern SMC-10 pp 781 (1980).

[12]E O Attinger. *op. cit.*

[13](1) A L Cochrane. *Effectiveness and Efficiency: Random Reflections on Health Services.* London: Burgess (1972). (2) H G Mather *et al. Acute myocardial infarction: a comparison between home and hospital care for patients.* Brit Med J pp 926 (1976).

[14]I Illich. *Limits to Medicine.* London: Boyars (1976).

[15]H S Abraham, G L Moore and F B Westervelt. *Suicidal behaviour in chronic dialysis patients.* Amer J Psychiatry 127 pp 119 (1971).

Congress soon after its introduction in 1972, for the lack of proof of its benefit to the health of either individuals or groups in society[17]. Cynics have since argued that medical technologies exist to diagnose, not to cure[18].

This is where the problem-oriented technology assessment sets in. To some, the recognition that there are non-medical determinants of health, still comes as a revelation[19], yet this concept has an established history. The socio-economics of health formed part of the *credo* of the French Revolution[20], and a first formal investigation was carried out in the 1830s and 40s [21]. Comprehensive studies of the recent past, the Black report[22] commissioned by the DHSS, and the Britsh Medical Association discussion paper[23], have conclusively shown that there are social-class determinants of health. At the same myths about diseases of affluence were exposed. The commonly held view that coronary heart disease or stomach ulcers are 'executive illnesses' was rejected on the basis of recent investigations, and the BMA commented laconically that "within the UK the only major cause of death that is clearly related to higher social class is malignant melanoma". Coronary heart disease is now more prevalent in the lower occupational grades[24], and shift workers have been shown to be at increased risk of ischaemic heart diease[25]. The social class gradient is thought to be related to the ability to

---

[16] H V Finneberg. *Advances and dilemmas in computed tompgraphy.* Proc IEEE 67 pp 1272 (1979).

[17] U.S. Congress, Office of Technology Assessment. *Development of medical technology: opportunities for assessment.* Washington DC (1976).

[18] T P Bleck, book review. IEEE Techn Soc pp 13 (March 1982).

[19] A Williams. *Expensive medical technologies: which can we afford?* in: 3rd Ann Meeting ISTAHC, see (7).

[20] Lanthenas. "*Who, then, should denounce tyrants to mankind if not doctors, who make man the sole study, and who, each day, in the homes of the poor and rich, among ordinary citizens and among the highest in the land, in cottage and mansion, contemplate the human miseries that have no other origin but tyranny and slavery.*" De l'influence de la liberté sur la santé. Paris (1792). in: M Foucault. *The Birth of the Clinic. An Archeology of Medical Perception.* Tavistock (1973).

[21] E Chadwick. Report on the sanitary conditions of the labouring population of Great Britain. (1842).

[22] *Report of the Working Group on Inequalities in Health (the Black Report).* DHSS London (1980).

[23] British Medical Association. *Deprivation and Ill-Health.* Discussion Paper (May 1987).

[24] M G Marmot. *Stress, social and cultural variations in heart disease.* Psychosom Res 27 pp 377 (1983).

[25] A Knutsson, T Akerstedt, B G Jonsson and K Orth-Gromer. *Increased risk of ischaemic heart disease in shift workers.* Lancet pp 89 (1986).

cope with stress and to the degree of control a person believes to have over sources of stress[26]. Infant mortality with unknown main causes during the first year of life ('cot death') is more than twice as high in the lower social classes[27], and respiratory disorders, thought to be linked to these deaths, have been associated with poor living conditions[28]. Similarly, lung diseases of external causes are markedly concentrated in the less skilled manual occupations[29]. Asbestos, for example, has long been recognised as a high risk material, but the introduction of tighter safety regulation merely led to the relocation of asbestos plants to South Africa[30], together with the occupational hazards.

What confounds and impedes the conscientious use of medical technologies is the pervasive character of technology which influences both health care providers and consumers. On the part of the patient, the imperative character of available medical technologies has reached dimensions where confrontations with the drawbackes of an implemented technology are tolerated by "anticipated decision regret"[31]. The physician's approach to medical care is dominated by a technological imperative[32], not least because of the legal safeguards[33].

A working group has recently been set up by the IFMBE to explore the social and economic implications of biomedical innovation, and the role of the engineer has been considered central to the analysis. It is to be hoped that such activities will be a first step toward the recognition of *qua* duties, or professional ethics, based on conscientiousness *i.e.* an awareness of surroundings, others, and one's self.

---

[26] S Fisher. *Stress and Strategy.* Lawarence Erlbaum Associates (1986).

[27] OPCS. *Occupational mortality. Childhood supplement.* HMSO London (1988).

[28] D J P Barker and C Osmond. *Infant mortality, childhood nutrition and ischaemic heart disease in England and Wales.* Lancet pp 1077 (1986).

[29] OPCS. *Occupational mortality. The Registrar General's decennial supplement for Great Britain,* 1979-80, 1982-83. HMSO London (1986).

[30] (1) *Killer asbestos moves south.* Africa Now (June 1981). (2) *Deadly dust threatens workers.* Africa Now (Feb 1983).

[31] Tj Tymstra. *The imperative character of medical technology and the meaning of 'anticipated decision regret'.* in: 3rd Ann Meeting ISTAHC, see (7).

[32] V R Fuchs. *Who shall live? Health, economics, and social choice.* New York: Basic Books (1974).

[33] L R Tancredi and J A Barondess. *The problem of defensive medicine.* Science 200 pp 879 (1978).

CHAPTER I

POSTSTENOTIC FLOW DISTURBANCES

1. Objectives

This study concerns poststenotic flow instabilities — their sensitivity to ambient flow perturbations and the phenomenological modelling of the flow 'locking-on' process. The experimental part of the study is a susceptibility investigation of oscillatory flow velocity fluctuations downstream of model stenoses under both steady and pulsatile flow conditions. The modelling part aims at applying nonlinear oscillator concepts to the flow regularisation phenomena observed experimentally.

1.1 Specific Goals

The aim behind the susceptibility analysis is to ascertain in model experiments the applicability of the *in vitro* existence of, amongst other forms of poststenotic flow velocity fluctuations, laminar oscillations originating in the separated shear layer, to flows *in vivo*. Complicating factors there include arterial wall vibrations that are related to poststenotic dilatation, an arterial condition occurring just downstream of partial obstructions to arterial flow. Both wall vibrations and separated shear layer oscillations are believed to have been observed *in vivo* (Kitney *et al* 1986). This suggests that not only are *in vitro* findings applicable to poststenotic flows *in vivo*, but also that the flow characteristics are not significantly altered by ambient perturbations. The assumed separability of the two signals further implies that in pulsatile flow the separated shear layer is a structurally stable phenomenon in the sense that it is insensitive to low level ambient noise. This has possible implications for the noninvasive diagnosis of the early stages of arterial deformation and is investigated experimentally here.

The aim behind the modelling study is of less instrumental character. This part is an investigation into the dynamical systems approach to modelling a time-periodically bifurcated flow. Flows exhibiting single-frequency 'self-sustained' oscillations have been successfully modelled by nonlinear oscillators (Hartlen and Currie 1970, Provansal *et al* 1987), yet no such approaches — apart from speculations — are known for the unstable free shear layer. The existence of a spectrally broad band of fluctuations does not lend itself readily to the traditional view of 'self-sustained' flow oscillations. Here the laminar shear layer fluctuations will be regarded as functionally composite nonlinear oscillations. Thus, whilst retaining the

self-sustained oscillation concept, the spectral character of free shear layer oscillations is accounted for. This description provides a phenomenological model of the 'locking-on' and the suppression of broadband fluctuations in forced poststenotic flows.

1.2 Structure of the Thesis

The remainder of this Chapter is an outline of the pathogenesis of arterial disease, and its non-invasive diagnosis based on the analysis of poststenotic flow disturbances. The Chapter ends with a discussion of haemodynamically complicating factors like arterial wall vibrations.

In Chapter II the fluid dynamics background of poststenotic separated flows is discussed. Emphasis is on the laminar instability of the free shear layer, in particular its high sensitivity — caused by the convective instability — to low level ambient noise.

The results of the experimental investigation of the susceptibility of poststenotic separated flows, including both steady and pulsatile flow conditions, are presented and discussed in Chapter III. The differences in susceptibility between steady and pulsatile flow are stressed. Also included are flow visualisations of steady and pulsatile flow past a nonsymmetric stenosis model, showing additional flow features that may be of haemodynamic relevance. Results of an experimental and theoretical analysis of the frequency tracking noise inherent in laser Doppler velocimetry are included in the Appendix.

Chapter IV introduces the second part of this thesis with a comprehensive discussion of synchronisation phenomena in simple nonlinear oscillators and populations of interacting oscillators. Both interacting identical and non-identical oscillators are considered.

This forms the basis for the phenomenological modelling, in Chapter V, of the experimentally observed synchronisation of the separated shear layer with an external excitation. The co-operative dynamics of a coupled-oscillator system with non-identical oscillators are shown to account for the flow synchronisation, and a number of other aspects of forced free shear layers. The limitations of the model are discussed.

A model system of more relevance to hydrodynamic stability theory is investigated in Chapter VI. The Ginzburg-Landau equation, the simplest field of identical nonlinear oscillators, is a generic amplitude equation for fluid problems where a continuum of wavenumbers becomes unstable as a control parameter, such as the Reynolds number, is increased above a finite threshold. A modification of this equation is introduced that gives rise to a subharmonic cascade, typically associated with the free shear layer growth. The relevance to the free shear layer is discussed.

The thesis concludes in Chapter VII with a recapitulation of the various aspects of this research, and suggestions for further work are outlined.

2. Atherosclerosis — Pathogenesis and Diagnosis

Atherosclerosis[1] is a patchy disease that occurs in the large systemic arteries. There is a clear predilection to more severe localised disease at certain selected sites in the arterial tree, including the coronary arteries, the branches of the aortic arch and the bifurcations of the carotid arteries. Atherosclerotic disease is particularly severe in the latter site — in the carotid bulb and the first few diameters of the internal carotid artery — and research has confirmed that ischaemic cerebrovascular strokes and transient ischaemic attacks are the result of atherosclerosis in the neck or the aortic arch.

A detailed knowledge of the local haemodynamics of preferential arterial sites is of importance to an understanding of the pathogenesis of this disease and to its — noninvasive — diagnosis at an early stage. Haemodynamic factors are generally thought to be of relevance to the initiation of atherosclerosis. On the other hand, the assessment of severity of arterial lesions by Doppler ultrasound techniques requires an intimate understanding of the poststenotic flow field.

2.1 Atherogenesis

The development of atherosclerotic plaque on the intimal of the artery is usually the first recognisable evidence of atherosclerosis and is a frequent finding in young adults (Enos *et al* 1953, McNamara *et al* 1971). Causative factors include heredity, high cholesterol levels, obesity, smoking and stress states. The preferential distribution of atheromatous plaque has several possible explanations. One is related to variations in the arterial wall properties. Experiments indicate that the non-uniformity in the permeability of the endothelium to lipoproteins — on which cholesterol is transported in the blood plasma — correlates with the development of fatty streaks, thought to be the precursors of the atheromatous plaque. Other than assuming genetic predisposition for the wall property variations, external influences may be sought that control the permeability of the endothelium. In particular, haemodynamic factors have been suggested to influence permeability. These include pressure and wall shear stress, the latter of which has emerged as the central but, at the same time, controversial issue. There is evidence that an elevated mean pressure enhances wall permeability, though not by a

[1] A note on the terminology — 'atherosclerosis' comprises the largest subset (90%) of the generic pathologic description 'arteriosclerosis' (Ku 1983).

pressure-driven filtration mechanism. Indeed, chronic high blood pressure is known to be a predisposing factor in the development of atherosclerosis. However, an elevated mean pressure affects arterial walls uniformly whereas wall shear stress varies with time, throughout the cardiac cycle, and with position in the arterial tree.

Fry (1968) studied the effect of wall shear stress on mass transport at the endothelial surface of dog aortas. He showed that the endothelial surface was irreversibly damaged when the wall shear stress exceeded — unphysiologically — high levels, and suggested that wall permeability increases with increasing shear stress. Fry postulated that atherosclerosis occurs preferentially at sites experiencing high wall shear stress. However, it is low permeability to large molecules that is expected to lead to fatty streaks.

Another hypothesis has been that lesions develop most readily in areas where the mechanical wall shear is relatively low. Caro *et al* (1969, 1971) suggested that the local wall shear stress exercises control over atheroma formation through flow dependent diffusion of lipid away from the vessel wall. This leads to an accumulation of lipid in areas of low wall shear stress.

The controversy has been superseded as the result of more recent studies. It is now generally accepted that physiological shear stress levels are not large enough to erode endothelial cells from the wall. Experimental findings suggest that regions of low wall shear, such as separation and reattachment points, will be susceptable to atherosclerosis. While this is an attractive hypothesis, one of the main problems is in determining which regions experience high and low wall shear stress. It has been pointed out recently (Ku *et al* 1985) that, before attempting to relate shear stress to atherosclerosis, a detailed knowledge of both the time- and space-dependence of the wall shear stress is required.

2.2 Diagnosis

Despite significant advances in non-invasive diagnostic techniques, contrast arteriography is still the standard method for detecting arterial abnormalities and the gold standard for assessing the sensitivity and specificity of non-invasive methods. Like any invasive technique, contrast arteriography presents a small, but real risk in respect to morbidity and mortality. Also, besides the costs, discomfort and other complications of this invasive examination, the information provided is strictly anatomical and it is often impossible to estimate the haemodynamic significance of a stenosis[2], even with films taken in two planes. This is because atherosclerosis rarely produces an axisymmetric lesion within an artery. Therefore, the use of changes in velocity patterns appears to be promising for long-term studies

of disease progression.

Ultrasonic duplex scanning, as a non-invasive direct technique, combines pulsed Doppler ultrasound with real-time B-mode imaging. With the pulsed Doppler ultrasound it is possible to detect blood flow at and near a site of arterial stenosis, and the B-mode images are used as a guide for the placement of the sample volume of the pulsed Doppler. Importantly, ultrasonic duplex scanning provides a means of screening patients and may help in planning the (invasive) arteriographic procedure to be used subsequently. Current experience suggests that B-mode imaging is best suited for the detection and classification of early lesions. As the plaque becomes more complicated in terms of its constituents, the variations in acoustic absorption characteristics become wider and the accuracy of B-mode imaging in predicting the degree of arterial narrowing becomes less. However, on the presupposition that arterial stenoses at specific sites will produce predictable changes in local flow velocities, Doppler velocity waveform analysis permits a broad classification of lesions and the current trend is encouraging. In this respect the carotid circulation proves advantageous in that the flow does not appear to show the same changes commonly observed in peripheral arteries under a wide variety of conditions, for example changes in ambient temperature or variations in sympathetic activity (Bernstein *et al* 1985).

3. Poststenotic Flow Disturbances

The use of successively more sophisticated methods of waveform analysis has resulted in a steady increase in the number of disease categories. Early carotid artery velocity waveform analysis limited the classification of carotid disease into haemodynamically insignificant and significant diameter reduction. With the advent of better instrumentation, it is now possible to grade stenoses in six broad categories based on peak Doppler frequency and spectral broadening : (1) normal (unoccluded); (2) 1% to 10%; (3) 11% to 49%; (4) 50% to 79%; (5) 80% to 99% and (6) occlusion. Further advances in disease description may be possible through a greater knowledge of the fluid dynamics of poststenotic flows and of signal analysis methods capable of extracting relevant information from Doppler velocity measurements.

This has formed the starting point for many a model experiment study of poststenotic flows with well defined configurational characteristics. Khalifa and Giddens (1981) identified three major types of flow disturbances downstream of contoured symmetric model stenoses in a

[2]An atherosclerotic lesion is traditionally considered to be haemodynamically significant if the lumen diameter reduction is greater than 50% *i.e.* if the cross sectional area reduction is greater than 75%.

straight rigid tube :

(1) a start-up structure associated with the start-up process of each cycle;

(2) oscillations originating in the separated shear layer downstream of the model stenosis;

(3) random velocity fluctuations.

The start-up structure has a very repeatable velocity *vs.* time signature with each pulse and propagates at approximately the local flow velocity. This suggests that what is observed is some form of starting vortex known from impulsively started separated shear layers. In fact, the repeatability of the waveform is a distinguishing feature of the starting vortex generated by orifice flow started from rest (*cf.* CH III § 5.2.1.5).

What was classified as the second type of flow disturbance by Khalifa and Giddens is the result of the Kelvin-Helmholtz type instability of the separated shear layer downstream of the stenosis. The oscillations are generally amplitude and frequency modulated, and approximately scale with the local flow velocity and a characteristic length scale such as the reduced lumen diameter. For comparison, in free circular jets, the dominant frequency f_0 is related to the jet exit velocity U_j and the jet diameter D *via* $f_0 U_j/D \approx 0.25$ to 0.50. The scatter of this dimensionless number, the Strouhal number (*cf.* Ch II § 2), is mostly due to the residual noise present in individual flow facilities. It must be emphasised, however, that this scaling law applies only if the ratio of jet diameter and initial shear layer momentum thickness is above some critical value.

Finally, the random velocity fluctuations are typically initiated not by the start-up structure but by the shear layer instability. Again, in free jets the turbulent structure represents the small-scale transition behind the end of the potential core. In confined jets, on the other hand, the break-up of coherent structures is more probably due to interference with the downstream bounding walls. Attempts have been made at scaling turbulence spectra in poststenotic flows, calculated from the data of an entire pulse cycle. The energy is non-dimensionalised by the peak velocity and the frequency is transformed to a semi-local Strouhal number. The results show remarkable similarity between data obtained both *in vivo* and *in vitro*, over an extensive range of stenosis size, Reynolds number and axial position (Cassanova and Giddens 1978). In general, turbulence similarity is best if the degree of occlusion is sufficient and the Reynolds number is relatively large.

The flow features that are of possible interest in respect to the early stages of arterial disease are the starting structure and oscillatory flow velocity fluctuations of discrete frequency because they are the first to be observed as the degree of stenosis increases. As Giddens and Kitney (1986) noted, "*Lowering the threshold of recognition of localised arterial disease using*

flow disturbance analysis will best be achieved by understanding the role of coherent disturbance features, not by measurement of turbulence".

The relevance of the flow disturbance categories to arterial stenotic flows remains to be assessed but evidence appears to support the *in vivo* existence of similar flow disturbances. For example, Casty and Giddens (1984) studied several subjects using a pulsed Doppler system and observed coherent flow disturbances during peak systole in the common carotid artery of a patient with aortic valve failure and a systolic bruit radiated up the artery. In another example (Khalifa and Giddens 1978), the analysis of hot-film anemometer measurements of blood velocities in the descending aorta of dogs with induced stenoses (*figure* 1.1) demonstrated flow disturbance features that were speculated to represent shed vortices or arterial wall vibrations. The subsequent analysis of individual beats by homomorphic filtering (Kitney *et al* 1986) indicated the co-existence of two spectrally distinctive structures during peak systole. This investigation is briefly summarised here.

For the purpose of analysing the flow disturbances, superposed on the basic pulsatile flow waveform, the two components were separated by low-pass/high-pass filtering (f_c=100 Hz). The inspection of individual-beat disturbance velocities at various levels of occlusion indicated that an amplitude-modulation mechanism was operative (*figure* 1.2*a*). It was decided to demodulate the signal by homomorphic filtering (Oppenheim and Schafer 1975), a technique that is more generally applicable than the Hilbert-transform approach (*e.g.* Ktonas and Papp 1980) to decomposing narrowband AM-FM signals. In a homomorphic filter for multiplicative signals, the two signal components are separated by a logarithmic operation. Modelling the disturbance velocity signal $s(t)$ as

$$s(t) = e(t)\ v(t) \quad , \tag{1.1}$$

with $e(t)$ an envelope function always greater than zero, the two components, if spectrally distinctive from one another, may be separated by a complex logarithm operation, followed by linear filtering of the real part — lowpass filtering for $e(t)$ and highpass filtering for $v(t)$ — and finally complex exponentiation :

$$\begin{aligned} \tilde{s}(t) &= \tilde{s}_R(t) + \tilde{s}_I(t) \\ \tilde{s}(t) &= \log\{e(t)\ v(t)\} = \log\{e(t)\} + \log\{|v(t)|\} + j \arg\{v(t)\} \\ e(t) &= \exp\{L_l[\tilde{s}_R(t)]\} \qquad\qquad v(t) = \exp\{L_h[\tilde{s}_R(t)] + \tilde{s}_I(t)\} \end{aligned} \tag{1.2}$$

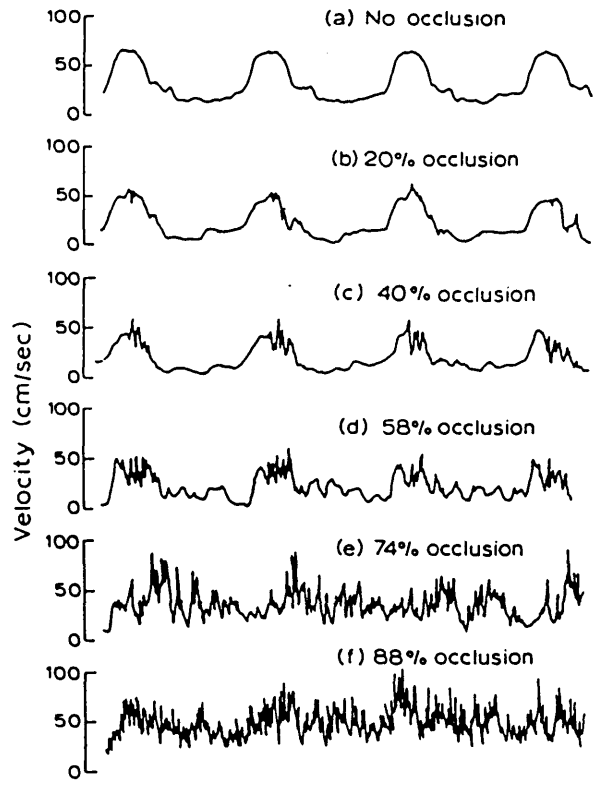

Figure 1.1 Poststenotic flow disturbances in the canine thoracic aorta, for various levels of occlusion. Flow velocities are measured with a hot-film probe located at the centre line, 2cm distal to the area of maximal constriction (after Giddens *et al* 1976, no time scale given).

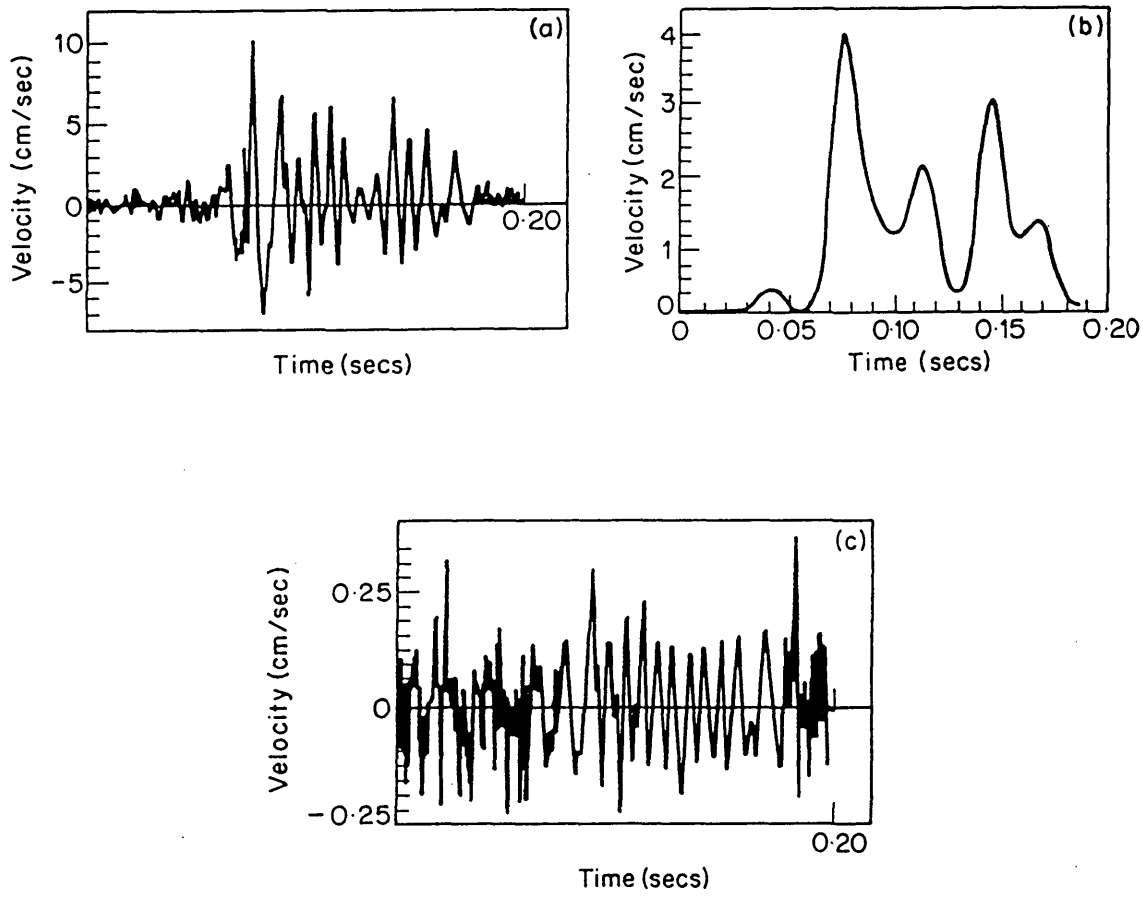

Figure 1.2 (*a*) A single highpass filtered beat (f_c=100 Hz) taken from 40% occlusion data. The low frequency envelope (*b*), and the high frequency content (*c*), obtained by homomorphic filtering.

where L_l and L_h are low- and high-pass filtering operators, respectively. Exemplary results of the demodulation are shown for the 40% occlusion level in *figure* 1.2. The large variations of the envelope $e(t)$ were thought to reflect the passage of large scale structures such as shed vortices. Indeed, the Strouhal number calculated from the basic frequency of variation of $e(t)$ and the peak velocity and constriction diameter was found to be around 0.5, a value representative of the vortex shedding in confined and free jets (*cf.* Ch II § 3.2). With regard to the carrier waveform $v(t)$, two somewhat contradictory explanations were offered. On the one hand, it was speculated that $v(t)$ represented "*finer scale phenomena within the vortex structure*". This, however, seems difficult to conceptualise. Lau and Fisher's (1975) analysis of hot-film measurements in jets conclusively showed that the signature of a vortex, passing the hot-film probe, consists of a single skewed spike. The details of this spike were explained physically.

Alternatively, the high-frequency fluctuations $v(t)$ were thought to result from arterial wall vibrations, as suggested previously by Khalifa and Giddens (1978). Thus the following scenario emerged: arterial wall vibrations are generated distally to the induced stenosis mainly during peak systole and cause high-frequency fluctuations. These in turn are modulated by the much lower frequency of vortex shedding from the stenosis.

To appreciate the significance of poststenotic vessel wall vibrations it is appropriate at this point to give an overview of this phenomenon.

4. Arterial Wall Vibrations and Poststenotic Dilatation

Arterial wall vibrations occur distally to atherosclerotic lesions and have been proposed as a noninvasive diagnostic tool for arterial disease (Lees and Dewey 1970). The technique, phonoangiography, is now successfully employed for the quantification of arterial deformations. The sound that is recognised as arterial bruit is produced by the transmission of vessel wall motion, induced by flow disturbances distal to the arterial stenosis, to the skin surface. Arterial wall vibrations are closely related to poststenotic dilatation, an enlargement of the artery in the low pressure region distal to a stenosis. Paradoxically, it is often the poststenotic dilatation that is easier to see radiologically than the stenosis itself. Poststenotic dilatation is a type of structural fatigue induced by the (resonant) wall vibrations which in turn are caused by flow disorder or turbulence. Correlation between the three has received considerable attention.

Roach (1963*a*) found from *in vivo* studies that only those stenoses, artificially induced in the femoral and carotid arteries of dogs, caused poststenotic dilatation that produced noticeable distal turbulence, indicated by a thrill and a bruit. A poststenotic dilatation

developed within the first 10 to 12 days of intervention and the dilated artery segments were more distensible than normal (Roach 1963*b*). A subsequent study *in vitro* (Roach and Harvey 1964) of isolated perfused human iliac arteries produced essentially the same result, *viz.* a degree of flow turbulence distal to the induced stenosis was required that was detectable by wall vibrations. Similar results, of somewhat lower accuracy due to different instrumentation, were obtained by Foreman and Hutchison (1970).

The obvious correlation between poststenotic arterial wall vibrations and the development of poststenotic dilatation led Boughner and Roach (1970) to investigate the effect of vibrations alone on the arterial wall. Again, isolated human iliac arteries were used. Different arteries were seen to respond, in terms of dilatation, to different frequency ranges, though no conclusive evidence of resonant behaviour was found. Resonance, however, was clearly observed by Hutchison (1974) in experiments on the frequency response of isolated canine carotid arteries, particularly at higher transmural pressures *i.e.* increased wall stiffness.

In contrast to Roach's (1972) hypothesis that flow turbulence is the *sine qua non* for poststenotic dilatation through arterial wall vibrations, there were speculations by Bruns *et al* (1959) and, more recently by Hussain (1977), that the vortex shedding from arterial stenoses interacts with the distal arterial walls, causing vibrations. Hussain went as far as conjecturing a possible link between the starting vortex shed during each cycle at the optimum Strouhal number St=0.4, with the resonant frequency of the vessel wall. Unfortunately, as far as flow conditions in the human carotid arteries are concerned, this is a rather unlikely situation.

A study that bears stronger on the findings of Khalifa and Giddens (1978), and subsequently Kitney *et al* (1986), is a comparison of model and *in vivo* experiments on vessel wall vibrations due to induced stenoses (Kirkeeide *et al* 1977). The model study utilised axisymmetric constrictions inserted into flexible tubes, with moduli of elasticity comparable to the canine femoral artery which was investigated *in vivo*. The relationships that were found between wall-vibration intensity and fluid dynamic parameters, were similar for the two experiments. Somewhat surprisingly, however, the amplitude of wall vibrations in the *in vivo* case was increased by a factor of approximately 20 in comparison to the model study. Concurrently, the axial position of maximum wall vibrations was consistently upstream of the position predicted by the model results. Kirkeeide *et al* (*ibid*) concluded that "*the unsteady flow system may be a more efficient generator of fluid oscillations than the steady flow system under similar conditions*".

Returning to the wall vibration measurements *in vivo*, although no frequency analysis was carried out due to the nonstationary character of the wall displacement signal, the *in vitro*

recordings showed clear resonance at frequencies of 600 Hz or 800 Hz, independent of flow rate. These values may not be physiologically relevant, however. Hutchison's (1974) findings indicated resonances in the range 50 to 150 Hz which is approximately the frequency range reported by Kitney *et al* (1986). As regards the amplitude of the vessel wall vibrations *in vivo*, despite the twenty-fold increase over comparable steady flow conditions, these are well in the sub-micron range, a figure that requires qualification. Firstly, the displacement transducer was a piezo-electric contact microphone which most probably influenced the vessel vibrations. Secondly, no independent calibration was undertaken. The experimental findings of Kirkeeide *et al* (1977) may therefore be taken as *in vivo* evidence of some form of poststenotic vessel wall vibrations, without detailed knowledge about either spectral composition or absolute vibration intensity.

5. Conclusions

The eduction of diagnostically meaningful non-turbulent flow disturbances from *in vivo* flow velocity waveforms is a non-trivial task. How much of the flow disturbance classification, derived from model experiments, survives in the *in vivo* context depends greatly on the degree of structural stability the particular type of flow disturbance possesses. Of the two coherent disturbance features, it is the large scale start-up structure that is very repeatable under a variety of flow conditions. This contrasts with the laminar shear layer oscillations which are significantly less structurally stable. Very low-level ambient background noise modifies the spectral content and the amplitude of these fluctuations. As will be seen in the following chapter, even under controlled laboratory conditions the most probable frequency (preferred mode) and the spreading rate of an initially laminar shear layer can show up to 100% variability in different flow facilities. It is conceivable therefore that resonant vessel vibrations feed back to the shear layer origin, modifying the flow evolution.

It is not attempted in this study to investigate such a feedback mechanism. The model experiment would entail too many *ad hoc* assumptions about the vessel geometry and elastic wall properties distal to the stenosis. Instead, it has been decided to study the susceptibility of the separated poststenotic shear layer *per se*. This affords control over the frequency content and the amplitude of the flow perturbations by artificially exciting the flow.

Literature Cited

Bernstein E F and Associate Editors (1985). Controversies in the non-invasive evaluation of extracranial arterial disease. *in: Noninvasive Diagnostic Techniques in Vascular Disease, 3rd Ed.* ed E F Bernstein (St Louis: Mosby).

Boughner D R and Roach M R (1970). The effect of low frequency vibration on arterial wall elastin. *Proc AGARD Conf on Fluid Dynamics of Blood Circulation and Respiratory Flow, Naples, Italy.*

Bruns D L, Connolly J E, Holman E and Stofer R C (1959). Experimental observations on poststenotic dilatation. *J Thorac Cardiovasc Surg* 38 pp 662.

Caro C G, Fitz-Gerald J M and Schroter R C (1969). Arterial wall shear and distribution of early atheroma in man. *Nature* 223 pp 1159.

Caro C G, Fitz-Gerald J M and Schroter R C (1971). Atheroma and arterial wall shear. Observation, correlation and proposal of a shear dependent mass transfer mechanism for atherogenesis. *Proc Roy Soc London B* 177 pp 109.

Cassanova R A and Giddens D P (1978). Disorder distal to modelled stenoses in steady and pulsatile flow. *J Biomech* 11 pp 441.

Casty M and Giddens D P (1984). 25+1 channel pulsed ultrasound Doppler velocimeter for quantitative flow measurements and turbulence analysis. *Ultrasound Med Biol* 10 pp 162.

Enos W F, Holmes R H and Beyer J (1953). Coronary disease among United States soldiers killed in action in Korea. *J American Med Ass* 152 pp 1090.

Foreman J E K and Hutchison K J (1970). Arterial wall vibration distal to stenoses in isolated arteries of dog and man. *Circ Res* 26 pp 583.

Fry D L (1968). Acute vascular endothelial changes associated with increased blood velocity gradients. *Circ Res* 22 pp 165.

Giddens D P, Mabon R F and Cassanova R A (1976). Measurements of disordered flows distal to subtotal vascular stenoses in the thoracic aortas of dogs. *Circ Res* 39 pp 112.

Giddens D P and Kitney R I (1985). Blood flow disturbances and spectral analysis. *in: Noninvasive Diagnostic Techniques in Vascular Disease, 3rd Ed.* ed. E F Bernstein (St Louis: Mosby).

Hartlen R T and Currie I G (1970). Lift-oscillator model for vortex-induced vibration. *Proc ASCE J Eng Mech* 96 pp 577.

Hussain A K M F (1977). Mechanics of pulsatile flow of relevance to the cardiovascular system. *in: Cardiovascular Flow Dynamics and Measurements.* eds N H C Hwang and N A Normann (Baltimore: Univ Park Press).

Hutchison K J (1974). Effect of variation of transmural pressure on the frequency response of isolated segments of canine carotid arteries. *Circ Res* 35 pp 742.

Khalifa A M A and Giddens D P (1978). Analysis of disorder in pulsatile flows with application to poststenotic blood velocity measurements in dogs. *J Biomech* 11 pp 129.

Khalifa A M A and Giddens D P (1981). Characterisation and evolution of poststenotic flow disturbances. *J Biomech* 14 pp 279.

Kirkeeide R L, Young D F and Cholvin N R (1977). Wall vibrations induced by flow through simulated stenoses in models and arteries. *J Biomech* 10 pp 431.

Kitney R I, Talhami H and Giddens D P (1986). The analysis of blood velocity measurements by autoregressive modelling. *J Theor Biol* 120 pp 419.

Ktonas P Y and Papp N (1980). Instantaneous envelope and phase extractions from real signals: theory, implementation, and an application to EEG analysis. *Signal Processing* 2 pp 373.

Ku D N (1983). Haemodynamics and atherogenesis at the human carotid bifurcation. Doctoral dissertation, Georgia Institute of Technology.

Ku D N, Giddens D P, Zarins C K and Glagov S (1985). Pulsatile flow and atherosclerosis in the human carotid bifurcation. Positive correlation between plaque location and low and oscillating shear stress. *Arteriosclerosis* 5 pp 293.

Lau J C and Fisher M J (1975). The vortex structure of 'turbulent' jets. Part 1. *J Fluid Mech* 67 pp 299.

Lees R S and Dewey C F Jr (1970). Phonoangiography: a new non-invasive diagnostic method for studying arterial disease. *Proc Natl Acad Sci USA* 67 pp 935.

McNamara J J, Molot M A, Stremple J F and Cutting R T (1971). Coronary artery disease in combat casualties in Vietnam. *J American Med Ass* 216 pp 1185.

Oppenheim A V and Schafer R W (1975). *Digital Signal Processing* (Englewood Cliffs: Prentice Hall).

Provansal M, Mathis C and Boyer L (1987). Bénard - von Kármán instability: transient and forced regimes. *J Fluid Mech* 182 pp 1.

Roach M R (1963*a*). An experimental study of the production and time course of poststenotic dilatation in the femoral and carotid arteries of adult dogs. *Circ Res* 13 pp 537.

Roach M R (1963*b*). Changes in arterial distensibility as a cause of poststenotic dilatation. *American J Cardiol* 12 pp 802.

Roach M R (1972). Poststenotic dilatation in arteries. *in*: *Cardiovascular Fluid Dynamics*, *Vol* 2. ed D H Bergel (London: Academic Press).

Roach M R and Harvey K (1964). Experimental investigation of poststenotic dilatation in isolated arteries. *Canadian J Physiol Pharm* 42 pp 53.

CHAPTER II

FREE SHEAR LAYER INSTABILITY

> "I happened to be one of a party of eight persons assembled after tea for the purpose of enjoying a private musical entertainment. Three instruments were employed in the performance of several of the grand trios of Beethoven, namely, the piano, violin, and violincello. Two *'fish-tail'* gas-burners projected from the brick wall near the piano. Both of them burnt with remarkable steadiness, the windows being closed and the air of the room being very calm. Nevertheless it was evident that *one* of them was under pressure nearly sufficient to make it *flare*.
>
> Soon after the music commenced, I observed that the flame of the last-mentioned burner exhibited pulsations in height which were *exactly synchronous* with the audible beats. This phenomenon was very striking to everyone in the room, and especially so when strong notes of the violincello came in. It was exceedingly interesting to observe how perfectly even the *trills* of this instrument were reflected on the sheet of flame. *A deaf man might have seen the harmony.*"
>
> John Leconte (1858). On the influence of musical sounds on the flame of a jet of coal-gas. *Phil Mag* 15 pp 235.

1. Introduction

Having given further details of his observations, Leconte then concluded "that the phenomenon which had fallen under my observation was nothing more than a *particular case* of the effects of sounds on *all kinds of fluid jets.*"

Leconte's delightfully vivid account of what is known as 'sensitive flames' conveniently sets out the theme of this chapter, namely the susceptibility of free shear layers to very low-amplitude perturbations. Two mechanisms constitute this susceptibility. Near the shear layer origin — in the linear region — the free shear layer acts as a large-gain narrowband amplifier of ambient background noise. In the nonlinear region, 'competition' between the natural broadband fluctuations and a periodic perturbation can lead to the suppression of broadband fluctuation levels and concentration of energy at the perturbation frequency. It is the combination of these two mechanisms that causes dramatic changes in the spatial development of the free shear layer.

Below, the basic properties of unforced and forced free shear layers are outlined. The discussion of more specific aspects of free shear layers is deferred until required (Ch III, V and VI). At first, however, the concept of dynamical similarity, of central importance to experimental fluid dynamics, is sketched briefly and the definitions for a few important dimensionless parameters are given.

2. Dynamical Similarity

Dynamical similarity is the cornerstone of physical modelling. Consider, for example, incompressible steady flow without any free surface. The dynamics of this hypothetical flow scale exhaustively with a single dimensionless parameter, the Reynolds number. That is, given two geometrically similar flows with otherwise different characteristics, they are expected to behave dynamically similar so long as the respective Reynolds numbers are the same. Problems with the similarity principle arise not because of its limited range of applicability, but because the underlying assumptions may break down if, for example, geometrical scales are greatly reduced *e.g.* whole blood is correctly treated as a Newtonian fluid only in the larger arteries (*cf* Ch III § 2.2).

The number of dimensionless parameters on which some physical process scales is equal to the difference between the number n of variables that constitute the – necessarily abstracted – formal description of the process and the number m of independent dimensions involved (Ipsen 1960). In rigid pipe flow, $n-m=1$. To demonstrate this, consider steady flow of an incompressible fluid in a rigid pipe. The number of variables that describe this flow is $n=4$: velocity (or pressure gradient), a length scale pertaining to the conduit, and the density and viscosity of the fluid. A typical dimensional base consists of mass, length and time, *i.e.* $m=3$. *q.e.d.*

Dimensionless products obviously have a meaning beyond the grouping of variables in dimensionless form. The Reynolds number

$$Re = \frac{U\,D}{\nu} \tag{2.1}$$

is the ratio of inertial to viscous forces, where U and D are a representative flow velocity and length scale, respectively, and ν is the kinematic viscosity $\nu=\mu/\rho$, ratio of dynamic viscosity and density. Thus, for any inviscid fluid, $Re=\infty$. When unsteady, or more specifically pulsatile, flows are considered another dimensionless product is required to account for the

added time scale. Depending on the physical meaning, this product can either be the Strouhal number

$$St = \frac{\omega\ D}{2\pi\ U}\ , \tag{2.2}$$

or the frequency parameter — also known as the Womersley number, in recognition of Womersley's contribution to the theory of oscillatory flows in rigid and elastic tubes (Womersley 1955, 1957),

$$\alpha = \frac{D}{2}\sqrt{\frac{\omega}{\nu}}\ , \tag{2.3}$$

or the Stokes layer thickness,

$$\delta = \sqrt{\frac{\nu}{\omega}}\ . \tag{2.4}$$

Between the Reynolds number, Strouhal number and Womersley number exists the relationship

$$\alpha^2 = \frac{\pi}{2}\ Re\ St\ . \tag{2.5}$$

The Stokes layer thickness is a measure of the distance that the effect of a boundary wall can diffuse away from the wall during one period of the oscillation. The Womersley number simply relates the Stokes layer thickness to a length scale such as the pipe radius,

$$\alpha = \frac{D/2}{\delta}\ . \tag{2.6}$$

The Strouhal number, on the other hand, relates a system length to the distance the fluid travels in one period.

3. Free Shear Layer Instability and Transition

This section considers natural mixing layers and free jets under steady flow conditions, for which the relevant scaling parameters are the Reynolds number and the Strouhal number.

3.1 The Mixing Layer

Consider the plane mixing layer formed by the merging of two parallel streams of respective velocities U_1 and U_2, separated by a splitter plate. A useful parameter is the quantity

$$R = \frac{U_1 - U_2}{U_1 + U_2}, \qquad U_1 > U_2 . \tag{2.7}$$

R is a measure of the magnitude of shear and describes various flow configurations. If $0 < R < 1$, both streams run in the same direction, while for $R > 1$ they flow in opposite directions. In the limiting case where $R=0$, there is no shear and when $R=1$, only one stream is present, as in the initial mixing region of a jet.

The spatially evolving flow downstream of the splitter plate is linearly inviscidly unstable to small perturbations *via* the Kelvin-Helmholtz instability mechanism. If the mixing layer is conceptualised as a superposition of interacting instability waves with space-time dependence $\exp(\beta x - j\omega t)$, that propagate and amplify in the downstream direction, the flow may be examined in Fourier space. Most calculations for linearly unstable free shear layers have been conducted for the one-parameter family of hyperbolic-tangent profiles

$$U(y,R) = \bar{U}\,(1 + R\tanh(\frac{\theta_0}{2y})) \qquad \bar{U} = (U_1 + U_2)/2 \tag{2.8}$$

where y is the cross-stream coordinate and θ_0 is the initial shear layer momentum thickness. The spatial growth rate β_r is found to be biggest for a wave with Strouhal number $St_n = \frac{\omega_n \theta_0}{2\pi \bar{U}} = 0.032$. This normalised frequency of the mixing layer changes by only 5% between $R=0$ and $R=1$. The phase velocity $c_r = \frac{\omega_n}{\beta_i}$ of the most amplified wave is equal to the average velocity $\bar{U}$ of the two streams. Spatial waves are dispersive below St_n and non-dispersive above, *i.e.* the phase velocity becomes independent of the normalised frequency St.

The analysis so far has been limited to small perturbations and a region where the basic flow is parallel. Both assumptions break down further downstream. As nonlinear effects come into play, the exponential growth of the linearly most unstable wave decreases. The instability wave evolves into a periodic array of vortices moving at the average velocity, with a wavelength $\lambda_n = \frac{2\pi}{\omega_n}$. At the same time, a subharmonic wave at half the frequency of the fundamental makes its appearance together with the expected higher harmonics. This constitutes one of the most striking features in mixing layer dynamics because it initiates

vortex pairing[1] *i.e* adjacent pairs of vortices begin to roll around each other, finally coalescing into a single vortex. The emergence of the subharmonic is the result of a parametric resonance mechanism. In its simplest formulation, the row of vortices is modelled by an array of point vortices. Linear analysis indicates that this configuration is most unstable to a disturbance of wavelength 2 λ_n (Lamb 1932). In a more representative description, the stability of a basic space-time periodic flow is investigated (Kelly 1967). It is found that the periodic flow can serve as a means by which waves with half the frequency and twice the wavelength *i.e.* with the same phase velocity $\bar{U}$, can be reinforced. The instability mechanism is thus one of principal parametric resonance (Nayfeh and Mook 1979) whereby the subharmonic can reproduce itself *via* quadratic interaction with the fundamental.

So far the shear layer instability has been a purely two-dimensional process. Following the appearance of the subharmonic, however, three-dimensional structure begins to form. The mixing layer becomes unstable to cross-stream disturbances and significant spanwise activity ensues in the form of longitudinal vortices. Eventually, the flow breaks down into turbulence. According to Miksad (1972), the entire process, from linear instability to turbulence, occurs in a distance of about five wavelengths of the fundamental instability wave.

3.2 The Free Jet

Jets, like mixing layers, are inviscidly unstable to small perturbations, with viscosity acting to stabilise the flow. However, this effect is rather small and jet flows become unstable at Reynolds numbers of the order of ten (Andrade 1939). Unlike the mixing layer, a free jet possesses two length scales. Apart from the initial shear layer thickness, another length scale is the diameter D of the axisymmetric nozzle, or the height H of the two-dimensional nozzle. In both kinds of jet, a potential flow issuing from the exit plane comes to an end about $5D$, or $3H$, downstream. As in the mixing layer, instability waves grow, eventually rolling up into axisymmetric, or two-dimensional, vortical structures. These large scale structures experience successive amalgamations that eventually lead to small-scale transition (*figure* 2.1). Beyond the tip of the potential core the vortices are more difficult to identify.

In accordance with the two lengths in the jet, θ_0 and D or H, there are two regions of scaling laws. Near the nozzle exit, the dominant instability wave is expected to scale with the initial shear layer momentum thickness θ_0. This is the high frequency *shear layer mode.* As

[1] This important point cannot be overemphasised (Ho and Huang 1982). Subharmonics are the catalyst of vortex pairing, not its outcome, as mistakenly assumed by Crow and Champagne (1971).

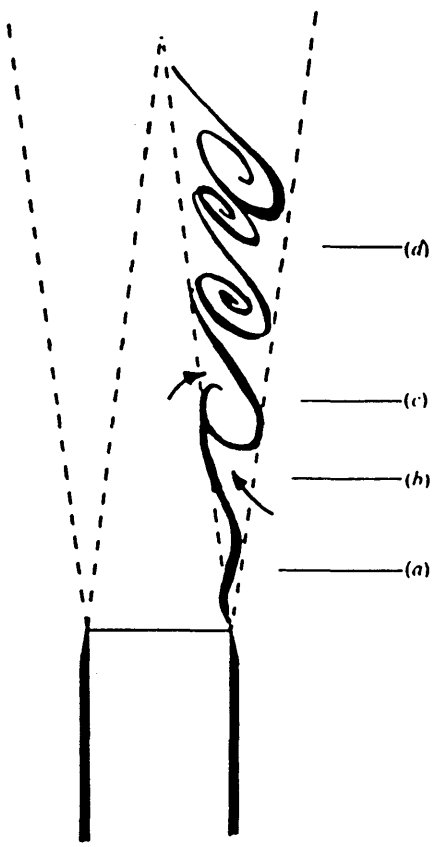

Figure 2.1 Schematic diagram of the development of the preferred mode in a free jet. (*a*) The shear layer oscillates. (*b*) Fluid becomes entrained — the shear layer rolls up. (*c*) Vortices form. (*d*) Vortices merge and the shear layer thickness grows (after Moore 1977). The potential core comes to an end about 5 D downstream.

Sato (1960) remarks for the two-dimensional jet :"*The shear layer at the one side of a jet does not know the existence of the shear layer at the other side.*" The passage frequency of vortical structures at the end of the potential core scales with the jet diameter or height, provided the initial momentum thickness is small compared to D, or H, $\frac{D}{2\theta_0} \gg 1$, or $\frac{H}{\theta_0} \gg 1$. This instability is the *preferred mode* or *jet-column mode*, and for length scale ratios greater than about 150, the number $\frac{\omega_p D}{2\pi U_j}$, or $\frac{\omega_p H}{2\pi U_j}$, is constant. In circular jets, the Strouhal number is found to vary between 0.25 and 0.5. The scatter is due the shear layer sensitivity. A similar Strouhal number range applies to the two-dimensional jet.

Obviously, the existence of the shear layer mode depends on the state of the boundary layer shed from the jet nozzle. If the boundary layer is tripped the preferred mode will develop directly from the turbulent free jet shear layer. If the boundary layer is laminar, both modes will exist and, particularly in forced jets, the two modes will interact to produce the necessary number of vortex pairings to connect the modes.

4. The Forced Free Shear Layer

To summarise this section, the sensitivity of the free shear layer is such that natural free shear layers are by nature excited flows.

4.1 Hyper-Sensitivity and Convective Instability

According to Gutmark and Ho (1983), disturbance levels as low as 10^{-3} % of the jet exit speed, or the average velocity $\bar{U}$ of the mixing layer, can generate 100% changes in the spreading rate, shear layer Strouhal number and jet-column Strouhal number. This hyper-sensitivity is a direct consequence of the convective instability of the linearly unstable free shear layer (Huerre and Monkewitz 1985). Very low-level disturbances are spatially amplified exponentially and can have a lasting effect on the downstream development of the flow. The hyperbolic-tangent profile (equation 2.8) was found to be convectively unstable even for mildly counter-flowing streams, $R < 1.315$. Cold jets with $R < 1$ are convectively unstable whilst inhomogeneous (hot) jets can be absolutely unstable. Wakes contain both convectively and absolutely unstable regions which explains their relative insensitivity.

We shall come back to these two types of instability in connexion with a model open flow system (Ch VI).

4.2 Means of Flow Forcing

It follows from the above discussion that flow excitation is most effective near the shear layer origin, *i.e.* at the jet nozzle or the trailing edge of the splitter plate. This was demonstrated for an acoustically excited jet by Brown (1935). A jet, partially shielded from the acoustic field, reverted to basically unforced conditions only when the immediate neighbourhood of the nozzle was screened. Often, however, free shear layers undergo a more subtle and insidious form of excitation. Facility forcing can cause unexpected flow organisation (Beavers and Wilson 1975), and is thought to account for the large scatter in measurements of various free shear layer parameters (Gutmark and Ho 1983).

Controlled types of free shear layer excitation include planar surging, azimuthal perturbation and mechanical vibrations with a ribbon or an oscillating flap. For the imposed excitation to be effective the forcing must be spatially coherent along the circumference or span. Planar surging is produced by employing an excitation source located in the supply stream (*e.g.* Crow and Champagne 1971, Moore 1977, Peterson 1978, Acton 1980) or in the downstream region (*e.g.* this study). Note, however, that surging, introduced upstream of the trailing edge of a splitter plate (*e.g.* Miksad 1972, Ho and Huang 1982), produces both streamwise and transverse velocity perturbations downstream of the trailing edge. In Kibens' (1980) forced jet experiments an azimuthally coherent perturbation was introduced locally at the nozzle exit through a thin slit surrounding the nozzle. Often, the excitation is not as well defined and the free shear layer is insonated with an acoustic source (Brown 1935, Sato 1960). Alternatively, periodic two-dimensional excitation can be applied at the initiation of mixing between the parallel streams by a thin oscillating flap mounted at the trailing edge of the splitter plate (*e.g.* Oster and Wygnanski 1982).

The main difference between the various methods of excitation lies in the manner in which the excitation source feeds energy into the fluctuating vorticity field. For example, the conversion of acoustic excitation into vortical instability waves at the trailing edge is an incompletely understood mechanism, whereas mechanical forcing acts in a straightforward way by converting a large portion of the input energy into instability waves.

4.3 The Forced Mixing Layer

What, then, is the effect of forcing on the mixing layer dynamics? In principle, low-level forcing regulates the spatial development of the mixing layer. The method has therefore been used to study the instability and transition of free shear layers (Miksad 1972). Flow excitation provides a means of educing the evolution of coherent structures and has been

instrumental in gaining an understanding of the vortex pairing process.

If the forcing frequency is near the natural instability, the otherwise irregularly forming vortices are phaselocked by the excitation and the spread of the mixing layer is suppressed. In the energy spectrum of vortex-induced flow velocity fluctuations, this manifests itself as a concentration of energy near the forcing frequency and a reduction elsewhere. Control over the flow in a distance of up to eight wavelengths is possible. Beyond the region of flow control, vortex merging resumes and the mixing layer grows linearly further downstream as in the unforced mixing layer.

If the forcing frequency is below a certain limit, the vortex formation frequency becomes a multiple of the fundamental forcing frequency and the location of vortex merging is localised, taking place over a distance of about one wavelength of the vortex passage frequency before merging. The mixing layer spreads very quickly around the merging positions but stays almost constant until further merging occurs. Vortex formation at up to four times the forcing frequency has been observed (Ho and Huang 1982), resulting in a cascade of three plateaus of constant vortex passage frequency, accompanied by two highly localised vortex pairings and the approximate doubling of the mixing layer thickness at each pairing location. The flow is regulated over a distance of nearly 20 diameters of the initial vortex formation frequency before the mixing layer reverts to unforced conditions. If the vortex formation is at an odd multiple of the forcing frequency, vortices typically merge in pairs and the new vortex merges with another one. At higher forcing levels the sequential vortex merging is bypassed. Vortices intially form in a wide band around the natural instability and merge collectively to produce vortices at the forcing frequency. The phenomenon is characterised by a large drop in vortex passage frequency and a high spreading rate.

The mixing layer is less sensitive to excitation at frequencies above the most probable frequency of vortex formation because of the smaller spatial growth rates at these frequencies.

4.4 The Forced Free Jet

The same sensitivity considerations apply to the excitation of the shear layer mode and the jet column mode in free jets. The natural instability of the initial shear layer of an untripped circular jet is effectively manipulated by forcing levels of the order of 10^{-5} % (Laufer and Zhang 1983) to 10^{-3} % (Gutmark and Ho 1983) of the jet exit speed. At very low forcing frequencies, comparatively higher amplitude levels are required to offset the small amplification rates prevailing in the low Strouhal number range. Crow and Champagne (1972) used forcing levels of about 2% to manipulate the preferred mode of a tripped axisymmmetric jet, the level

in Moore's (1977) experiments on an untripped jet was of the order of 0.1%, and in the numerical simulation of Acton (1980) flow regulation was achieved at levels around 2%.

In contrast to the plane mixing layer where subharmonic forcing is necessary to manipulate the vortex merging process effectively, long-range control is effected in axisymmetric jets by harmonic forcing (Kibens 1980). At forcing frequencies f_f near the shear layer mode, a vortex pairing cascade $f_f/2$, $f_f/4$, $f_f/8$ with three localised pairing locations is possible. This scenario is most pronounced when the ratio of the shear layer mode and the jet-column mode is eight. The two instability modes interact most strongly then and the energy transfer to successively lower frequencies is largest.

Provided the forcing amplitude is sufficiently high, the jet-column mode may be excited directly. In the case of an untripped jet boundary layer, this amounts to the collective merging scenario of the strongly forced plane mixing layer, the main difference being the resonant behaviour near the preferred mode.

5. Conclusions

If natural free shear layers are by nature excited flows, then any quantitation of the shear layer instability must be treated with some caution. In most circumstances an *a priori* knowledge of possible sources of flow perturbation is essential because the perturbations may not be amenable to measurement due to the low perturbation intensity strength.

It must be borne in mind that the above discussion applies to steady separated flows. Under pulsatile flow conditions, the free shear layer exhibits qualitatively new behaviour including a starting vortex and flow destabilisation during flow deceleration. It is the purpose of the experiments described in the following chapter to assess the flow susceptibility of poststenotic flows under steady and puslatile flow conditions.

Literature Cited

Acton E (1980). A modelling of large eddies in an axisymmetric jet. *J Fluid Mech* 98 pp 1.

Andrade E N da C (1939). The velocity distribution in a liquid-to-liquid jet. Part 2. The plane jet. *Proc Phys Soc* 51 pp 784.

Beavers G S and Wilson T A (1970). Vortex growth in jets. *J Fluid Mech* 44 pp 97.

Brown G B (1935). On vortex motion in gaseous jets and the origin of the sensitivity to sound. *Proc Phys Soc* 47 pp 703.

Crow S C and Champagne F H (1971). Orderly structure in jet turbulence. *J Fluid Mech* 48 pp 547.

Gutmark E and Ho C-M (1983). Preferred modes and the spreading rates of jets. *Phys Fluids* 26 pp 2932.

Ho C-M and Huang L-S (1982). Subharmonics and vortex merging in mixing layers. *J Fluid Mech* 119 pp 443.

Ho C-M and Huerre P (1984). Perturbed free shear layers. *Ann Rev Fluid Mech* 16 pp 365.

Huerre P and Monkewitz P A (1985). Absolute and convective instabilities in free shear layers. *J Fluid Mech* 159 pp 151.

Ipsen D C (1960). *Units, Dimensions and Dimensionless Numbers* (New York: Mc Graw Hill).

Kelly R E (1967). On the stability of an inviscid shear layer which is both periodic in space and time. *J Fluid Mech* 27 pp 657.

Kibens V (1980). Discrete noise spectrum generated by an acoustically excited jet. *AIAA J* 18 pp 434.

Lamb L (1932). *Hydrodynamics* (New York: Dover).

Laufer J and Zhang J Q (1983). Unsteady aspects of low Mach number jets. *Phys Fluids* 26 pp 1740.

Miksad R W (1972). Experiments on the nonlinear stages of free-shear-layer transition. *J Fluid Mech* 56 pp 695.

Moore C J (1977). The role of shear layer instability waves in jet exhaust noise. *J Fluid Mech* 80 pp 321.

Nayfeh A H and Mook D T (1979). *Nonlinear Oscillations* (New York: Wiley).

Oster D and Wygnanski I (1982). The forced mixing layer between parallel streams. *J Fluid Mech* 123 pp 91.

Peterson R A (1978). Influence of wave propagation on vortex pairing in a jet. *J Fluid Mech* 89 pp 469.

Sato H (1960). The stability and transition of a two-dimensional jet. *J Fluid Mech* 7 pp 19.

Womersley J R (1955). Method for the calculation of velocity, rate of flow and viscous drag in arteries when the pressure gradient is known. *J Physiol* 127 pp 553.

Womersley J R (1957). An elastic tube theory of pulse transmission and oscillatory flow in mammalian arteries. *WADC Techn Rep TR* 56-614.

CHAPTER III

POSTSTENOTIC FLOW EXPERIMENTS

PART A – METHODS

Summary

Steady and pulsatile poststenotic flows are subjected to low-level periodic flow excitation. Corresponding to poststenotic oscillatory flow disturbances that are larger in pulsatile flow than what is predicted by quasi-steady analysis, the separated shear layer is found to be less susceptible to perturbations under pulsatile flow conditions. In steady flow, on the other hand, complete flow synchronisation, characterised by a suppression of broadband fluctuations, is possible.

Starting and stopping flow experiments prove useful for interpreting pulsatile flow phenomena and flow visualisations indicate the presence in pulsatile flow of a vortex wave, thought to be due to a low Reynolds number instability.

1. "Pulsatile Laminar Flow at Intermediate Reynolds Numbers"

Thus blood flow in the large arteries is described within the framework of classical fluid mechanics (Young 1979). The model experiments described here may be summarised as the investigation of steady and pulsatile flow of a Newtonian fluid in a rigid locally constricted tube. The assumptions entailed by this approach to the study of arterial stenotic flow are discussed below.

Interestingly, it was the rigid pipe model of arterial blood flow that stimulated the mathematical treatment of important laminar flows *viz.* steady flow in a circular tube by the physician Poiseuille (1840), and oscillatory flow by, amongst others, Womersley (1955).

1.1 Configurational Characteristics

The study described here concerns fluid flow in a rigid straight tube of circular cross section with a geometrically well defined local constriction. The implications of these restrictions are evident. We exclude, in the order of the above specifications, wall distensibility, secondary flow phenomena, more general cross sectional geometries and non-localised constrictions of non-simple shape.

How are these boundary conditions rationalised? In general, arterial walls exhibit nonlinear viscoelastic behaviour that is further complicated by anisotropy and inhomogeneities. Additionally, arterial wall properties change with age. The wall becomes thicker and less distensible due to degenerative histological changes. Yet these properties are less important in determining fluid motion. They are important for the propagation of pressure waves[1]. The net effect of distensibility on actual wall movement throughout a cardiac cycle is considered to be of the order of about $\pm$ 2% in arterial diameter or, in cross sectional area, $\pm$4% (Lighthill 1972).

Pipe curvature produces secondary flow velocities at right angles to the streamlines of a primary flow. For example, given a fully developed laminar flow at the entry of a curved tube, transverse secondary fluid motion is set up immediately by the action of centrifugal forces as a result of the curvature. The greatest axial velocities occur near the outside wall. In contrast, if fluid enters a curved tube from rest, velocities will be greatest near the inside wall and secondary motion will not become important until a long way downstream when the flow approaches its fully developed form.

Curvature affects both wall shear stress and flow transition. It is obvious that wall shear stress is greater at the outside wall for fully developed flow. Somewhat unexpectedly, the same behaviour also applies to entry flow. Within about one tube diameter the initial shear stress distribution — greater at the inside of the tube — is reversed, effected by the thin boundary layer on the walls near the entrance. According to Lighthill (1975), pipe curvature suppresses flow transition, increasing the critical Reynolds number from about 2000 to 6000. Among the large blood vessels secondary flow phenomena are most prominent in the ascending aorta and, of course, in branched arteries.

The cross sectional shape of a blood vessel is ideally circular but depends on the magnitude of compressive circumferential stresses. Collapse of a vessel is resisted by the effects of stretching, tethering and the thickness of the walls. Some veins and pulmonary arteries normally have elliptic cross sections, indicating a degree of collapse associated with the compressive stress in their walls However, this is not known for the larger (non-pathologic) arteries.

Atherosclerotic lesions can have geometrically ill-defined shape but studies seem to indicate that most uncomplicated lesions are mainly eccentric or non-axisymmetric intimal

---

[1]This view (Caro *et al* (1978)) has been contested by Doo *et al* (1984) on the basis of preliminary findings. They noted differences in flow distribution of up to 4.9% between rigid wall tubes and distensible tubes of appropriate elasiticity.

deposits with concave lesion surfaces and circular or oval lumen transverse cross section (Glagov and Zarins 1983). The transition between arterial wall and the lesion is gradual and the lesion edge is wedge-shaped. Atherosclerotic lesions are typically localised in longitudinal extent, but multiple arterial stenoses are not uncommon (Vonruden *et al* 1964).

1.2 Flow Conditions

In the experimental flow facility, industrial water is used as the flow medium and steady and oscillatory (sinusoidal) flow components are adjusted independently. The Reynolds number, based on flow rate throughout this study, and the frequency parameter are adjustable from 200 to 2000 and from 7 to 30, respectively.

Whole blood, however, is not readily equated with a Newtonian fluid. Blood is a suspension of some 40% to 50% by volume in the blood plasma of deformable bodies *viz.* erythrocytes, leucocytes and thrombocytes. By far the most numerous are erythrocytes of diameter about 8 μm and they completely dominate the mechanical properties of blood. Whilst the blood plasma can be regarded as a homogenous Newtonian fluid this is true for whole blood only under certain circumstances. In blood vessels of diameter greater than about 100 μm, the scale of the micro-structures is much smaller than that of the flow and blood becomes homogeneous on the larger scale. Typically, whole blood exhibits Newtonian behaviour at low shear rates. However, at the higher shear rates commonly found in the larger arteries (above approximately 1 mm in diameter), the effective viscosity of blood is largely independent of shear rate.

The physiological range of the Reynolds number is from a few hundred to several thousand and the frequency parameter is between 1 and 20, respectively (Lighthill 1972). To give an example, in the human carotid artery the mean Reynolds number is about 380 with a maximum of 830 to 1200 and a frequency parameter[2] around 10 (Balasubramanian 1983).

2. The Experimental Flow Facility

The experimental flow rig used in this study is sketched in *figure* 3.1. This set-up allows flow visualisation and the non-intrusive measurement with a laser Doppler velocimeter of local flow velocities in steady or pulsatile flow around model stenoses under controlled flow conditions.

[2]It is tacitly assumed that the relevant time scale is given by the period of the heart beat. The effective frequency parameter is possibly higher due to the fast systolic rise of the arterial waveform, followed by sustained forward flow.

2.1 Extraneous Factors

The susceptibility study of poststenotic shear layer instabilities is partly stimulated by observations of great flow sensitivity to ambient background vibrations, made during initial experimentation with the flow rig. It therefore proved advantageous for the flow facility to be set up in a basement hydraulics laboratory where the influence of environmental disturbances can be kept to a minimum. Movement about the laboratory itself, or in neighbouring laboratories, has no discernible effect on the flow. However, as indicated above, structural vibrations induced by wind-tunnel turbine machinery on another floor do influence the flow evolution and measurements are carefully avoided during wind-tunnel operation. Fluctuations in room temperature are small. The water temperature is found to vary between 16^0C and 17^0C over the course of experiments, resulting in a 2.4% variability of the Reynolds number.

2.2 Description of Experimental Apparatus

The experimental flow rig (*figure* 3.1) provides gravity driven water flow supplied by a constant head reservoir of capacity 170 litres. All major components of the flow facility are made of transparent material to avoid the uncontrolled formation of air pockets in the flow system. The use of industrial water ensures operation of the flow system for a continuous number of days without the development of algae.

The fluid enters the upstream pipe of inner diameter D=2.54 cm and length 66 D through a smoothly converging nozzle that was originally designed for starting/stopping flow experiments (Parker 1977). Flow measurements are carried out in a perspex[3] test section of dimensions 70 x 70 x 30 mm. The fluid leaves through a downstream pipe which branches after 44 D. One branch is connected to a pair of rotameter type flowmeters (Q_1=0.2–2 l min^{-1}, stainless steel float; Q_2=1–10 l min^{-1}, korannite float) with flow control valves. The two meters provide low accuracy flow rate measurements. The other branch is attached to a piston-cylinder combination that is driven by a scotch-yoke mechanism. This oscillatory flow generator is driven by a variable-speed drive and produces highly sinusoidal oscillatory flow of variable peak flow rate and oscillation period. Note that the oscillatory flow generator is mounted directly to the downstream pipe. Vibrations induced in the test section by the motor drive, however, are largely absorbed by the strong aluminium support. Also, the typical frequency of vibration is greater by orders of magnitude than the natural flow instabilities. The fluid is fed back to a recollection tank from which the water is pumped by a centrifugal pump

[3] polymethylmethacrylate, refraction index n=1.49.

into a separate chamber of the constant head reservoir to avoid spurious fluid motion in the upper tank.

2.3 Flow Excitation

Controlled planar flow surging is generated by means of a solenoid valve connected in parallel to the two main flow control valves. The flow rate through the solenoid valve (maximum flow rate Q_{max}=0.76 l min^{-1}) is controlled by a serially connected flow control valve. Very low levels of flow excitation are produced at zero net flow rate solely by the open/shut mechanism of the solenoid valve, with the control valve shut. The solenoid valve responds accurately to frequencies up to about 11 Hz, above which inertial effects become noticeable.

3. The Test Section

The test section comprises a perspex block that allows flow measurements and visualisation up to approximately 6 D on either side of an exchangeable constriction. Four variants of the test section are employed here : (1) a straight tube section for determining LDV accuracy and for calibration of the flow meters; (2) a second straight section with a pressure transducer mounted flush to the inside wall; (3) a test section with exchangeable orifice plates, and (4) a test section for stenosis models of streamwise length 2 D.

3.1 Model Stenosis Geometry

Three different stenosis types are employed in this study with standard geometries that have been widely used in similar experiments. The sharp edged orifice plate (Cox 1977, Cassanova and Giddens 1978, Djilali 1978, Yongchareon and Young 1979, Bernardinis *et al* 1981) provides a fixed locus of flow separation and can thus be thought of as a reference with regard to separated flow instabilities for the contoured stenosis models.

A geometry considered to be physiologically more relevant is given by the contoured symmetric shape (Lee and Fung 1970, Young and Tsai 1973, Yongchareon and Young 1979, Giddens and co-workers)

$$r/D = 1 - \frac{\delta}{2}\left[1 + \cos(2\pi x/X_0)\right], \qquad |x| \leq X_0/2 \tag{3.1}$$

with longitudinal extent X_0 and $(1-\delta^2)$% area constriction. Its cross-sectional 'lumen' is circular and the transition from the tube walls is smooth.

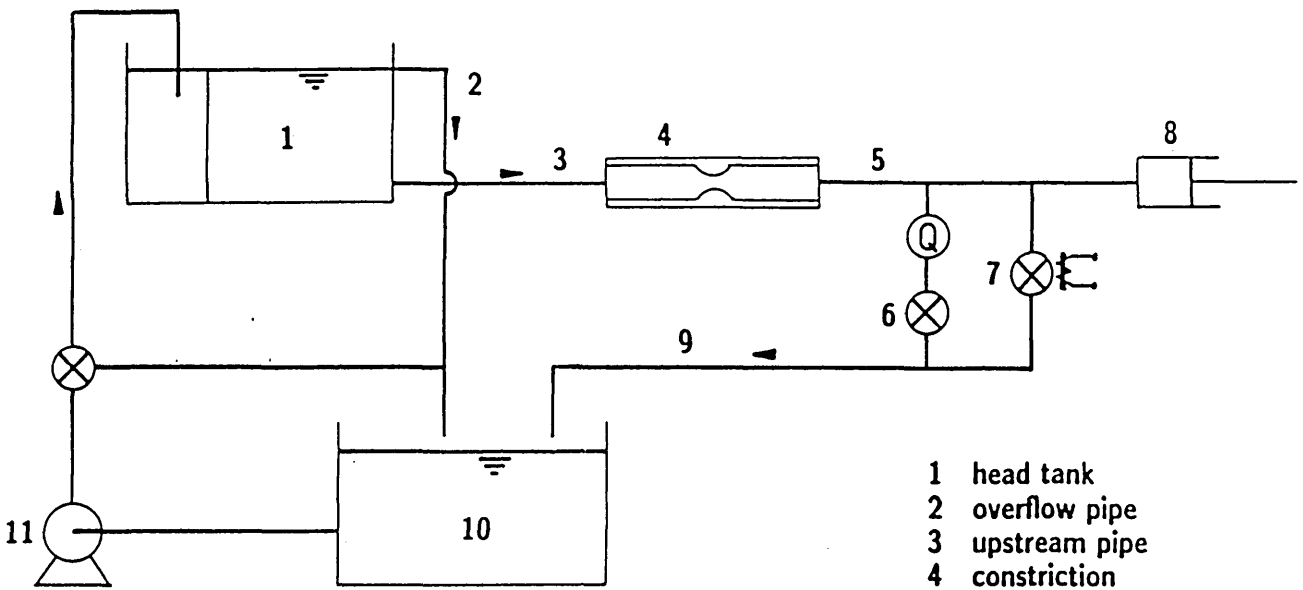

Figure 3.1 Schematic of the experimental apparatus. Flow velocities are measured in the test section [4] with a laser Doppler velocimeter.

The third stenosis model represents possible eccentricity of atherosclerotic lesions and is formed by an isolated protuberance from one wall (Young and Tsai 1973, Mates *et al* 1978). The geometry of this nonsymmetric stenosis is described by a cylindrical section inserted transversely into the circular tube.

A representative area reduction of 50% for all three stenosis geometries is chosen for our investigation, a value that separates haemodynamically mild stenoses from the more severe stenoses. Preliminary experiments with models of 75% area reduction showed that flow disturbances, related to the separated shear layer instability, were much more developed whereas for area reductions less than 50% the contoured symmetric stenosis produced only minimal flow disturbances. This is in agreement with observations made by Cassanova and Giddens (1978). Also, a minimal area reduction is required for simple practical reasons. Velocity measurements and flow visualisations in our experiments are only possible in a region extending six diameters downstream.

The longitudinal extent for this investigation, $X_0=2D$, is a widely used value, although studies with $4D$ sized stenosis models exist. With regard to characteristic hydrodynamic factors, including pressure drop, separation and turbulence, X_0 appears to play a subordinate role as compared to the area reduction (Young and Tsai 1973), which is why the latter parameter is the commonly used stenosis-specifying geometric characteristic.

4. Instrumentation

Local and global flow field properties of stenotic flows are determined in this study by non-intrusive optical techniques. In both laser Doppler velocimetry (LDV) and particle image velocimetry (PIV), light is used as an information carrier whereby information is impressed on a light beam by the flow. The flow is visualised by micro-particles whose motion is assumed representative of the flow. The light scattered by the illuminated particles – the scattering angles are 0° and 180° for LDV and 90° for PIV – is collected by an optical receiving unit and processed for flow velocity calculation. The requirements for successful application of the two techniques are readily apparent from this outline : (1) a known relationship between particle motion and flow velocity; (2) sufficient flow seeding; (3) matching of light source intensity and particle scattering properties; and (4) a low-noise optical receiver. If these conditions are not properly met, flow measurements can be seriously impaired. Some of the problems typically encountered are discussed below.

4.1 Laser Doppler Velocimetry (LDV)

4.1.1 Outline of LDV Theory and Practice

Laser Doppler velocimetry is a flow visualisation technique for the non-intrusive measurement of the local, instantaneous velocity of tracer particles suspended in a liquid or gaseous flow. The formation of an interference pattern allows the determination of particle velocity by measuring the transit time of the particle across a number of interference fringes with known spacing. Since it is the particle velocity that is measured, the relationship between the particle and fluid velocity must be known if the fluid velocity is to be evaluated.

A basic laser Doppler velocimeter comprises several optical and signal processing components and is shown schematically in *figure* 3.2. Independent of the particular arrangement (dual-beam, reference beam, two-scattered beam), the crossing of two coherent light beams gives rise to an interference pattern. Part of the volume of interference is observed by a light collecting system and imaged on a photodetector. The photodetector current is then processed by an appropriate signal-processing arrangement.

A number of features of laser Doppler signals is analysed both qualitatively and quantitatively on the basis of an 'interference fringe' model proposed by Rudd (1969). For a differential or dual-beam Doppler system the measuring volume can be visualised as a set of fringe planes occupying an ellipsoidal volume at the beam intersection point. The Doppler signal is explained as the superposition of the scattered light intensity distribution from randomly arriving particles.

Two practical problems are readily identified by this analysis. First, the signal quality, or 'fringe visibility', depends strongly on the particle size[4]. Secondly, the more or less random distribution of particles in the flow results in the 'transit-time broadening' of the Doppler spectrum.

For an in-depth account of the theory and practice of laser Doppler velocimetry the reader is referred to the monographs by Durst *et al* (1976) and Durrani and Greated (1977).

4.1.2 Measurement Accuracy

In this study an LDV system operating in dual-beam forward scattering mode is employed. The system comprises a 5 mW He-Ne laser (Model Spectra Physics 120, safety class 3A) of wavelength 623.8 nm, a 50 mm beam splitter (Model TSI 915), a Bragg cell for acousto-

[4]Fringe visibility at the same time exposes the limitations of the fringe model. The fringe model predicts that velocity measurements cannot be carried out for large particles. This is in disagreement with experimental findings. Rudd's model is physically incomplete because the scattering process itself is not accounted for.

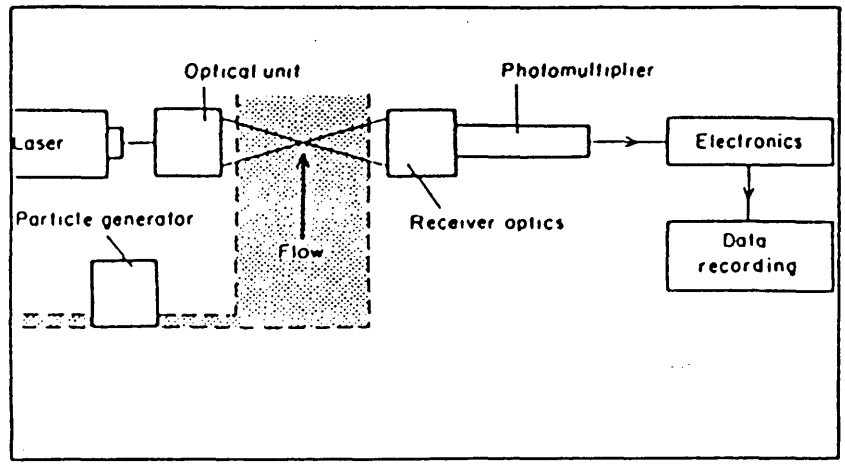

Figure 3.2 Basic components of a laser Doppler velocimeter (after Durst *et al* 1976).

optical frequency shifting, a transmitter-receiver set of lenses of 104 mm focal length and a photomultiplier of aperture size 0.254 mm (which had been found experimentally to yield the best signal-to-noise ratio). The complete optical set-up rests on a heavy table with traversing facilities in the three major axis. The positioning accuracy of the table is $\pm 100\mu$m. The photodetector current is demodulated with a Model TSI 1090 frequency tracker. Industrial water is used as the flow medium, with no artificial scattering particles added.

The tracker operates at an average tracking rate of 50 %. This somewhat low figure is connected to the large amount of optical noise, characteristic of the experimental set-up *i.e.* small measuring volume and a low-power light source. The tracking performance is not improved considerably by artificially seeding the flow, for example by adding homogenised milk (George and Lumley 1973) but indicates that the LDV system is operating in the many particle range ('continuous LDV'), an assumption we shall make in a theoretical analysis of tracking properties (*cf* § 8).

In view of the problematic tracking performance it was decided that the influence of the tracking process on the accuracy of local flow velocity measurements should be investigated in some detail. The results of that investigation are given in the Appendix (§ 8). Below, the findings are summarised.

4.1.2.1 Summary and Implications

Confronted with experimental circumstances that may lead to a low tracking performance of the LDV frequency tracker, the frequency-tracking study was undertaken with the purpose of assessing the quality of LDV measurements of local flow velocity in the presence of tracking noise.

Employing a simple Poisson process description of the transitions between lock and unlock, two readily available parameters of tracking performance, tracking rate λ and unlock frequency ν, were used to quantify effects of dropouts on velocity measurements, thereby offering a simple tool of assessing the significance of 'dropout noise' to be expected in specific cases. It was shown that the unlock frequency is of crucial importance in determining the degree of signal corruption by intermittent loss of tracking.

Transit time noise measurements were then evaluated by means of a simulation and an estimate for the scattering volume was obtained. The dimensions are approximately 0.08mm in streamwise direction, and 0.36mm in cross-stream direction. Moreover, the two parameters λ and ν were found to be a convenient means of determining the overall velocity-signal bandwidth.

As a consequence, the unlock frequency is monitored in the LDV experiments described below, and non-interference with the spectral bandwidth of those velocity fluctuations that are of interest in this study, is ensured. LDV measurements in pulsatile flow typically result in an even lower tracking rate, $\lambda=0.45$, but present no additional accuracy problems.

4.2 Particle Image Velocimetry (PIV)

PIV allows the quantitative determination of an instantaneous velocity field over a complete plane of interest in a flow. Flow velocities are measured by the double (or multiple) exposure recording of patterns of scattered light radiation from micro-particles suspended in the flow. For PIV the light source need not be coherent so that the particle photography reduces to the usual multi-exposure technique of flow visualisation. The main difference to the flow visualisation lies in the use of Young's fringes obtained by illuminating sections of the multi-exposure photographic slides with a coherent plane wave *e.g.* an unexpanded He-Ne laser beam. In the back focal plane of a converging lens placed behind the slide, Young's fringes appear whose spacing and orientation is a measure of local flow motion in the illuminated section. It is the analysis of the fringe patterns that has been automated (Meynart 1983, Gray and Greated 1987), but a preliminary study (Thiriet *et al* 1988) showed that the complete analysis of the specklegram may be accurately carried out by image processing techniques.

The advantages and shortcomings related to PIV are those typical of flow visualisation techniques. The main advantage is that flow field information of an entire plane of interest is measured instantaneously. This contrasts with a plethora of outstanding problems *viz.* the need for an appropriate light source for flow illumination, adequate flow seeding, fast and high-resolution recording material and, importantly, directional ambiguities of the recorded flow field. In analogy to LDV, it has been suggested to resolve this ambiguity by subjecting the recording material to a defined (translational) movement between successive exposures (Adrian 1986).

4.2.1 Experimental Apparatus

Originally designed for flow velocity measurements with the hydrogen bubble technique (Djilali 1978), the test section is readily adapted to PIV. The light source is a 35mW He-Ne laser (safety class 3B – potentially hazardous) whose unexpanded beam is directed at a rotating hexagonal mirror, driven by a high-precision dc motor. The reflected beam describes a plane illuminating the horizontal centre plane downstream of the constriction over the first few diameters. This has the advantage over beam expansion techniques with a cylindrical lens that

the light intensity necessary for illuminating micro-particles is preserved without the need for an extra light pulsing mechanism. Particles are continuously supplied to the upstream reservoir near the nozzle exit, carefully avoiding any disturbances of the exit flow. Soluble starch (estimated particle size 5 to 50 μm) is used for flow seeding in the flow visualisation experiments reported below, but experimentation with other seeding material showed that acrylic beads (ICI) of average diameter 50 μm and density 1.18 g $cm^{-3}$are equally well suited. The scattered light – note that the scattering angle is 90^0 which explains the requirement for a high intensity light source – is recorded on high resolution photographic film (ASA 400, uprated to ASA 1000) with a Minolta X700, f=2.8, 105 mm focus.

PART B – RESULTS

5. Results

5.1 Flow Conditions Near the Test Section

In order to establish the pertinent flow conditions and calibrate the flow meters and the oscillatory flow generator setting, measurements of axial flow velocity profiles for steady and pulsatile flow as well as pressure measurements are carried out 5 D upstream of the constriction.

5.1.1 Steady Flow

Axial flow velocity profiles in the centre plane are determined for a range of flow rates. The centre plane is traversed in steps of 1 mm. Conveniently, the LDV system need not be realigned during a radial traverse, $r \in [0, D/2]$. Near-wall velocity measurements tend to be very noisy and are found to be reliable only for wall distances greater than about 1 mm. Velocity profiles are found to be near-parabolic for Reynolds numbers from 940 to 1910, with a maximum absolute error of 11.2%. This is reasonable in view of an entrance length of x/D=60 for a value of Re=2000. Flow rates are calculated from the velocity profiles and used to calibrate the rotameters.

5.1.2 Pulsatile Flow

In laminar pulsatile flow the velocity profile is time dependent and not described by a parabolic law because inertial effects cause phase variations along the radius. Theoretical

profiles for pulsatile flow in a straight rigid tube have been derived by a number of workers (Witzig 1914, Sexl 1930, Lambossy 1952, Womersley 1955, Uchida 1956). In bio-fluid dynamics, probably the most well known derivation is due to Womersley. His results are summarised here.

5.1.2.1 Theory

Consider a circular rigid pipe of length l and radius R, filled with a viscous incompressible liquid of densitiy ρ and viscosity μ. The liquid is driven by a pulsating pressure gradient

$$\frac{p_1-p_2}{l} = A_0 + A_1\cos(\omega t) \tag{3.2}$$

The longitudinal velocity $u(r,t)$ at distance r from the pipe axis is then found by superposing the Poiseuille solution for steady flow

$$u_0(r,t) = \frac{A_0}{4\mu}(R^2-r^2) \tag{3.3}$$

and the solution for oscillatory flow with frequency parameter, or Womersley number, $\alpha = R\sqrt{\frac{\omega}{\nu}}$,

$$u_1(r,t) = \frac{A_1 R^2}{\mu\alpha^2} M_0{}'(r/R)\,\sin(\omega t+\epsilon_0(r/R)) , \tag{3.4}$$

where functions M'_0 and ϵ_0 are related to the Bessel function of order zero and complex argument $J_0(\alpha x\, e^{j3/4\pi}) = M_0(x)\, e^{j\theta_0(x)}$ through

$$\begin{aligned} M'_0(x) &= \sqrt{1+h_0(x)^2-2h_0(x)\,\cos\delta_0(x)} \\ \tan\epsilon_0(x) &= \frac{h_0(x)\,\sin\delta_0(x)}{1-h_0(x)\,\cos\delta_0(x)} \end{aligned} \tag{3.5}$$

where $h_0(x) = M_0(x)/M_0(1)$ and $\delta_0(x) = \theta_0(1)-\theta_0(x)$. Since the governing equation for oscillatory flow is linear, the solution contains no higher harmonic terms. The velocity $u_1(r,t)$ follows the pressure gradient with a given phase lag and amplitude distribution. Note that in equation (3.4) the phase and amplitude are functions of the frequency parameter only.

5.1.2.2 Practice

The oscillatory flow generator is set to operate at an intermediate frequency parameter, $\alpha=10$, and the steady and oscillatory flow rates are chosen so as to minimise the difference between the measured velocity profile and the theoretically predicted one. *Figure* 3.3*a* shows the temporal evolution of experimentally determined axial flow velocities over one flow cycle. The pulsatile flow is very close to what is predicted by theory (*figure* 3.3*b*). The parameters A_0 and A_1 of the theoretical profile are optimised with respect to the measured profile. The absolute error has an average value of 0.29 cm s^{-1} and a peak value of 1.1 cm s^{-1} which occurs near the wall for flow reversal. Flow rates are calculated from the experimental results for calibration purposes.

5.1.3 Flow Excitation

At the smaller forcing amplitudes, the induced periodic veocity fluctuations are buried in the LDV system noise and cannot be detected. Determination of specific excitation levels therefore requires measurements with a high sensitivity differential pressure transducer (0−75mbar, PDCR 42, Druck Leicester UK). Simultaneous measurements of pressure and velocity at higher forcing amplitudes may then be used to extrapolate values for the small-amplitude range. The rms pressure−velocity relationship near the LDV noise level is shown in *figure* 3.4*a*. The functional dependence is approximately linear, in agreement with the linearised Bernoulli equation. The lowest rms forcing level − at zero net flow rate −, employed in the steady flow experiments, is established to be $u'_{p,rms}=0.042$ cm/s. Note that this value is for an unobstructed tube and needs to be corrected to represent perturbation velocities in the throat of the constriction. In pulsatile flow, higher amplitudes are required to influence the poststenotic flow appreciably. These perturbations can be measured directly.

By the same method, the spectral content of the excitation is determined. The result for zero net flow is given in *figure* 3.4*b*. The response of the solenoid valve is highest for frequencies near 2 Hz. The 3dB bandwidth is approximately 11 Hz, sufficient to cover the range of dominant flow instabilities. At the lower forcing frequencies, the excitation is rich in harmonics, but becomes more sinusoidal toward higher values.

5.2 Flow Around Model Stenoses

Having established the appropriate flow conditions, we now proceed to the results of a comprehensive investigation of the susceptibility to periodic excitation of steady and pulsatile poststenotic flows. The bulk of this analysis is carried out using the laser Doppler velocimeter

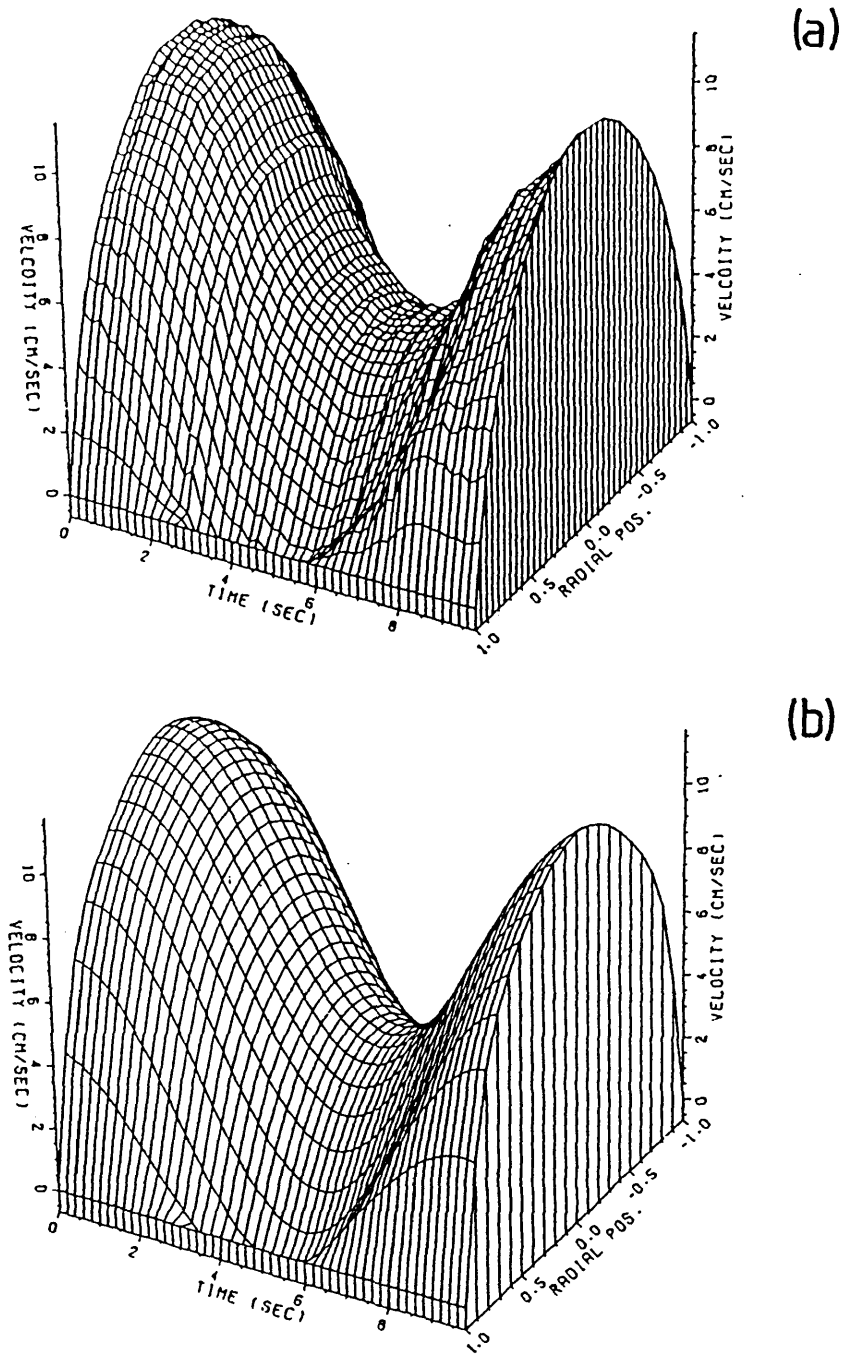

Figure 3.3 Comparison between (*a*) pulsatile flow velocities measured in the experimental flow system, and (*b*) Womersley's (1955) solution for fully developed laminar flow. The average error is 0.29 cm s^{-1}. The largest error, 1.1 cm s^{-1}, occurs near the wall during flow reversal.

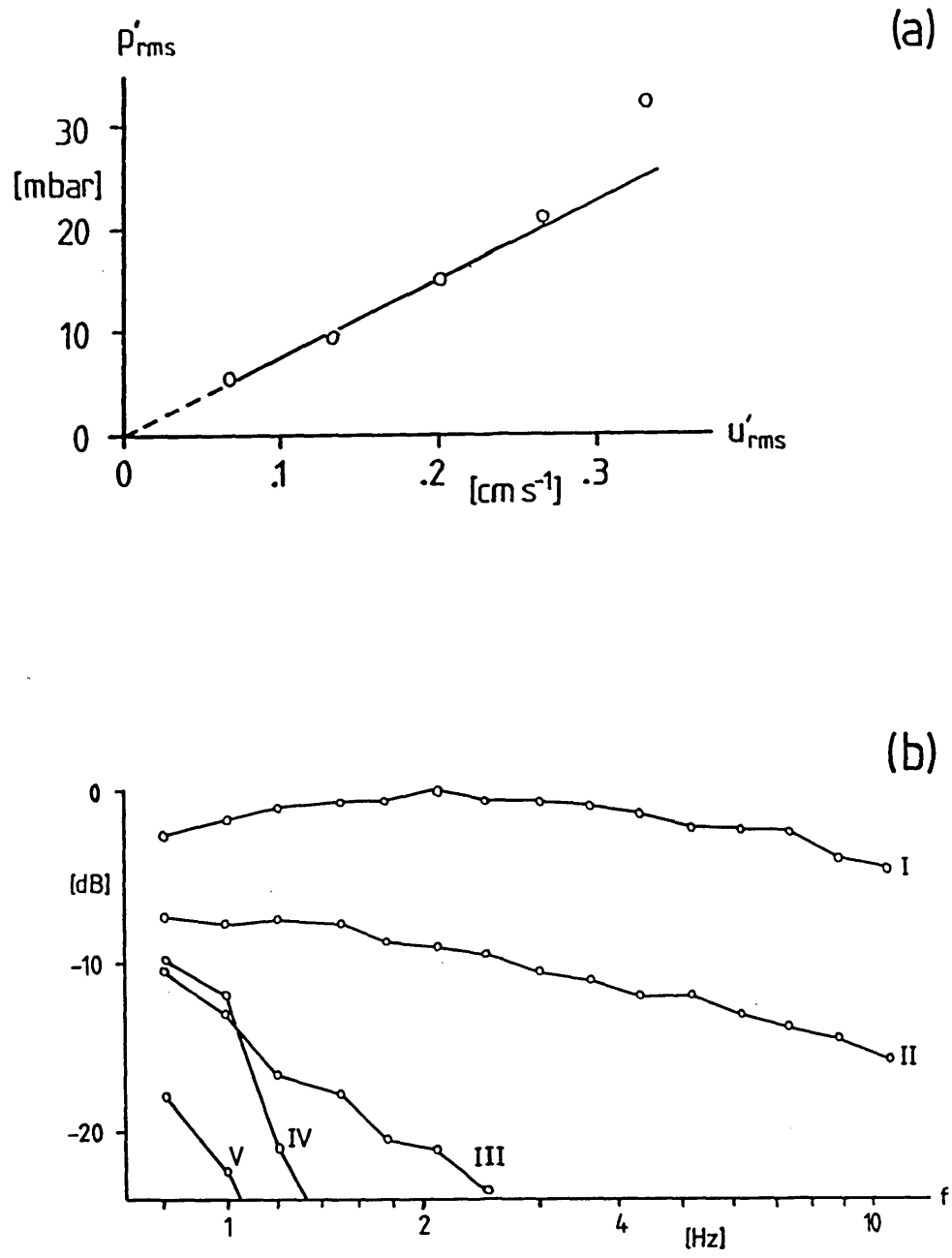

Figure 3.4 Characteristics of low-level flow excitation (at zero net flow through the solenoid valve). (*a*) The excitation amplitude is calculated from the experimentally determined rms pressure—velocity relationship by linear extrapolation. The LDV noise level is approximately 0.07 cm s^{-1}. (*b*) Variation of the harmonic content of the flow excitation with forcing frequency (I — fundamental, II — 2nd harmonic, III — 3rd harmonic, IV — 4th harmonic, V — 5th harmonic).

but some flow visualisation results of unforced steady and pulsatile flow are given here as well. The visualisations indicate the existence of flow phenomena that are not necessarily related to the primary separated shear layer instability around which the flow forcing exercise centres.

5.2.1 LDV Measurements

The point measurements of axial flow velocities downstream of three different stenosis geometries indicate that flow disturbances can be considerably greater in pulsatile flow than what is predicted by assuming quasi-steadiness. This finding is thought to be related to transient vortex structures observed in flows started from rest, and has important implications for the susceptibility of poststenotic shear layer instabilities.

5.2.1.1 Steady Flow – Without Forcing

5.2.1.1.1 Signal Analysis

Following conventional practice, the Eulerian local flow velocity $u(\underline{s},t)$ is decomposed into its time average

$$U_0 = \frac{1}{T}\int_0^T u(\underline{s},t)\,\mathrm{d}t \tag{3.6}$$

and its residual $u'(\underline{s},t) = u(\underline{s},t) - U_0$. Of the residual we shall require the additional quantity, the root-mean-square value

$$u'_{rms}(\underline{s}) = \frac{1}{T}\Big(\int_0^T [u'(\underline{s},t)]^2\,\mathrm{d}t\Big)^{1/2} \tag{3.7}$$

Power spectral estimates for $u'(\underline{s}_0,t)$ at measuring location $\underline{s}_0$ are obtained from averaged periodograms (Oppenheim and Schafer 1975). The periodograms are calculated using a 4-term Blackman-Harris window (Harris 1978) which gives spectral estimates with greatly suppressed side lobe levels (-72 dB), thus increasing spectral resolution.

5.2.1.1.2 Results

Axial flow velocity measurements are taken downstream of the model stenoses over distances, limited by the test section geometry, from 1 D (for the orifice plate) and 1.5 D (for the spatially extended stenoses) to 5 D at four different flow rates, Re=940, 1260, 1590 and 1910. Flow velocities are typically measured at the centre line[5], with the exception of the nonsymmetric constriction for which radial velocity profiles are determined. This will prove

useful in explaining anomalies of the axial profile of centreline velocities for the nonsymmetric constriction (*figure* 3.5). In that figure, axial profiles of the mean axial velocity on the centre line and of the rms axial fluctuations are given for the three stenosis geometries with Reynolds number as parameter. The noise level of the LDV measurements is around 0.07 cm s^{-1}, indicated by the hatched regions in the rms graphs. For the orifice plate, as for the contoured stenosis, the mean velocities decrease monotonically with distance from the throat section suggesting that the *vena contracta* region is either located further upstream or, because of the mild constrictions, not observable. The peaking of the U_0 profiles for the nonsymmetric constriction does not indicate *vena contracta* flow, but rather points to the flow asymmetry (*figure* 3.6).

Regarding the flow disturbances u', several phenomena are noted. Again, for the orifice plate, at low flow rates (I and II) the fluctuations grow monotonically (nearly linearly or faster) with downstream distance. At higher flow rates, however, the spatial growth rate decreases either because nonlinear effects come into play or because of wall interference. Compared with the orifice plate, the flow behind the smooth constriction evolves on much longer length scales. The average velocity decreases gradually and no saturation occurs up to $x/D=5$. In fact, measurements at flow rate I and II are of limited interest because the flow disturbances are buried in measurement noise over the first few diameters. Obviously, results for the nonsymmetric flow constriction must be treated with some caution. This not only applies to the mean velocity but to variations in rms levels as well. Higher fluctuation amplitudes may simply signify a change in the distance of the measurement volume from the shear layer region. For instance, the distance from the location of steepest velocity gradient increases with downstream distance (*figure* 3.6).

The flow disturbances are fairly narrowband in character, and exemplary waveforms are shown in *figure* 3.7. Average frequencies for these recordings are readily obtained from the power spectral estimates and are summarised in *figure* 3.8. The frequencies for all three stenosis geometries are non-dimensionalised by a representative constriction diameter $d=D/\sqrt{2}$ and the peak axial velocity downstream of the constriction. The Strouhal number for the orifice plate is seen to be relatively independent of flow rate, and is well within the range of the preferred mode Strouhal number of free axisymmetric jets. This suggests that wall effects play only a minor role. The Strouhal number scaling for the contoured symmetric constriction is less

[5] With regard to the optimal recording position for identifying vortical structures in jet like flows, axial centre line measurements are certainly not the most representative. Acton (1980) found that the radial velocity component measured inside the jet shear layer represented vortical structures most truthfully.

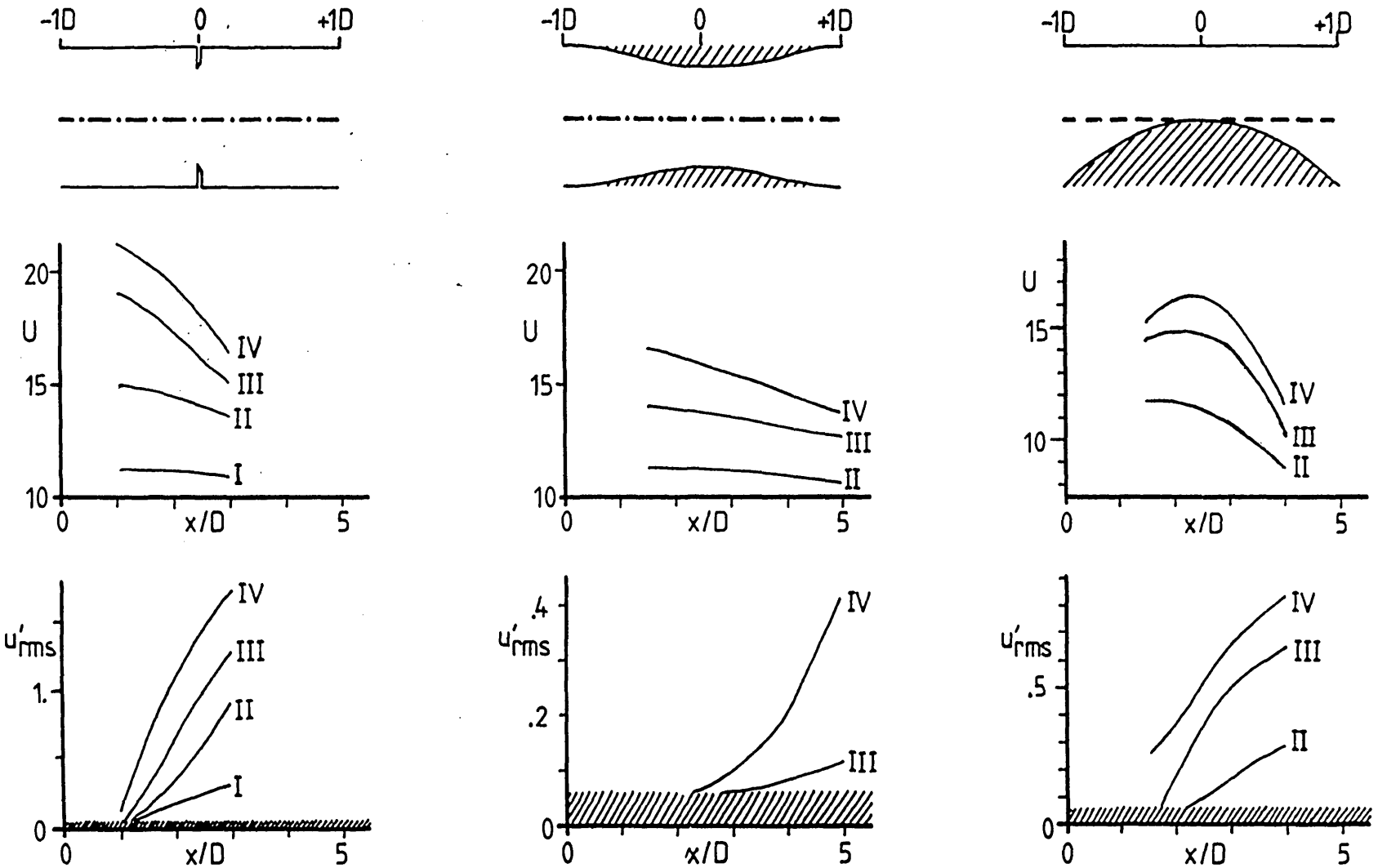

Figure 3.5 Axial profiles of the mean centreline axial velocity $U(x)$ and the rms centreline axial velocity fluctuations u'_{rms} (all values in [cm s^{-1}]), for Reynolds numbers (I) Re=940, (II) Re=1260, (III) Re=1590 and (IV) Re=1910.

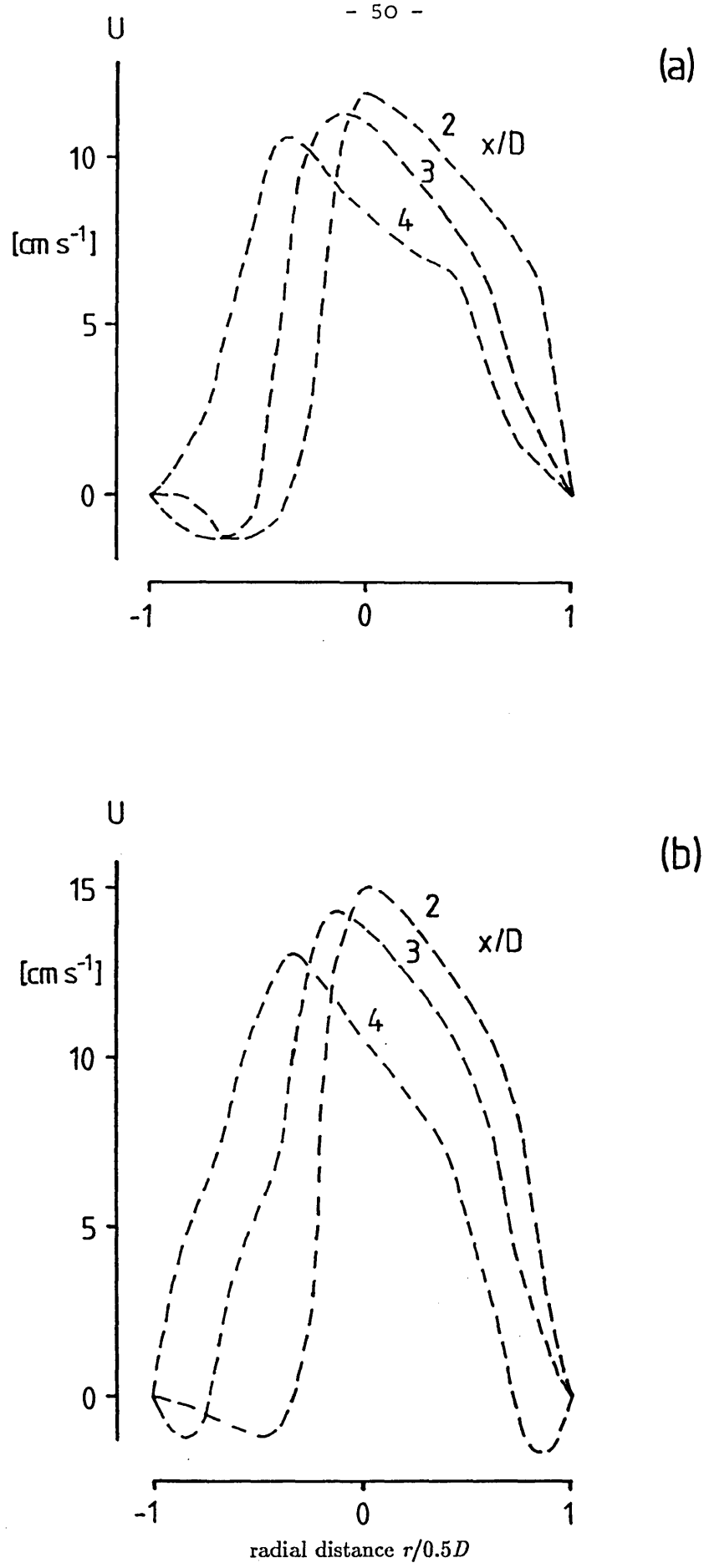

Figure 3.6 Downstream evolution of the axial velocity behind the non-symmetric model stenosis, in the plane of symmetry. (*a*) $Re=1260$. (*b*) $Re=1590$.

convincing, although St is of comparable magnitude, and is obviously related to the quite different flow separation. The Strouhal number for the nonsymmetric constriction agrees reasonably well with the corresponding values of the orifice plate. The similarity with the orifice plate is somewhat unexpected, for the flow conditions are hardly comparable. However, forced flow experiments support the similarity between the two flows.

The spatial evolution of disturbance spectra shows an increased broadening, but no significant change in average frequency (*figure* 3.9). Instead, with growing downstream distance the definition of an average frequency becomes less meaningful as the spectrum approaches a broadband 'noise' spectrum. This is evident for the orifice plate even at flow rate I, but the broadening is more obvious at higher flow rates. Similar observations are made for the nonsymmetric constriction, whereas the downstream evolution of the flow through the contoured constriction is rather more gradual, and the break up of vortex structures — if it occurs at all — takes place well outside the test section.

The flat portion of these spectra in the higher frequency range represents the measurement noise, and is not related to the analogue-to-digital conversion. With 12 bits resolution, the noise 'floor' is at approximately -72dB, with regard to the largest signal power (Oppenheim and Schafer 1975).

5.2.1.2 Steady Flow — With Forcing

Forced flow experiments prove an excellent means for ascertaining the nature of poststenotic flow velocity fluctuations and can offer conclusive evidence that the velocity fluctuations with Strouhal numbers from 0.2 to 0.5 reflect shear layer instabilities of poststenotic separated flows.

The three stenotic flows are subjected to a comprehensive flow excitation investigation, covering a range of excitation frequencies and different flow rates. The minimum forcing level *i.e.* closed valve operation, is chosen because of the extreme sensitivity of the flows to perturbations. Using a conservative estimate of the excitation level of $2u'_{p,rms}=0.084$ cm s^{-1}, the forcing is seen to be at most 0.8% of the maximum axial throat velocity, but is typically lower. Representative waveforms for all three stenosis models are shown in *figure* 3.10. It is immediately apparent that the separated flow 'resonates' at the forcing frequency or higher harmonics thereof. This resonance clearly is a nonlinear phenomenon because the forcing signal is not simply amplified but, importantly, seems to regulate the flow. For example, the flow conditions for the orifice plate (*figure* 3.10$a1,a2$) are the same as in undisturbed flow (*figure* 3.7a). At a forcing frequency $f_f=2.1$ Hz near the natural instability $f_m=2.3$ Hz, the amplitude

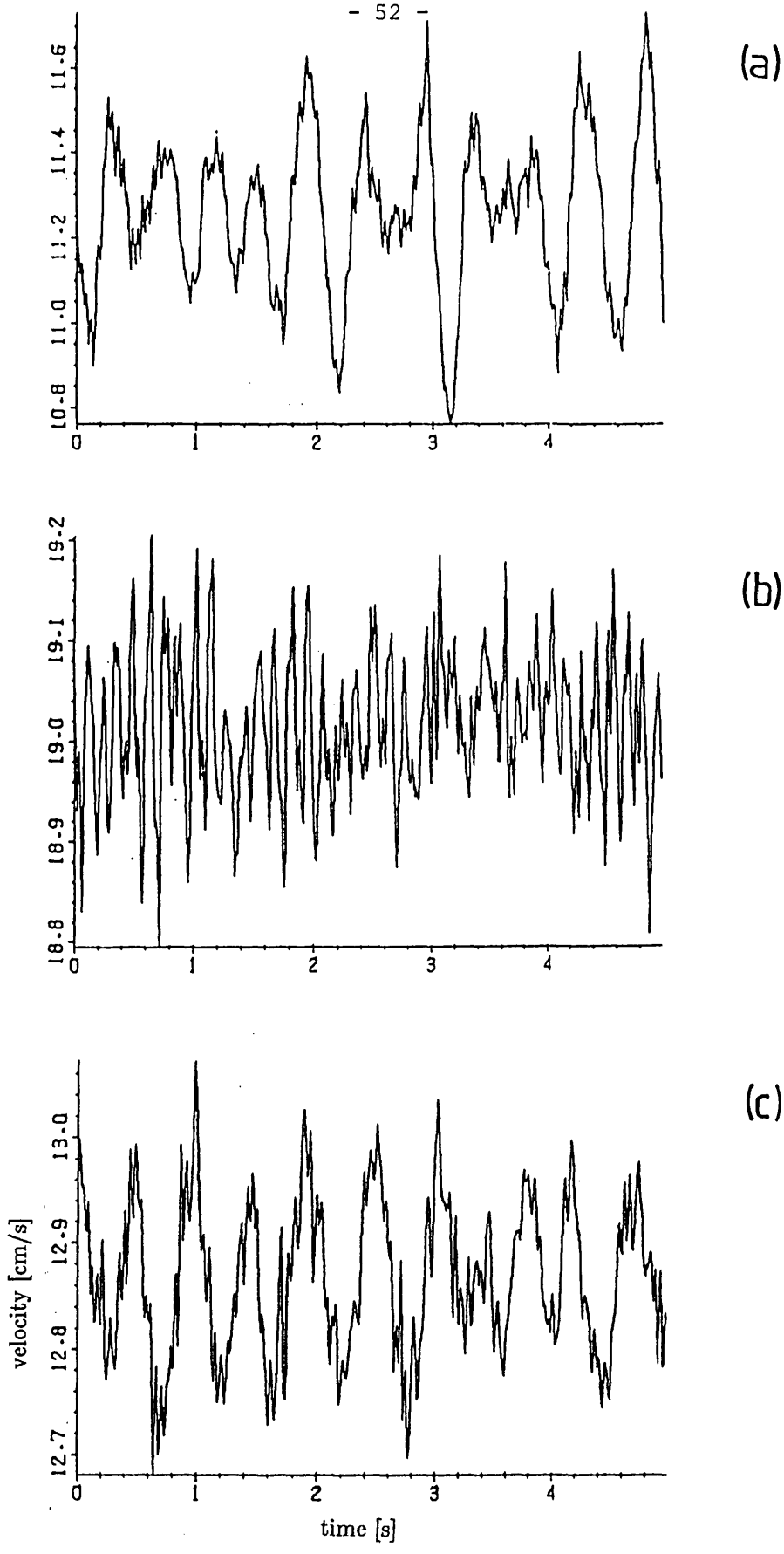

Figure 3.7 Natural (unperturbed) centreline axial flow velocity fluctuations in poststenotic steady flow (all velocities in [cm s^{-1}], time in [s]). (*a*) Orifice plate, $x/D=2$, $Re=940$. (*b*) Orifice plate, $x/D=1$, $Re=1590$. (*c*) Contoured symmetric constriction, $x/D=4$, $Re=1590$. (*d*) Nonsymmetric constriction, $x/D=2$, $Re=1590$. (*e*) Nonsymmetric constriction, $x/D=3$, $Re=1590$.

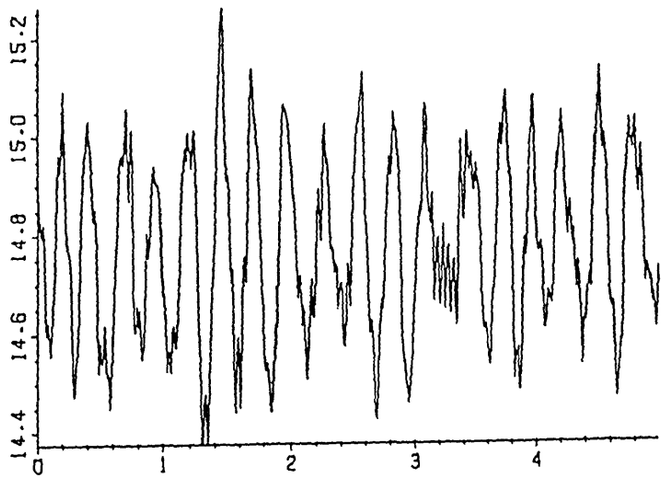

(d)

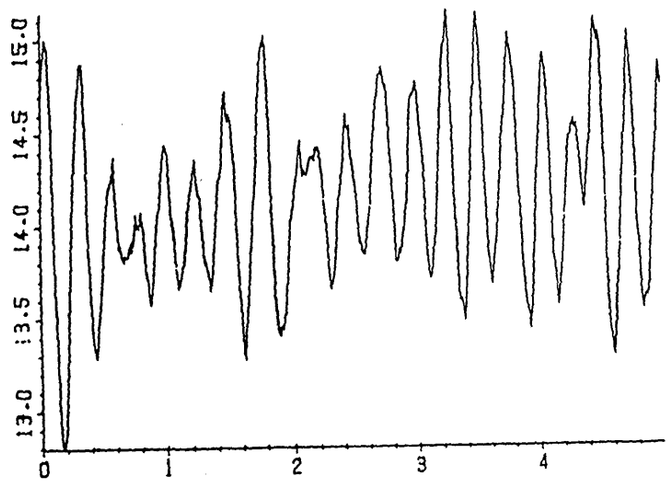

(e)

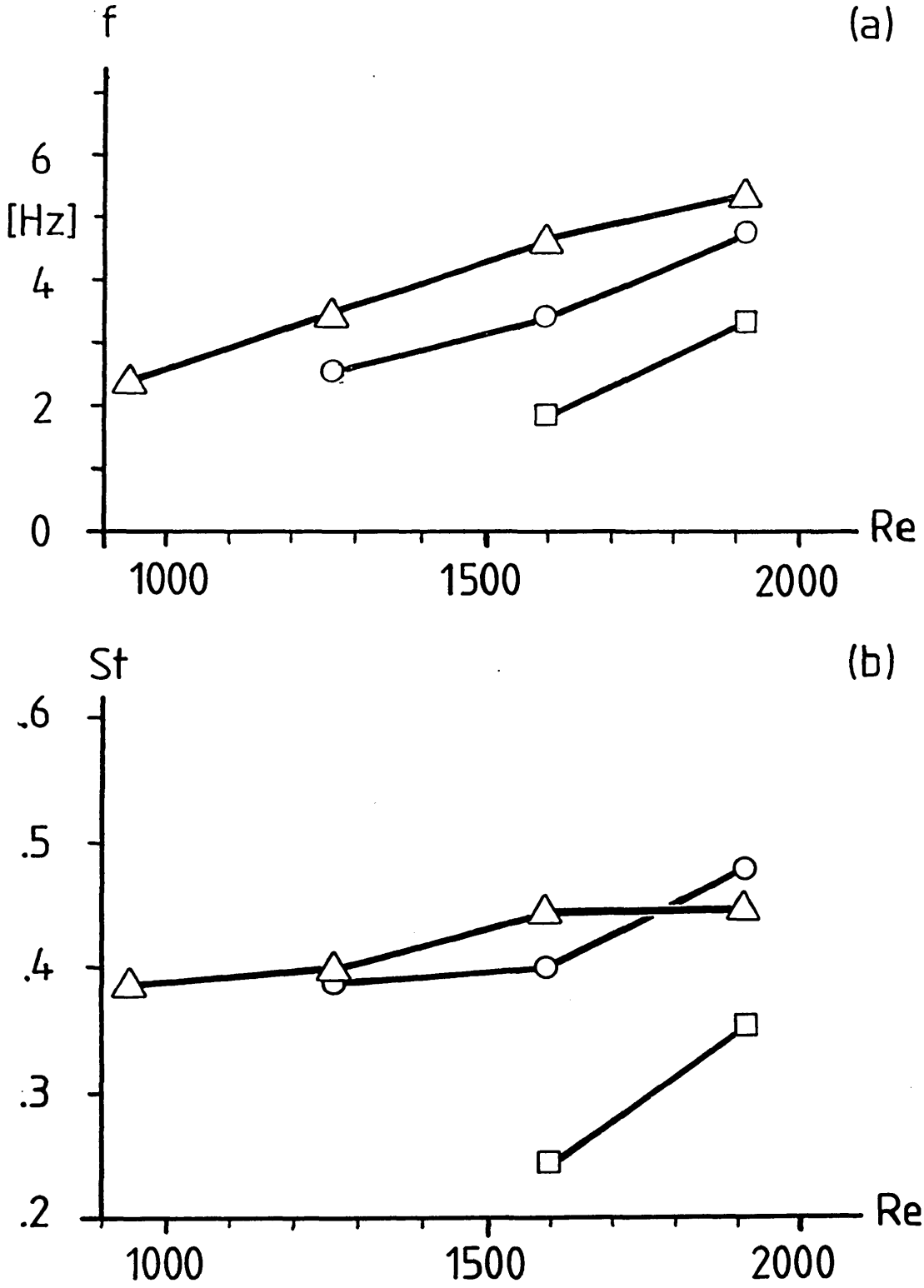

Figure 3.8 (*a*) Variation of the dominant frequency of axial velocity fluctuations with Reynolds number, in unforced poststenotic flow (Δ—orifice plate, □—contoured symmetric constriction, o—nonsymmetric constriction). (*b*) Dominant frequency, non-dimensionalised by the representative constriction diameter $d=D/\sqrt{2}$, and the peak poststenotic axial velocity.

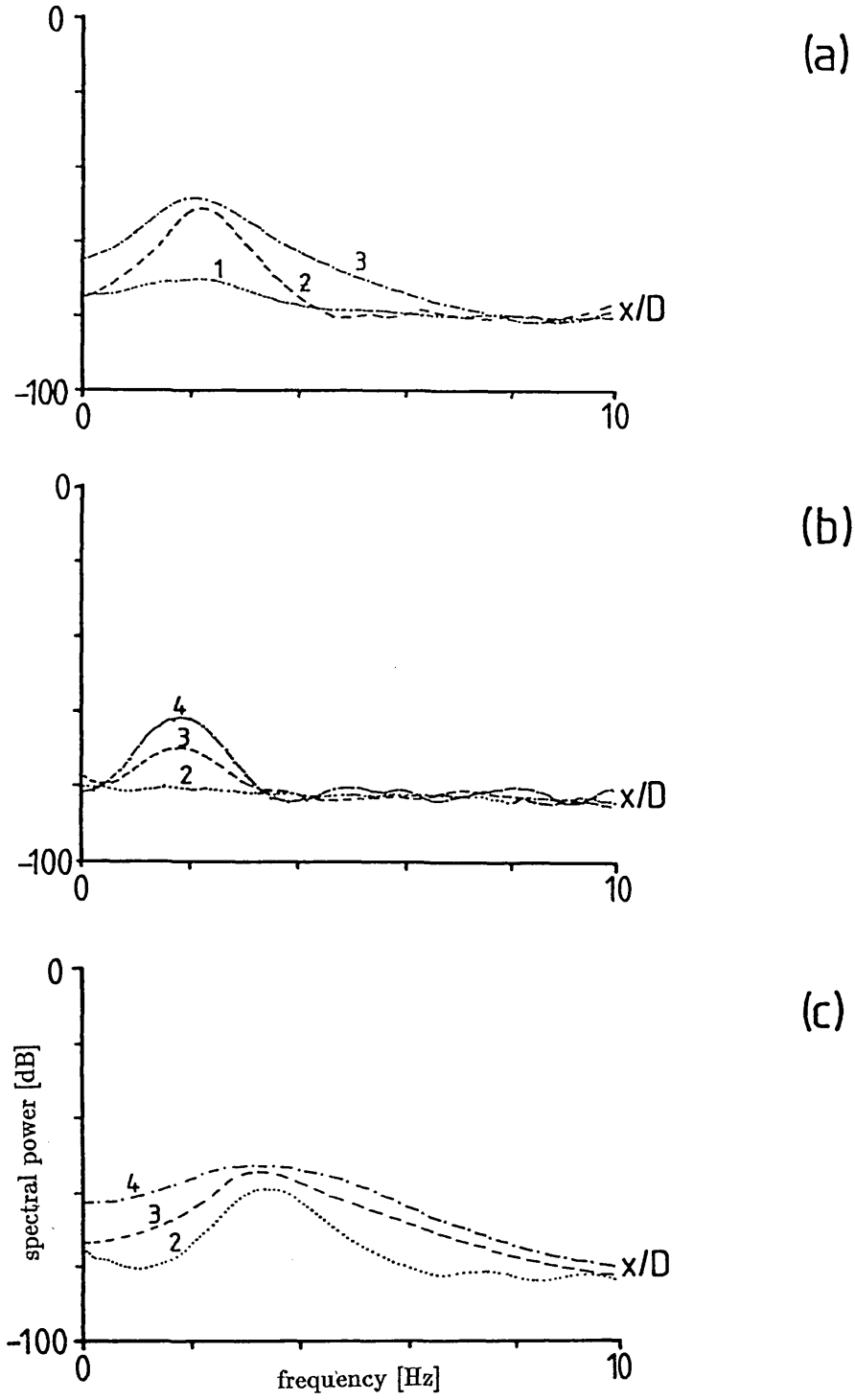

Figure 3.9 Downstream evolution of the power spectral estimates of centreline axial velocity fluctuations in poststenotic flow (frequency in [Hz], spectral power in [dB]). (*a*) Orifice plate, Re=940. (*b*) Contoured symmetric constriction, Re=1590. (*c*) Nonsymmetric constriction, Re=1590.

is at least twice as high and there is virtually no amplitude modulation. At a higher forcing frequency, f_f=3.6 Hz, the response is less dramatic and a certain degree of amplitude modulation is observed. However, as will be seen more clearly from power spectral estimates (*figure* 3.11*a*), there is some spectral activity at the first subharmonic of f_f, an observation that is also made for the contoured symmetric constriction. Higher harmonic response, on the other hand, is well illustrated for the nonsymmetric constriction (*figure* 3.10*e*1 – *e*3). The natural instability frequency is f_m=3.4 Hz, and for a forcing frequency of f_f=1.0 Hz the flow response is at the fourth harmonic (*figure* 3.10*e*1), for f_f=1.8 Hz at the second harmonic. Finally, for f_f=3 Hz the separated shear layer resonates most strongly (*figure* 3.10*e*3). It is noted that the fourth-harmonic response is accompanied by a significant drop in mean velocity, indicating increased entrainment of fluid by the large forced vortex structures.

The flow resonance and regularisation in the presence of forcing is illustrated by comparing the power spectral estimates of the natural velocity fluctuations with those of the excited flow (*figure* 3.11). Two sets of power spectra are shown, for the orifice plate (*figure* 3.11*a*) and for the contoured symmetric stenosis (*figure* 3.11*b*), each set covering forced flow measurements at minimal forcing level and different forcing frequencies, f_f=0.8 – 4.3 Hz. In view of the fact that no qualitatively different behaviour is observed for the nonsymmetric stenosis model, it has been decided to summarise results for this geometry in the form of a response *diagram* 3.12, only.

The broken line indicates the respective undisturbed flow. The mean velocity of the undisturbed flow is chosen as 0 dB reference point. Recalling that the minimum forcing level used in the steady flow experiments is buried in the measurement noise, it is readily seen that the forcing signal is greatly amplified in the region of the dominant natural flow velocity fluctuations. Most strikingly, however, the excitation actually suppresses the natural broadband fluctuations. This is observed convincingly for the orifice plate at f_f=2.5 Hz, and for the symmetric constriction at f_f=2.1 Hz. It is this property of forced free shear layers that suggests some form of nonlinear mode competition between a collection of instability waves. If the shear layer acted as a compound amplifier, the flow excitation spectrum would simply be superposed on the natural broadband fluctuations. In chapter V we shall attempt to model this scenario by multiple-degree-of-freedom oscillations.

Both poststenotic flows show some form of subharmonic response, as mentioned above. For the contoured symmetric stenosis, this takes place at a lower forcing frequency, f_f=3.0 Hz, in agreement with the lower natural frequency of oscillation, f_m=1.9 Hz. Also, for the same stenosis model, there is no response above 3.6 Hz, suggestive of the narrowband character of

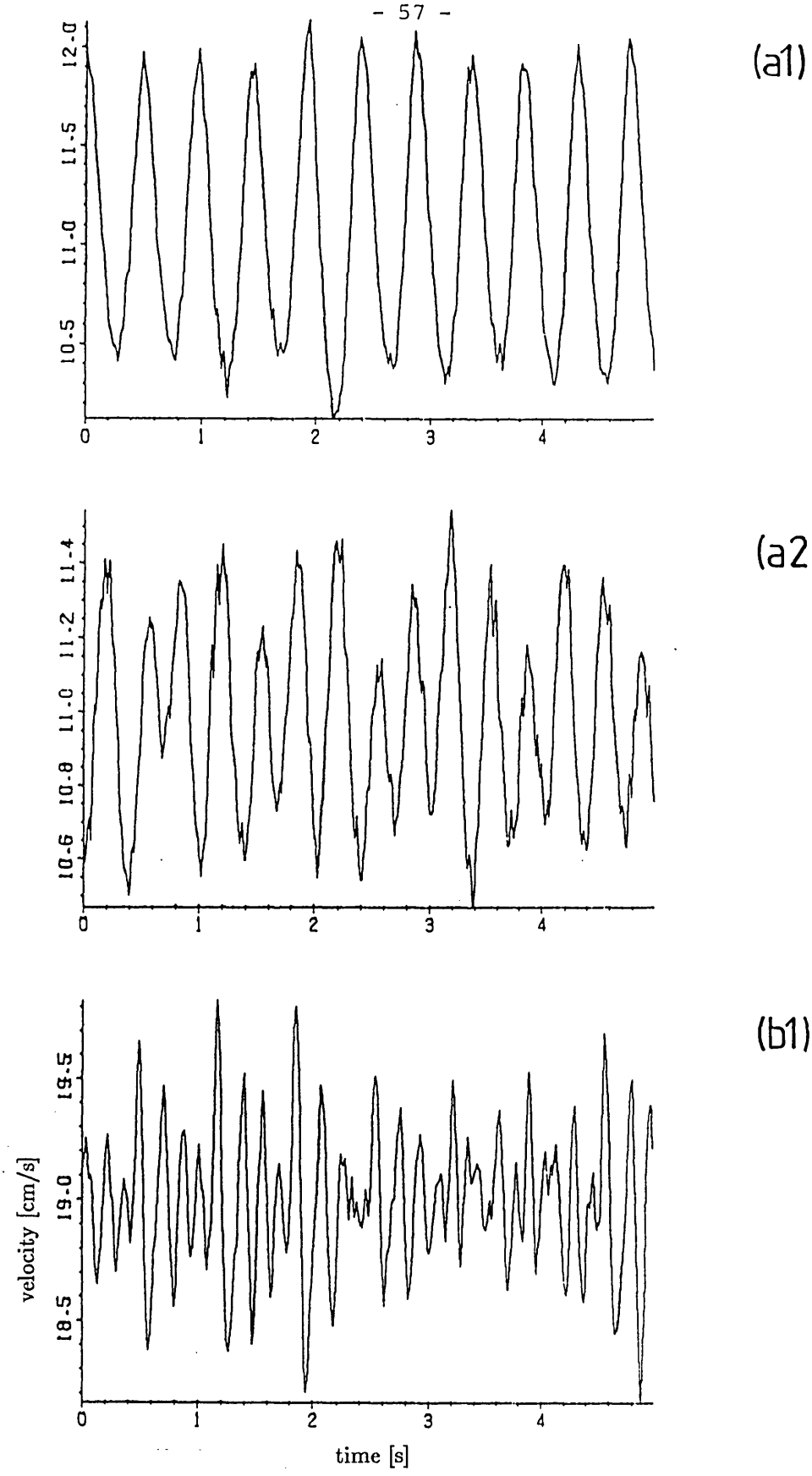

Figure 3.10 Forced centreline axial velocity fluctuations in poststenotic steady flow (all velocities in [cm s^{-1}], time in [s]). (*a*) Orifice plate, $x/D=2$, $Re=1260$. (1) $f_f=2.1$ Hz. (2) $f_f=3.6$ Hz. (*b*) Orifice plate, $x/D=1$, $Re=1590$. (1) $f_f=1.5$ Hz. (2) $f_f=2.5$ Hz. (*c*) Contoured symmetric constriction, $x/D=4$, $Re=1590$, $f_f=1.8$ Hz. (*d*) Nonsymmetric constriction, $x/D=2$, $Re=1590$. (1) $f_f=0.8$ Hz. (2) $f_f=3.0$ Hz. (*e*) Nonsymmetric constriction, $x/D=3$, $Re=1590$. (1) $f_f=1.0$ Hz. (2) $f_f=1.8$ Hz. (3) $f_f=3.0$ Hz.

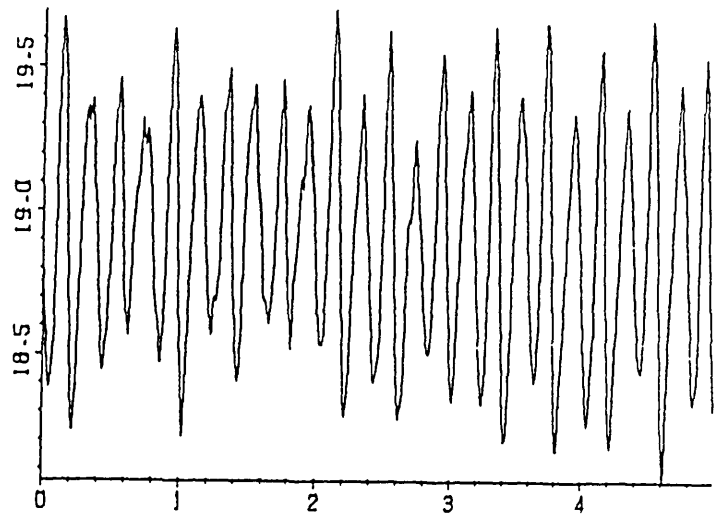

(b2)

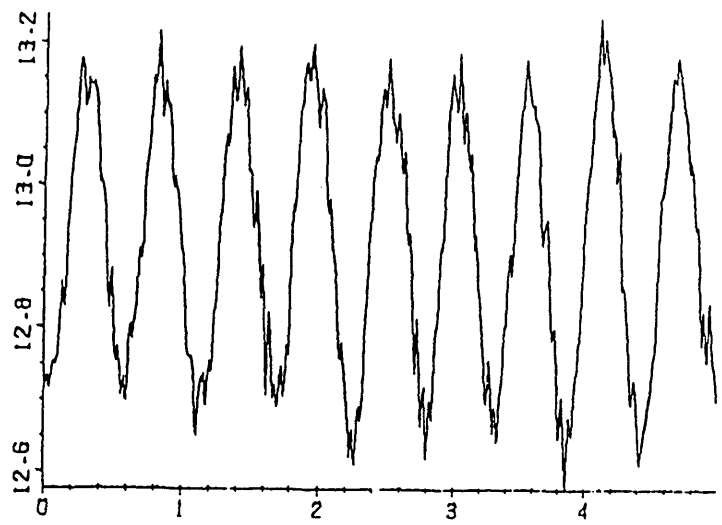

(c)

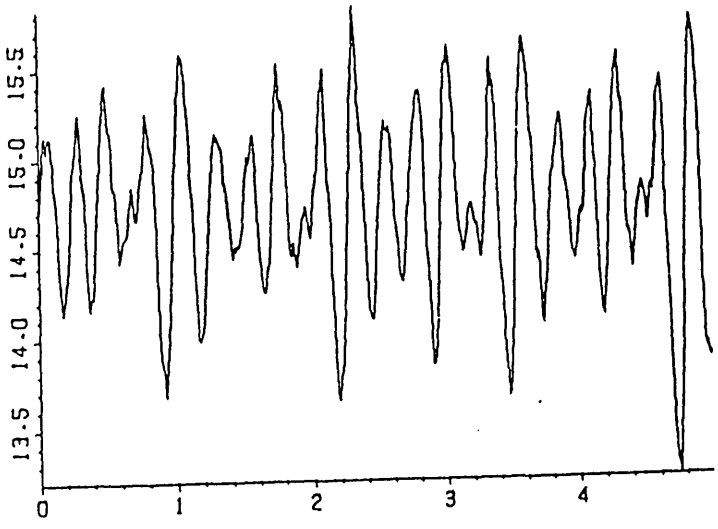

(d1)

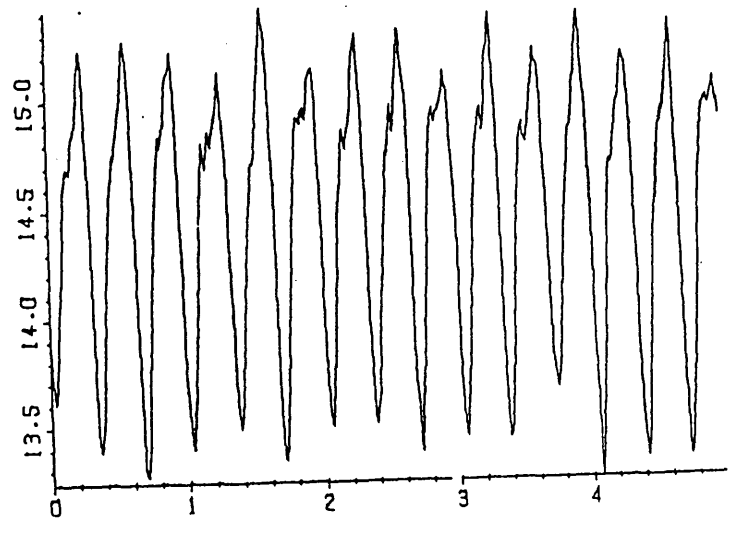

(d2)

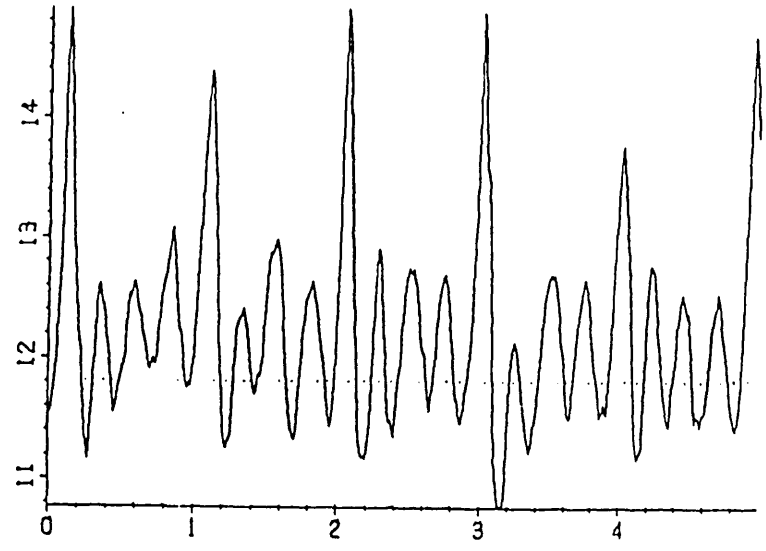

(e1)

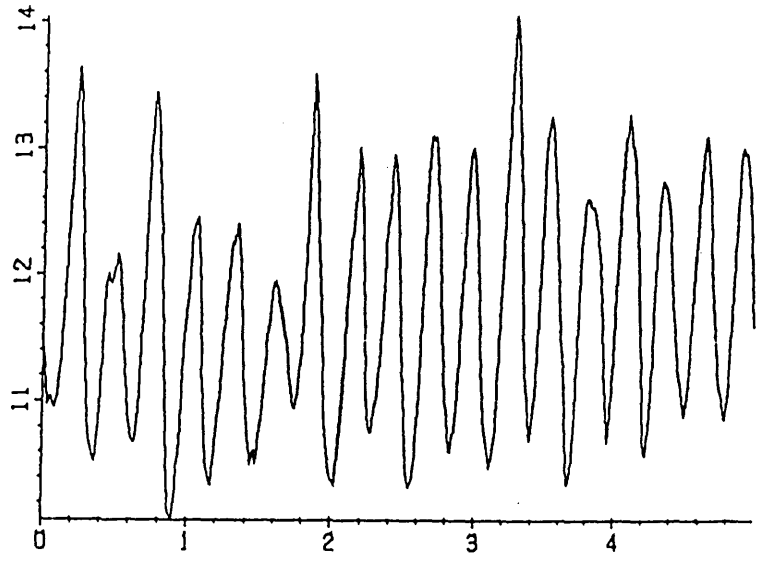

(e2)

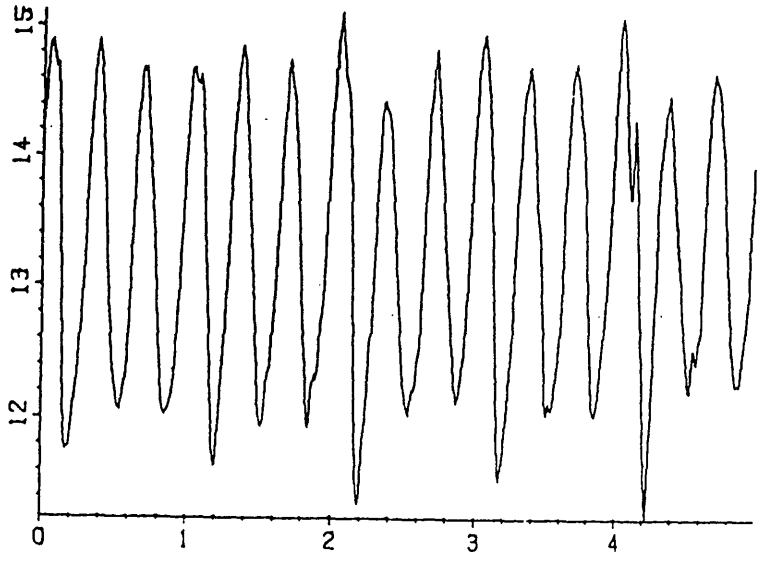

(e3)

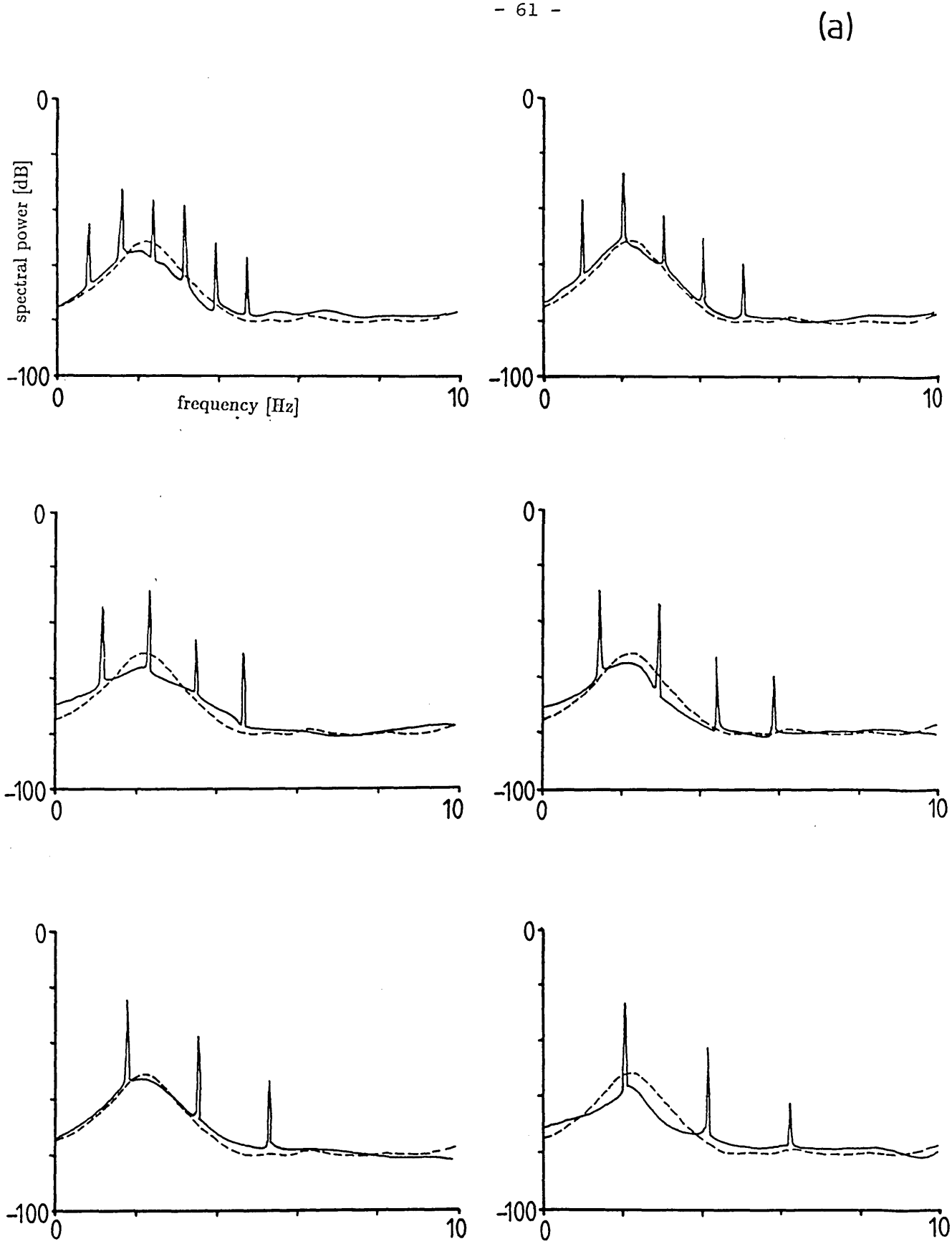

Figure 3.11 Power spectral estimates of forced axial flow velocity fluctuations, at the centreline, in poststenotic flow (frequency in [Hz], spectral power in [dB]). The broken line indicates unforced flow. The forcing frequencies are (from left to right, top to bottom): 0.8, 1.0, 1.2, 1.5, 1.75, 2.1, 2.5, 3.0, 3.6 and 4.3 Hz. (*a*) Orifice plate, $x/D=2$, $Re=940$. (*b*) Contoured symmetric constriction $x/D=4$, $Re=1590$.

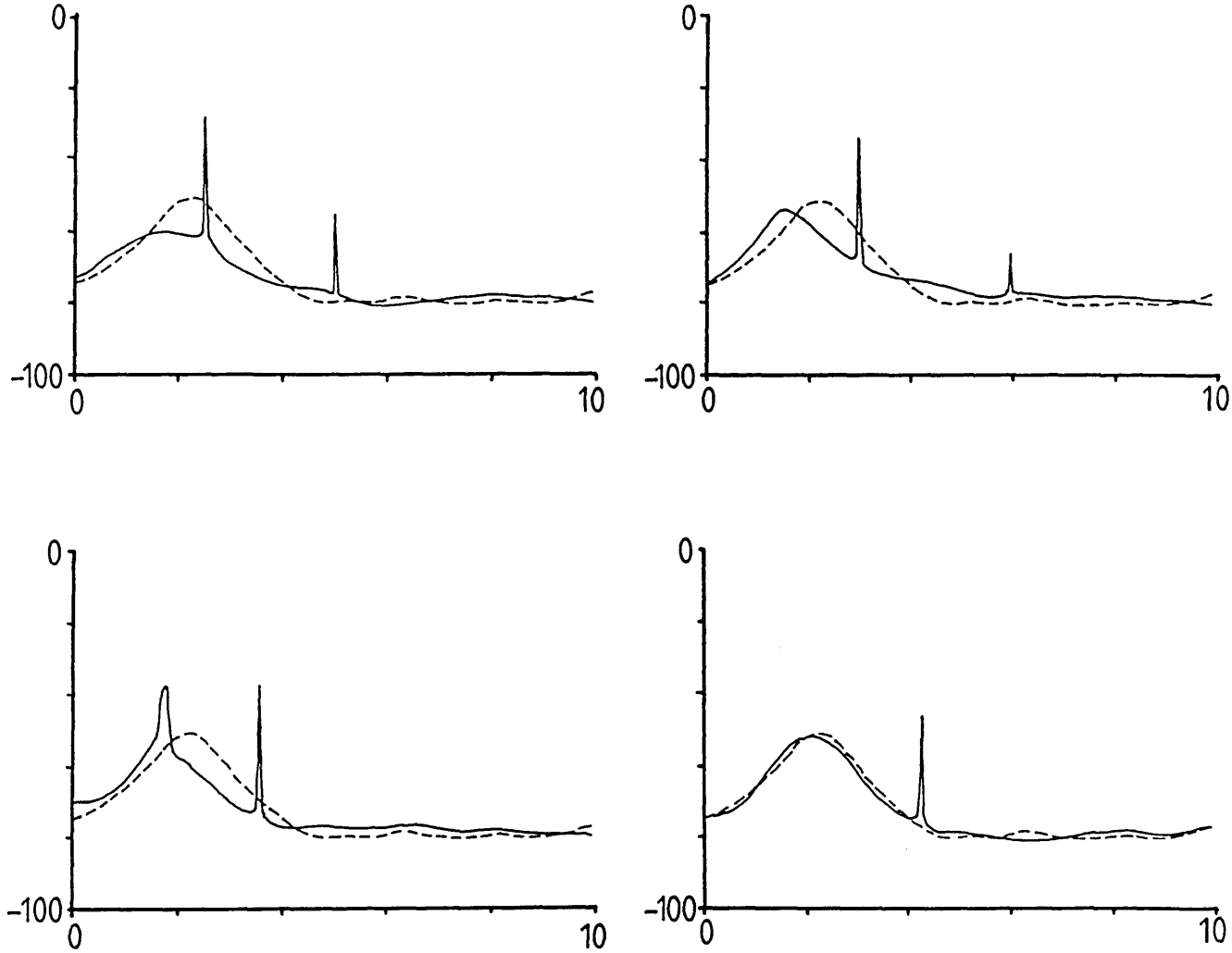
0
-100
0
10
0
-100
0
10
0
-100
0
10
0
-100
0
10

(b)

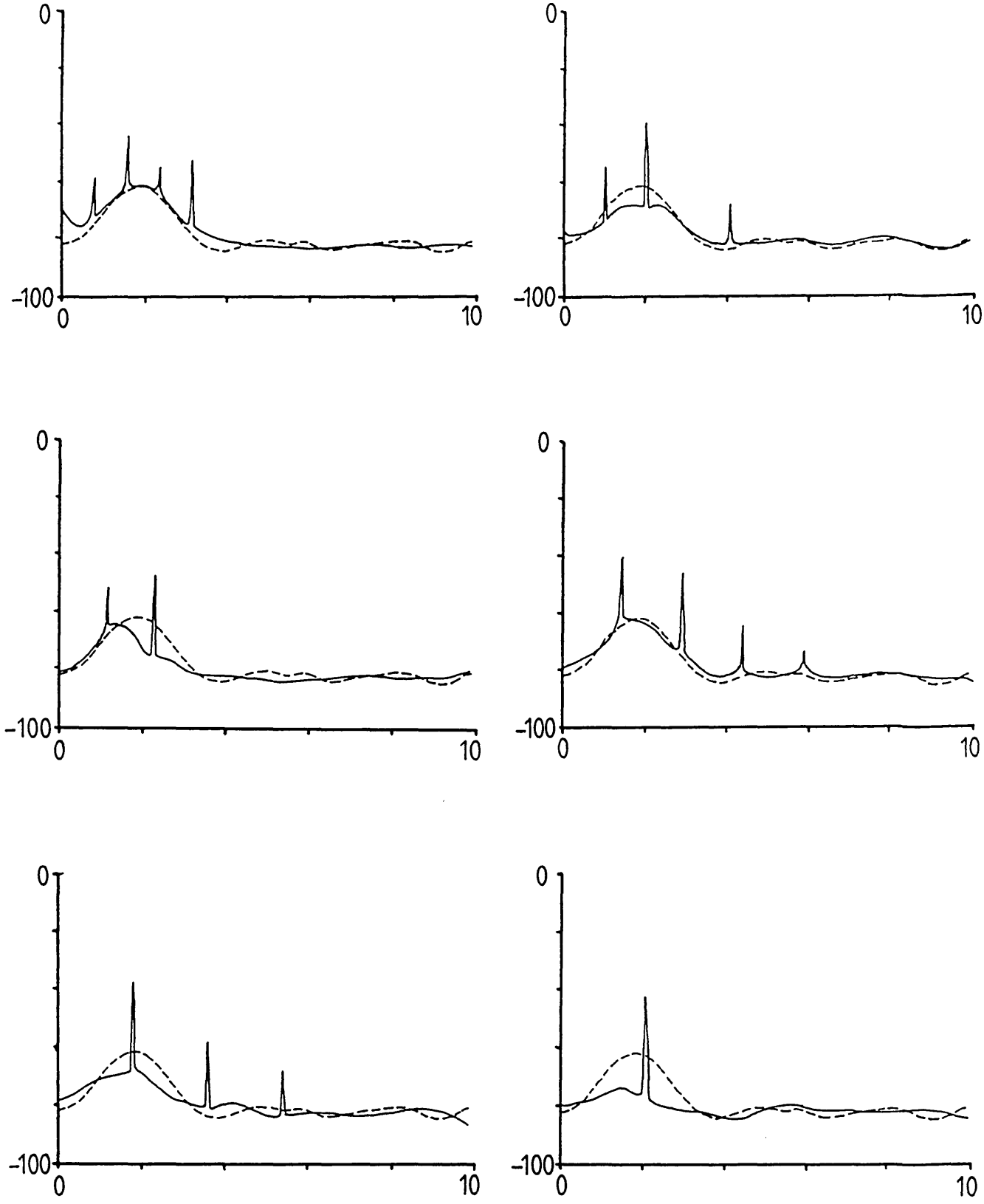

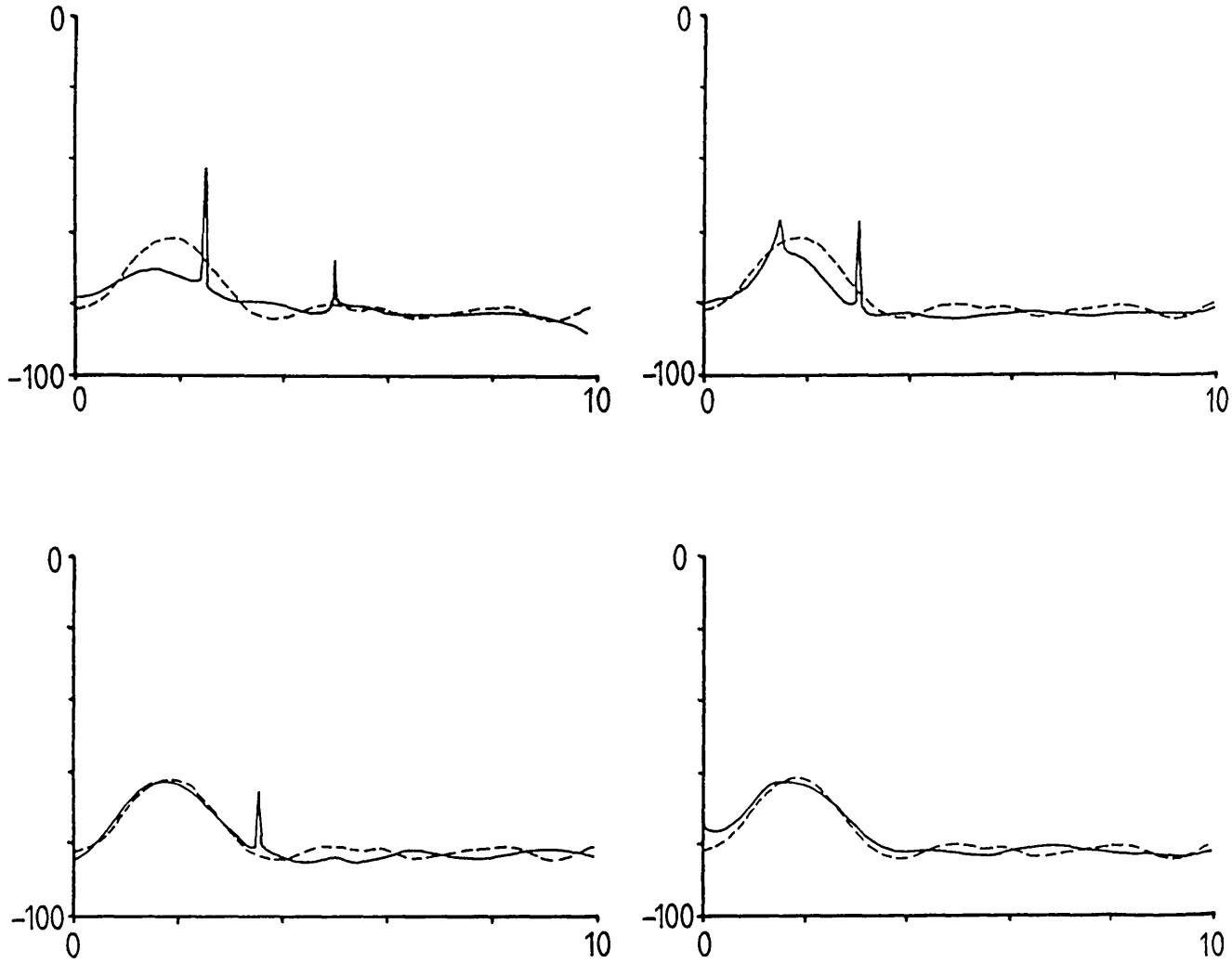
0
-100
0
10
0
-100
0
10
0
-100
0
10
0
-100
0
10

the spatial amplification.

Figure 3.12 shows response frequency diagrams that relate the dominant frequency of flow velocity fluctuations to the forcing frequency. This response is most marked for the nonsymmetric constriction where resonance at up to the fifth harmonic of the fundamental forcing frequency is observed. As the forcing frequency is increased, the response frequency jumps discontinuously between different modes of (higher) harmonic response. Note that no third-harmonic response is observed which may simply be due to the step size used for sweeping the range of forcing frequencies. As regards the half-harmonic response in the case of the orifice plate and the contoured symmetric constriction, this phenomenon is observed clearly under pulsatile flow conditions (§ 5.2.1.4), although only in orifice flow.

5.2.1.3 Pulsatile Flow – Without Forcing

Axial flow velocities are measured at successive downstream positions for the three different stenosis geometries under pulsatile flow conditions, as described in § 5.1.2.2 with $\alpha=10$, mean Reynolds number $Re_m=1090$ and oscillatory Reynolds number $Re_{m\omega}=810$. The measurements for the symmetrical constrictions are taken on the centreline but for the nonsymmetric constriction the measurement position is a short distance off centre ($r=0.16D/2$) This allows a better detection of the vortex structures.

5.2.1.3.1 Signal Analysis

As in the steady flow experiments, the emphasis in pulsatile flow is on the velocity fluctuations u' superimposed on the time-varying mean velocity $U_0(t)$. As to the exact definition of 'mean velocity' in pulsatile flow, the view taken here is that the two components are spectrally separable.

It may be expected that, by assuming a quasi-steady relationship between pulsatile and steady flow conditions, the velocity fluctuations will follow the instantaneous flow rate in spectral content. It was therefore decided to analyse the temporal evolution by a simple autoregressive (AR) tracking method that is used in a variety of applications *e.g.* biological rhythms (Linkens 1979), frequency demodulation (Kitney and Giddnes 1986) and power system load prediction (Hartmann and Treiber 1986). On the assumption that, on time scales short compared to flow rate variation, the time-varying velocity fluctuations are described by a parametric model, AR model parameters are determined successively for a moving data window. Importantly, no parametric description of the temporal evolution of the AR parameters themselves is assumed. This allows the tracking of rapid changes in the spectral

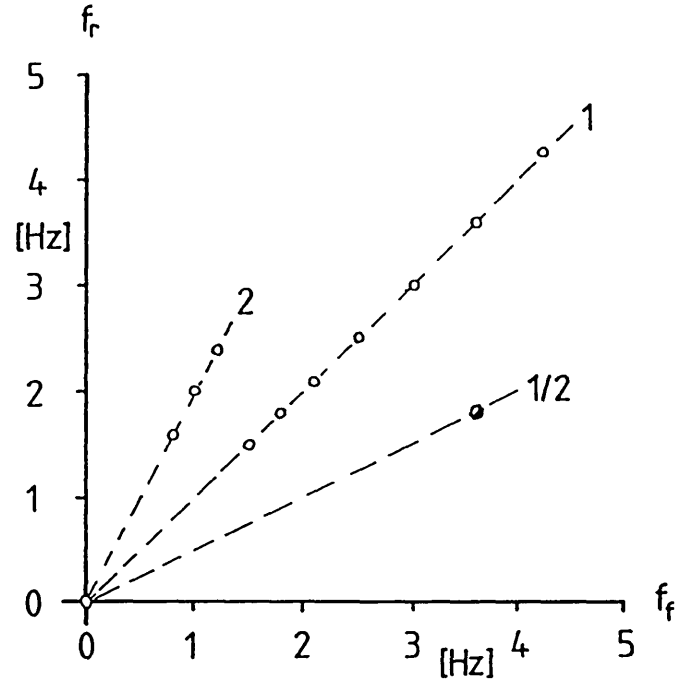

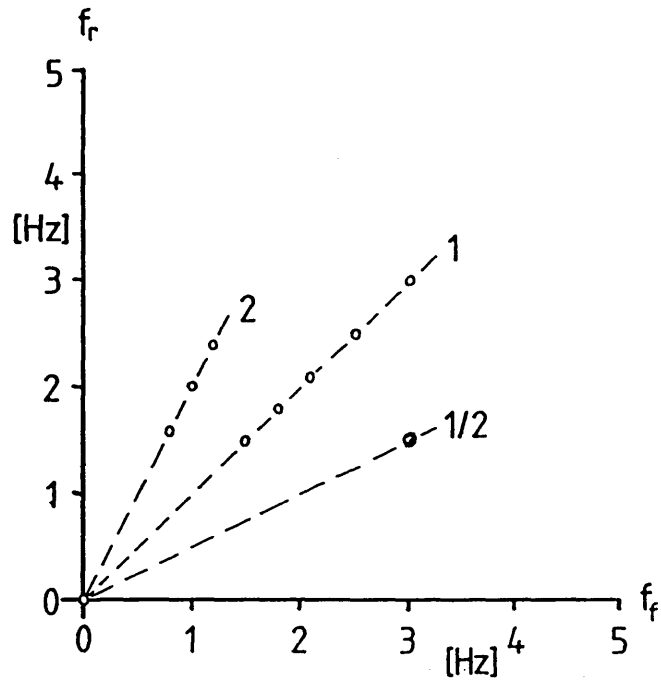

Figure 3.12 Dominant response frequency f_r *vs.* forcing frequency f_f in poststenotic flow. (*a*) Orifice plate. (*b*) Contoured symmetric constriction. (*c*) Nonsymmetric constriction. The half-harmonic response (◕) co-exists with response at the harmonic.

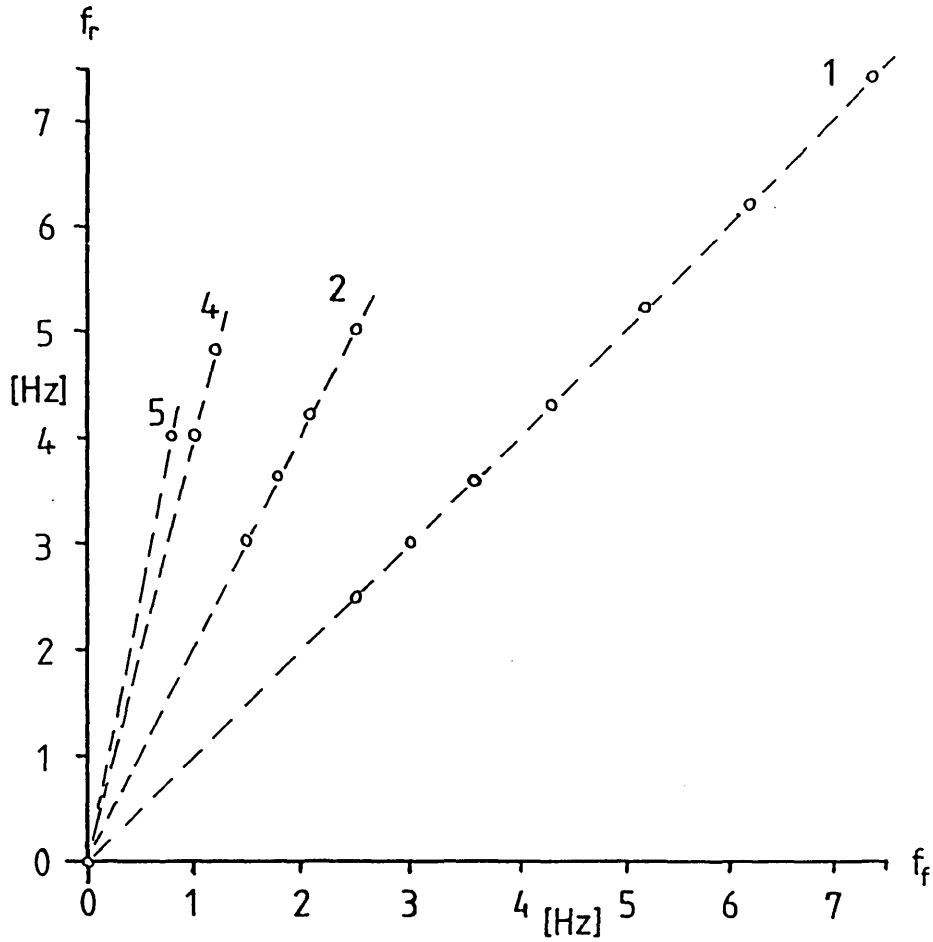

(c)

properties of the data, but requires a great deal more calculations than recursive AR estimation techniques. The appropriate window size for AR modelling is a compromise between the spectral resolution of very low frequencies and the quasi-steadiness of the data. The AR model order is usually determined on the basis of empirical rules (Haykin 1979, Linkens 1979), unless one is prepared to determine some optimal model order anew at each step.

5.2.1.3.2 Results

Typically, each pulsatile flow recording comprises a batch of 20 to 25 successive flow cycles. These are analysed individually by the tracking technique discussed above. Before, the flow velocity component u' is extracted by high-pass filtering (f_c=1 Hz). The data window size for the signal tracking is t_w=1 s, and a fixed AR model order $N/4$ is found to be sufficient for resolving spectral components in the frequency band of interest. The analysis shows that the pulsatile flow velocity variations are reproduced qualitatively in each cycle. Some variability is noted in the large disturbances at the beginning and the end of a cycle, but oscillatory activity is greatly repeatable with regard to the evolution of the dominant frequency and the rms values. In view of the fact that the forcing signal is not locked to the cycle of pulsation (*cf* § 5.2.1.4), no attempts are made at investigating ensemble averaged profiles. The phase relationship between the excitation and the flow cycle varies thus initiating the resonant response at varying time instants during a cycle.

Representative waveforms for all three stenosis geometries and successive downstream locations are shown in *figure* 3.13. For comparison with the steady flow results, the corresponding steady flow values of u'_{rms} and f_m for peak flow rate in pulsatile flow are given in the *diagrams* (3) and (4), respectively. Starting with the orifice plate constriction, the mean velocity variation is fairly sinusoidal at x/D=0.5 and the fluctuation intensity is rather small. The measurement noise level is larger than in steady flow – about 0.13 cm s^{-1} – , a result that is confirmed by the decrease in average tracking rate from λ=0.5 to λ=0.45.

There is some surprisingly stable low-level activity of about 2 Hz in the acceleration phase whose origin is not entirely clear. Two prominent features that are also observed at downstream locations x/D=1.0 and 1.5, are a 'start-up' structure in mid-acceleration and a similar structure in mid-deceleration. Oscillatory activity of greater intensity and better understood origin is measured at x/D=1.0. Low-level activity of about 2 Hz is observed even before the start-up structure at t=3.25 s, suggesting that the 2 Hz activity is related to disturbances from previous cycles. Following the large scale structure, high-intensity fluctuations build up immediately. The fundamental frequency is about 5.5 Hz and corresponds

to what is expected in steady flow for peak Reynolds number. However, the intensity of the fluctuations in pulsatile flow is greater by a factor of about five. The oscillations become less distinct with the onset of the deceleration phase — the frequency estimate behaves rather erratically — and a large scale disturbance terminates the oscillatory fluctuations.

Similarly, at $x/D=1.5$, large amplitude oscillations are preceded and terminated by two large scale structures. The frequency during peak flow is slightly lower than further upstream — about 5 Hz — and drifts off again in the deceleration phase. The intensity of the oscillations has grown further, to a peak value of 2 cm s^{-1}, compared to its steady flow equivalent of 0.65 cm s^{-1}.

Pulsatile flow through the contoured symmetric stenosis behaves rather differently. The mean velocity evolves with more triangular shape, *i.e.* fairly linear acceleration and deceleration slopes, and no noticeable structures at the beginning and end of cycle are observed. At $x/D=2.0$ regular oscillatory fluctuations of frequency about 2.3 Hz are seen to build up quickly. They reach highest intensity at peak flow, approximately 0.6 cm s^{-1}, and then fall off more gently, accompanied by a decrease in frequency. The behaviour is qualitatively similar at $x/D=3.0$, but at $x/D=4.0$ the oscillatory activity sets in later during cycle and there is a return to laminar flow, *i.e.* the fluctuations decrease gradually in intensity and frequency. Unlike in pulsatile flow downstream of the orifice plate, the dominant frequency during peak flow is somewhat lower than the frequency expected in comparable steady flow. On the other hand, the flow velocities show similar differences, suggesting that no fundamentally different behaviour is observed. Again, the fluctuation intensity is much greater. Note that in steady flow, even at highest Reynolds number, the rms level is always below 0.5 cm s^{-1}.

Not unexpectedly, the mean velocity for pulsatile flow downstream of the nonsymmetric constriction bears little resemblance to the upstream sinusoidal waveform. Similar to the orifice plate flow, there are large scale disturbances at the beginning and the end of the cycle, probably related to previous cycles. In particular the disturbance near the end of the cycle is variable, its magnitude changing with each cycle. At $x/D=1.2$, oscillatory activity of about 4 Hz and rms level 0.6 cm s^{-1} is seen to be confined to the high velocity plateau during peak flow. At $x/D=1.5$, the oscillatory fluctuations, though impulsively started at the end of the rapid acceleration phase, extend well into the deceleration phase. The intensity is somewhat larger and the dominant frequency is reasonably constant. Further downstream, at $x/D=2.0$, the onset of coherent fluctuations is less abrupt but the fluctuation levels have not grown. Finally, at $x/D=2.5$, a prominent reproducible structure at the beginning of the cycle is observed, followed by oscillations that tend to become less distinct in the deceleration phase.

In summary, the 4 Hz activity is in broad agreement with steady flow fluctuations and the rms levels are not dramatically different.

5.2.1.4 Pulsatile Flow With Forcing

It is seen from the above results that both the spectral content and the mean fluctuation level of the flow velocity component u' are subject to variations during the pulse cycle. This, of course, raises the question of defining an appropriate forcing function. For example, it may be expected that a hypothetical source of flow excitation in arterial flow exhibits cyclic variations with the basic period of the flow pulsation due to some fundamental flow coupling.

In this study, the flow excitation is of fixed frequency and amplitude thus avoiding *ad hoc* assumptions about the phase relationship between a periodically varying forcing signal and the pulsatile flow rate, as well as the waveform of the periodic forcing signal variations. The view taken is that the most significant flow velocity fluctuations are those with the highest mean fluctuation level u'_{rms}, because they constitute the flow feature most readily detected and observed *in vivo*. In addition, in physiological flows the periodic mean flow variations are far from sinusoidal, typically characterised by a short acceleration phase and prolonged deceleration. Note also that even for sinusoidally varying pressure gradients the poststenotic mean flow velocity can be far from sinusoidal (*figure* 3.13*c*) with very short acceleration and deceleration phase and a dominant plateau of constant-frequency oscillations.

No attempts are made at quantifying exactly the forcing level at which the dominant pulsatile flow fluctuations start to be regulated by the excitation. Rather it is found from qualitative analysis of forced pulsatile flow results that at a forcing frequency near the natural frequency, forcing levels around 0.2 cm s^{-1} are required to achieve flow resonance in a significant portion of the cycle. Clearly, because the forcing frequency is matched to the natural instability, these forcing levels represent a minimum with regard to more general forcing types and conditions.

The phase relationship between the forcing function and the waveform of pulsation is disregarded here, although it is acknowledged that this may have some influence on the separated shear layer response, in particular at the lower forcing frequencies where the phase is not negligible.

Representative results are shown in *figure* 3.14. The pulsatile flow through the sharp edged orifice plate is forced at a fundamental frequency of 5 Hz and at a level of about 0.2 cm/s. At position x/D=0.5, the poststenotic flow acts as a compound amplifier and resonance

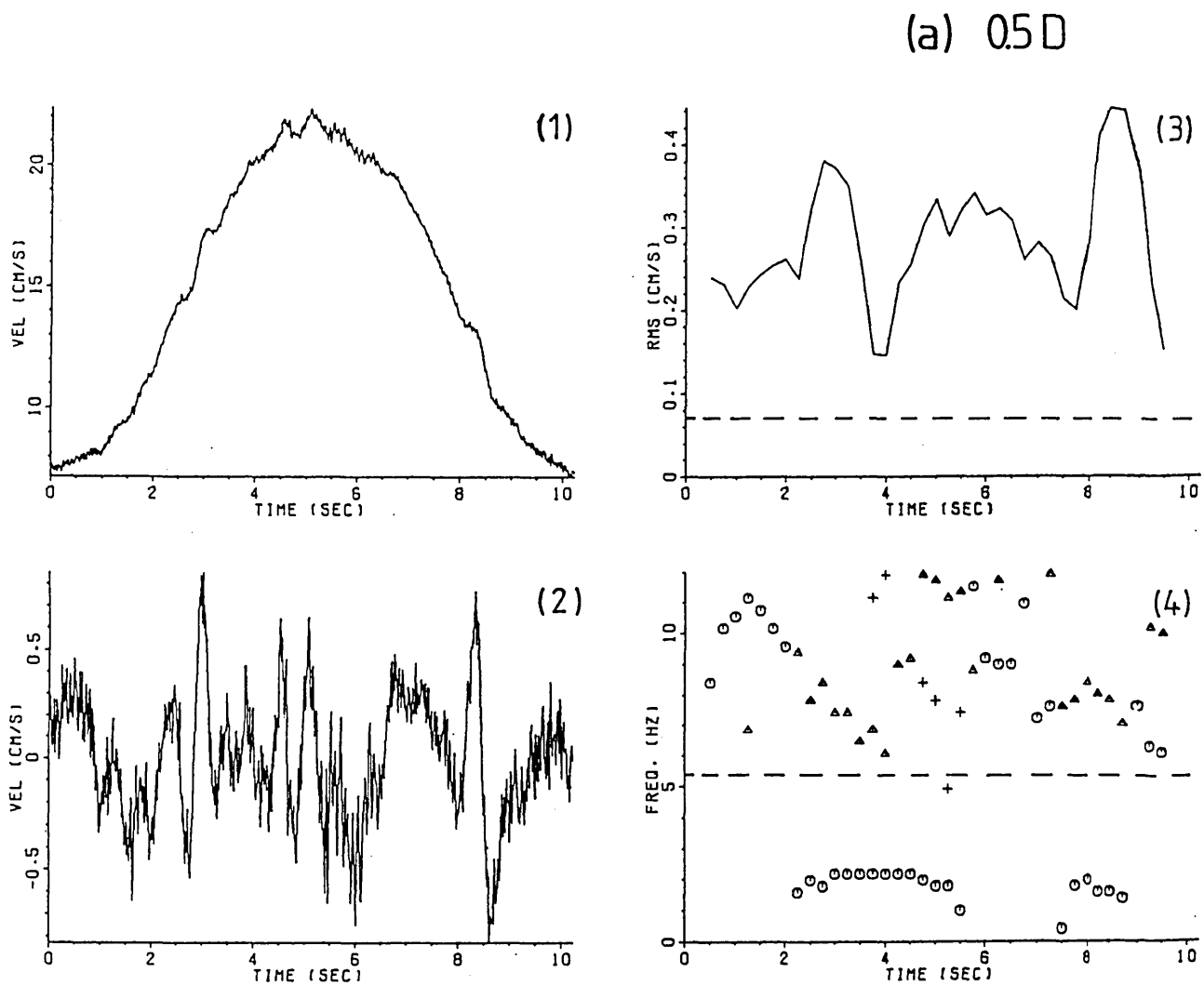

Figure 3.13 Unforced axial velocities in pulsatile poststenotic flow, with mean Reynolds number Re_m=1090, and oscillatory Reynolds number $Re_{m\omega}$=830 (all measurements at centreline except nonsymmetric constriction, r=0.16D/2). A single pulse (1) is highpass-filtered (f_c=1Hz) to obtain the flow disturbances (2). Rms values (3) and frequency content (4) (peak frequency: o, 2nd peak: Δ, 3rd peak: +) are determined by AR tracking (window size t_w=1 s, 75% window overlap, AR order: N/4). The horizontal lines in *diagrams* (3) and (4) indicate the corresponding steady flow values for peak Reynolds number. (*a*) Orifice plate, x/D=0.5, 1.0 and 1.5. (*b*) Contoured symmetric constriction, x/D=2, 3 and 4. (*c*) Nonsymmetric constriction, x/D=1.2, 1.5, 2.0 and 2.5.

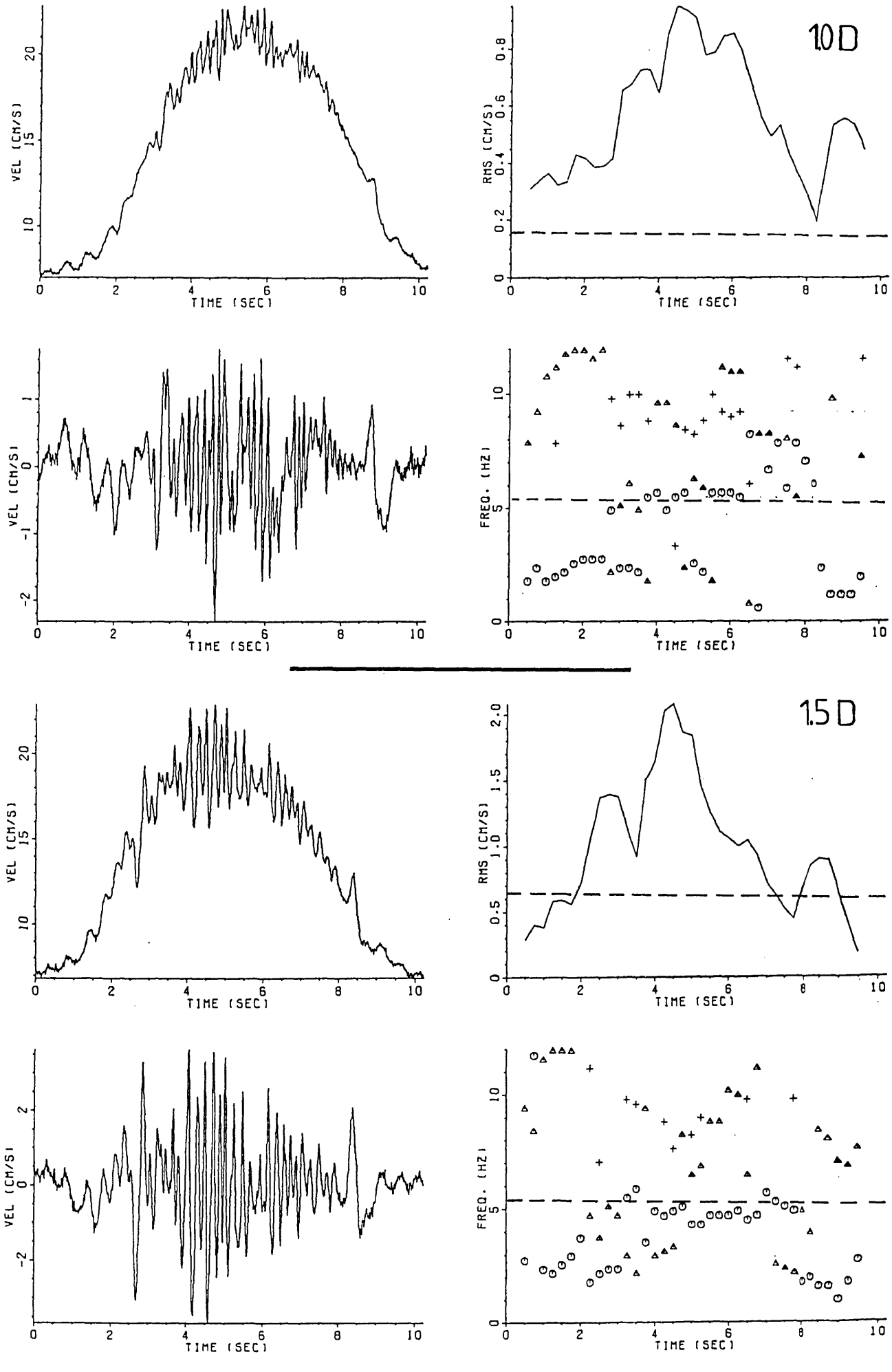
1.0 D
VEL (CM/S)
RMS (CM/S)
FREQ. (HZ)
TIME (SEC)
1.5 D
VEL (CM/S)
RMS (CM/S)
FREQ. (HZ)
TIME (SEC)

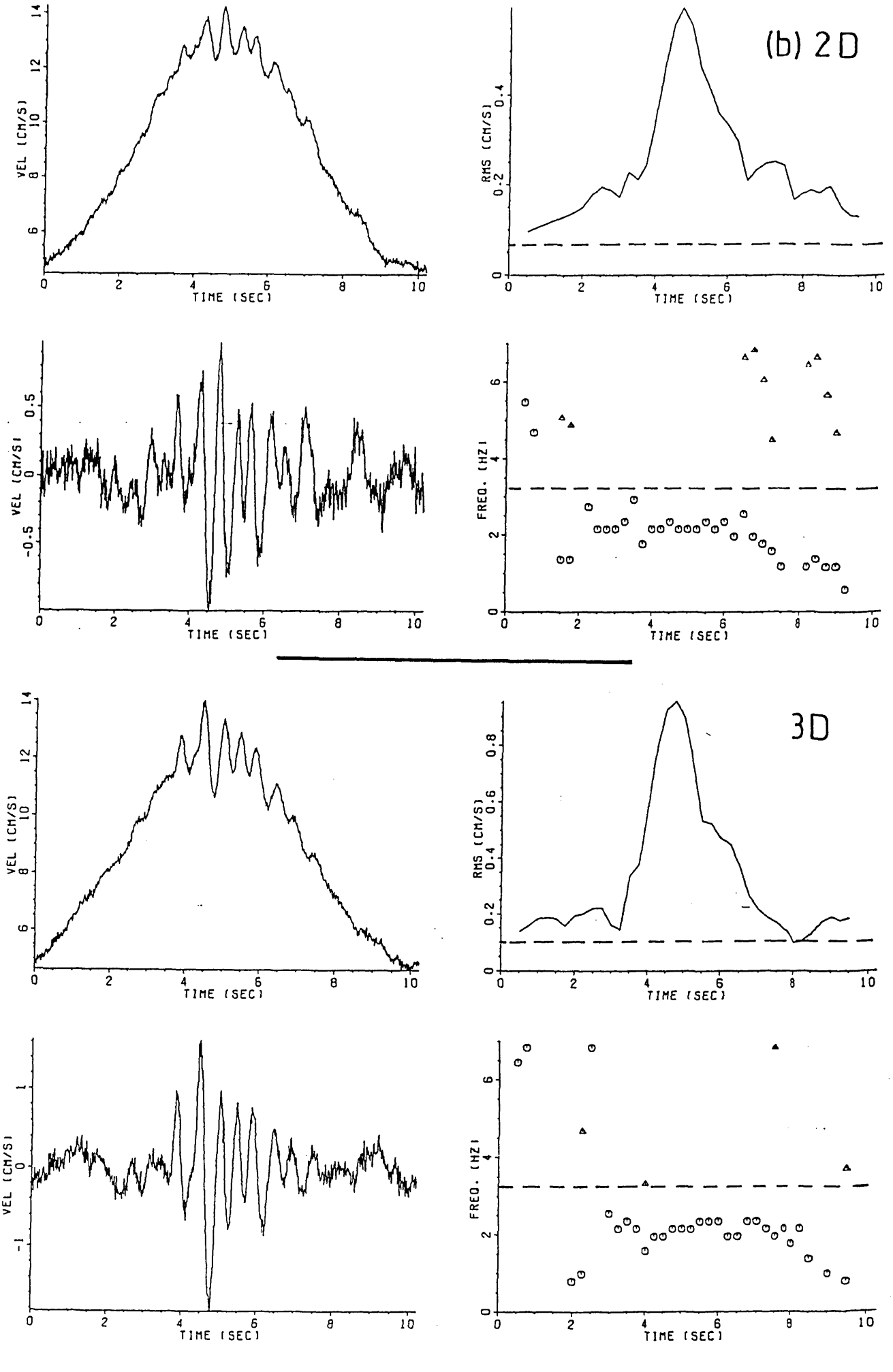
(b) 2D
VEL (CM/S)
TIME (SEC)
RMS (CM/S)
TIME (SEC)
VEL (CM/S)
TIME (SEC)
FREQ. (HZ)
TIME (SEC)
3D
VEL (CM/S)
TIME (SEC)
RMS (CM/S)
TIME (SEC)
VEL (CM/S)
TIME (SEC)
FREQ. (HZ)
TIME (SEC)

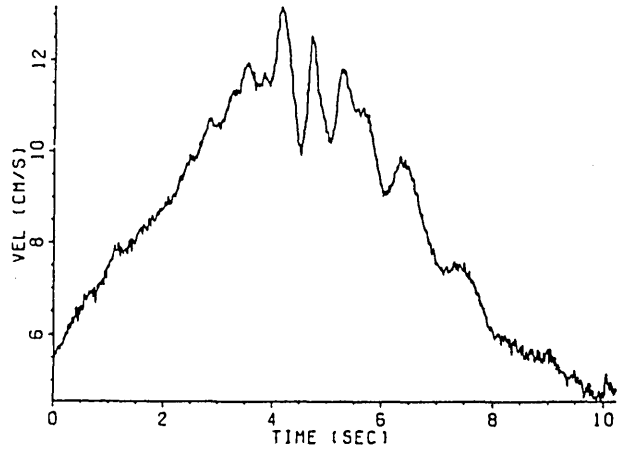
VEL (CM/S)
6
8
10
12
0
2
4
6
8
10
TIME (SEC)

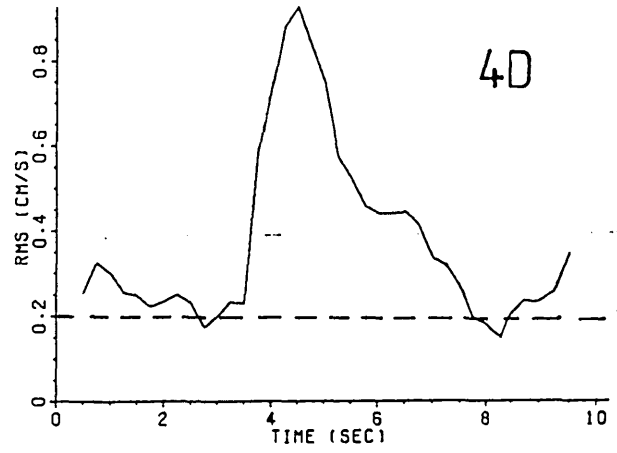
4D
RMS (CM/S)
0
0.2
0.4
0.6
0.8
0
2
4
6
8
10
TIME (SEC)

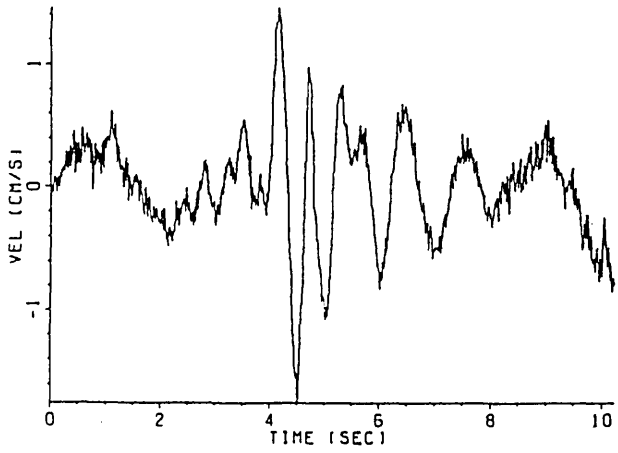
VEL (CM/S)
-1
0
1
0
2
4
6
8
10
TIME (SEC)

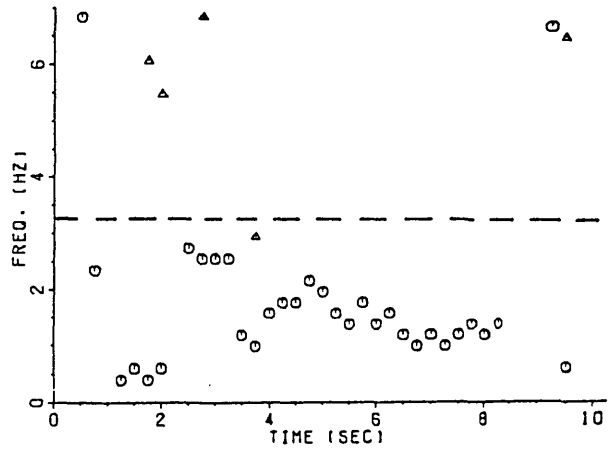
FREQ. (HZ)
0
2
4
6
0
2
4
6
8
10
TIME (SEC)

(c) 1.2D

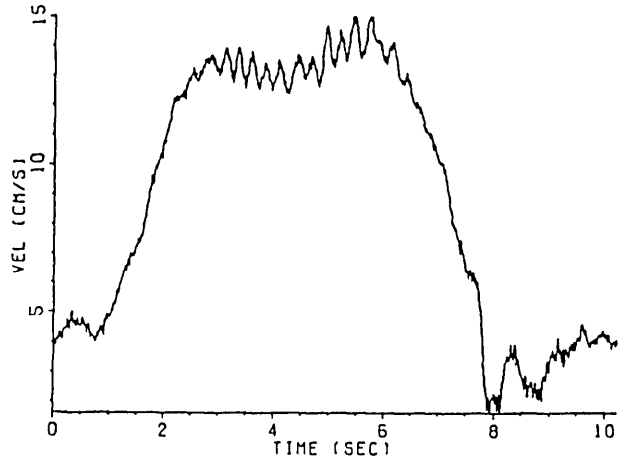
VEL (CM/S)
TIME (SEC)

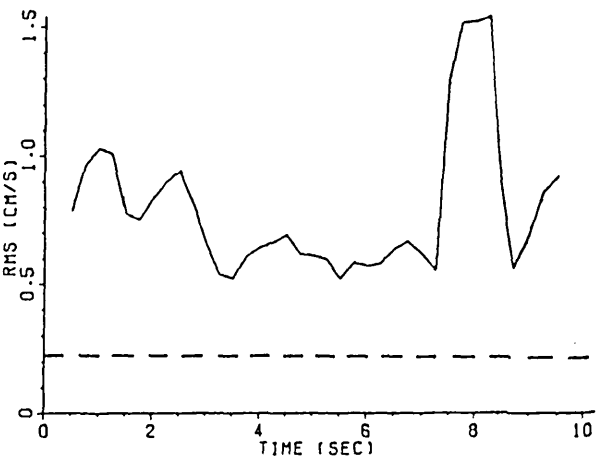
RMS (CM/S)
TIME (SEC)

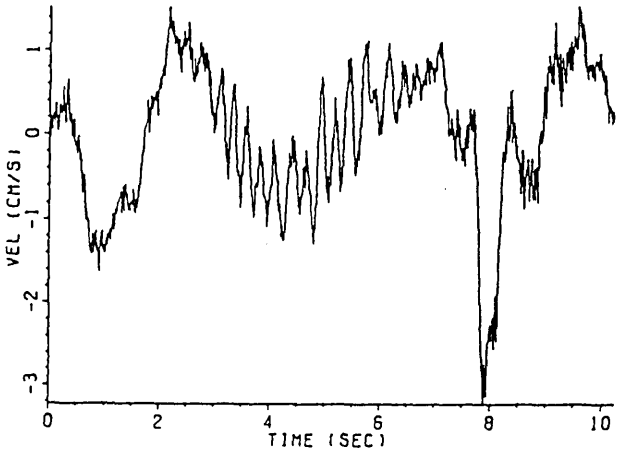
VEL (CM/S)
TIME (SEC)

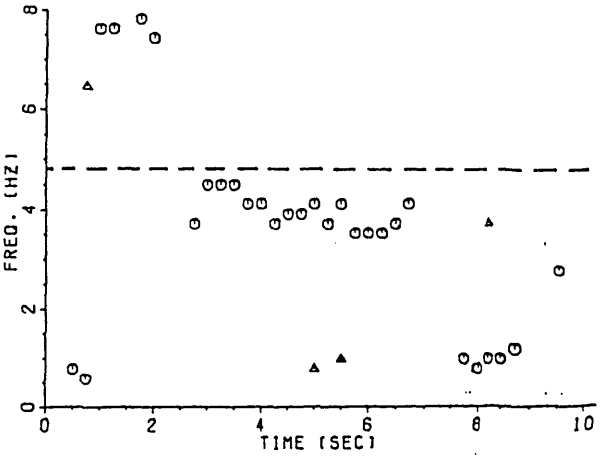
FREQ. (HZ)
TIME (SEC)

1.5D

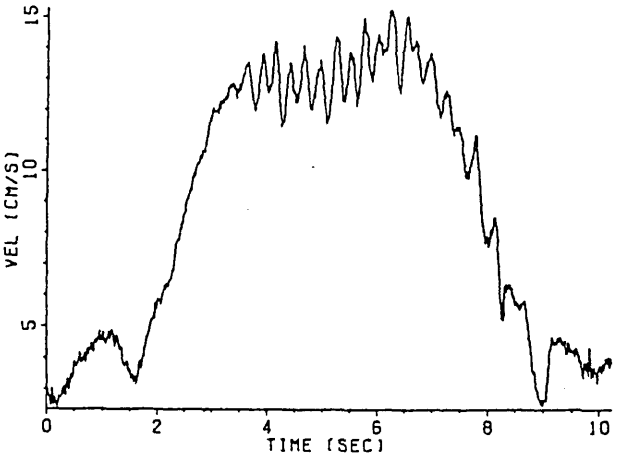
VEL (CM/S)
TIME (SEC)

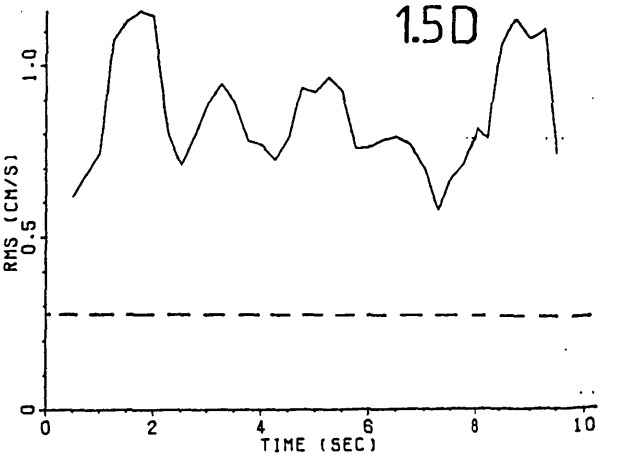
RMS (CM/S)
TIME (SEC)

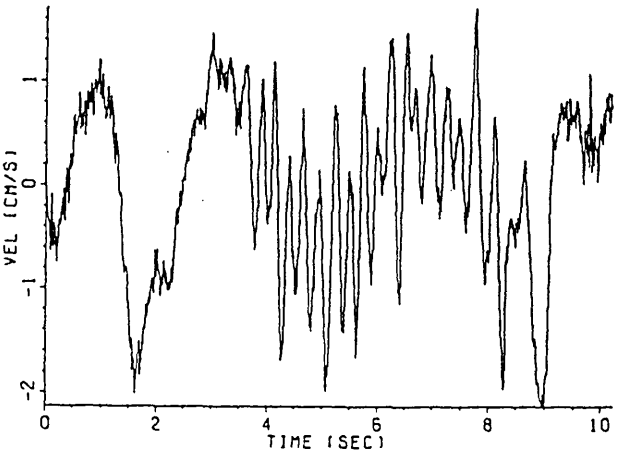
VEL (CM/S)
TIME (SEC)

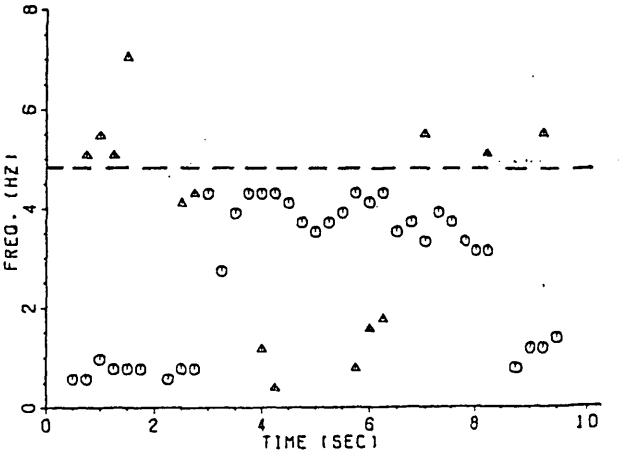
FREQ. (HZ)
TIME (SEC)

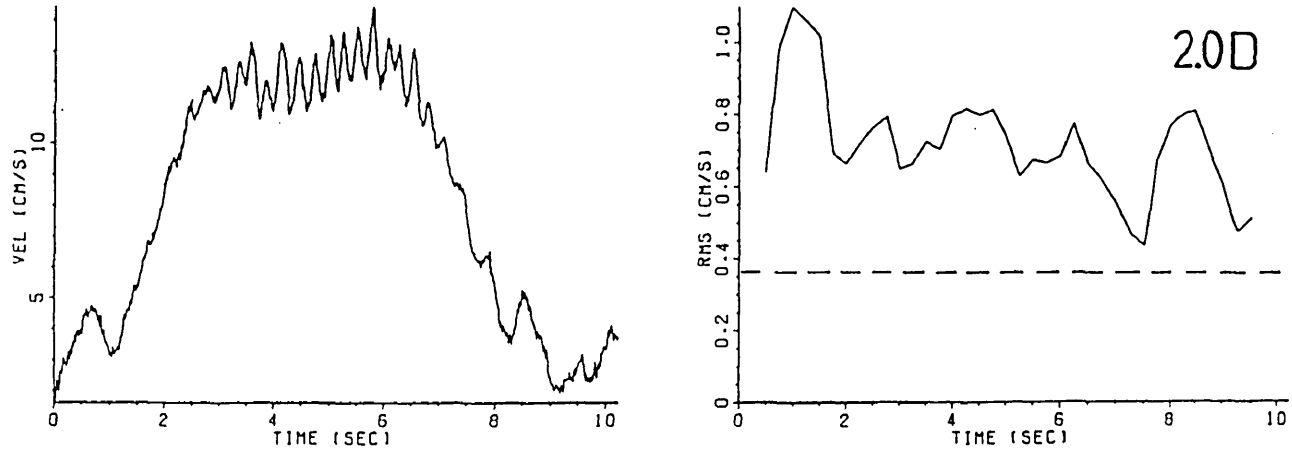
VEL (CM/S)
TIME (SEC)

2.0D
RMS (CM/S)
TIME (SEC)

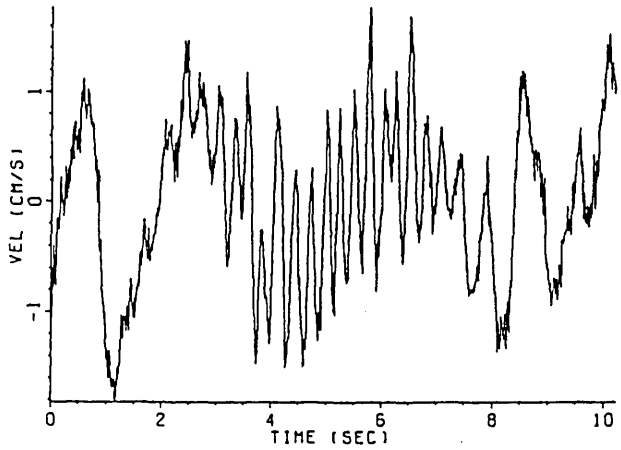
VEL (CM/S)
TIME (SEC)

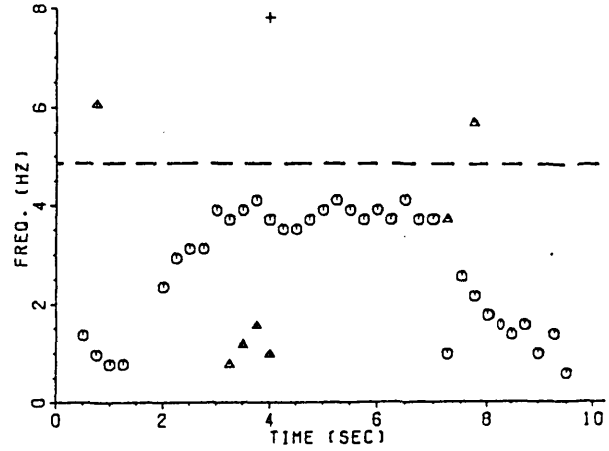
FREQ. (HZ)
TIME (SEC)

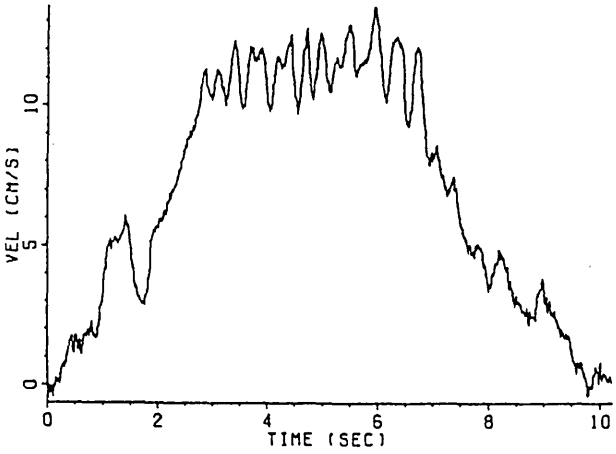
VEL (CM/S)
TIME (SEC)

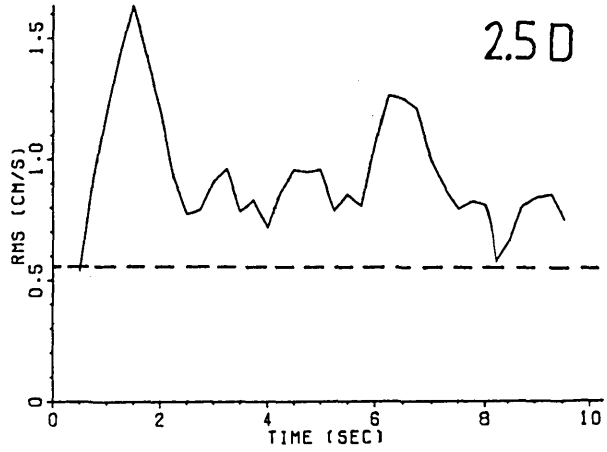
2.5D
RMS (CM/S)
TIME (SEC)

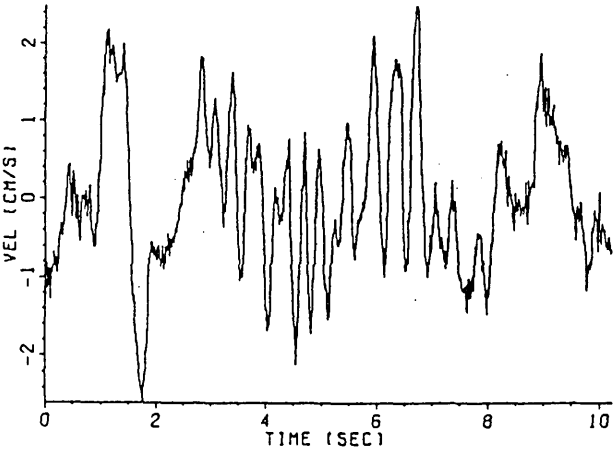
VEL (CM/S)
TIME (SEC)

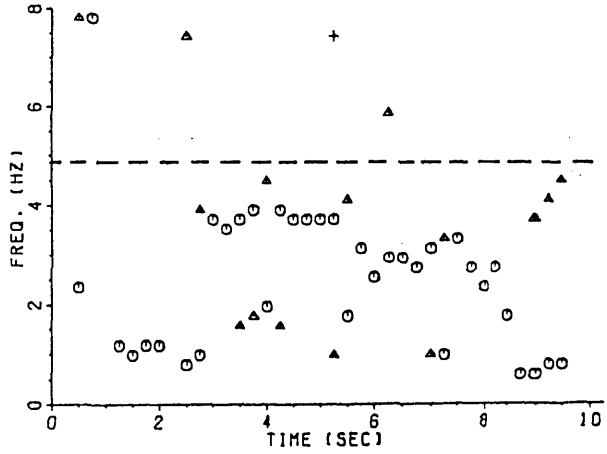
FREQ. (HZ)
TIME (SEC)

is observed. The excitation signal, amplified by approximately a factor three, is seen to be superimposed on the undisturbed flow velocity fluctuations. The second harmonic of the fundamental forcing frequency (*cf.* § 5.1.3) is clearly visible in the spectral evolution diagram. At $x/D=1.0$, where the unforced flow exhibits distinct fluctuations of about 5 Hz during peak flow rate the resonance phenomenon is more pronounced. In the acceleration phase, the fluctuations lock onto the half harmonic of the excitation and then switch discontinuously to the fundamental in late acceleration. The amplification of the forcing signal has doubled to a factor six. In late deceleration, the locking-on is lost and a large scale disturbance is observed that also exists in the unforced flow. The excitation is further amplifed at $x/D=1.5$, and the large vortical structures formed at the forcing frequency appreciably affect the mean flow $U_0(t)$ — the peak velocity is almost 10% lower. Again, the flow initially responds at half the fundamental forcing frequency and switches discontinuously to the fundamental. The spike at $t=5.6$ s indicates the passage of a single vortical structure close to the measuring position. Beyond $x/D=1.5$, the flow loses its spectrally distinct character as the large vortical structures begin to interact violently with the boundary wall.

In flow through the smooth constriction (*figure* 3.14*b*), the amplification of the excitation is far more gradual. At $x/D=2.0$, the flow resonates at the fundamental forcing frequency $f_f=2.5$ Hz, but fluctuation levels only amplify from 0.6 to 0.9 cm s^{-1}. At $x/D=3.0$, the decelerating flow resonates more strongly and the mean velocity is somewhat lower. A change of phase occurs during late acceleration, together with a sudden increase in fluctuation amplitude. In the deceleration phase, gradual loss of tracking is observed. At $x/D=4$, the fluctuations have grown further, and the same phase discontinuity is seen. In addition, the dominant spectral response is clearly not at the forcing frequency but below, and in late deceleration the 'quasi-locking' is lost.

The forcing frequency for the nonsymmetric stenosis geometry is 3 Hz, *i.e* below the dominant natural frequency of the flow instability. Near the constriction, at $x/D=1.2$, the fluctuations are not much greater than in the unforced case, but they are clearly locked to the excitation. Again, the second harmonic of the fundamental forcing frequency is present. The behaviour is similar at $x/D=1.5$. The fluctuations barely grow with downstream distance. At $x/D=2.5$, flow regulation during peak flow together with the gradual loss of locking are well illustrated.

To conclude this section, half-harmonic locking-on, although observed for both the smooth symmetric constriction and the orifice plate in steady flow, is only seen for the orifice plate in pulsatile flow. This suggests that, because the flow separation point is fixed for the

orifice plate geometry, the spectral evolution of the flow instability downstream of the orifice plate in pulsatile flow is explained to first approximation by quasi-steady analysis. Note, however, that this does not apply to the intensity of oscillatory flow velocity fluctuations.

5.2.1.5 Transient Flow

The significance of poststenotic flow velocity fluctuations that are considerably larger in pulsatile flow than what is predicted by quasisteady analysis has been stressed repeatedly and possible links with 'starting vortices' have been hinted at. These vortices are an intrinsic feature of jet flows started from rest into an initially irrotational fluid[6]. The starting vortex generated during the start-up flow transients possesses significantly greater vorticity than the vortical structures formed by the ensuing shear layer roll-up. Starting vortices have been identified as a potential source of error in orifice-type flowmeters under pulsatile flow conditions (Bajura and Pellegrin 1975) and were associated with the start-up structures in poststenotic flow (Khalifa and Giddens 1978).

Starting flow through a locally constricted tube — as a limiting form of accelerated stenotic flow on greatly reduced time scales — can provide valuable information about the nature of transients of flow velocity fluctuations in pulsatile poststenotic flows. Considering for the moment starting flow in a circular rigid pipe that settles to fully developed Poiseuille flow after transients have died out, it is readily appreciated that, given a fast acting flow valve, the centre line velocity suffers a discontinuous jump from zero velocity to half its steady state value immediately after the valve opening. This scenario is identical, in reversed time, to stopping flow (Parker 1977). The pressure wave caused by the valve action sets up a flow of uniform velocity which, on a much longer time scale, then develops into the parabolic profile. This has been verified experimentally for unobstructed tube flow[7] (*figure* 3.15). The velocity signal overshoot observed in starting as well as stopping flow is most probably due to mechanical transients of the solenoid valve.

The same scenario applies to impulsively started poststenotic flow. *Figure* 3.16*a* gives results of centreline axial velocity measurements taken 2 D downstream of the 50% orifice plate. The starting vortex is found to be a highly reproducible feature of this transient flow, as can be seen from the two exemplary recordings. For times $t > 2.7$ s, the fluctuations become

[6] An aesthetically very pleasing example of a starting vortex is shown in the excellent flow visualisation on the front cover of Batchelor's *An Introduction to Fluid Dynamics.*

[7] Interestingly, the velocity discontinuity offers an immediate check of how well developed the flow is.

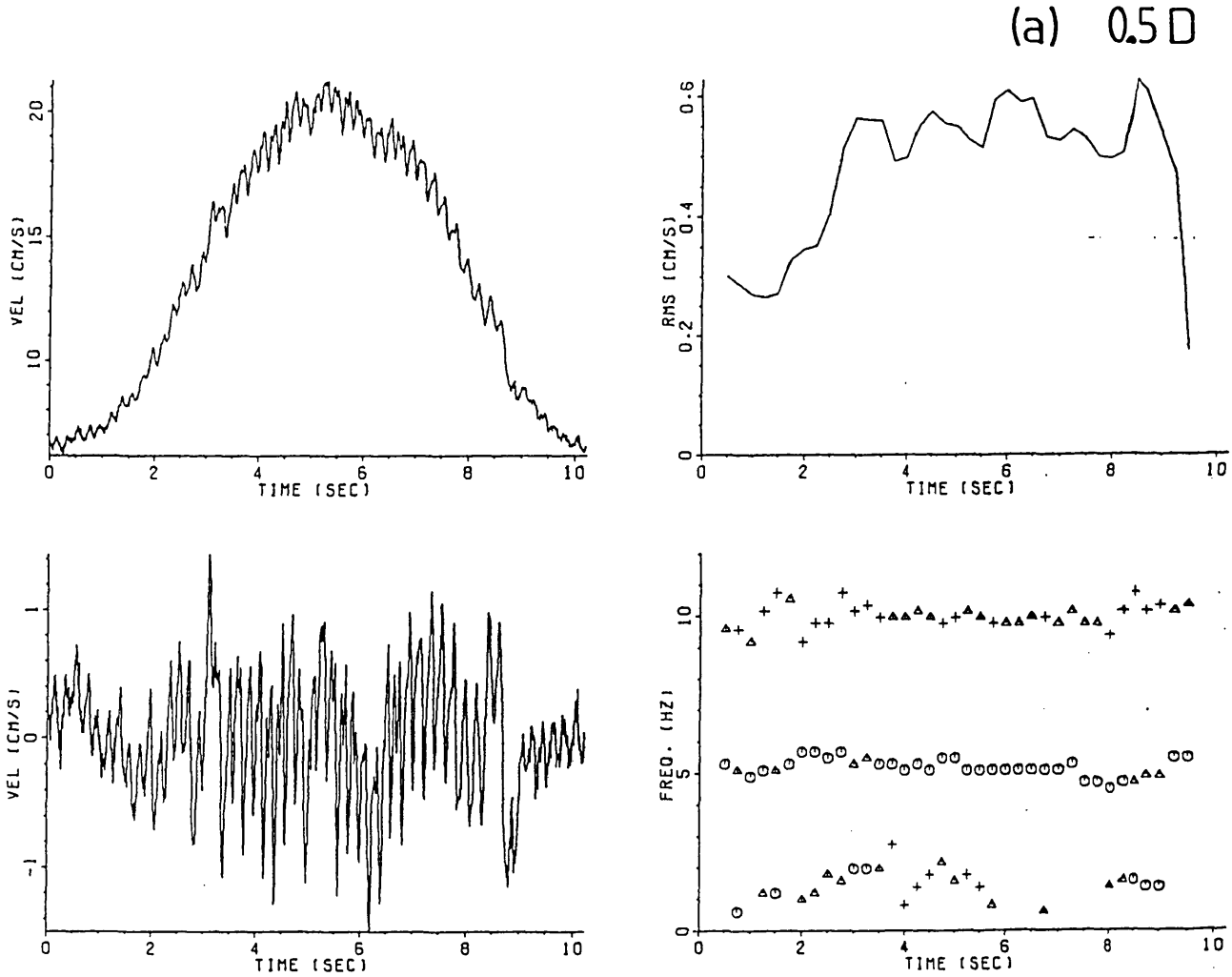

Figure 3.14 Forced axial velocities in pulsatile poststenotic flow. Flow conditions and measurement positions as for *figure* (3.13). (*a*) Orifice plate, f_f=5.0 Hz. (*b*) Contoured symmetric constriction, f_f=2.5 Hz. (*c*) Nonsymmetric constriction, f_f=3.0 Hz.

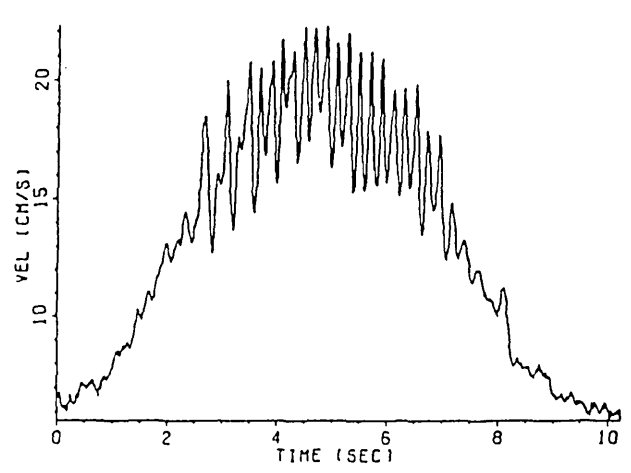
VEL (CM/S)
TIME (SEC)

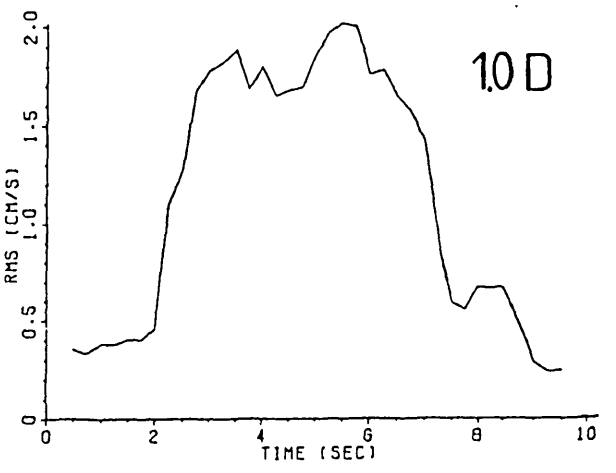
1.0 D
RMS (CM/S)
TIME (SEC)

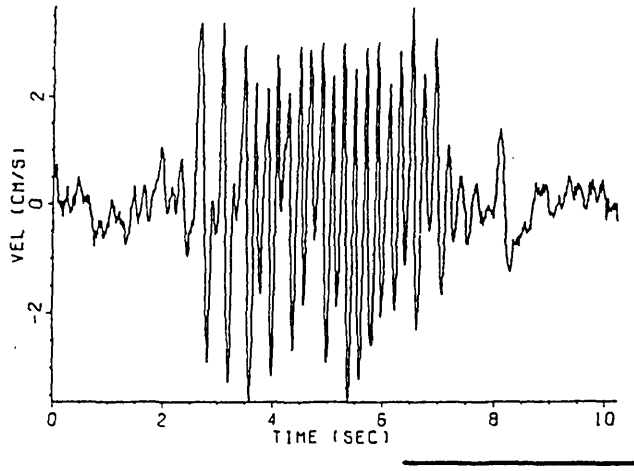
VEL (CM/S)
TIME (SEC)

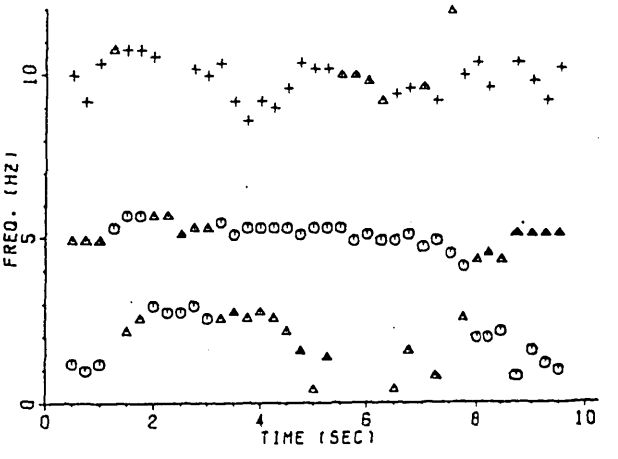
FREQ. (HZ)
TIME (SEC)

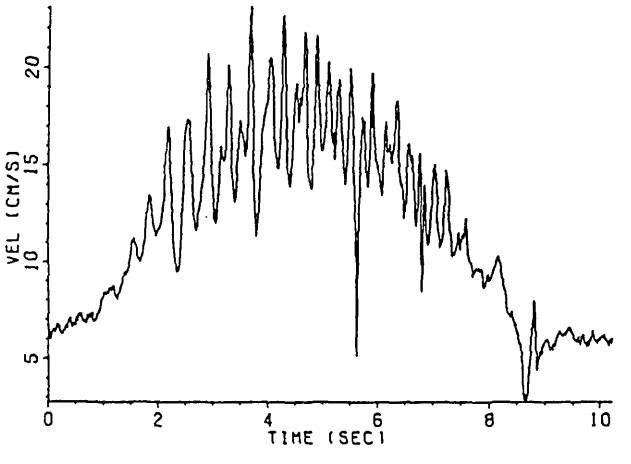
VEL (CM/S)
TIME (SEC)

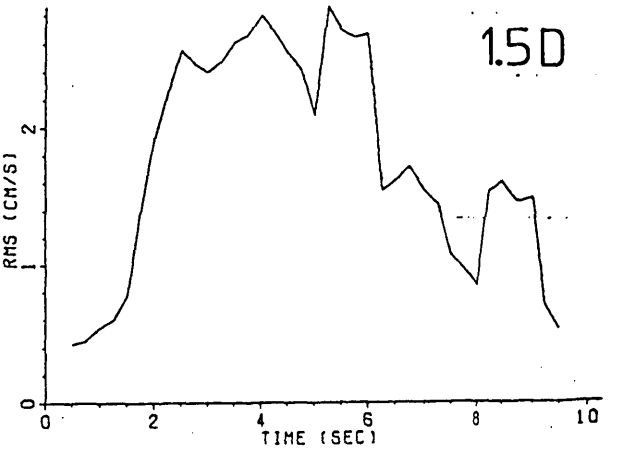
1.5 D
RMS (CM/S)
TIME (SEC)

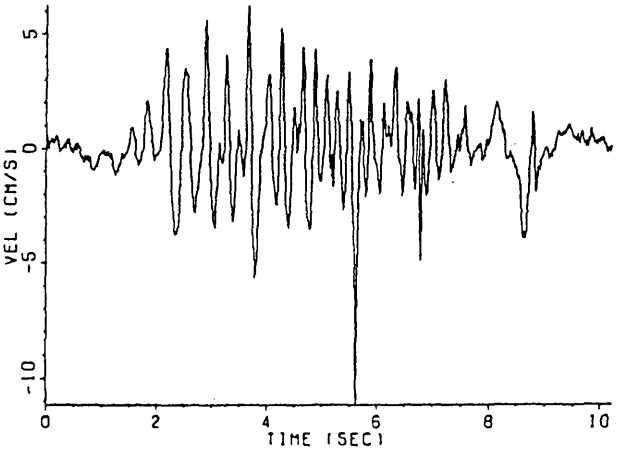
VEL (CM/S)
TIME (SEC)

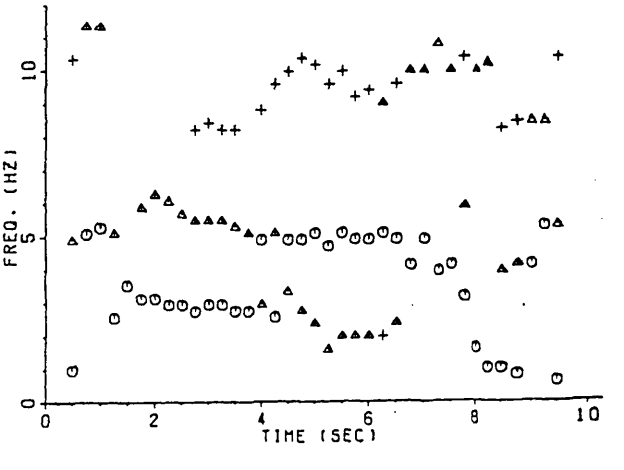
FREQ. (HZ)
TIME (SEC)

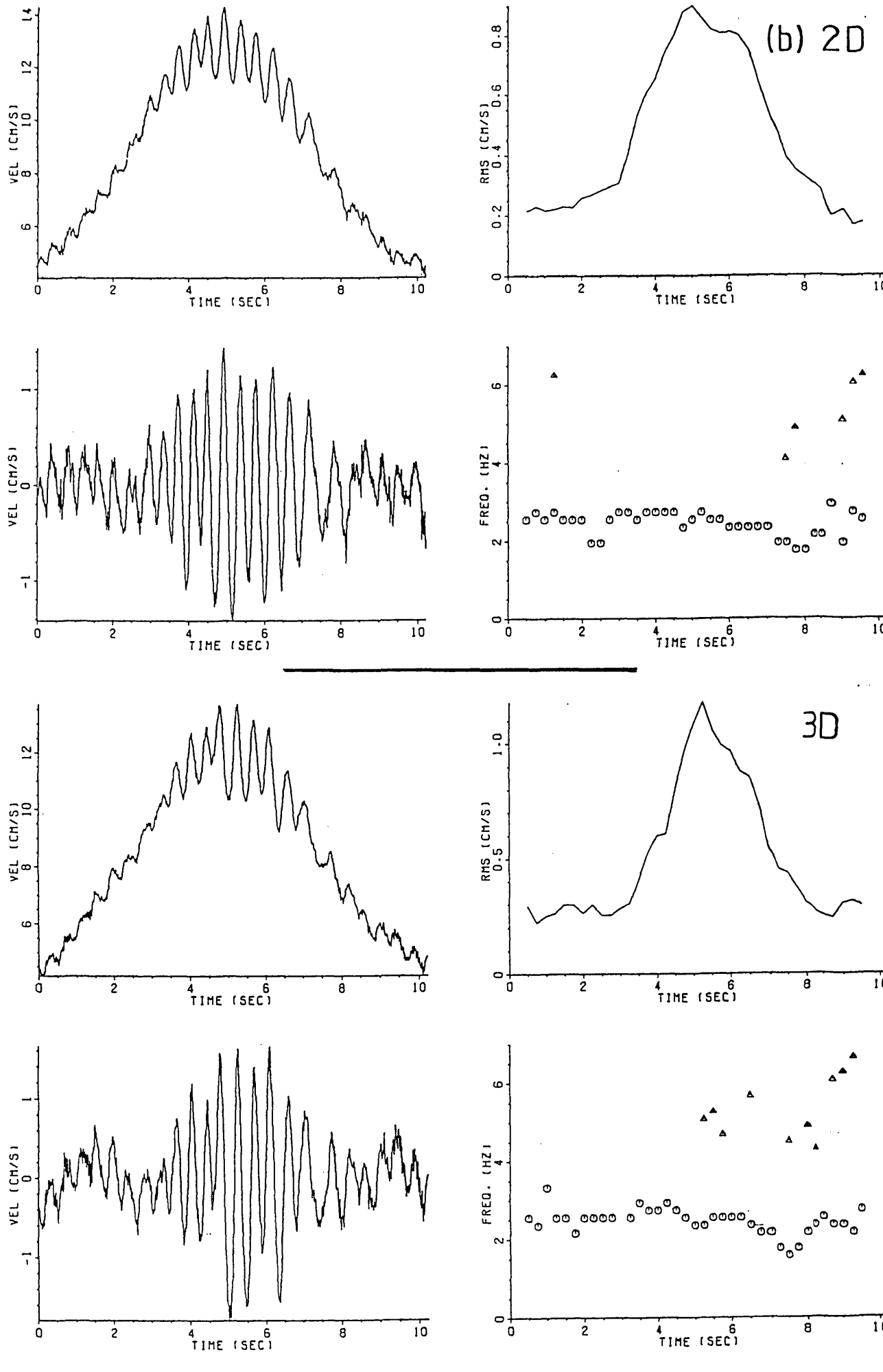
(b) 2D
3D
VEL (CM/S)
RMS (CM/S)
FREQ. (HZ)
TIME (SEC)

4D

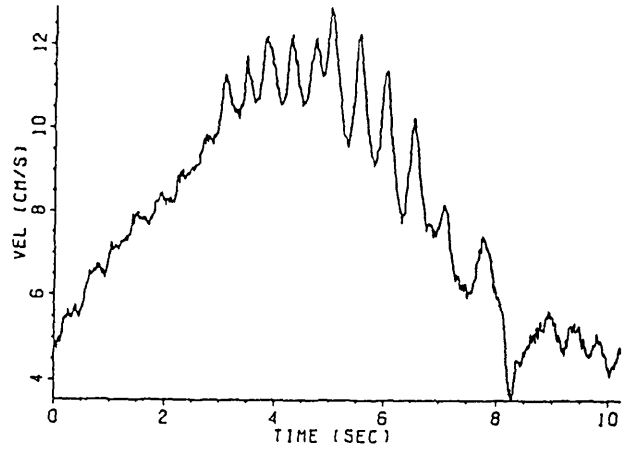
VEL (CM/S)
TIME (SEC)

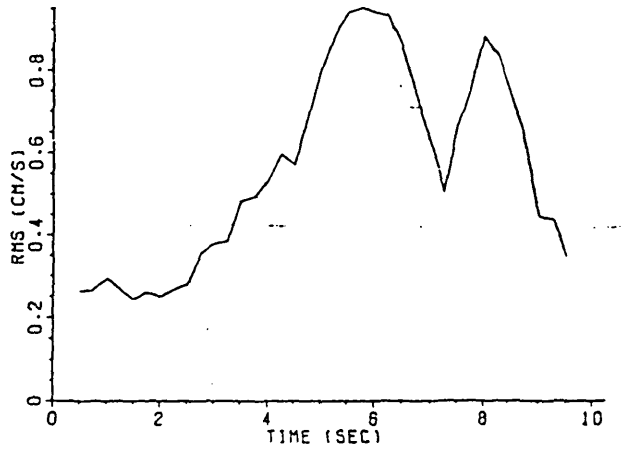
RMS (CM/S)
TIME (SEC)

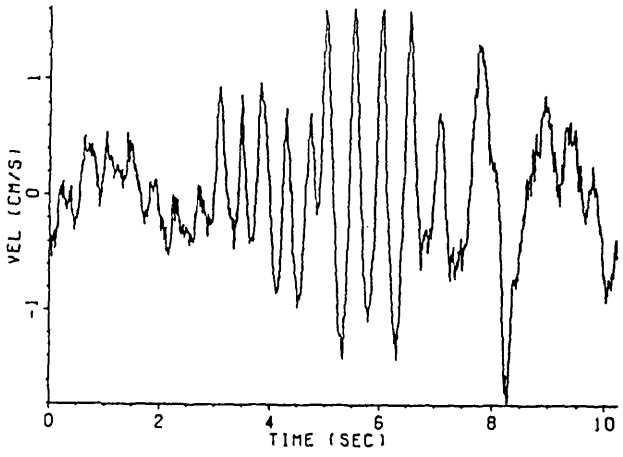
VEL (CM/S)
TIME (SEC)

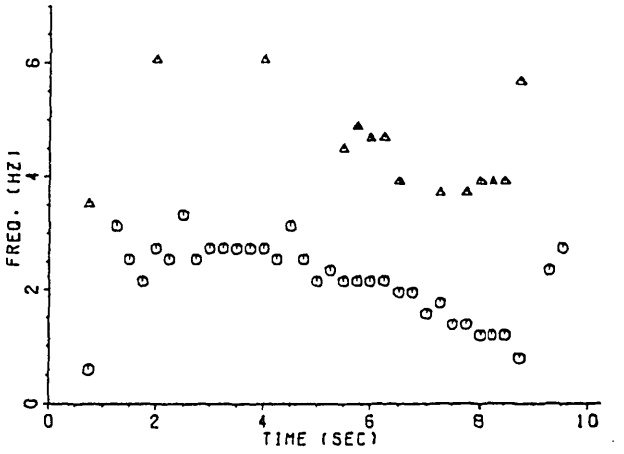
FREQ. (HZ)
TIME (SEC)

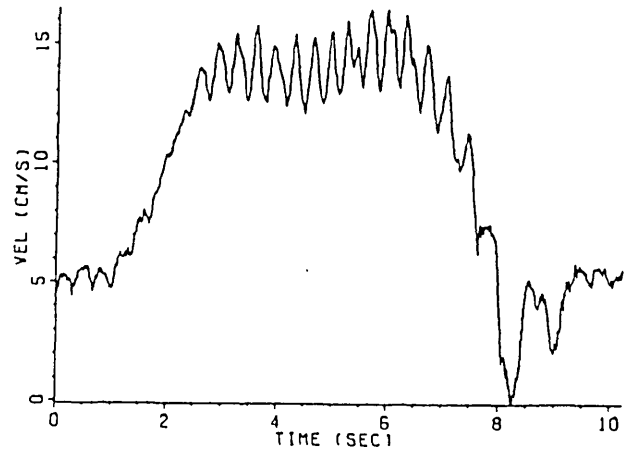
VEL (CM/S)
TIME (SEC)

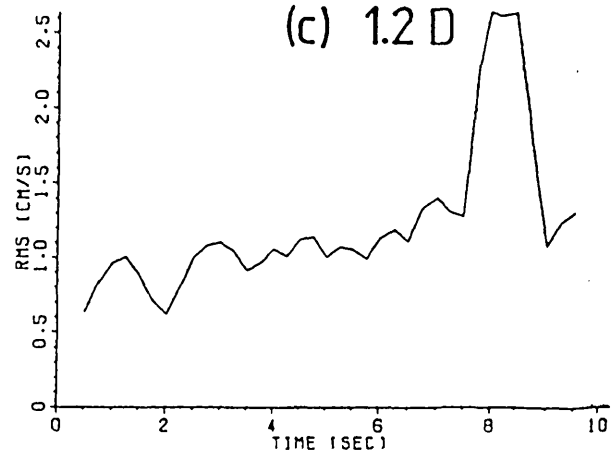
(c) 1.2 D
RMS (CM/S)
TIME (SEC)

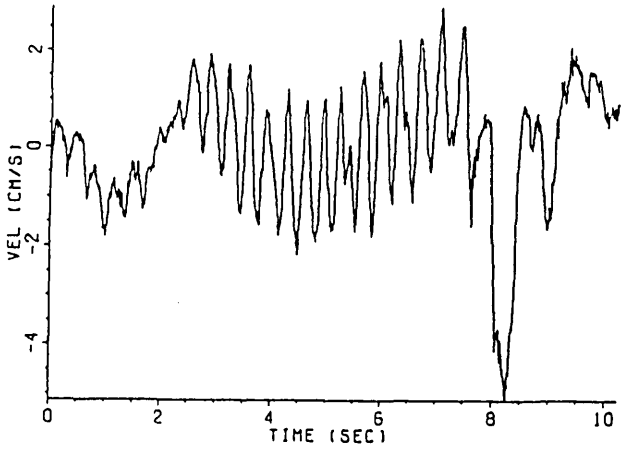
VEL (CM/S)
TIME (SEC)

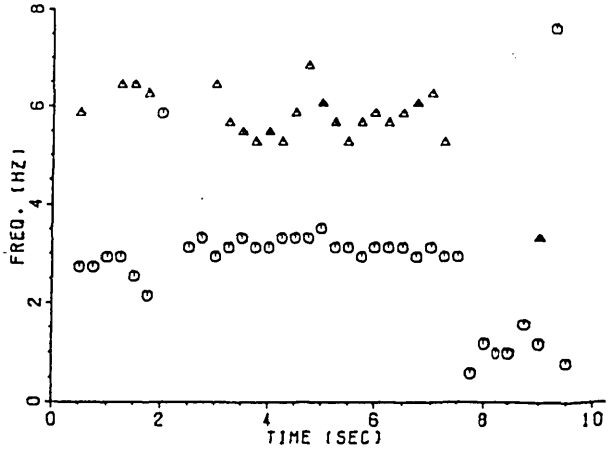
FREQ. (HZ)
TIME (SEC)

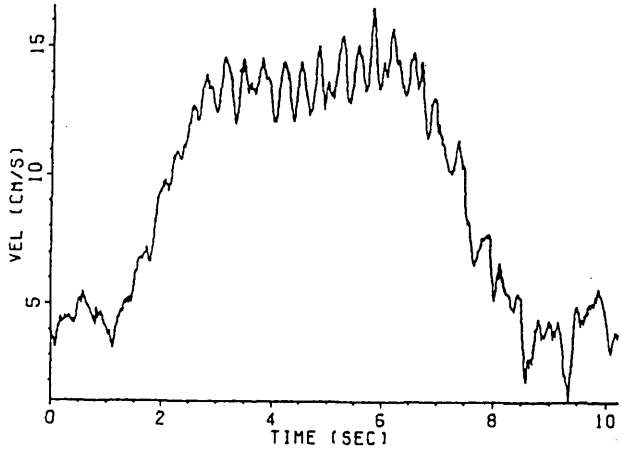
VEL (CM/S)
TIME (SEC)

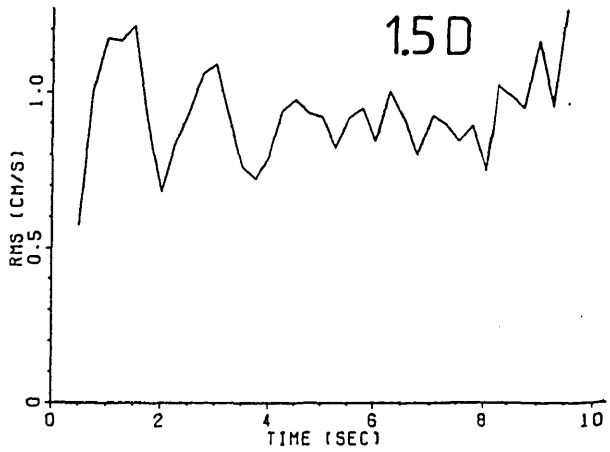
1.5 D
RMS (CM/S)
TIME (SEC)

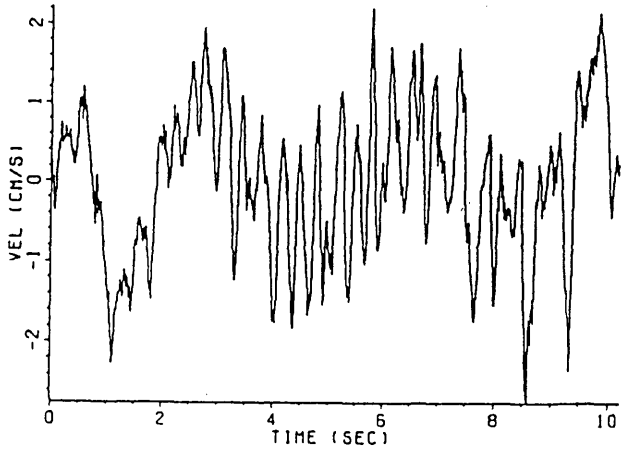
VEL (CM/S)
TIME (SEC)

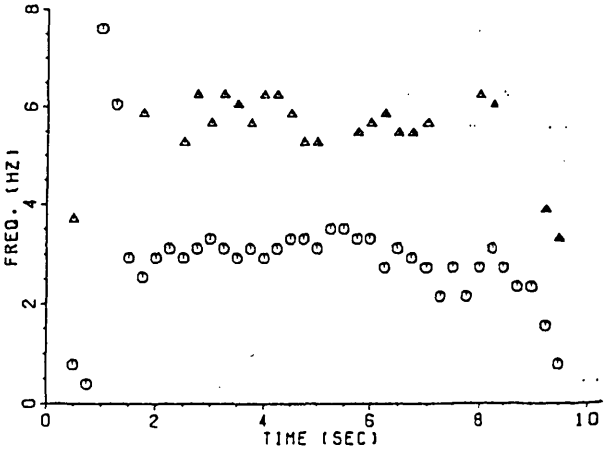
FREQ. (HZ)
TIME (SEC)

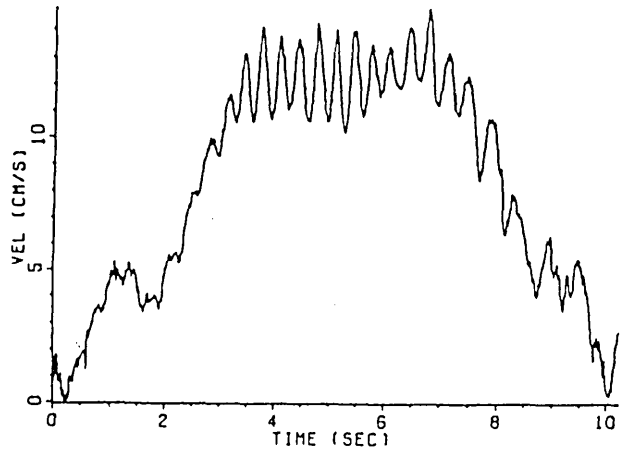
VEL (CM/S)
TIME (SEC)

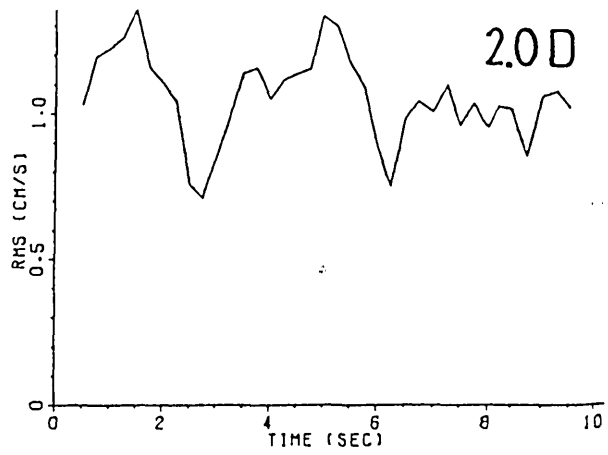
2.0D
RMS (CM/S)
TIME (SEC)

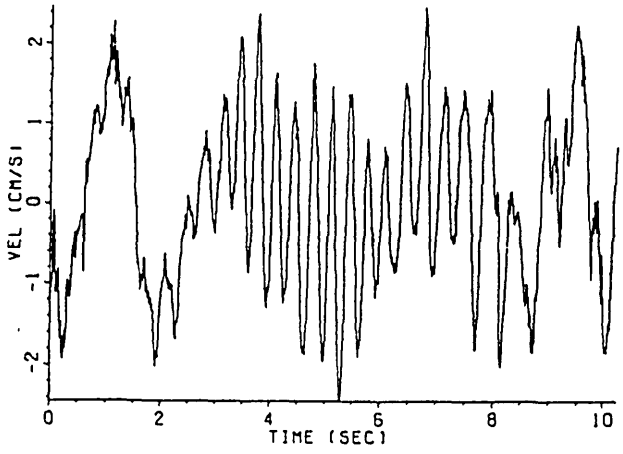
VEL (CM/S)
TIME (SEC)

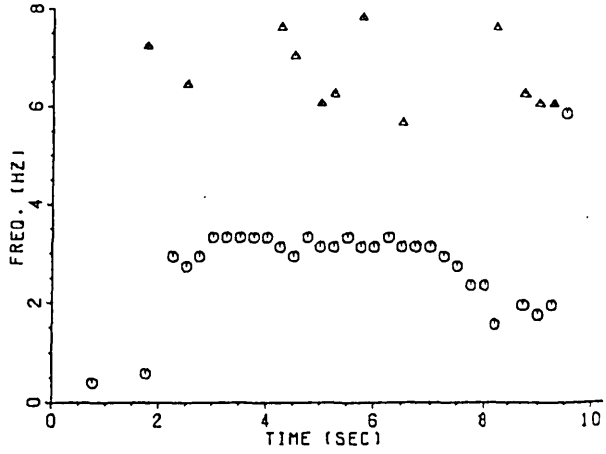
FREQ. (HZ)
TIME (SEC)

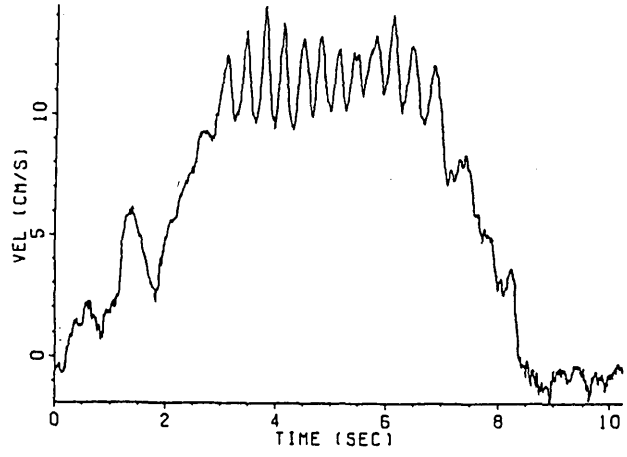
VEL (CM/S)
TIME (SEC)

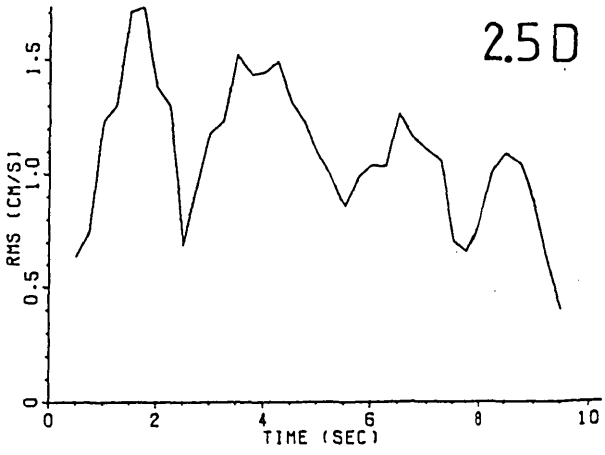
2.5D
RMS (CM/S)
TIME (SEC)

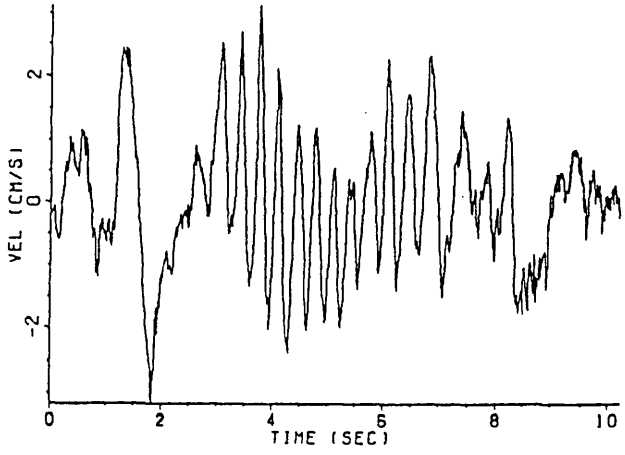
VEL (CM/S)
TIME (SEC)

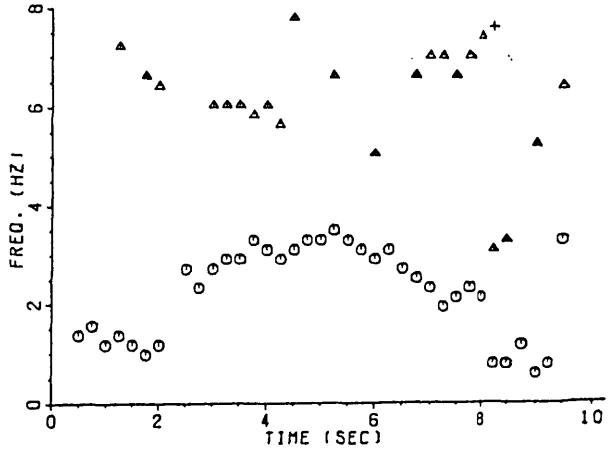
FREQ. (HZ)
TIME (SEC)

more variable in nature suggesting that the flow behind the starting structure is already sensitive to background noise. In *figure* 3.16*a*1, for example, the starting vortex is followed by a series of spiky velocity excursions of similar appearance, and in the interval $4\ \mathrm{s} > t > 8\ \mathrm{s}$ by a train of very organised vortical structures. Eventually, the flow settles to the characteristic broadband fluctuations. Alternatively, the transient structures immediately behind the starting vortex can be much less developed (*figure* 3.16*a*2) and, although fluctuations in the time interval $4\ \mathrm{s} > t > 8\ \mathrm{s}$ are greater compared to what is observed once the transients have died out, their appearance is much less organised.

In conclusion, the flow transients that are considered of potential relevance to pulsatile flow phenomena are those succeeding the initial large vortex. This starting vortex must be associated with the very short time scale transient *i.e.* the sudden rise in the mean velocity, whereas the following vortex structures, in particular the ones in the interval $4\ \mathrm{s} > t > 8\ \mathrm{s}$, are related to the much longer time scale of transition to fully developed laminar flow. Regarding the transient fluctuations of *figure* 3.16*a*, one may speculate as to the regulating effect of time-varying mean velocities. A steadily increasing mean velocity ('ramp') possibly provides a phase reference for the shear layer instability *via* parametric interaction and deserves further investigation.

Finally, stopping flow through a locally constricted tube — as a limiting form of decelerated stenotic flow on greatly reduced time scales — can give clues about the type of stopping structures to be expected in the late deceleration phase of poststenotic pulsatile flow. By the same mechanism that underlies impulsively started Poiseuille flow, the centre line axial velocity suffers a discontinuity from the steady state value to half that value (*figure* 3.15), and a similar sudden drop is observed in poststenotic flow (*figure* 3.16*b*). The overshooting is again due to the valve shutting transients. Compared to the immediate velocity decay in unobstructed laminar flow, the orifice flow is characterised by some distinct acitivity in the first 1.5 seconds. Two extreme examples of stopping poststenotic flow are shown in *figure* 3.16*b*. In the first case, the stopping structure is very pronounced, whilst in the second example the stopping activity is identified by the change in the rate of velocity decay. Typically, the stopping structure is confined to approximately the first 1.5s, and will lie between the two extremes. The variability in this structure is presumably due to the state of the flow just before stopping. Curiously, the core flow reverses slightly before approaching zero velocity. This is thought to be related to the stopping vortex shed upstream of the orifice plate.

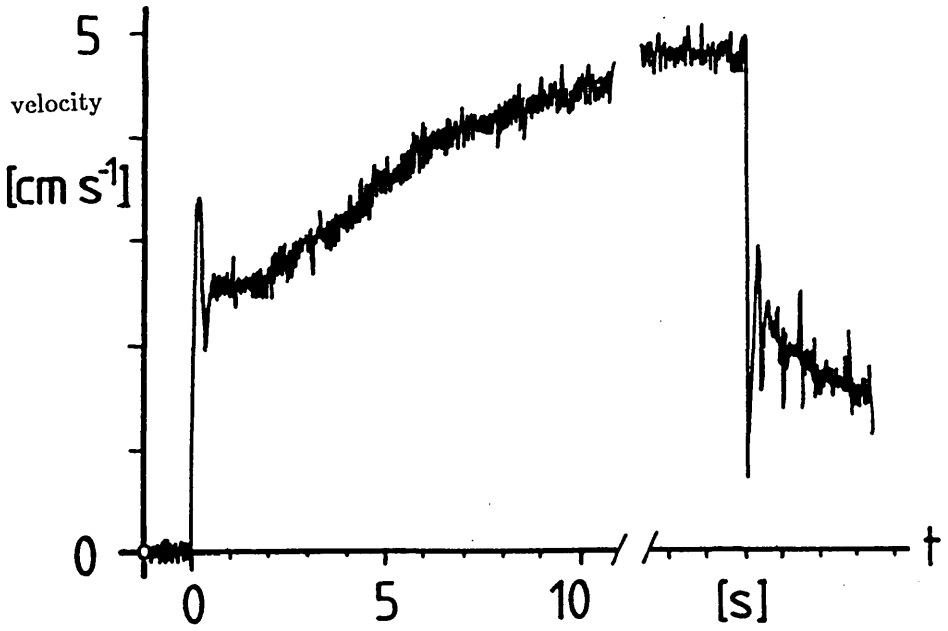

Figure 3.15 Impulsively started and stopping flow in a straight tube. The centreline axial velocity is shown. The steady flow Reynolds number is Re=780. The large spikes are due to valve mechanical transients.

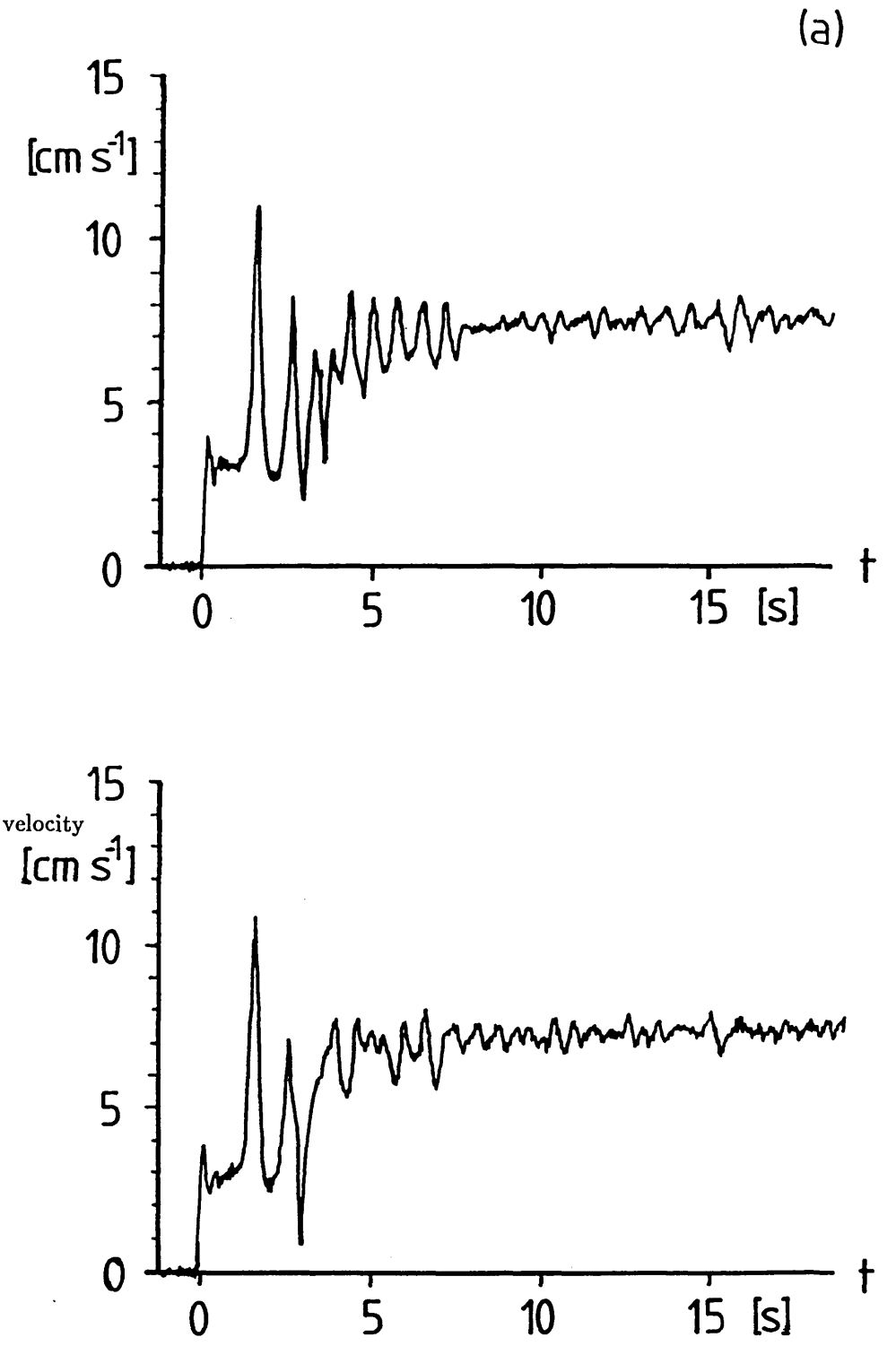

Figure 3.16 Examples of (*a*) starting and (*b*) stopping flow downstream of the orifice plate. The centreline axial velocity 2 *D* downstream is shown. The steady flow Reynolds number is $Re=780$.

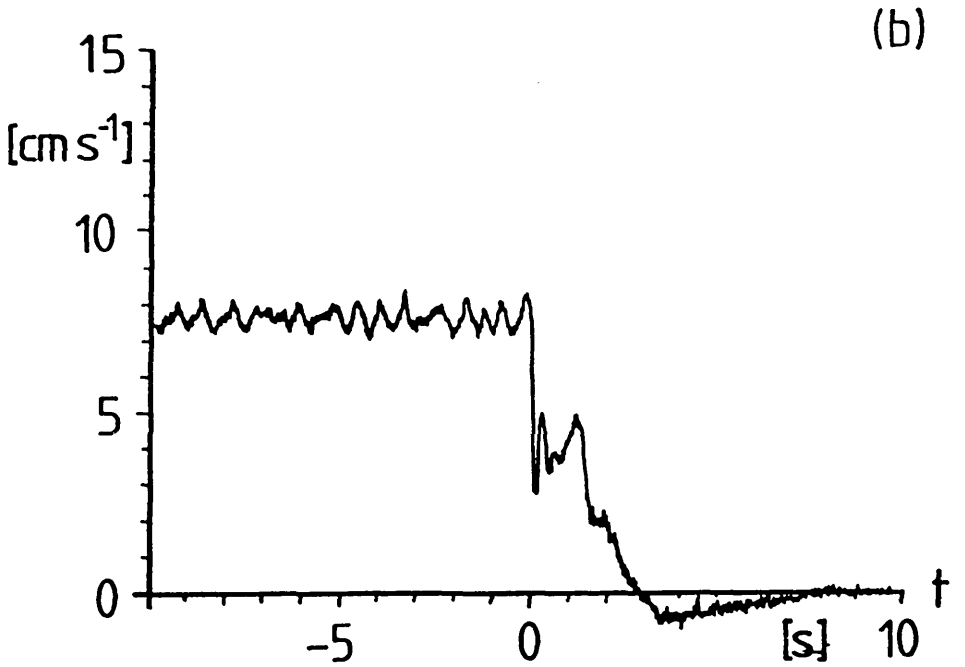
(b)
15
[cm s-1]
10
5
0
-5
0
[s]
10
t

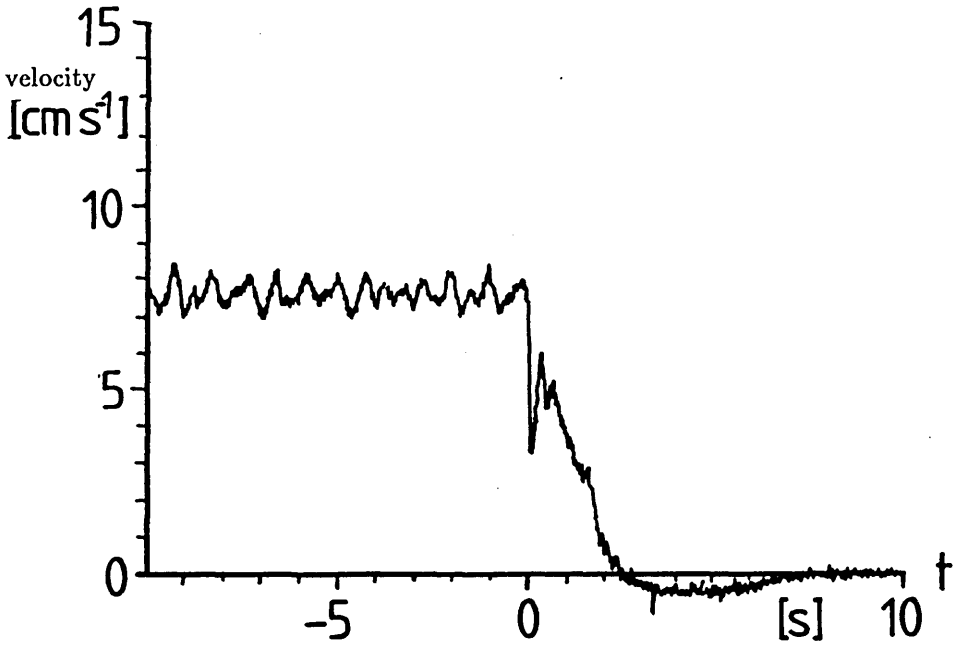
15
velocity
[cm s-1]
10
5
0
-5
0
[s]
10
t

The stopping structure is not unlike what is observed in pulsatile flow, particularly behind the orifice plate. Similar experiments for the smooth constriction geometries would be instrumental in this regard.

5.2.2 Flow Visualisation

Further experimentation with the experimental apparatus is required before the flow visualisation technique employed here can produce quantitative results. The successful visualisation is marred by, amongst other factors, the inadequacy of the light source and the scatterers. The light source is very low power and not matched to the size and scattering properties of the seeding particles. The scatterers are highly unevenly distributed in the flow and show a tendency to settle out. Flow visualisation results are included here mainly because the visualisation shows flow phenomena that are suspected to be largley unrelated to the shear layer instabilities investigated so far.

The flow visualisation is by no means comprehensive. Emphasis is on the nonsymmetric stenosis geometry for which a complete pulsatile flow cycle was recorded. Invariably, the results have a somewhat anecdotal character but they are supported by systematic studies of two dimensional flows of comparable geometry (Betram and Pedley 1983, Armaly *et al* 1983).

5.2.2.1 Steady Flow

Flow visualisation results for steady flow through the contoured symmetric and nonsymmetric model stenoses are shown in *plate* 3.1. The Reynolds number is the same for both geometries, $Re=1470$. The nonuniform seeding is immediately apparent, and so is the inadeqate particle size and the seeding density. Furthermore, the illumination is not uniform and only in the far downstream region of the flow past the nonsymmetric stenosis model – which protrudes from the upper wall – the multi-exposure character of the technique becomes visible. Note finally the artefact caused by reflections at the tube curvature and seen on all photographs as a bright line parallel to the upper wall.

The bright elongated patch just downstream of the symmetric constriction (*plate* 3.1 *a*) shows particles that are progressivley deposited in the separated flow region. The flow itself has a wavy core flow structure with vortices attached, not symmetrically, to either wall. Visual inspection of the steady flow showed that the vortices retain a relatively fixed position at the upper and lower wall and, if some form of axisymmetry is assumed, the two prominent vortices may in fact be connected through a ring-like structure.

A series of three successive visualisations of nonsymmetric-stenosis flow is shown in *plate* 3.1*b*, *c* and *d*, with the stenosis protruding from the upper wall. The core flow describes a sinuous path and large vortices are observed at either wall. Surprisingly, in the immediate flow separation region no large 'primary' vortex is seen. The vortex further downstream at the upper wall seems at times to interact with a neighbouring smaller vortex, and the vortex attached to the lower wall is clearly seen to split up into two vortices. The succession of photographs suggests that the vortices do not appreciably change their position.

Somewhat unexpectedly, the flow velocity fluctuations associated with the separated shear layer instability are virtually absent, compared to the more outstanding flow characteristics, the large vortices. Upon closer inspection, some small scale activity is identified in the region $x/D=1$ to $x/D=2$ of the separated shear layer. The scale is very small yet comparable to the type of early shear layer roll-up observed in dye-injection flow visualisations undertaken at an early stage of the project[8]. It is to be recalled that flow velocity fluctuations induced by the shear layer roll-up are of the order of 3% of the mean velocity for the nonsymmetric constriction, and below 1% for the contoured symmetric constrictions. This can serve as an explanation for the apparent disparity between flow velocity measurements and the visualisation.

5.2.2.2 Pulsatile Flow

Pulsatile flow past the nonsymmetric constriction is shown in *plate* 3.2. The photographs form a complete cycle of pulsation, starting with early acceleration in *plate* 3.2*a*, $t=T/8$. The peak flow is reached at $t=T/2$ in *plate* 3.2*d*, and the cycle is completed in *plate* 3.2*h* at $t=T$. The flow during acceleration is qualitatively similar to the steady flow but already more wavy (*plate* 3.2*c*). At peak flow, the wave like nature of the core flow is more pronounced but the greatest degree of 'activity' is clearly observed in early deceleration, at $t=3T/4$. This particular flow structure is already discernible at $t=5T/8$ but quickly disintegrates shortly after, at $t=7T/8$. At the minimum flow rate, apart from a small primary vortex little activity is observed and the vortex at the lower wall is scarcely visible. Again, the separated shear layer instability is obscured in the visualisation by the large vortices. Note also, that the maximum downstream position for LDV measurements is $x/D=2.5$ only, whereas vortex activity extends well beyond $x/D=4$.

These flow results are of interest for two reasons. Firstly, we are probably observing a 'vortex wave' the genesis of which does not come from the separated shear layer instability.

[8] See also Cassanova and Giddens (1978) for a visualisation of the shear layer roll-up.

Plate 3.1 Flow visualisation of steady poststenotic flow, $Re=1470$. The displayed region extends from $x/D=1$ to approximately $x/D=5.3$ downstream of the model stenosis. The pressure taps visible at the upper and lower walls are at $x/D=2$. (a) Contoured symmetric constriction. (*b*), (*c*) and (*d*). Nonsymmetric constriction, successive photographs. The protuberance is from the upper wall.

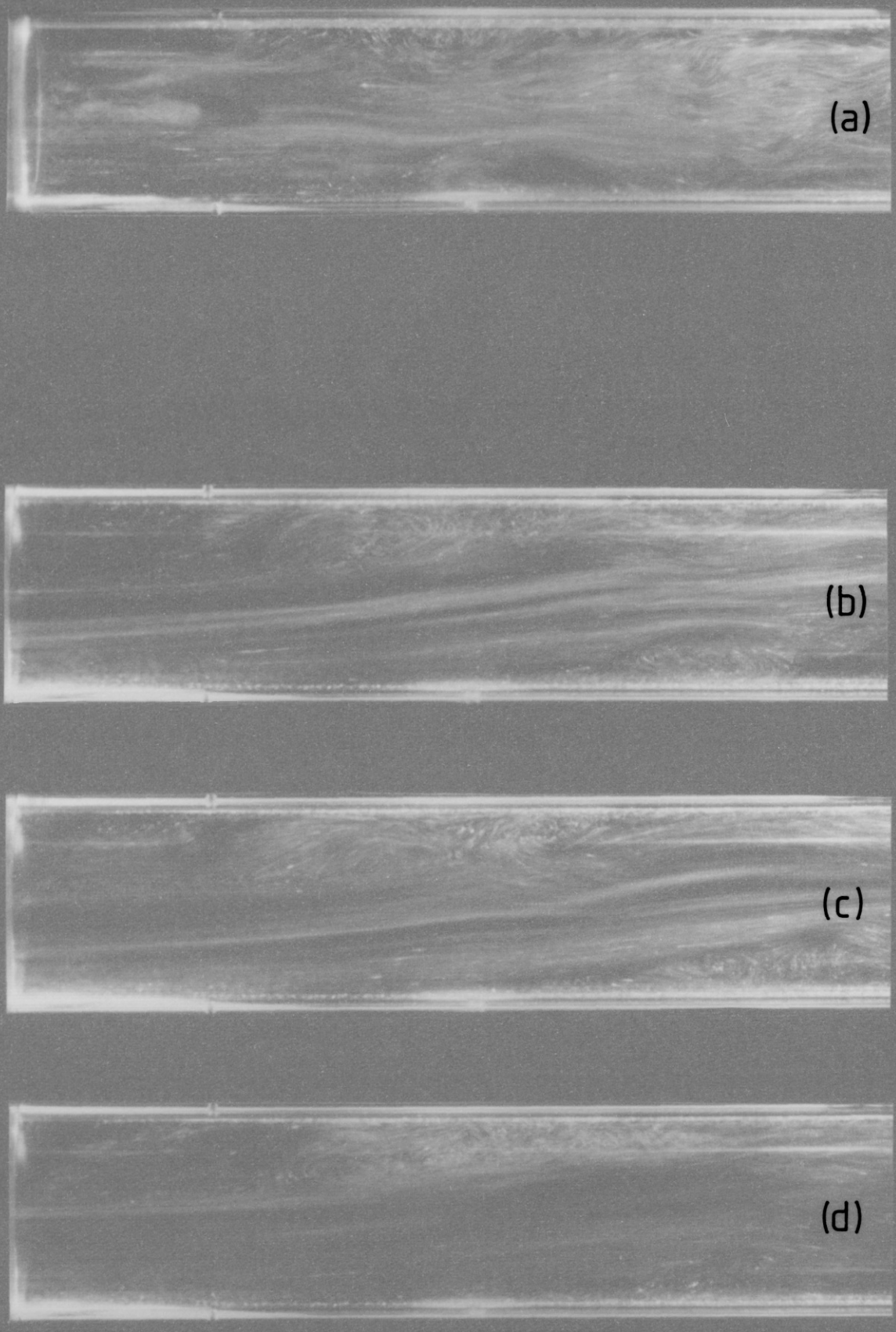
(a)
(b)
(c)
(d)

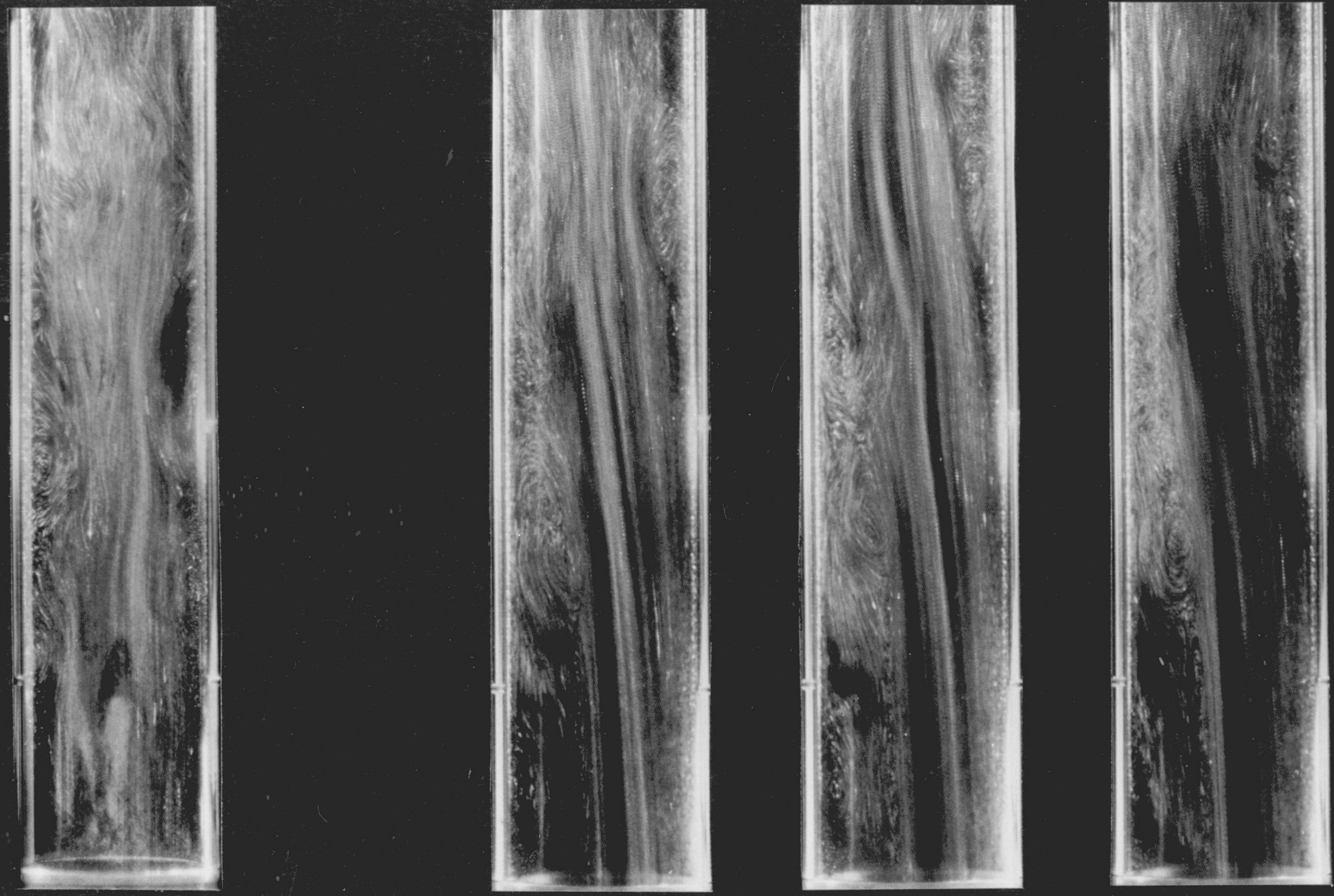

Plate 3.2 Flow visualisation of one cycle (T=10 s) of pulsatile flow downstream of the nonsymmetric model stenosis, starting with acceleration. The stenosis protrudes from the upper wall. (*a*) $t = T/8$ . . . (*h*) $t = T$.

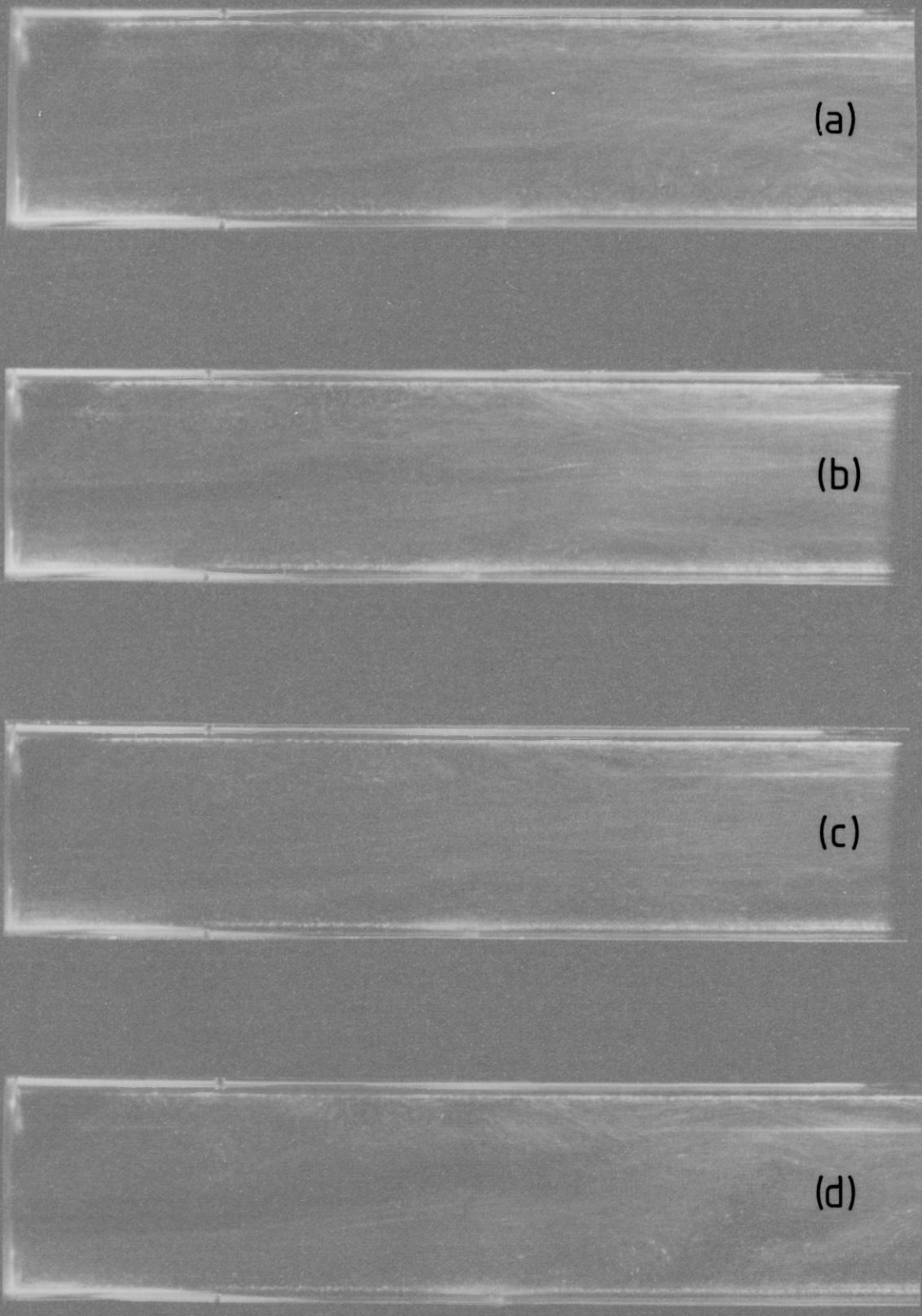
(a)
(b)
(c)
(d)

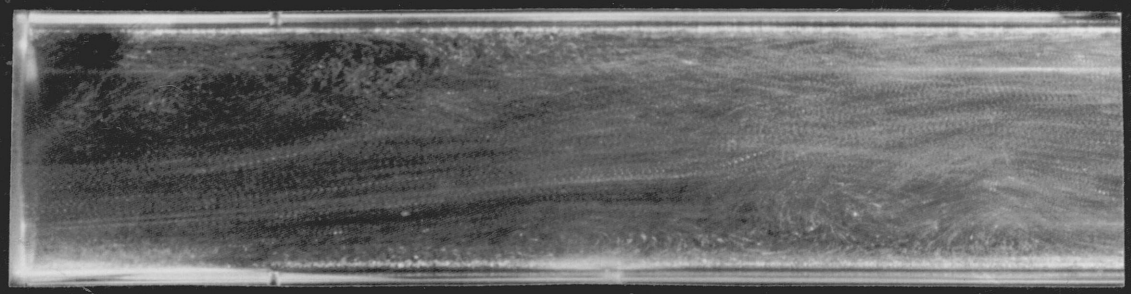

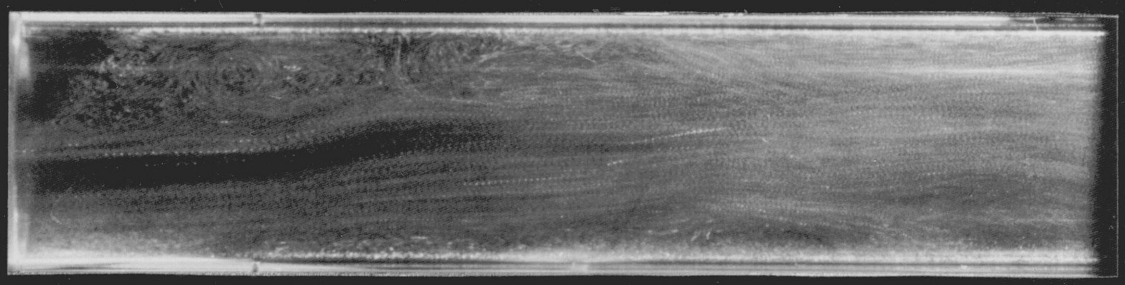

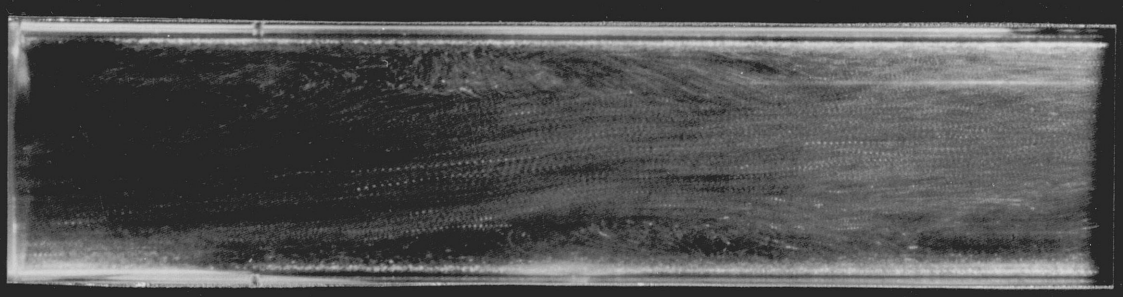

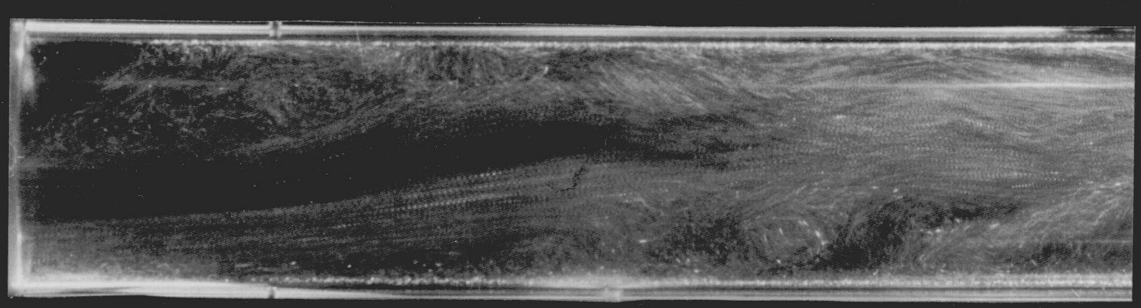

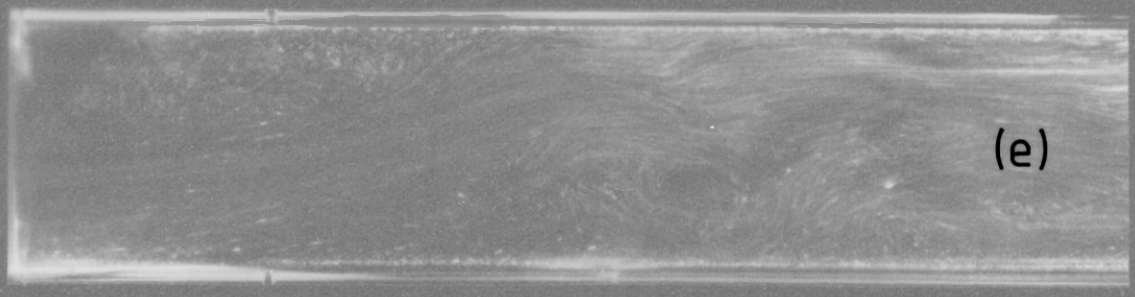
(e)

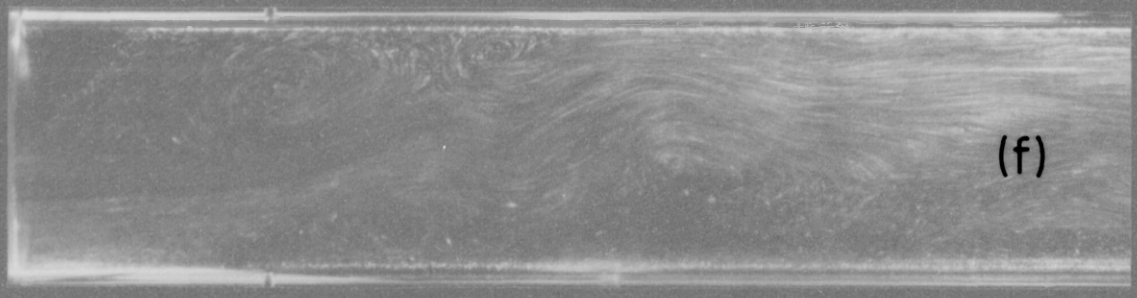
(f)

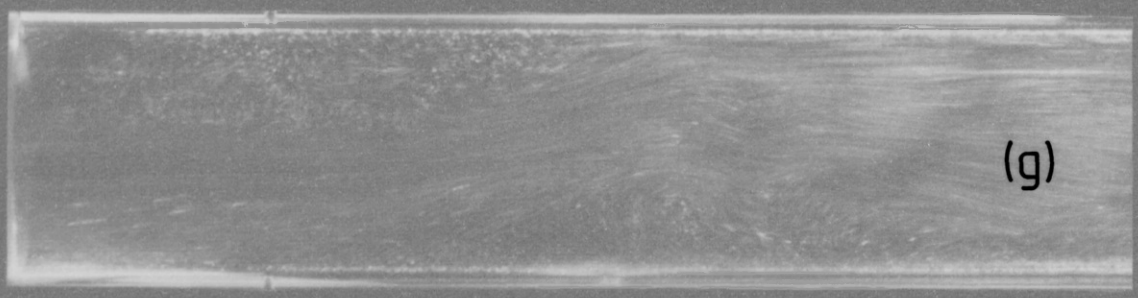
(g)

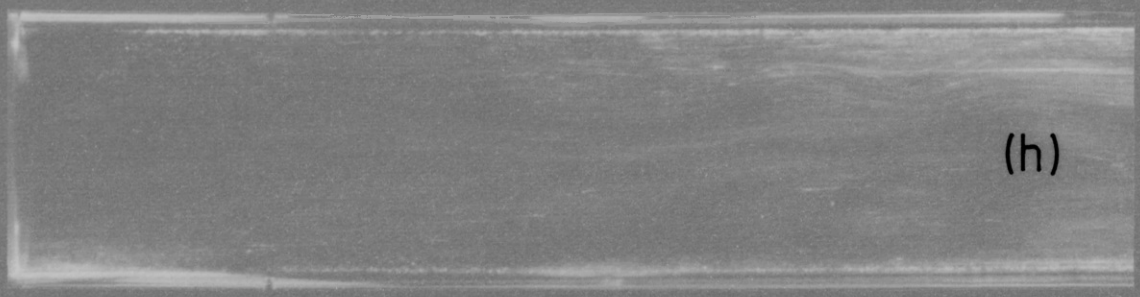
(h)

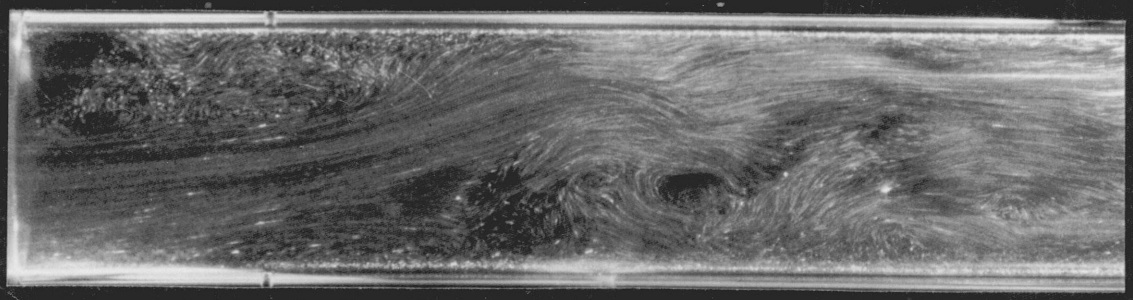

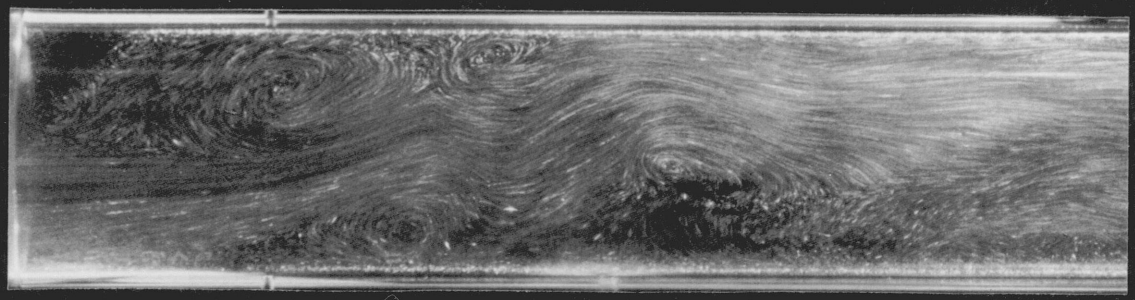

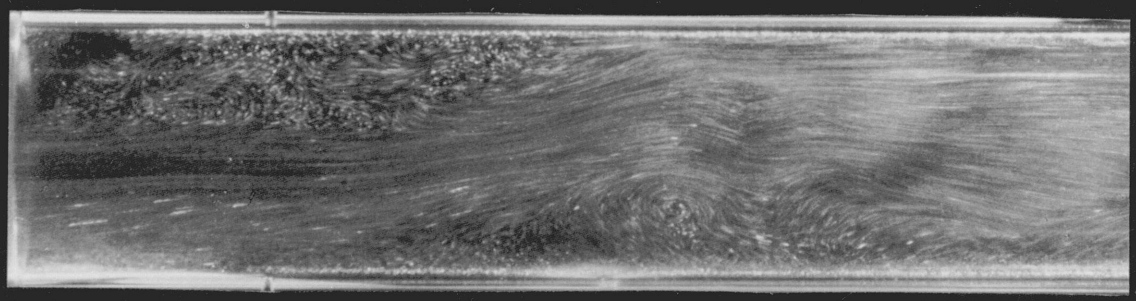

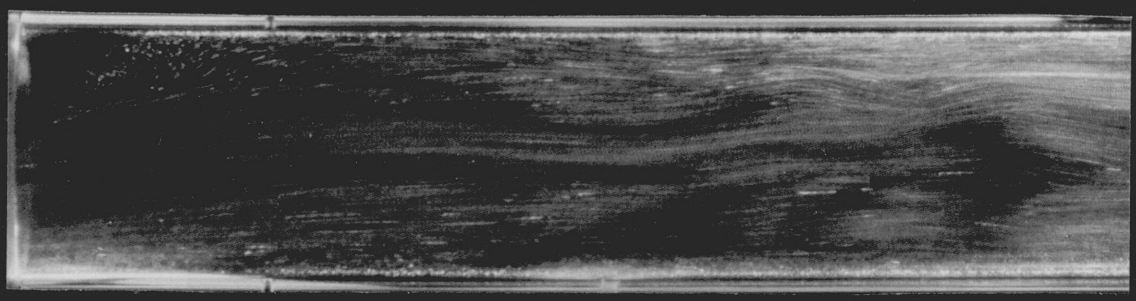

Secondly, the vortices may be important haemodynamically because the magnitude of the wall shear beneath a vortex can be very high. Importantly, the location of high wall shear can be far from the constriction causing it.

5.2.2.3 Post—Processing

The limitations of the present flow visualisation set-up have been outlined, and it is hoped that the quality of the visualisation can be improved sufficiently to allow flow field quantitation. In the mean time a preliminary investigation (Thiriet *et al* 1988) of high quality double exposure photographs of waves in channel flow (Greated and co-workers 1987) showed that the analysis of the photographs need not involve the two step process of (1) determining Young's fringes, and (2) extracting the planar flow vector, as carried out conventionally (*e.g.* Gray and Greated 1987). Instead, two-dimensional autocorrelation methods applied to a digitised version of the flow field photograph provide accurate and speedy velocity vector estimates. The image processing of flow field visualisations increases the spatial resolution considerably. In contrast to fringe analysis where the spatial correlation region is of fixed size and requires the rescaling of the flow field photographs, spatial autocorrelation estimates by image processing may be obtained for arbitrarily sized local flow regions, the main limitation being the particle density.

PART C – DISCUSSION

6. Discussion

Poststenotic flows downstream of model stenoses with geometries identical to our models have been investigated by a number of researchers and the findings reported herein for unforced steady and pulsatile flow are in broad agreement.

6.1 Steady Flow

To begin the discussion with steady unforced flow, the *vena contracta* flow phenomenon is generally observed in orifice plate flows (Bajura and Pellegrin 1975, Djilali 1978), but less distinct in flow through smooth constrictions, at least for area constrictions of up to 75 % (Cassanove and Giddens 1978). For even more severe constrictions (89 %), Young and Tsai (1973) reported *vena contracta* flow behind contoured symmetric constrictions and

nonsymmetric protuberances, albeit close to the throat of the constriction (at about x/D=0.3).

Effects of the downstream bounding walls on flow development were discussed by Cassanova and Giddens (*ibid*), based on flow visualisation experiments. At low Reynolds numbers the presence of the tube walls retarded the formation of vortices ('image vortex'). In contrast, at higher Reynolds numbers the disintegration of vortex patterns occured at a downstream location closer to the constriction than in the free jet case.

With regard to the spatial development of flow instabilities (*figure* 3.5), a stability investigation by Yongchareon and Young (1979) indicated that the orifice flow is the least stable since the velocity gradient at the separated shear layer is high due to the relatively flat velocity profile at the orifice exit. On the other hand, the streamlined symmetric constriction provides the most stable flow since the separated shear layer is close to the wall which may tend to damp out small disturbances. In this description the behaviour of the nonsymmetric constriction is expected to lie between the two extremes. The separation point is downstream of the throat but the shear layer distance to the wall is thought to be greater than for the symmetric constriction.

This also explains the Strouhal number variability (*figure* 3.8). The orifice plate flow comes closest to a free jet flow with a fairly well defined jet column mode, largely unaffected by wall interference. The flow downstream of the contoured symmetric model stenosis scales less well because the initial shear layer thickness is not negligible compared to the throat diameter (Ho and Huerre 1984). Finally, the flow past the nonsymmetric constriction is least representative of a jet flow, and the dominant instability frequency is comparable to the flow through the orifice plate mainly because of similar flow conditions.

There is considerably less evidence in support of our findings for the forced poststenotic flow experiments under steady flow conditions, and the discussion relies mostly on forced free shear layer investigations.

In connection with orifice flow meters, Bajura and Pellegrin (1977) studied the effect of flow excitation on high Reynolds number flow (Re=8000 to 24000) through a sharp-edged orifice plate in a circular pipe (35%, 50% and 75% area reduction), at high excitation levels (5% to 30% of the mean jet exit speed) and for a range of forcing frequencies (St=0 to 1.8).Their observations included greater flow sensitivity at Strouhal numbers 0.4 to 0.8, increased shear layer spreading and a decrease in flow rate.

Studies of free forced jets are more numerous. Observations of rather anecdotal character were reported by Beavers and Wilson (1975) for the free circular jet at moderate Reynolds numbers (500 to 3000), excited (unintentionally!) by presumably very low level

building vibrations at Strouhal numbers 0.43, 0.61 and 0.98. In a jet with Re=470 and Re=770 and vortex shedding frequency St=0.63, low level excitation at St=0.43 and St=0.98, respectively, resulted in the locking of the vortex shedding frequency onto the excitation, accompanied by a dramatic regulation of the flow evolution and a slight decrease in mean jet exit velocity.

A more systematic study, at considerably higher Reynolds number of order 10^5, is that of Crow and Champagne (1971). They considered the periodic forcing at intermediate levels (2%) of a circular jet with tripped boundary layer. The natural jet column response was at St=0.30 and the effect of forcing was strongest around this Strouhal number. A mild decrease in mean velocity was observed near the jet exit ($0 < x/D < 8$), the reason being the greater entrainment of fluid in the forced jet. What is of particular interest is the effect the forcing had on the background turbulence, expressed by the power spectrum of the axial flow velocity fluctuations. Importantly, Crow and Champagne's findings clearly showed that forcing does suppress background noise. This phenomenon is considered of central importance and will be addressed in chapter V.

A rather different study (Ho and Huang 1982) is of possible relevance to the instability of the separated shear layer behind the nonsymmetric stenosis model. The investigation concerned the forced laminar mixing layer formed by the merging of two parallel water streams of velocities U_1=9.5 cm s^{-1} and U_2=5.0 cm s^{-1}. The natural frequency of the mixing layer instability was 5.06 Hz and the spreading was greatly regulated by forcing. It is not entirely clear from the description of the experimental apparatus whether the excitation was purely monochromatic (dc-motor driven butterfly valves are employed). Nonetheless, the mixing layer responded not only at the fundamental but at up to the fourth higher harmonic of the forcing frequency, and the response diagram is qualitatively very similar to *figure* 3.12. In addition, Ho and Huang observed hysteresis between the various higher harmonic modes. In contrast to our findings, third harmonic resonance was clearly present in the forced mixing layer.

6.2 Pulsatile Flow

Let us turn the discussion to pulsatile flow now. Apart from the consistently observed disparity in rms levels of flow velocity fluctuations between pulsatile and steady flow, pulsatile unforced flow through the model stenoses exhibits further behaviour worth looking into. For example, the large disturbances at the beginning and end of a cycle, most clearly observed in the orifice flow, and to some extent in the flow past the nonsymmetric constriction, are most probably related to the starting vortex and the stopping structure of the transient flow

experiments. Both the large vortex in starting flow and the disturbance during the mid-acceleration in pulsatile flow are characterised by rapid changes in local flow velocity, whilst the structure in suddenly stopped flow and the large disturbance during mid-deceleration in pulsatile flow are more sluggish in appearance. 'Start-up' structures were identified by Khalifa and Giddens (1981) as one of three types of flow disturbances typically encountered in poststenotic flow. A detailed investigation showed that these structures are very repeatable with each pulse and are created anew with the initiation of a cycle.

Other phenomena are related to pulsatile flow stability. The orifice flow seems to be the only one that exhibits some form of transition to randomness during the deceleration phase, whereas the flow downstream of the contoured symmetric constriction exhibits the opposite behaviour *viz.* a tendency toward relaminarisation. Obviously, the orifice flow is the most unstable and transition is therefore most probable for this flow. It is a well documented phenomenon that the transition — if it occurs — is first observed in the deceleration phase of pulsatile flow. Young and Tsai (1973) reported that for a contoured symmetric stenosis (56% area reduction) the initiation of turbulence is retarded by pulsating flow. This observation is in agreement with the results of a comprehensive investigation into the effect of pulsatility on transition in a straight tube (Sarpkaya 1966)[9]. More specifically, Gerrard (1971) found that the acceleration phase reduces turbulence intensity but the deceleration increases it. This served as the rationale for Parker and co-workers (Weinbaum and Parker 1975, Hall and Parker 1976, Parker 1977) to concentrate on the instability investigation of the simplest decelerating flow, a suddenly stopped steady Poiseuille flow in a pipe or channel. Flow destabilisation by deceleration is thought to have been observed in experiments on pulsatile flow through contoured symmetric model stenoses (Cassanova and Giddens 1978). For steady flow a 50% stenosis was required to cause substantial flow disturbances. However, for pulsatile flow, disturbances were created during deceleration by a stenosis of as little as 25% area reduction.

With regard to the oscillatory activity in pulsatile poststenotic flow during peak flow and early deceleration, this phenomenon was identified by Khalifa and Giddens (*ibid*) as the second type of flow disturbance. They observed a change in frequency associated with corresponding changes in mean flow velocity, and a merging of the start-up structure and the oscillations further downstream. Strouhal numbers were found to be about 0.3 for a 50% contoured symmetric stenosis. Curiously, explanations for the difference to the free jet number $St=0.5$ were sought in the flow pulsatility. Our experiments, on the other hand, indicate that the contoured symmetric stenosis does not scale convincingly even in steady flow.

[9]For a more recent study see Stettler and Hussain (1987).

Comparison with other work on the effect of pulsating flow on the intensity levels of oscillatory activity is, to say the least, very difficult. For instance, energy spectra of flow velocity fluctuations on which a comparison of steady and pulsatile flow by Cassanova and Giddens (1978) was based, were calculated for pulsatile flow using an entire cycle! We therefore turn to the starting flow results for an explanation. If the vortex transients were related to the stability problem of accelerating flow, the opposite behaviour would be expected *i.e.* a decrease in fluctuation levels during the transients due to the stabilising effect of the acceleration. In fact, the opposite is true for the impulsively started 'confined jet' flow. For want of a more detailed investigation into this phenomenon we speculate, as outlined in § 5.2.1.5, on the possible relevance of the fluctuations, following the highly repeatable starting structure. It was pointed out there that these fluctuations are related to the much longer time scales of the transient flow and that they are not fully reproducible due to the assumed sensitivity of the instability transient. Of course, impulsively started flow is the simplest form of accelerating flow and a continuously varied mean flow such as a steady flow with superimposed oscillatory flow certainly has an effect on the formation of vortical structures, possibly in a flow regulating form. Finally, what must not be overlooked is the fact that the steady state flow rate in the starting flow experiment is only about half the value that applies to peak flow under pulsatile flow conditions, and instabilities are expected to develop more intensely.

The results for forced pulsatile flow are very much in accordance with what is observed in steady forced flow. As an aside, it is noted that the resonant response of the forced separated shear layer in pulsatile flow provides a means of identifying velocity fluctuations that are directly related to laminar shear layer instabilities. For instance, it is common practice in steady separated flow experiments to exert some control over an otherwise randomly evolving separated shear layer by means of forcing, in order to study the details of the flow. In pulsatile flow, the detailed understanding of flow velocity fluctuations is further complicated by a wealth of nonstationary disturbances, ranging from temporally varying flow separation points to disturbances originated in previous flow cycles. It is therefore suggested that, by subjecting pulsatile flow to excitation of appropriate frequency and amplitude, oscillatory shear layer instabilities may be clearly separated from other forms of flow disturbances.

The half-harmonic frequency locking observed during acceleration in pulsatile orifice flow is clearly a consequence of the fixed flow separation locus provided by the sharp edged orifice plate. To a first approximation, pulsatile flow through the orfice plate may be thought of as simply generating a time-varying version of the steady flow jet shear layer instability. It is then perfectly possible that the instability first locks onto the half-harmonic of the

fundamental forcing frequency, and at higher flow rates switches to harmonic response. Complications caused by temporal variations in the separation point and the degree of wall interference in flow through the contoured symmetric constriction, let alone the nonsymmetric constriction, clearly do not support a forced shear layer response scenario as simple as in orifice flow.

A few other points are worth mentioning. The decrease in axial velocity for forced pulsatile orifice flow again reflects — as in forced steady flow — the greater degree of fluid entrainment accompanied by a faster spreading of the shear layer. The phenomenon is more pronounced in pulsatile flow because the vortical structures possess considerably greater vorticity. Secondly, again in pulsatile orific flow the forcing seems to suppress the transition to randomness in the decleration phase, as is clearly seen at location $x/D=1.0$ (*figure* 3.14). At $x/D=1.5$, however, the vortical structures have reached such a size that wall interference begins to influence the resonant response of the velocity fluctuations.

Another interesting phenomenon is observed in pulsatile flow through the contoured symmetric constriction. At downstream position $x/D=3.0$, the flow is greatly regulated, however the resonant fluctuations are not necessarily locked by the forcing frequency. At time about $t=5$ s, a discontinuity occurs after which stable oscillatory activity at a frequency noticeably below 2.5 Hz dominates. Apparently the phase reference provided by the flow excitation serves to regulate oscillatory flow activity at a frequency not harmonically related to the forcing frequency.

6.3 Flow Visualisation

The emphasis in the flow visualisation experiments described in § 5.2.2 has been on the nonsymmetric model stenosis because of the possible insight into a poststenotic flow with a lesser degree of symmetry than in the case of the axisymmetric stenoses. Implicit in the choice of a plane of visualisation through the tube axis is of course the tacit assumption that the flow is reasonably symmetric about the plane of visualisation. It is obvious, however, that our flow visualisation need neither be an exhaustive description of the main characteristics of the poststenotic flow, nor representative at all. Yet remarkably similar observations were made in flow through a two-dimensional channel expansion at low Reynolds numbers. In steady flow, $Re < 640$, downstream of a right-angled expansion (backward facing step), Armaly *et al* (1983) observed one or two standing 'secondary' vortices attached to the wall downstream of, or opposite to, the primary vortex in the lee of the channel expansion. At Reynolds numbers of

the order of 100, Sobey (1985) observed no actual secondary vortex but a region of significantly reduced shear.

The situation changed dramatically if the flow through the channel expansion was oscillatory. For the same range of Reynolds numbers and a frequency parameter of order 1, wavy core flow with eddies alternating on the two walls was observed. Sobey referred to this scenario as *vortex wave*. A strong secondary eddy was present already in early acceleration and the vortex wave was most pronounced in the deceleration phase. Similar findings applied to a 45^0 channel expansion. Sobey mentioned the splitting of vortices into two in oscillatory flow when the Reynolds number was varied and contributed it to the delicate bifurcation phenomenon that can exist in separated flows.

Bertram and Pedley (1983) studied impulsively started flow through a right-angled expansion. The final Reynolds number was 800 and they observed a distinct vortex street during the flow transients which they contributed to "*the quasisteady instability of a velocity profile with an inflexion point.*" Sobey (*ibid*) however conjectured that what was observed in their experiment was another example of a vortex wave. The important difference is with regard to the type of instability associated with either flow structure. A vortex street is essentially the result of a shear layer instability whilst the genesis of a vortex wave is thought to relate to a large-amplitude damped Tollmien-Schlichting wave. Sobey believed that he was observing a vortex street in oscillatory flow through a symmetric channel expansion, based on observations (flow visualisation as well as numerical simulation) of movement of the vortices. Once vortices were formed they were convected with a velocity somewhat less than the mean flow. In an asymmetric channel, vortices were not convected by the flow once they had formed.

Returning to the flow visualisation of pulsatile flow past the nonsymmetric constriction (*plate* 3.2), the vortices most visible are in photographs (*e*), (*f*) and (*g*). In that flow the average upstream velocity is about 7.5 cm s^{-1} and the time elapsed between two consecutive photographs is 1.25 s implying that convective movement of vortices is clearly not observed. In fact, between photographs (*e*) and (*f*) the vortices seem to have moved upstream some distance.

The reason these unsteady flow phenomena are of possible interest to the haemodynamics of arterial stenoses is related to the high wall shear beneath a vortex. A recent investigation of vortex waves in flow in a channel with a moving indentation (Ralph and Pedley 1988) – the moving wall flow reported in (Stephanoff *et al* 1983) had prompted Sobey's oscillatory channel flow study – showed that wall vorticity can be 5 to 6 times greater than what is expected by assuming a quasisteady flow. Also vortex doubling seemed to be a

regular feature of the vortex waves.

No doubt the flow visualisations of pulsatile poststenotic flow are at best anecdotal evidence of flow instabilities unrelated to the Kelvin-Helmholtz type instability of the separated shear layer, yet the similarities with two-dimensional flows certainly exist and seem very intriguing indeed.

7. Conclusions

With regard to arterial flows the separated shear layer sensitivity appears to be of minor importance. With forcing levels between approximately 1% of the peak axial centreline velocity for the orific plate and about 1.5% for the contoured symmetric stenosis, the poststenotic oscillatory flow disturbances may be considered fairly structurally stable, particularly because the above estimates apply to perturbations at frequencies near the natural instability. To give an idea of the haemodynamic relevance, at an assumed heart rate of 60 beats per minute, the peak flow disturbances will fall into a frequency range of *ca.* 20 to 60 Hz, provided the stenosis is moderate and flow rates are high (*cf.* § 1.2). Assuming arterial wall vibrations to be a source of potential flow perturbations, these are generally thought to resonate at somewhat higher frequenices. As to the magnitude of these vibrations, the evidence is spurious. Considering therefore the flow 'perturbations' observed by Kitney *et al* (1986), even such high fluctuations, of amplitude about 5% of the peak flow velocity and frequency 100 Hz will not necessarily synchronise the flow instability, because the estimated natural instability occurs at approximately one third of the frequency of the perturbation.

J. Phys. E: Sci. Instrum. 20 (1987) 1404–1411. Printed in the UK

8. Appendix

Influence of dropouts on flow velocity measurements with an LDV frequency tracking system

J Treiber and R I Kitney
Biomedical Systems Group, Department of Electrical Engineering, Imperial College, London SW7 2BT, UK

Received 23 September 1986, in final form 11 February 1987

Abstract. Dropouts can greatly affect the accuracy of flow measurements in the case of low-SNR Doppler signals. The dependence of the measurement accuracy on easily determined dropout parameters has been studied theoretically and experimentally.

Based on a gaussian narrowband representation of the Doppler signal, the dropout process is characterised by two parameters, tracking rate and unlock frequency, and modelled as alternating renewal process. It is found that velocity estimates are poorest for unlock frequencies of the order of the signal bandwidth but improve at higher and lower values.

Laminar flow experiments indicate that the transitions between lock and unlock are best described by a Poisson process. An application of this finding to the determination of the LDV scattering volume demonstrates that even under adverse tracking conditions useful volume-dimension estimates may be obtained.

1. Theoretical investigation

1.1. Introduction

Owing to limits of tracking range and slew rate, in frequency tracking systems, tracking flow velocity fluctuations cannot be free of error in situations of large frequency variations, which may result from local flow velocity variations or, indirectly, from the Doppler signal falling below a certain noise level thereby causing a sudden change in signal spectral composition. Here the level of noise depends on the contributions of individual noise sources, namely, optical, photodetection and electronic system noise (Durrani and Greated 1977) with optical noise usually dominating.

Whereas the former case of frequency variations can be avoided by carefully matching the LDV parameters to the flow conditions, large variations in signal envelope are inherent in Doppler signals and express the random interference pattern of large numbers of light scatterers. Consequently, even for high-SNR signals, destructive interference may cause the envelope to fall below the noise level occasionally (figure 1).

The frequency tracker then ceases to function (drops out) and resumes normal tracking operation only when a valid Doppler signal is detected. During dropout the tracker output is held constant, either at the signal value immediately before dropout (e.g. Wilmshurst and Rizzo 1974) or at zero voltage or the signal average, depending on the strategy employed.

Systematic studies into the degradation of the LDV signal by background noise (Durrani and Greated 1974) have elucidated the dependence of dropouts on noise level and tracking filter bandwidth. Also a Markov chain model of the dropout process has been conjectured (Buchave *et al* 1979) and its implications have been studied theoretically.

0022-3735/87/111404 + 08 $02.50 © 1987 IOP Publishing Ltd

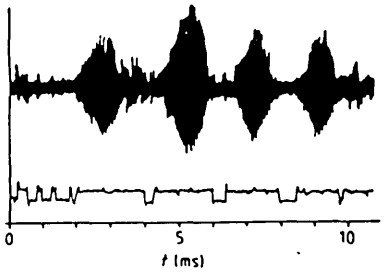

Figure 1. Amplitude variations of the photodetector signal (top) and their effect on frequency tracking performance (bottom; low signal level indicates dropout).

An analysis presented here will show that dropout effects in LDV trackers may be effectively quantified in terms of tracking rate and dropout frequency. Information about these two parameters is provided in most commercially available trackers by displaying a running-average form of tracking rate defined as the percentage time of locked operation. In addition, a synchronisation signal is available giving information (cf § 2.2) about the frequency of unlock transitions.

1.2. Calculation of the tracking rate and the unlock frequency

1.2.1. Theoretical background. The analysis of the dropout characteristics of the LDV frequency tracker is based on a gaussian narrowband process representation of the photodetector current $i(t)$ (e.g. George and Lumley 1973, Durrani and Greated 1977),

$$\begin{aligned} i(t) &= F(t)\cos(KX(t)) + G(t)\sin(KX(t)) \\ &= (F^2(t)+G^2(t))^{1/2}\cos[KX(t)-\tan^{-1}(G(t)/F(t))], \end{aligned} \tag{1}$$

where $i(t)$, $F(t)$ and $G(t)$ are gaussian random variables, K represents a scattering wavenumber for the particular velocimeter configuration and $X(t)$ is an effective displacement. Furthermore, $R_{FF}(\tau)=R_{GG}(\tau)$ and $R_{FG}(\tau)\equiv 0$ for all practical purposes,

$$R_{FF}(\tau)=R_{FF}(0)\exp[-\tfrac{1}{2}(\Delta\omega_F\,\tau)^2]$$

and

$$\begin{aligned} R_{ii}(\tau) &= R_{FF}(\tau)E\{\cos[K(X(t)-X(t+\tau))]\} \\ R_{ii}(0) &= R_{FF}(0)=\sigma_i^2. \end{aligned} \tag{2}$$

The instantaneous frequency function $f(t)$ of the photodetector current is given by the sum of two uncorrelated signals,

$$f(t)=f_0(t)+n(t)$$

$$R_{f_0 n}(\tau)\equiv 0$$

with $f_0(t)$ proportional to the volume-averaged Eulerian velocity at the centre of the measuring volume (which, in fact, may be a biased estimate of the mean velocity at the centre of the measuring volume due to velocity gradients, e.g. Kreid 1974),

$$f_0(t)=\frac{K}{2\pi}u_0(t)$$

and $n(t)$ representing transit-time noise of infinite variance and spectral density

$$S_{nn}(\omega)=\frac{\Delta\omega_F}{16\pi^{5/2}}\sum_{K=1}^{\infty}\frac{1}{K^{3/2}}\exp\left[-\frac{1}{4K}(\omega/\Delta\omega_F)^2\right] \tag{3}$$

(a result that was first derived by Rice (1948) in his classic paper on FM detection and random noise) with half-power bandwidth $\Delta\omega_n \simeq 2.7\Delta\omega_F$.

1.2.2. Tracking rate. Dropout parameters are now calculated by employing the analytical model introduced in the previous section. Defining the tracking rate λ as the probability that the envelope $r(t)=(F^2(t)+G^2(t))^{1/2}$ is above a given level L, $\lambda = P\{r>L\}$, we obtain, by noting that r has a Rayleigh density

$$f_R(r)=(r/\sigma_i^2)\exp(-r^2/2\sigma_i^2),$$

$$\lambda=\exp(-1/2\,\mathrm{SNR}) \qquad \mathrm{SNR}=(\sigma_i/L)^2 \tag{4}$$

where the ratio σ_i/L has conveniently been chosen as a measure of the signal-to-noise ratio. According to figure 2 the tracking rate reaches values of 0.5 for SNRs as low as 0.72, whereas rates above 0.9 require much greater SNRs, SNR > 4.75.

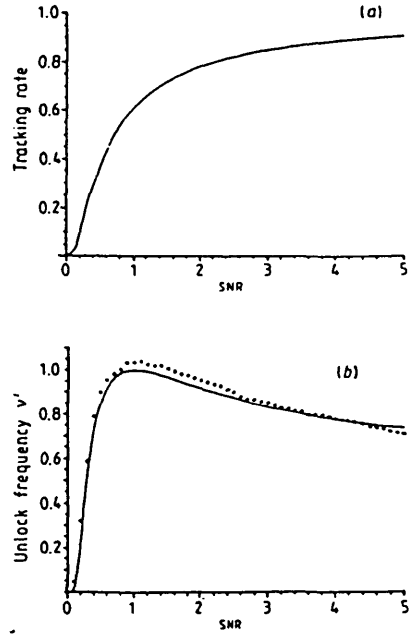

Figure 2. Functional dependence of (*a*) tracking rate λ and (*b*) normalised unlock frequency $\nu'=\nu/(\Delta\omega_F/\sqrt{2}\pi)$ on signal-to-noise ratio. ν' is compared with results of a simulation of the level crossing process.

1.2.3. Unlock frequency. An expression for the unlock frequency ν may be found by noting that the level crossing density $\eta_{L,\dot{x}}$ of a stationary differentiable process $x(t)$ for a level L is

$$\eta_{L,\dot{x}}=f_x(L)E\{\dot{x}(t)|x(t)=L\} \tag{5}$$

with $f_x(x)$ the probability density function (PDF) of x (Blanc-Lapierre 1963). It is readily appreciated that trying to evaluate equation (5) for the envelope function $r(t)$ is, at best, highly involved, if not impossible. However, by assuming a normal process $x(t)$ for which $\mathrm{d}x(t)/\mathrm{d}t$ and $x(t)$ are orthogonal and therefore independent, equation (5) assumes the more tractable form

$$\eta_{L,\dot{x}}=\frac{1}{\pi}\left(\frac{-\ddot{R}_{\tilde{x}\tilde{x}}(0)}{R_{\tilde{x}\tilde{x}}(0)}\right)^{1/2}\exp\left(-\frac{\tilde{L}^2}{2R_{\tilde{x}\tilde{x}}(0)}\right) \tag{6}$$

$$\tilde{x}=x-E\{x(t)\} \qquad \tilde{L}=L-E\{x(t)\}.$$

The density $f_r(r)$ will therefore be approximated by a gaussian density centred at the maximum of $f_r(r)$ and of the same variance. The autocorrelation (ACF) of $r(t)$ is given by (Lawson

and Uhlenbeck 1950)

$$R_{rr}(\tau)=R_{FF}(0)\,|2E(\rho(\tau))-(1-\rho^2(\tau))K(\rho(\tau))|$$

$$\rho(\tau)=R_{FF}(\tau)/R_{FF}(0)$$

where $E(\rho)$ and $K(\rho)$ are complete elliptic integrals of the first and second kind, respectively. Expanding the expression $2E(\rho)-(1-\rho^2)K(\rho)$

$$R_{rr}(\tau)=\tfrac{1}{2}\pi R_{FF}(0)\,(1+\tfrac{1}{8}\rho^2(\tau)+\tfrac{3}{64}\rho^4(\tau)+\ldots).$$

Therefore,

$$R_{rr}(\tau)\simeq\tfrac{1}{2}\pi\sigma_i^2\left(1+\frac{R_{FF}^2(\tau)}{4R_{FF}^2(0)}\right).$$

Now,

$$\nu=\tfrac{1}{2}\eta_L=\frac{\Delta\omega_F}{\sqrt{2}\pi}\exp\left|-\frac{4}{\pi}\left(\frac{\bar{L}}{\sigma_i}\right)^2\right|. \tag{7}$$

which is the desired unlock frequency expressed in terms of bandwidth $\Delta\omega_F$ and the variance of the photodetector current. The unlock frequency is proportional to the product of the envelope bandwidth and a non-linear function of SNR, $f(\text{SNR})\in[0,1]$. As expected, ν is highest for SNRs around 1.0 (corresponding to the zero crossing density of process $r(t)-E\{r(t)\}$, figure 2). Also given in figure 2 are the results of a simulation of the level crossing process, which agree very well with the analytical form and substantiate the gaussian density approximation.

1.3. A model of the dropout process

The tracker output will be represented as

$$\tilde{f}(t)=f(t)U(t)+f'(t)\bar{U}(t)$$

with $f(t)$ the instantaneous frequency of the Doppler signal, $U(t)$ a modulating function taking values zero and one during unlock and lock, respectively, $\bar{U}(t)$ a function taking the negated values of U, $\bar{U}=1-U$, and $f'(t)$ a function that depends on the strategy employed for handling dropouts.

In an *ad hoc* approach to simplifying the discussion of the statistical properties of $f(t)$, the functions $U(t)$ and $f(t)$ are assumed to be statistically independent. It should be noted, however, that the gaussian narrowband process model implicitly assumes a certain degree of correlation between the envelope function and the instantaneous frequency, i.e. drops in envelope $r(t)$ are accompanied by spiky excursions of the instantaneous frequency. Therefore it is only through experimental validation that the above simplification can be justified (cf § 2.5).

Viewing output $f(t)$ as an estimate of $f(t)$, it may be shown that, on the basis of mean square error P,

$$P=E\{(f(t)-\tilde{f}(t))^2\}$$

a strategy of holding the signal value constant prior to dropout,

$$f'(t)=f(t_k-0)\text{ for }t\in[t_k,t_{k+1}];\ t_k\text{: unlock transitions}$$

is superior to letting $f'(t)=0$ or $f'(t)=E\{f(t)\}$. It is noted that the sample-hold strategy is implemented in the TSI 1090 tracker, used in this study.

Statistical properties of process $U(t)$ are studied by decomposing $U(t)$ into two random sequences $\{U_1,U_2,\ldots\}$ and $\{\bar{U}_1,\bar{U}_2,\ldots\}$ comprising interval durations of tracking ($U(t)=1$) and unlock ($U(t)=0$), respectively, with unlock interval $\bar{U}_i$ succeeding lock interval U_i. Theoretical and experimental studies on the level-crossing problem of the envelope function of a gaussian narrowband process (Rice 1958) and the zero-crossings of low-pass gaussian processes (McFadden 1958, Blötekjaer 1958) indicate that the up or down crossing interval PDF is basically of a unimodal shape. Furthermore, intervals of duration greater than the average interval duration asymptotically follow an exponential distribution and successive zero-crossing intervals may be taken to be statistically independent in the case of smoothly decaying low-pass spectra. The exponential-tail property of the interval PDF is clearly a consequence of the chance of a crossing in $(t,t+h]$ being quite independent of what happens up to t, for large t.

On this basis, the transition times of $U(t)$ are modelled as alternating renewal process, i.e. the sequences $\{U_i\}$ and $\{\bar{U}_i\}$ are mutually independent sequences of independent identically distributed random variables of densities $f_U(U)$ and $f_{\bar{U}}(\bar{U})$, respectively. The autocorrelation of $U(t)$ may now be calculated as

$$R_{UU}(\tau)=\left(\frac{m_U}{m_U+m_{\bar{U}}}\right)^2\left(1+\frac{m_{\bar{U}}}{m_U}R_*(\tau)\right)$$

$$R_*(\tau)=\mathcal{L}^{-1}\left(\frac{1}{s}-\frac{m_U+m_{\bar{U}}}{m_U m_{\bar{U}}}\frac{1}{s^2}\frac{(1-\varphi_U(s))(1-\varphi_{\bar{U}}(s))}{1-\varphi_U(s)\varphi_{\bar{U}}(s)}\right) \tag{8}$$

where

$$m_U=\int_0^\infty x f_U(x)\,dx \qquad m_{\bar{U}}=\int_0^\infty x f_{\bar{U}}(x)\,dx$$

and $\varphi_U(s)$ and $\varphi_{\bar{U}}(s)$ are the Laplace transforms of f_U and $f_{\bar{U}}$ (appendix 1).

Employing the sample–hold strategy for estimating $f(t)$ and assuming independence, we obtain

$$R_{\tilde{f}\tilde{f}}=R_{ff}R_{UU}+R_{f'f'}R_{\bar{U}\bar{U}}+R_{ff'}R_{U\bar{U}}+R_{f'f}R_{\bar{U}U}. \tag{9}$$

Now,

$$R_{U\bar{U}}=E\{U\}-R_{UU}$$

$$R_{\bar{U}U}=R_{U\bar{U}}$$

$$R_{\bar{U}\bar{U}}=1-2E\{U\}+R_{UU}.$$

Calculation of the auto- and cross-correlations $R_{f'f'}$, $R_{ff'}$ and $R_{f'f}$ is somewhat involved and only the end results will be given here (see appendix 2 for complete derivation)

$$R_{f'f'}(\tau)=\int_0^\infty R_{ff}(t)p''(t,\tau)\,dt$$

$$R_{f'f'}(-\tau)=R_{f'f'}(\tau)$$

and

$$R_{ff'}(\tau)\int_{-\infty}^{+\infty}R_{ff}(t)p'(t-\tau)\,dt$$

with p' and p'' PDFs of the transformed lags τ.

Discussion of the estimate $R_{\tilde{f}\tilde{f}}$ of R_{ff} is simplified by relating the expectations m_U and $m_{\bar{U}}$ to the dropout parameters:

$$\lambda=\frac{m_U}{m_U+m_{\bar{U}}} \qquad \nu=\frac{1}{m_U+m_{\bar{U}}}. \tag{10}$$

Now, equation (9) assumes the form

$$R_{\tilde{f}\tilde{f}}=\lambda^2R_{ff}+(1-\lambda^2)R_{f'f'}+\lambda(1-\lambda)(R_{ff'}+R_{f'f})$$
$$+\lambda(1-\lambda)[R_{ff}+R_{f'f'}-(R_{ff'}+R_{f'f})]R_*. \tag{11}$$

As is expected, the estimate $R_{\tilde{f}\tilde{f}}$ asymptotically approaches the true autocorrelation function for high tracking rates λ. Independently of this observation, the unlock frequency distinctly influences the quality of the estimate. Relating ν to a measure of correlation-bandwidth of $f(t)$, f_{corr} (or correlation-time τ_{corr}, $\tau_{corr}\propto 1/f_{corr}$), it is found that if $\nu\ll f_{corr}$ then $R_*\simeq 1$, $R_{f'f'}$ and $(R_{ff'}+R_{f'f})$ are approximately constant over the significant part of $R_{ff}(\tau)$. Thus,

$$R_{\tilde{f}\tilde{f}}(\tau)=\lambda R_{ff}(\tau)+\text{constant}.$$

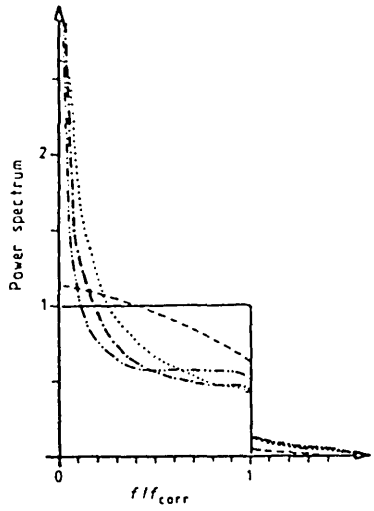

Figure 3. Power spectrum of ideal low pass signal affected by Poisson type dropout process (at tracking rate 0.5). ——, $\nu=\infty$; – – –, $\nu=2$; · · · ·, $\nu=1$; · – · –, $\nu=\frac{1}{2}$; · · · – · · ·, $\nu=\frac{1}{4}$.

On the other hand, if $\nu \gg f_{corr}$ then $R_{ff}(\tau)$ may be approximated by a delta function and $R_{f'f'} \simeq R_{ff}$, $(R_{ff'} + R_{f'f}) \simeq 2R_{ff}$. Hence,

$$R_{\tilde{f}\tilde{f}}(\tau) = R_{ff}(\tau).$$

Finally, as ν becomes of order f_{corr} the quality of the estimate $R_{\tilde{f}\tilde{f}}$ greatly deteriorates.

The above discussion has been quantified for a velocity signal with an ideal low pass power spectrum (figure 3). Assuming a Poisson process formulation of the transitions between lock and unlock that allows a complete description of the dropout process in terms of tracking rate and unlock frequency (cf § 2.4), power spectra were calculated for various ν at $\lambda = 0.5$.

1.4. Implications for LDV measurements at intermediate tracking rates

From the above discussion it is obvious that for low to intermediate tracking rates ν will have to be either much greater or much smaller than f_{corr} in order to get useful estimates of the instantaneous frequency. However, this only applies to attempts of measuring 'signal plus noise'. As described in § 1.2.1 the transit-time noise is not correlated with the volume-averaged velocity fluctuations. It is readily seen that this property holds for the modified signals $\tilde{f}_0(t)$ and $\tilde{n}(t)$ also. Therefore, influences of ν on the quality of estimates $\tilde{f}_0$ and $\tilde{n}$ may be treated separately and the estimates may be recovered by some optimal noise filter (e.g. Wiener filtering). Subsequently a tracking rate $\lambda = 0.5$ (at SNR = 0.72) will be assumed, implying an unlock frequency $\nu \simeq \frac{1}{2}\Delta\omega_F$. Consequently, estimates of the transit time noise, which has a bandwidth of $\Delta\omega_n \simeq 2.7\Delta\omega_F$ (i.e. $\nu \simeq \frac{1}{13}\Delta\omega_n$) cannot be expected to be reliable (specific cases may have to be analysed by simulating the unlock process, cf § 2.5). Furthermore, measurements of turbulent or highly disturbed flows are not primarily limited by transit time effects (George and Lumley 1973), but instead by the requirement for a spectral bandwidth of velocity fluctuations $f_{corr} \ll \frac{1}{2}\Delta\omega_F$ (the case $f_{corr} \gg \frac{1}{2}\Delta\omega_F$ has no practical value because then the velocity signal cannot be distinguished from the noise).

2. Experimental investigation

2.1. Description of the experimental apparatus

LDV experiments were carried out as part of a study of transit-time broadening effects in laminar flow measurements and the estimation of the scattering volume dimensions.

Axial velocity measurements were taken at the centre line position of a 1 in (25.4 mm) ID straight perspex tube in developed liquid flow, 66 diameters downstream from a constant head reservoir, connected with the tube by a converging nozzle. The flow was observed through a test section, consisting of a block of perspex of dimensions 63.5 × 63.5 × 254 mm³, to avoid refractions at the pipe curvature.

The LDV system, operating in dual beam forward scattering mode comprised a 5 mW He–Ne laser (Model Spectra Physics 120) of wavelength 623.8 nm, a 50 mm beam splitter (Model TSI 915), a Bragg cell for acousto-optical frequency shifting, a transmitter–receiver set of lenses of 104 mm focal length and a photomultiplier unit of aperture size 0.254 mm (which has been found experimentally to yield the best signal-to-noise ratio). The photodetector current was demodulated with a Model TSI 1090 frequency tracker, operating in *open loop* condition so as to avoid any possible tracking of noise.

Industrial water was used as the flow medium, with no artificial scattering particles added. The tracker operated at an average tracking rate of 0.5. Operation of the LDV system in the 'many particle' range (continuous LDV) – as implied by the gaussian narrowband process model – was ensured by comparing tracking rate and unlock frequency at various particle densities (addition of homogenised milk). The tracking parameters were indeed found to be independent of particle density. This result also identified the optical system as the major source of noise resulting in this somewhat low tracking rate.

2.2. Recovery of the unlock signal

Information about the unlock and recapturing behaviour of the phase locked loop (PLL) was obtained by low-pass filtering the synchronisation signal available at the TSI tracker. Because of the signal validation circuitry employed in the particular tracker, in the case of perfect tracking this signal is a train of equally spaced pulses with a pulse repetition frequency of $\frac{1}{10}$ the Doppler frequency. Loss of tracking is indicated by pulse spacings greater than in the ideal case and the tracker output is held constant at the last validated value until the PLL has recaptured the FM signal.

Low-pass filtering of the synchronisation signal at a bandwidth slightly lower than a tenth of the signal frequency thus yields a signal (figure 4) that, after passing through a threshold device, represents the unlock process $U(t)$. However, information about the very short unlock intervals is lost – a fact that has to be accounted for when analysing statistical properties of $U(t)$.

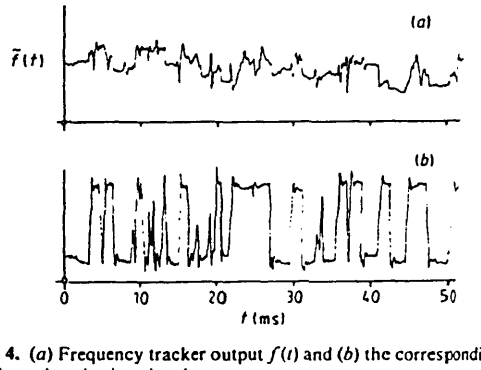

Figure 4. (*a*) Frequency tracker output $f(t)$ and (*b*) the corresponding filtered synchronisation signal.

Table 1. Moments of PDF estimates normalised by the first moment of the convolved PDFs.

	$f(U)*f(U)$	$f(U_i+U_{i-1})$	$f(\bar{U})*f(\bar{U})$	$f(\bar{U}_i+\bar{U}_{i-1})$	$f(U)*f(\bar{U})$	$f(U_i+\bar{U}_i)$
m_1/m_1^*	1.000	1.001	1.000	1.000	1.000	1.000
$m_2/(m_1^*)^2$	1.290	1.300	1.268	1.274	1.489	1.488
$m_3/(m_1^*)^3$	2.040	2.067	1.946	1.968	2.956	2.943
$m_4/(m_1^*)^4$	3.825	3.862	3.501	3.555	7.327	7.200

2.3. Testing the independence of lock and unlock intervals

Centre line velocity measurements were taken at four different Reynolds numbers (Re = 650–1100, based on the flow rate) and the recorded samples of $U(t)$ and $f(t)$ were digitised for analysis on a CDC mainframe computer. From sample records of $U(t)$ the lock and unlock sequences $\{U_i\}$ and $\{\bar{U}_i\}$ of sample sizes between $N = 1000$ and 2000 were then derived and auto- and cross-correlation coefficients $\rho_U(k)$, $\rho_{\bar{U}}(k)$ and $\rho_{U\bar{U}}(k)$ were estimated for the first few lags $k = 0, 1, \ldots 10$. Consistently, an upper bound of $\rho = 0.05$ for these coefficients was found. Although the postulated independence implies a lack of correlation, which is indeed supported by the above findings, the reverse line of reasoning only holds for gaussian random variables. Therefore, a further test was included, based on estimates of the probability density fuctions of $\{U_i\}$ and $\{\bar{U}_i\}$.

The independence of two random variables a and b of PDFs $f_a(a)$ and $f_b(b)$ may be determined by comparing $f_{a+b}(a+b)$ with the convolved PDFs $f_a(a)*f_b(b)$. The random variables a and b can be considered independent if, within the limitations of finite sample size operations and the smoothing property of the convolution operator, $f_{a+b}(a+b) = f_a(a)*f_b(b)$. Here, equivalence of f_{a+b} and f_a*f_b was tested by comparing sample moments, a technique that has been successfully employed in the testing of the renewal property of series of events (Sayers 1970). (For completeness it should be noted that in general a PDF is not fully specified by its moments, unless its moment generating function is analytic at the origin.)

In practice, sample moments of a higher order than four are dominated by finite sample size effects (Yule and Kendall 1953) and, therefore, of limited value. Hence, only the first four moments were considered. The independence test was carried out with samples from experiments of varying Re numbers and exemplary results are given in table 1 and figure 5. Clearly the convolution-predicted moments agree very well with the experimentally determined values. Comparison between the distributions further supports the independence hypothesis.

2.4. Investigation of the interval-duration distribution

With the aim of determining simple parametric descriptions of the lock- and unlock-interval distributions, sample PDFs were tested for the exponential tail property (cf § 1.3). However, the results of least-squares fittings of an exponential density $f_U(U) = \gamma \exp(-\gamma U)$ to the data indicated that this function could well be used to describe the complete sample PDF, which is, of course, a truncated estimate of the true PDF. Percentage mean-squared errors of fitting were consistently below 6% with an average value of 3.2% (figure 6). This finding was further substantiated by comparing the experimentally determined ACFs of $U(t)$ with the predicted ACF, which, for PDF estimates $f_U(U) = \alpha \exp(-\alpha U)$, $E\{U\} = 1/\alpha$ and $f_{\bar{U}}(\bar{U}) = \beta \exp(-\beta U)$, $E\{\bar{U}\} = 1/\beta$, is (equation (8))

$$R_{UU}(\tau) = \frac{\beta^2}{(\alpha+\beta)^2} + \frac{\alpha\beta}{(\alpha+\beta)^2} \exp[-(\alpha+\beta)|\tau|] \qquad (12)$$

with parameters α and β related to the dropout parameters by

$$\lambda = \frac{\beta}{\alpha+\beta} \qquad \nu = \frac{\alpha\beta}{\alpha+\beta}.$$

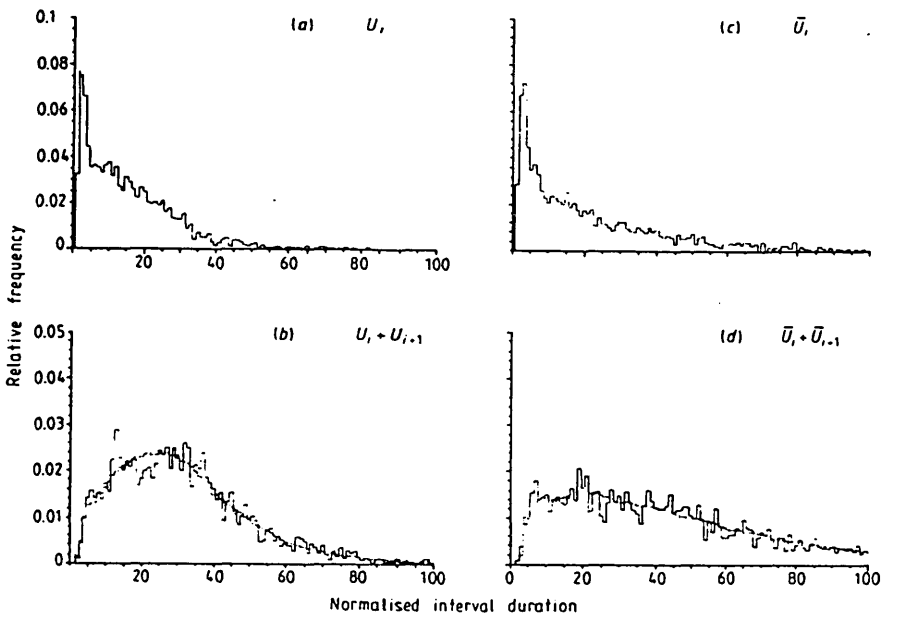

Figure 5. Comparison between PDF estimates of random variable $U_i + U_{i-1}(\bar{U}_i + \bar{U}_{i-1})$ and convolution $f_U * f_U(f_{\bar{U}} * f_{\bar{U}})$ – dotted curves in (*b*) and (*d*).

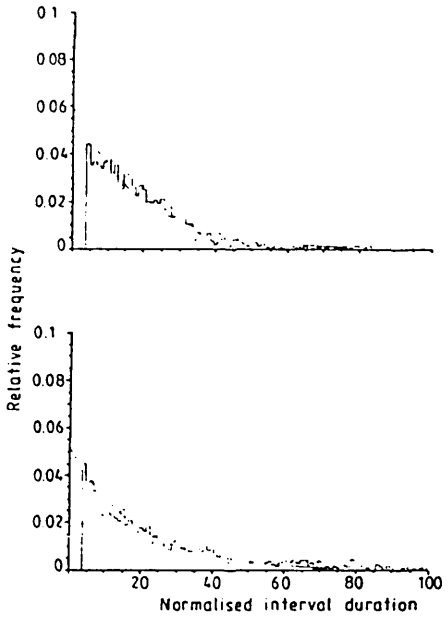

Figure 6. Least-squares fit of exponential density function to PDF estimates (the very short interval values are ignored because they cannot be considered representative).

Specifically, correlation times $\tau_{corr.exp}$ and $\tau_{corr} = 1/(\alpha+\beta)$ were compared (table 2). As the measured autocorrelations did not show any oscillatory component in their tails, which is a potential feature according to equation (8) in the case of higher order PDFs (in terms of their Laplace transforms), it may be assumed that the concept of alternating Poisson process satisfactorily describes the unlock process.

Table 2. Lock and unlock durations $1/\alpha$ and $1/\beta$ are averages of five independent runs at each flow rate (I–IV). Auto-correlation time $1/(\alpha+\beta)$ is compared with corresponding averaged values of measured τ_{corr}. All values in ms.

	$1/\alpha$	$1/\beta$	$1/(\alpha+\beta)$	Expt
I	1.892	1.843	0.918	0.940
II	1.421	1.479	0.725	0.731
III	1.184	1.373	0.636	0.617
IV	0.993	1.182	0.540	0.553

It should be pointed out that the exponential-density model does not contradict the unimodal shape characteristic mentioned earlier. Although the sample PDF, as an estimate of the truncated form of the true PDF, is potentially masking a PDF maximum in the short interval range, it is the much longer intervals that determine the correlation time of R_{UU} and affect $f(t)$.

2.5. Application to the determination of the LDV scattering volume

The analysis of transit-time effects in laminar flow measurements provides a means of verifying the calculation of scattering volume dimensions based on the optical configuration.

Given the beam crossing angle φ, the focal length l_0 of the lens, the $1/e^2$ intensity beam diameter D and the wavelength λ_L, the three characteristic dimensions of the scattering volume are

$$\sigma_x = \sigma/(\sqrt{2}\cos\tfrac{1}{2}\varphi)$$
$$\sigma_y = \sigma/(\sqrt{2}\sin\tfrac{1}{2}\varphi) \qquad (13)$$
$$\sigma_z = \sigma/\sqrt{2}$$

with

$$\sigma = \frac{\sqrt{2}}{\pi}\frac{l_0\lambda_L}{D}.$$

In laminar flow, if transit-time effects dominate the spectral broadening (i.e. negligible curvature of the flow profile across the scattering volume),

$$\Delta\omega_F^2 = \bar{u}^2/2\sigma a_x^2$$

with flow velocity $\bar{u}$ and the direction of flow corresponding to the x direction. This bandwidth may be determined either directly by spectral analysis of $i(t)$ (e.g. Berman and Dunning 1973) or by studying $f_L(t) = f_0 + n_L(t)$. The second approach was chosen here in an attempt to study the effects of the unlock process in situations $\nu \simeq \Delta\omega_F$. Based on scattering-volume

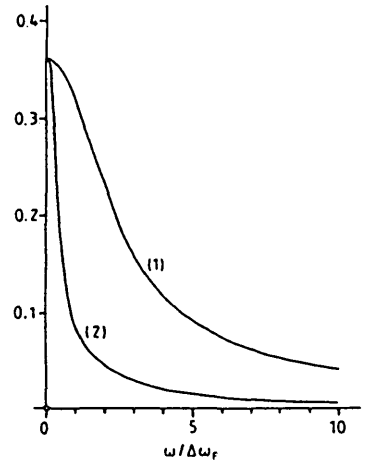

Figure 7. Normalised power spectrum $S_{nn}(\omega)/(\Delta\omega_F/4\pi^2)$ (1) and simulation $S_{\dot{n}\dot{n}}(\omega)/(4\pi^2/\Delta\omega_F)S_{nn}(0)$ (2).

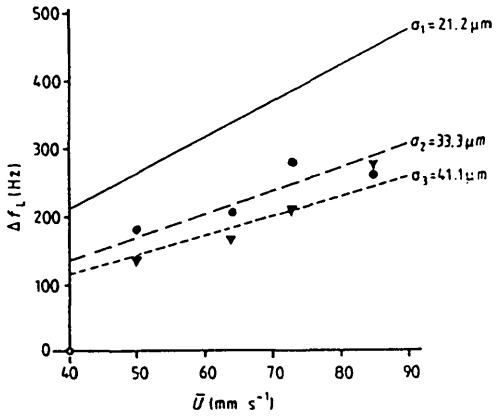

Figure 8. Comparison of theoretically predicted (——) and measured (●) transit time noise bandwidths. Also given is the scattering volume dimension in flow direction σ_x, as calculated from the optical configuration (σ_1), from noise measurements and simulations (σ_2) and from estimates of λ and ν (▼) (σ_3).

dimensions according to equation (13) of $\sigma_1 = 21.2\,\mu$m, $\sigma_1 = 88.3\,\mu$m and $\sigma_2 = 20.6\,\mu$m and estimates of parameters λ and ν, the spectral density of $f(t)$ was calculated (equation (12)) and compared with the theoretical curve (figure 7). Half-power bandwidths of the calculated spectra were then used to estimate the bandwidths of the experimentally measured noise spectra. Also included was a calculation of noise-bandwidths by making use of the functional relationship $\Delta\omega_F = f(\lambda, \nu)$ (equations (4) and (7)). Results of all three types of calculations are given in figure 8. In view of practical limitations to perfect optical alignment and the avoidance of stray beams, the actual scattering volume is clearly greater than that found from optical data. Furthermore, the estimate based on the unlock characteristics is surprisingly close to the transit-time noise estimate, suggesting that the level-crossing model (including the $U(t)$–$f(t)$ independence assumption) is an adequate description of the unlock process.

3. Conclusions

Confronted with experimental circumstances that may lead to a low tracking performance of the LDV frequency tracker, this study was undertaken with the purpose of assessing the quality of LDV measurements of local flow velocity in the presence of tracking noise.

Employing a simple Poisson process description of the transitions between lock and unlock, two readily available parameters of tracking performance, tracking rate and unlock frequency, were used to quantify the effects of dropouts on velocity measurements, thereby offering a simple tool of assessing the significance of 'dropout noise' to be expected in specific cases. Transit time noise measurements were then evaluated by means of simulation and an estimate for the scattering volume was obtained. Moreover, the two parameters were found to be a convenient means of determining the overall velocity-signal bandwidth.

Appendix 1

The autocorrelation of two-state ('on', 'off') process $U(t)$ is found by noting (Cox 1962) that for an alternating renewal process the equilibrium probability P_E, given that U is in state 1 at the (arbitrarily chosen) time origin t_0, that $U(t_0 + t)$ is also in state 1 is

$$P_E(t) = \mathcal{L}^{-1}\left(\frac{1}{s} - \frac{1}{m_1}\frac{1}{s^2}\frac{(1-\varphi_1(s))(1-\varphi_2(s))}{1-\varphi_1(s)\varphi_2(s)}\right)$$

with

$$\lim_{t\to\infty} P_E(t) = \frac{m_1}{m_1+m_2} \qquad \text{and} \qquad \lim_{t\to 0} P_E(t) = 1.$$

Here, $\varphi_1(s)$ and $\varphi_2(s)$ are the Laplace transforms of the state 1 and state 2 PDFs and m_1, m_2 are the respective average durations. Now,

$$R_{UU}(\tau) = E\{U(t)U(t+\tau)\} = P\{U(t+\tau)=1 \mid U(t)=1\}\,P\{U(t)=1\}$$

$$= P_E(\tau)\frac{m_1}{m_1+m_2}.$$

Appendix 2

The autocorrelation function of the sample-hold signal $f'(t)$ is readily seen to be a smoothed version of $R_{ff}(\tau)$, namely

$$R_{f'f'}(\tau) = \int_0^\infty R_{ff}(t)\,p''(t,\tau)\,dt \qquad \text{for} \qquad \tau \geqslant 0$$

$$R_{f'f'}(-\tau) = R_{f'f'}(\tau).$$

Here, $p''(t, \tau)$ is the PDF of the random variable

$$t = \begin{cases} \tau - (\Delta_2 - \Delta_1) & \Delta_2 \leqslant \tau \\ 0 & \Delta_2 > \tau \end{cases}$$

with Δ_2 and Δ_1 the backward recurrence times from $t = \tau$ and $t = 0$, respectively (figure 9). As the interval PDF $f_{U'}(U')$ of process $f'(t)$ is given by the convolution of the lock- and unlock-interval PDFs, the backward recurrence time Δ has a density

$$f_\Delta(\Delta) = \frac{1 - F(\Delta)}{m}$$

with $F(\Delta)$ the cumulative distribution of $f_U * f_{\bar{U}}$ and $m = E\{U_i + \bar{U}_i\}$. Furthermore, recurrence times Δ_1 and Δ_2 are

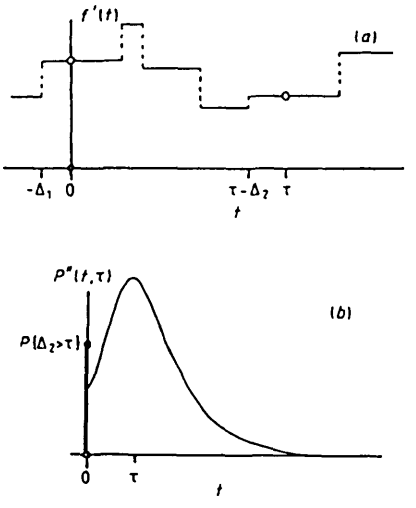

Figure 9. (*a*) Derivation of $R_{f'f'}$. As $f'(t)$ is a sample-hold version of $f(t)$, lag τ of R_{ff} translates to $t = \tau - (\Delta_2 - \Delta_1)$ of $R_{f'f'}$. (*b*) PDF of t, based on backward recurrence times Δ_1 and Δ_2.

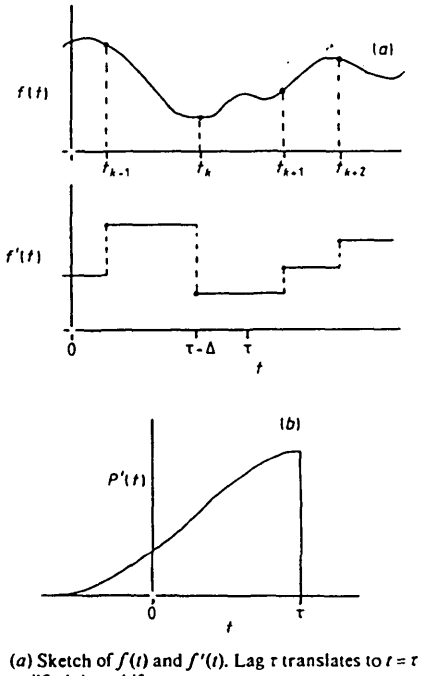

Figure 10. (*a*) Sketch of $f(t)$ and $f'(t)$. Lag τ translates to $t = \tau - \Delta$. (*b*) PDF of modified time shift.

independent for $\tau > \Delta_2$. Hence,

$$p''(t, \tau) = P\{\Delta_2 > \tau\}\delta(\tau) + f_{\Delta_2} * f_{\Delta_1} \qquad \delta(\tau) = 0 \qquad \tau \neq 0.$$

Similarly, the cross-correlation $R_{ff'}(\tau)$ is given by

$$R_{ff'}(\tau) = \int_{-\infty}^{+\infty} R_{ff}(t)p'(t-\tau)\,dt$$

with $p'(t)$ the PDF of backward recurrence time Δ (figure 10).

References

Berman N S and Dunning J W 1973 Pipe flow measurements of turbulence and ambiguity using laser-Doppler velocimetry
J. Fluid Mech. **61** 289

Blanc-Lapierre A 1963 *Modèles Statistiques pour l'Etude des Phénomènes des Fluctuations* (Paris: Masson)

Blötekjaer K 1958 An experimental investigation of some properties of band-limited gaussian noise
IRE Trans. Information Theory **IT-4** 100

Buchhave P, George W K and Lumley J L 1978 The measurement of turbulence with the laser-Doppler anemometer
Ann. Rev. Fluid Mech. **11** 443

Cox D R 1962 *Renewal Theory* (London: Methuen)

Durrani T S and Greated C A 1974 Theory of LDV tracking systems
IEEE Trans. Aerospace and Electron. Systems **AES-10** 418

Durrani T S and Greated C A 1977 *Laser Systems in Flow Measurement* (New York: Plenum)

George W K and Lumley J L 1973 The laser-Doppler velocimeter and its application to the measurement of turbulence
J. Fluid Mech. **60** 321

Kreid D K 1974 Laser-Doppler velocimeter measurements in nonuniform flow: error estimates
Appl. Opt. **13** 1872

Lawson J L and Uhlenbeck G E 1950 Threshold signals
MIT Radiation Laboratory Series, vol. 24

McFadden J A 1958 The axis crossing intervals of random functions – II
IRE Trans. Information Theory **IT-4** 14

Rice S O 1948 Statistical properties of a sine wave plus random noise
Bell Systems Tech. J. **27** 109

Rice S O 1958 Distribution of the duration of fades in radio transmission
Bell Systems Tech. J. **37** 14

Sayers B McA 1970 *Inferring Significance from Biological Signals in : Biomedical Engineering Systems* ed. M Clynes and J H Milsum (London: McGraw-Hill)

Wilmshurst T H and Rizzo J E 1974 An autodyne frequency tracker for laser Doppler anemometry
J. Phys. E: Sci. Instrum. **7** 924

Yule G U and Kendall M G 1953 *An Introduction to the Theory of Statistics* 14th edn (London: Griffin)

Literature Cited

Adrian R J (1986). Multi-point optical measurements of simultaneous vectors in unsteady flow – a review. *Int J Heat Fluid Flow* 7 pp 127.

Acton R E (1980). A modelling of large eddies in an axisymmetric jet. *J Fluid Mech* 98 pp 1.

Ahmed S A and Giddens D P (1984). Pulsatile poststenotic flow studies with laser doppler anemometry. *J Biomech* 17 pp 695.

Armaly B F, Durst F, Pereira J C F and Schönung B (1983). Experimental and theoretical investigation of backward facing step flows. *J Fluid Mech* 127 pp 473.

Bajura R A and Pellegrin M T (1977). Studies of pulsating incompressible flow through orifice meters. *Proc Symp on Flow in Open Channels and Closed Conduits, NBS, Gaithersburg MD, USA.*

Balasubramanian K (1983). An experimental investigation of steady flow at an arterial bifurcation. Doctoral dissertation. Georgia Inst Techn USA.

Beavers G S and Wilson T A (1975). Vortex growth in jets. *J Fluid Mech* 44 pp 97.

Bernardinis B de, Graham J M R and Parker K H (1981). Oscillatory flow around disks and through orifices. *J Fluid Mech* 102 pp 279.

Bertram C D and Pedley T J (1983). Steady and unsteady separation in an approximately two-dimensional indented channel. *J Fluid Mech* 130 pp 315.

Caro C G, Pedley T J, Schroter R C and Seed W A (1978). *The Mechanics of the Circulation* (Oxford Univ Press).

Cassanova R A and Giddens D P (1978). Disorder distal to modelled stenoses in steady and pulsatile flow. *J Biomech* 11 pp 441.

Cox J T (1977). Description of a pulsatile flow field downstream from an orifice-like stenosis. Doctoral dissertation. Univ Houston, Houston, Texas.

Crow S C and Champagne F H (1971). Orderly structure in jet turbulence. *J Fluid Mech* 48 pp 547.

Djilali N (1978). Oscillatory flow through a sharp-edged orifice plate. MSc Thesis, Imperial College London).

Doo I, Jedrich W T, Kennedy J S, Adams P F and Rodkiewicz Cz M (1984). Wall distensibility effect on arterial flow distribution. *J Biomech* 17 p 643.

Durrani T S and Greated C A (1977). *Laser Systems in Flow Measurement* (New York: Plenum).

Durst F, Melling A and Whitelaw J H (1976) *Principles and Practice of Laser-Doppler Anemometry* (London: Academic Press).

George W K and Lumley J L (1973). The laser-Doppler velocimeter and its application to the measurement of turbulence. *J Fluid Mech* 60 pp 321.

Gerrard J H (1971). An experimental investigation of pulsating turbulent water flow in a tube. *J Fluid Mech* 46 pp 43.

Glagov S and Zarins C K (1983). Quantitating atherosclerosis: problems of definition. *in*: *Clinical Diagnosis of Atherosclerosis*: *Quantitative Methods of Evaluation.* eds Bond M G *et al* (New York: Springer Verlag).

Gray C and Greated C A (1987). The application of particle image velocimetry to the study of water waves. *Preprint* (Edinburgh Univ).

Hall P and Parker K H (1976). The stability of decaying flow in a suddenly blocked channel. *J Fluid Mech* 75 pp 305.

Harris F J (1978). On the use of windows for harmonic analysis with the discrete Fourier transform. *Proc IEEE* 66 pp 51.

Hartmann I and Treiber J (1986). Forecasting of daily power system loads. *Contr and Comp* 14 pp 84.

Haykin S, ed. (1979). *Nonlinear Methods of Spectral Analysis* (New York: Springer-Verlag).

Ho C-M and Huang L-S (1982). Subharmonics and vortex merging in mixing layers. *J Fluid Mech* 119 pp 443.

Ho C-M and Huerre P (1984). Perturbed free shear layers. *Ann Rev Fluid Mech* 16 pp 365.

Hussain A K M F (1977). Mechanics of pulsatile flow of relevance to the cardiovascular system. *in*: *Cardiovascular Flow Dynamics and Measurements.* eds N H C Hwang and N A Normann (Baltimore: Univ Park Press).

Khalifa A M A and Giddens D P (1978). Characterisation and evolution of poststenotic flow disturbances. *J Biomech* 14 pp 279.

Kitney R I and Giddens D P (1986). MEDINFO 86 Pt 2 pp 672.

Lambossy P. (1952). Oscillations forcées d'un liquide incompressible et visqueux dans un tube rigide et horizontal. Calcul de la force de frottement. *Helv Phys Acta* 25 pp371.

Lee J-S and Fung Y-C (1970). Flow in locally constricted tubes at low Reynolds numbers. *J Appl Mech Trans ASME* pp 9.

Lieber B B and Giddens D P (1988). Apparent stresses in disturbed pulsatile flows. *J Biomech* 21 pp 287.

Lighthill M J (1972). Physiological fluid dynamics: a survey. *J Fluid Mech* 52 pp 475.

Lighthill M J (1975). *Mathematical Bio-fluid Dynamics* (SIAM, Philadelphia).

Linkens D A (1979). Empirical rules for the selection of parameters for autoregressive analysis of biomedical rhythms. *Signal Processing* 1 pp 243.

Mates R E, Gupta R L, Bell A C and Klocke F J (1978). Fluid dynamics of coronary artery stenoses. *Circ Res* 42 pp 152.

Meynart R (1983). Instantaneous velocity field measurements in unsteady gas flow by speckle velocimetry. *Appl Optics* 22 pp 535.

Oppenheim A V and Schafer R W (1975). *Digital Signal Processing* (Englewood Cliffs: Prentice-Hall).

Parker K H (1977). Instability in arterial blood flow. *in: Cardiovascular Flow Dynamics and Measurements.* eds N H C Hwang and N A Normann (Baltimore: University Park Press).

Poiseuille J L M (1840). Recherches experimentales sur les mouvement des liquides dans les tubes de trés petits diamètres. *C R Acad Sci (Paris)* 11 pp 961, pp 1041.

Ralph M E and Pedley T J (1988). Flow in a channel with a moving indentation. *J Fluid Mech* 190 pp 87.

Rudd M J (1969). A new theoretical model for the laser Doppler meter. *J Phys E: Sci Instr* 2 pp 55.

Sarpkaya T (1966). Experimental determination of the critical Reynolds number for pulsating Poiseuille flow. *J Basic Eng Trans ASME* 88 pp 589.

Sexl T (1930). Über den von E.G. Richardson entdeckten Annulareffekt. *Z Phys* 61 pp 349.

Sobey I J (1985). Observation of waves during oscillatory channel flow. *J Fluid Mech* 151 pp 395.

Stephanoff K D, Pedley T J, Lawrence C J and Secomb T W (1983). Fluid flow along a channel with an asymmetric oscillating constriction. *Nature* 305 pp 692.

Stettler J C and Hussain A K M F (1987). On transition of the pulsatile pipe flow. *J Fluid Mech* 170 pp 169.

Thiriet M, Treiber J and Graham J M R (1988). Velocimetrie par imagerie du deplacement de particules. *XIII Congres de la Societe de Biomecanique*, Louvain-en-Woluwe (Bruxelles).

Uchida S (1956) Pulsating viscous flow superposed on the steady laminar flow motion. *Z Angew Math Phys* 7 pp 403.

Vonrunden W J, Blaisdell F W, Hall A D and Thomas A N (1964). Multiple arterial stenoses: effect on blood flow. *Arch Surg* 89 pp 307.

Weinbaum S and Parker K H (1975). The laminar decay of suddenly blocked channel and pipe flows. *J Fluid Mech* 69 pp 729.

Witzig K (1914). Über erzwungene Wellenbewegungen zäher, inkompressibler Flüssigkeiten in elastischen Röhren. Dissertation. Bern, Switzerland.

Womersley J R (1955) Method for the calculation of velocity, rate of flow and viscous drag in arteries when the pressure gradient is known. *J Physiol* 127 pp 553.

Yongchareon W and Young D F (1979). Initiation of turbulence in models of arterial stenoses. *J Biomech* 12 pp 185.

Young D F (1979). Fluid mechanics of arterial stenoses. *Trans ASME J Biomech Eng* 101 pp 157.

Young D F and Tsai F Y (1973). Flow characteristics in models of arterial stenoses — I. Steady flow. *J Biomech* 6 pp 395.

Young D F and Tsai F Y (1973). Flow characteristics in models of arterial stenoses — II. Unsteady flow. *J Biomech* 6 pp 547.

CHAPTER IV

ON NONLINEAR OSCILLATIONS IN NONCONSERVATIVE SYSTEMS

[Fig. 75.]

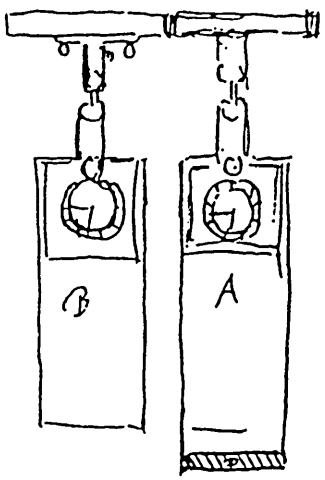

"Diebus 4 aut 5 horologiorum duorum novorum in quibus catenulae [Fig. 75], miram concordiam observaveram, ita ut ne minimo quidem excessu alterum ab altero superaretur. sed consonarent semper reciprocationes utriusque perpendiculi. unde cum parvo spatio inter se horologia distarent, sympathiae quandam quasi alterum ab altero afficeretur suspicari coepi. ut experimentum caperem turbavi alterius penduli reditus ne simul incederent sed quadrante horae post vel semihora rursus concordare inveni."[1]

Christiaan Huygens, 22nd February 1665.

Summary

Attempts at demarcation through negation are invariably expansive in character and require qualification. This chapter provides an overview of what van der Pol termed relaxation oscillations, with a single or multiple degrees of freedom. The van der Pol oscillator itself is reviewed briefly but is regarded too complex a quantitative model of harmonic synchronisation[2]. However, the emphasis here is on weakly perturbed oscillators for which important dynamical reductions are possible. These reductions allow the (analytical) treatment

[1] "For four or five days I had observed wonderful concord between two new clocks on this support [Fig. 75], such that neither was ahead by the most minimal difference yet. Instead, the reciprocations of the two perpendicle were in perfect harmony. I began to suspect that, because of the small distance between the clocks, they affected each other. By way of experiment, I perturbed the return of one of the penduli so they did not swing in simultaneously, but after a quarter or half an hour, I found them moving in harmony again". Christiaan Huygens, Vol 17, *Oeuvres Completes de Christiaan Huygens*. Societé Hollandaise des Sciences, La Haye, M Nijhoff, 1932.

[2] The terminology used here is not strict, in the sense that no distinction is made between the terms 'synchronisation' and 'frequency entrainment'. The former term is sometimes reserved for phenomena observed in populations of identical oscillators to distinguish them from the interactions observed in populations of non-identical oscillators, described by the latter term.

coupling, congruent with the modelling conventions for spatio-temporal systems with local dynamics.

1. Introduction

Huygens seems to have been the first to consciously observe synchronisation in a two-oscillator system. However, his accidental discovery of this phenomenon was presumably rather premature (Zeitgeist theory, Ogburn and Thomas 1920). In the end, the notion of mutual synchronisation had to await rediscovery more than two centuries later. Although cursory mention was made by John Ellicott[3] in 1739, it was Lord Raleigh (1894), who introduced what is referred to as Raleigh's equation or van der Pol oscillator, when studying the negative-damping effect of dry friction on a violin string. Eventually, in the early 1920s synchronisation was deemed important enough to receive theoretical treatment (Appleton 1922, van der Pol 1922).

The concept of synchronisation of self-excited oscillations with an external excitation found its way into fluid mechanics only much later, although 'lock-in' or 'locking-on' phenomena are known for a number of flow instabilities, *e.g.* for the Bénard - von-Kármán vortex street, free shear layer instabilities and oscillations of impinging flows. This comes as no surprise, as the Navier-Stokes equations cannot be viewed as an assembly of a large number of coupled identical systems with local dynamics. Every term on the right-hand side of this equation represents 'interaction' because a spatial gradient is involved.

Early interest in synchronisation phenomena in fluid flows focused on the vortex shedding process from oscillating bluff bodies in moving fluids in which case an analogy with nonlinear oscillators was readily suggested by the presence of a fairly discrete frequency component, characterising the flow instability.

Observations of harmonic and sub-harmonic entrainment of vortex shedding from an oscillating cylinder as well as beating phenomena and hysteretic response led Bishop and Hassan (1964) to speculate on the existence of a 'fluid oscillator' and they referred to Appleton's work. These experimental findings and conjectures were taken up by Hartlen and Currie (1970), who used a simple van der Pol type oscillator to describe typical features of oscillating cylinder/wake combinations. Subsequently, Iwan and Blevis (1974) made an attempt at rationalising the concept of nonlinear self-sustained oscillations by resorting to basic

[3]For further historic detail on this subject see "*Les horloges sympathiques de Huygens, les phénomènes connexes et les oscillations principales et composeés que présentent deux pendules fixeś à un mécanisme à un seul degré de liberté, par D J Korteweg*",Archives Neérl. des Sciences ex. et nat., Série II, T. XI, la Haye, M Nijhoff, 1906.

fluid mechanic principles. Further studies of bluff-body dynamics aimed at a more comprehensive modelling of observed phenomena (*e.g.* Berger *et al* 1979) but, as Bearman (1984) notes, nonlinear oscillator models "are unable to reproduce all the observed effects".

Recently, renewed interest in dynamical systems (Hirsch and Smale 1974) has stimulated the use of more realistic 'fluid oscillator' models. For example, the various instability regimes of a wake downstream of a cylinder have been modelled by a nonlinear harmonic oscillator (Provansal *et al* 1987), known in nonlinear hydrodynamic stability theory from a perturbation analysis of the Navier-Stokes equations, and speculations were made as to employing a distributed oscillator model.

In contrast to bluff-body wake dynamics, free shear layer instabilities have proved more elusive to a modelling by self-sustained oscillation. Wake flows contain absolutely unstable flow regions with a fairly discrete frequency component, whereas free shear layers are typically convectively unstable and velocity fluctuations are broadband in character. Speculations exist as to the use of multiple-degree-of-freedom nonlinear oscillators or, in the continuum limit, fields of oscillators. This will form the central theme of chapter V.

In the subsequent sections the groundwork is laid for the nonlinear-oscillator treatment of free shear layer instabilities, with a discussion of simple and coupled nonlinear oscillator systems.

2. Single-Degree-of-Freedom Oscillations

By way of clarification, the definition of 'degrees of freedom', as used in the context of oscillations, does not follow the conventions of thermodynamics or statistical mechanics. Instead of identifying the number of degrees of freedom with actual state space dimension, the relevant space is, for one-degree-of freedom oscillations, the ring $\mathbb{S}^1$, and for several-degree-of-freedom oscillations the torus $\mathbb{T}^n$. Only when dealing with the simplest oscillators of state space dimension two, is this definition consistent with conventions in mechanics (Feynman *et al* 1964).

2.1 The van der Pol Oscillator Revisited

A discussion of nonlinear oscillations would surely be incomplete without mention of the van der Pol oscillator, classic example of a second-order system exhibiting relaxation oscillations. Not only was this equation the first to be analysed theoretically, but more significantly, it was the first nonconservative system[4] in which chaotic behaviour was studied

(Cartwright and Littlewood 1945, Levinson 1949), eventually leading to the development of a modern mathematical theory of dynamical systems during the 1960's (Smale 1967).

2.1.1 Frequency Entrainment

The unforced (autonomous) van-der-Pol equation

$$u_{tt} - \epsilon\,(1-u^2)\,u_t + u = 0\,, \quad \epsilon > 0 \tag{4.1}$$

models a simple triode oscillator (*figure* 4.1*a*) with assumed nonlinearity $i(u)=-u+u^3$ and possesses a single stable limit cycle, apart from an unstable focus at the origin (*figure* 4.1*b*). For weak nonlinearity $\epsilon<<1$, the limit cycle is nearly circular and solutions have the form $u(t)=\cos(t+\theta_0)$, but as ϵ, often referred to as waveshape factor, becomes larger, solutions approach highly nonlinear relaxation oscillations (*figure* 4.1*c*), of frequency $\frac{1}{1.614\epsilon}$, determined by the relaxation time $\tau_{rel}= R\ C$ (Stoker 1950).

Adding a forcing term with dc-offset $B\cos(\nu t)+B_0$ to the right-hand side of equation (4.1) and introducing a new variable $v=u-B_0$, yields an alternative form

$$v_{tt} - \mu\,(1-\beta v-\gamma v^2)\,v_t + v = B\cos(\nu t) \tag{4.2}$$

where $\mu = (1-B_0{}^2)\,\epsilon\,, \qquad \beta = \frac{2B_0}{1-B_0{}^2}$ and $\gamma = \frac{1}{1-B_0{}^2}$.

The dc-component is seen to introduce a quadratic term in the nonlinearity, $i(v) = -v + \beta v^2 + \gamma v^3$, and must satisfy $B_0<1$ if a stable limit cycle is to be maintained.

For weak nonlinearity harmonic, higher-harmonic and sub-harmonic oscillations as caused by frequency entrainment, may be investigated by the method of harmonic balance (Krylov and Bogoliubov 1947). Solutions for equation (4.2) are assumed to have the form

$$v(t) = \frac{B}{1-\nu^2}\cos(\nu t) + b_1 \sin(n\nu t) + b_2 \cos(n\nu t)\,. \tag{4.3}$$

---

[4] Chaos in conservative, Hamiltonian systems, on the other hand, had been observed much earlier in problems concerning the three-body-problem of celestial mechanics. Poincaré remarks on highly irregular movements of a parametrically excited pendulum : "*One is struck by the complexity of this figure that I am not even attempting to draw. Nothing can give us a better idea of the complexity of the three-body problem...*" (Vol 3, Les Méthodes Nouvelles de la Mécanique Celeste, Gauthier-Villars, Paris, 1899)

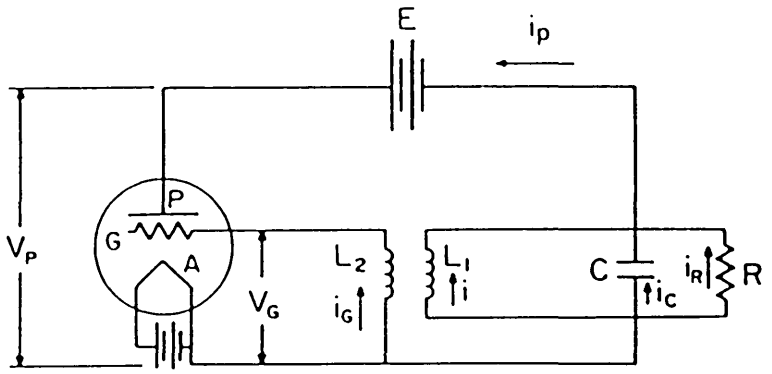

(a)

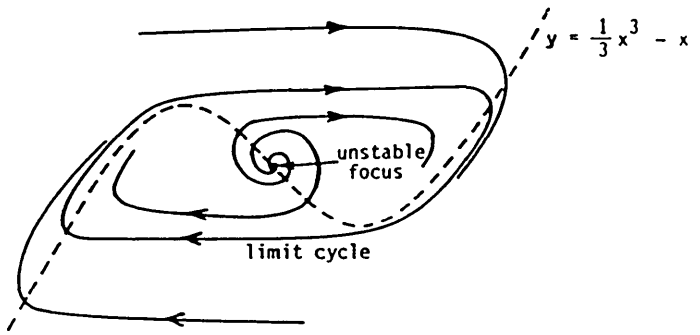

(b)

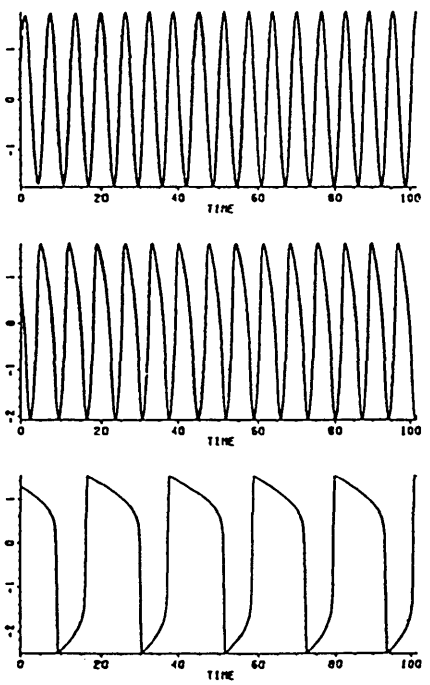

(c)

Figure 4.1 (a) Electronic circuit diagram of the van der Pol oscillator. (b) Limit cycle attractor of the (autonomous) van der Pol oscillator for large ϵ. (c) Relaxation oscillations for various values of the waveshape factor ϵ (0.1, 1.0, 10.0) and B_0=0.5. Note the asymmetry of the oscillations.

Here, the integer number n defines higher (n=2,3,...) and sub- ($n=\frac{1}{2},\frac{1}{3},...$) harmonics, respectively. The amplitude $\frac{B}{1-\nu^2}$ of the harmonic term is determined by disregarding nonlinear terms in equation (4.2), an approximation that is justified even for large nonlinearities (Mandelstam and Papalexi 1932).

Substituting into equation (4.2) and equating coefficients of like terms, the amplitude and phase of the entrained oscillation are found. Stability of this solution is then analysed by solving the variational equation of the Hill type[5] (Hayashi 1964), dividing the response curves into stable and unstable regions (*figure* 4.2*a*).

Numerical results (Hayashi *ibid*), that agree well with the harmonic-balance analysis – apart from a small, but noticeable difference in intrinsic frequency – are shown in figures 4.2*a* and 4.2*b*. The response curve for harmonic entrainment relates the forcing frequency (or, in normalised form, the 'detuning' $\sigma_1 = \frac{1-\nu^2}{\mu\nu}$) to the amplitude r_1 of the entrained oscillation, for various forcing amplitudes B. For higher and sub-harmonic entrainment only the stable regions of attraction are depicted in the (B, ν) - plane. As for the harmonic entrainment region, the size of the higher and subharmonic regions depends on parameters ϵ and B_0. By increasing the dc-term, the higher and subharmonic regions of even frequency ratio can be increased. Note, however, that the regions of odd integer ratio of frequency entrainment cannot be abolished completely, because the cubic term is essential for self-sustained oscillations.

Two points are worth mentioning at this point. Closer inspection of the response curve (*figure* 4.2, see also Stoker (1950) for a more detailed diagram), shows that potentially 'pathologic' behaviour may occur near σ=0.5 and $(\frac{B}{\mu\nu a_0})^2=\frac{8}{27}$, due to the multi-valued character of the graph. Indeed, two harmonic solutions, or a harmonic as well as an almost periodic oscillation, are known to co-exist stably in this rather limited region (Cartwright 1945). The two-solution region is characterised by jumps in amplitude and hysteresis. A recent account of the qualitative dynamics of this region can be found in (Guckenheimer and Holmes 1983), where detailed sketches of the topology of the forced weakly nonlinear van der Pol oscillator are given. This has prompted Thompson and Stewart (1986) to suspect mildly chaotic behaviour, a property of the weakly nonlinear van der Pol oscillator that generally seems to be overlooked (*e.g.* Kitney 1975).

---

[5] Conventional stability analysis *via* characteristic equation of the variational form fails to resolve instabilities resulting from the variations having different, typically commensurate, frequencies.

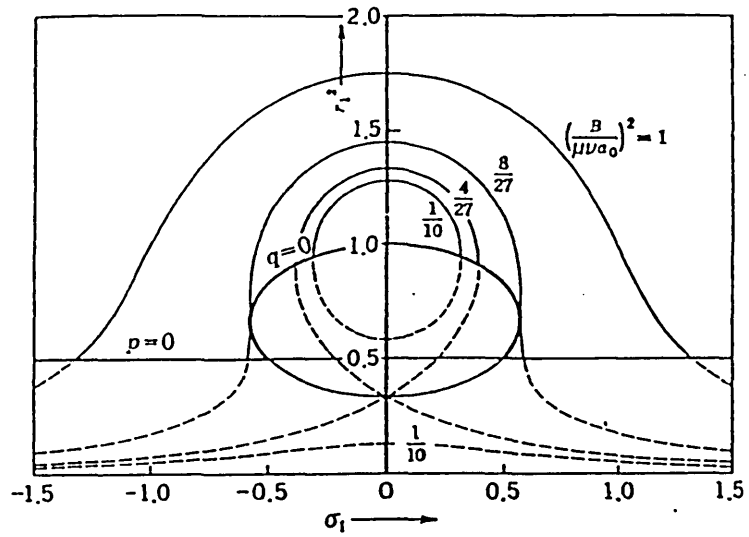

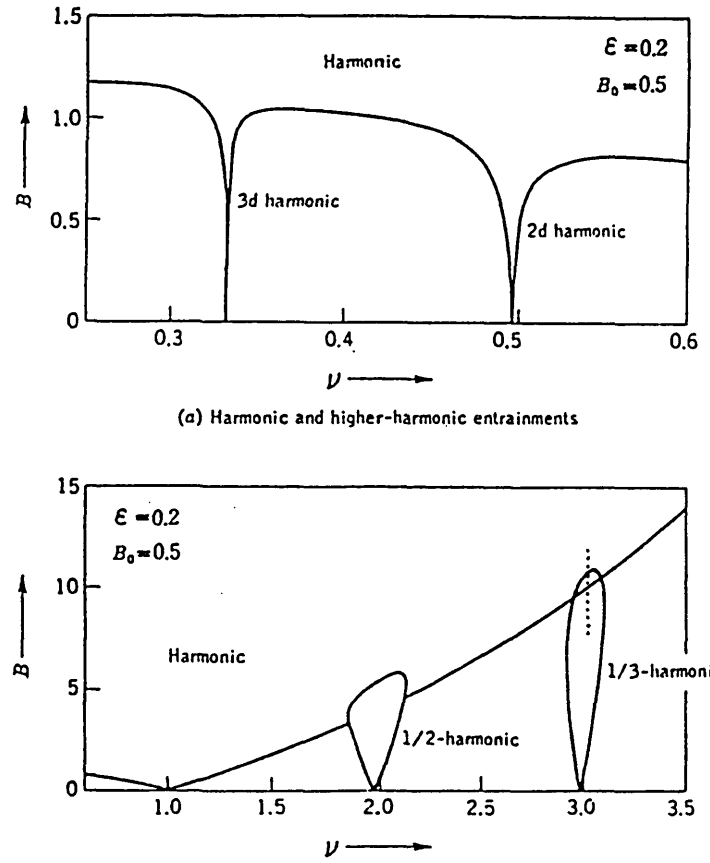

Figure 4.2 (*a*) Response curve of the van der Pol oscillator for harmonic entrainment. The entrained oscillator amplitude is given by r_1. (*b*) Harmonic, super- and sub-harmonic entrainment regions, obtained from analog-computer simulation. Note that, for higher and subh-harmonic entrainment, the apparent oscillator frequency differs from $\omega_0=1$, as the result of the non-sinusoidal waveform of the entrained oscillation. The overlap of the harmonic and 1/3-harmonic region indicates hysteresis (after Hayashi 1964).

Hysteresis is also observed in the region of harmonic and 1/3 harmonic entrainment overlap, for example when the forcing amplitude B is varied as indicated by the dotted line in figure (4.2*b*).

2.1.2 Phase Locking and Asynchronous Quenching

The above analysis of frequency entrainment in the van der Pol oscillator gives no indication that the entrainment mechanism for small forcing amplitudes may be essentially different from that for large amplitudes. Physically, though, two fundamentally different mechanisms are operative, *phase locking* and *asynchronous quenching*. Phase locking implies synchronisation by either systematic phase retardation or phase advancement of the self-sustained oscillation by virtue of the action of the external force on it. Asynchronous quenching, on the other hand, corresponds to the case where the effect of the external force is to abolish self-sustained oscillations. The system response then is that of a nonlinear resonator and the process of quenching the self-sustained oscillation is advantageously analysed by the describing function technique (Atherton 1975).

More rigorous forms of analysis were employed by Dewan (1972) to investigate the details of the entrainment mechanism. Using topological methods, he gave exact definitions for distinguishing between the different types of entrainment. Sketched briefly here, phase locking and asynchronous quenching are defined by the type of singularities associated with these forms of entrainment in the van der Pol plane. This variant of the two-dimensional phase plane has the added property that the dominant rotation at the forcing frequency is eliminated. Possible combinations of singularities are: (1) a single focus; (2) a saddle and two sinks; (3) a saddle, a sink and a source. Phase locking is identified by the existence of three singularities, one of which is a saddle point and the system is at rest at the stable node. For asynchronous quenching the system equilibrium points are stable foci.

Dewan notes that for the van der Pol oscillator all subharmonic entrainment seems to be of the phaselocking type. Other entrainment regions are of this type only for weak forcing.

2.1.3 Chaotic Response

Before entering into a discussion of 'irregular bahaviour' observed in certain dynamical systems, a few words on the terminology are in order. The attribute *chaotic* has been used to describe the random motion of trajectories on attractors with complicated geometric structures in dissipative systems, in distinction to *stochastic* motion in conservative, Hamiltonian systems (Lichtenberg and Lieberman 1983). Often, however, the usage is less stringent, and Mees

(1981) suggests to call *chaotic* any system behaviour that is more complicated than almost periodic motion.

To begin with, chaotic motion applies to deterministic dynamical systems and an essential property of deterministic randomness (*sic*) was explained eloquently by Henri Poincaré :

"*A very small cause which escapes our notice determines a considerable effect we cannot fail to see, and then we say that the effect is due to chance. If we know exactly the laws of nature and the situation of the universe at the initial moment, we could predict exactly the situation of that same universe at a succeeding moment. But even if it were the case that the natural laws had no longer any secret for us, we could still only know the initial conditions 'approximately'. If that enabled us to predict the succeeding situation with the 'same approximation', that is all we require, and we should say that the phenomenon had been predicted, that it is governed by laws. But it is not always so; it may happen that small differences in the initial conditions produce very great ones in the final phenomena. A small error in the former will produce an enormous error in the latter. Prediction becomes impossible, and we have a fortuitous phenomenon.*" (Science et Méthode, Paris: Flammarion, 1908).

To summarise Poincaré's account, this property is the sensitivity to initial conditions, reflected in the exponential divergence of trajectories, starting from a neighbourhood of initial conditions. A quantitative measure of divergence is provided by the Lyapunov exponent. For a given n-dimensional nonlinear system, the Lyapunov exponents are determined from the eigenvalues of the long-time product Jacobian, but non-analytical methods also exist (Wolf 1986). The other property by which chaotic motion is identified is quasi-recurrence, characterised by a power spectrum with broadband background noise, superimposed on which are relatively sharp peaks (Parker and Chua 1987).

For chaotic motion to occur, a minimum dynamical system complexity is required. According to the Poincaré-Bendixson theorem (Hirsch and Smale, 1974), autonomous systems of order less than three will always converge to a point or a closed curve. Furthermore, the synchronisation property of nonlinear oscillators has recently been associated with the existence of chaotic motion (Tang *et al* 1983).

Recalling that non-autonomous systems are readily transformed to autonomous form by defining new state variables for each external input, the forced van der Pol oscillator is seen to be a prime candidate for chaotic behaviour.

As mentioned earlier, it was Cartwright and Littlewood who studied a phenomenon that van der Pol and van der Mark (1927) had been aware of. The key observation made was that, for large ϵ (equation 4.1), there are parameter values for which two different sub-

harmonic solutions with periods that are odd multiples of the forcing period, co-exist stably. In this case, the start-up transients may jump between the two subharmonics for an arbitrarily long time before settling to one or the other. This irregular behaviour was analysed again for a simplifed van der Pol oscillator with the nonlinearity replaced by a piecewise-linear characteristic (Levinson 1949). In fact, Levinson's paper has been the starting point for the construction of prototype chaotic systems leading to a deepened understanding of chaos generating mechanisms.

Strangely enough, though, it is a hopeless undertaking to try to find chaotic solutions in laboratory experiments (Parker and Chua 1983). Indeed, an analysis shows that in the space of initial conditions, chaotic solutions form an infinitely thin set (Levi 1981). Ironically, chaos is clearly observable in a forced neon-bulb oscillator employed by van der Pol and van der Mark (*ibid*). For certain parameters they observed "irregular noise", but dismissed it as a subsidiary phenomenon. This noise has since been identified as chaotic behaviour (Kennedy and Chua 1986).

The hypothesised connection between irregular behaviour and synchronisation in nonlinear oscillators (Tang *et al*, *ibid*) becomes apparent now, but requires qualification. It is the overlap between different entrainment regions that provides the mechanism for chaotic behaviour. Consequently, irregular dynamics are not expected to be observed in simple oscillators with a harmonic catchment region of entrainment only. The effects of resonance overlap are illustrated rather well in (Tomita 1986) for the Brusselator (a second order chemical oscillator proposed by the Brussels school, Glansdorff and Prigogine 1971) (*figure* 4.3). We shall come back to the resonance overlap mechanism in § 2.4.

2.1.4 Concluding Remarks

The above comments on irregular behaviour in the forced van-der-Pol oscillator testify to the remarkably complex dynamics of this system. As yet the dynamics have not been fully understood, and modifications similar to those of Levinson are required to make the oscillator dynamics amenable to qualitative analysis (Levi 1981).

The value of the van der Pol oscillator for the quantitative modelling of harmonic entrainment seems questionable therefore. Glass *et al* (1986) remark on the difficulties with the van der Pol equation when trying to model cardiac rhythms and have opted for a phase description approach instead. In general, the expediency of alternative, averaged forms of the van der Pol equation is well established and numerical studies are greatly assisted if the oscillator dynamics are given in a more suitable coordinate system (such as polar coordinates).

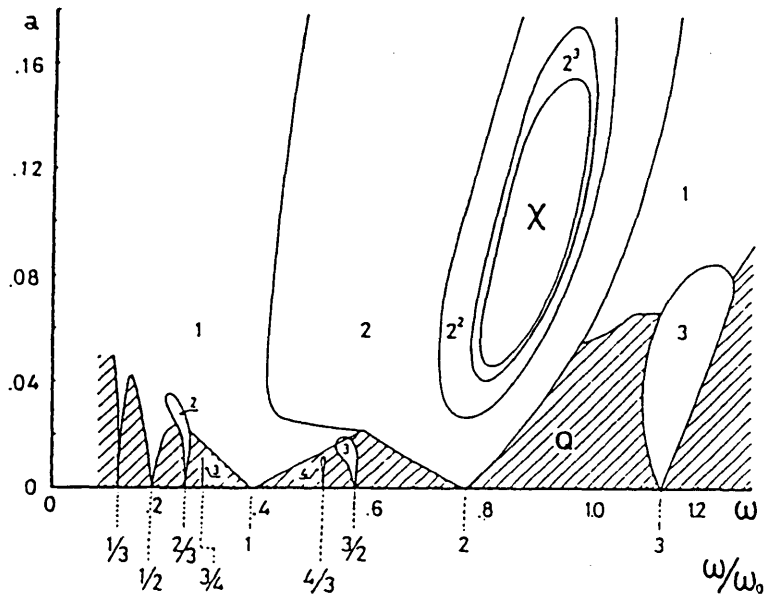

Figure 4.3 Entrainment regions of the forced Brusselator $x_t = x^2y - Bx + A + a\cos\omega t$; $y_t = Bx - x^2y$ ($A=0.4$, $B=1.2$). Chaotic response, caused by resonance overlap, is found in the region marked χ. In the shaded regions 'Q' almost periodic oscillations exist (after Tomita 1986).

Indeed, some coupled-oscillator models of the neural control of locomotion have been formulated in purely qualitative terms (Cohen and Wallen 1980, Cohen and Harris-Warrick 1984). Without diminishing the predictive power of these models, the qualitative approach avoids implications regarding complex synchronisation mechanisms.

It is the purpose of the following section to introduce and discuss a nonlinear oscillator with simple dynamics, closely related to an averaged form of the van der Pol oscillator.

2.2 The λ-ω Oscillator

Introduced in a paper by Kopell and Howard (1973*b*) to determine analytically certain wave patterns occurring in spatially oscillating chemical reactions, the λ-ω oscillator models the simplest, yet generic, form of a nonlinear harmonic oscillator (Kuramoto 1984*a*). This oscillator has found application in the synthesis of nonlinear periodic systems (Chua and Green 1974, Bardakjian and Sarna 1980) and is an example of a system displaying sub-/super-critical Hopf bifurcations which play an important part in hydrodynamic stability theory (Joseph, 1985). Given by equation

$$\begin{bmatrix} x_t \\ y_t \end{bmatrix} = \begin{bmatrix} \lambda(r) & -\omega(r) \\ \omega(r) & \lambda(r) \end{bmatrix} \begin{bmatrix} x \\ y \end{bmatrix} \quad ; \quad r^2 = x^2 + y^2 \tag{4.4}$$

or, in more 'natural' (defining!) polar coordinates,

$$\begin{aligned} r_t &= r\,\lambda(r) \\ \theta_t &= \omega(r)\ , \end{aligned} \tag{4.5}$$

the λ-ω oscillator possesses solutions for the particular case $\lambda(r) = R^2 - r^2$,

$$\begin{aligned} r^2(t) &= \frac{R^2\, r^2(0)}{r^2(0) + [R^2 - r^2(0)]\, \exp(-2R^2 t)} \\ \theta(t) &= \int_0^t \omega[r(\tau)]\, d\tau + \theta_0 \end{aligned} \tag{4.6}$$

where $r(0)$ and θ_0 are the initial values. In general, limit cycle solutions of radius r_0 are defined by the zeros of $\lambda(r)$ and stability is determined from $d\lambda(r)/dr$ at r_0.

It is worth mentioning that the property of defining limit cycles by zeros of λ allows

for easy mathematical description of multiple-limit-cycle systems such as encountered in aeroelastic galloping (*eg* Parkinson and Smith 1964).

Returning to the Hopf bifurcation property of the λ-ω system, such bifurcation behaviour is at the centre of a theorem of the same name that provides one of the few reliable methods of establishing the existence of limit cycles in high-dimensional systems. Briefly stated, Hopf's theorem says that in a system of ordinary differential equations that depend on a real parameter μ, if on linearising about an equilibrium point one finds that pairs of complex conjugate eigenvalues of the linearised system cross the imaginary axis as μ varies through certain critical values, then for near-critical values μ_c limit cycles close to the equilibrium point exist.

In the case of the λ-ω oscillator, so-called *supercritical* bifurcations with stable limit cycles are found for functions $\lambda(r)$ with dependence on a parameter μ as sketched in figure 4.4.*a*, whilst *subcritical* bifurcations together with unstable limit cycles and hysteresis result from functions $\lambda(r)$ (*figure* 4.4*b*).

Due to the generic character of the λ-ω system, it is possible to reduce a wide class of nonlinear oscillations to this form. For example, to first order the van-der-Pol equation is reducible to a system with $\lambda(r)= \frac{1}{2}- \frac{1}{8}\gamma r^2$ and $\omega(r)=1$. To demonstrate this, equation (4.2) is rewritten in polar coordinates,

$$\begin{aligned} r_t &= \mu\, r\,(1 - \beta\, r\cos\theta - \gamma\, r^2\cos^2\theta)\,\sin^2\theta \\ \theta_t &= 1 + \mu\ (\,1 - \beta\, r\cos\theta - \gamma\, r^2\cos^2\theta)\,\sin\theta\,\cos\theta \end{aligned} \tag{4.7}$$

By first-order averaging techniques (Hale 1969), it can be seen that (4.7) is equivalent to

$$\begin{aligned} r_t &= \mu\, r\,(\,\tfrac{1}{2} - \tfrac{1}{8}\gamma r^2\,) + \mathcal{O}(\mu^2) \\ \theta_t &= 1 + \mathcal{O}(\mu^2) \end{aligned} \tag{4.8}$$

Interestingly, the assumed general dependence of instantaneous frequency ω on amplitude, although not observed in the simple van der Pol system, is known for a self-oscillatory system with nonlinear restoring force, $v_{tt} - \mu(1-v^2)\, v_t + v^3 = B\cos(\nu t)$ (Hayashi 1964).

More generally, it may be shown (Kuramoto 1984*a*), how a small-amplitude equation valid near a Hopf bifurcation point is derived from a general system of ordinary differential

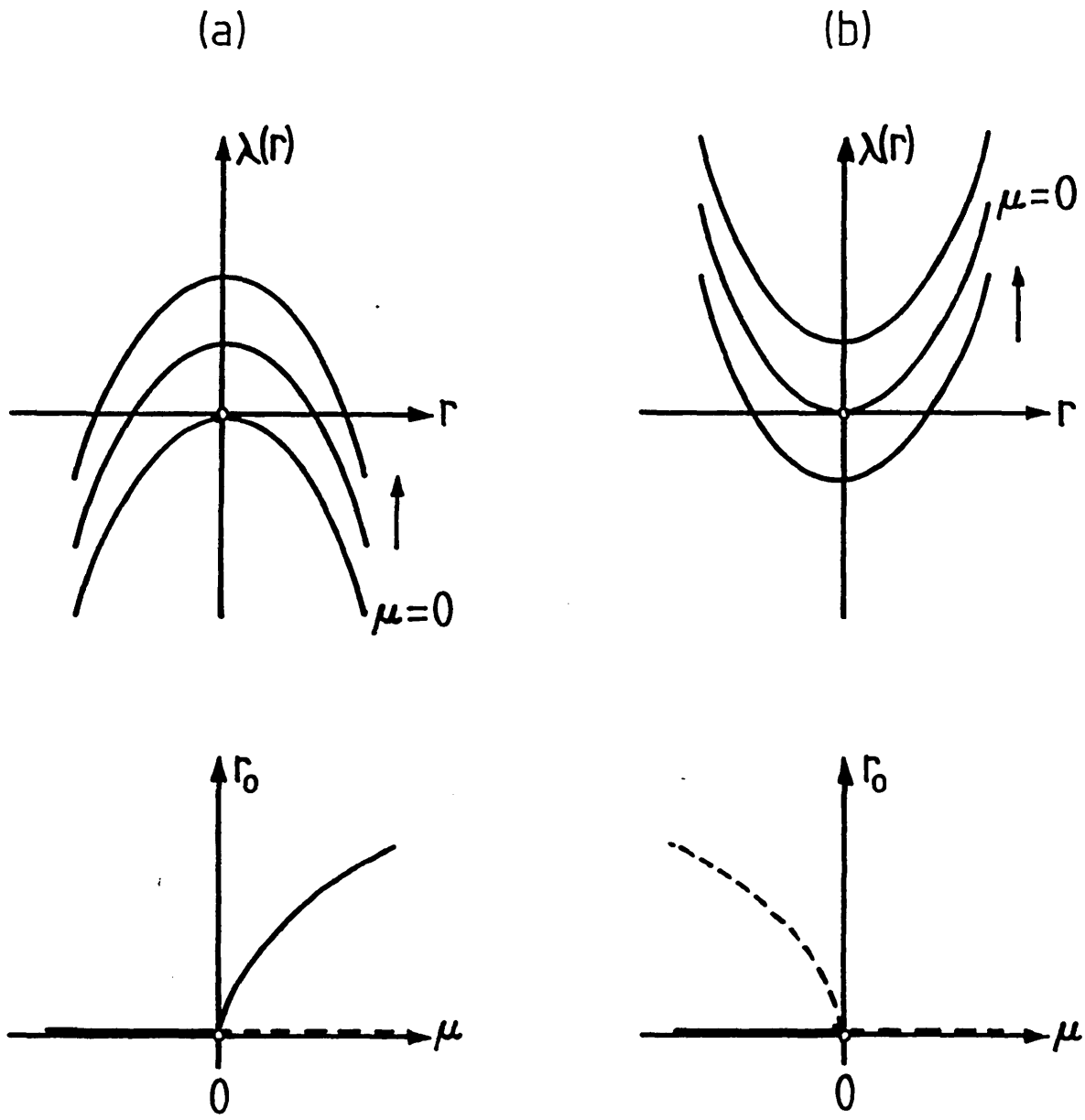

Figure 4.4 Hopf bifurcations of the $\lambda-\omega$ oscillator. $\lambda(r)$ varies with the control paramter μ as indicated. r_0 is the steady state amplitude. (*a*) Supercritical bifurcation — emergence of a stable limit cycle. (*b*) Subcritical bifurcation — loss of stability.

equations. This equation, called the Stuart-Landau equation, after Landau (1944), who was the first to derive this equation form on heuristic grounds, and Stuart (1960), who obtained it through an asymptotic method, has the form :

$$\psi_t = a\,\psi - c\,|\psi|^2\psi \qquad \psi,\ a,\ c\ \in\ \mathbb{C} \tag{4.9}$$

By letting $\psi = r\,e^{j\theta}$, equation (4.9) is seen to be a λ-ω oscillator with defining functions $\lambda(r) = a_r - c_r r^2$ and $\omega(r) = a_i - c_i r^2$, where the subscripts r and i denote real and imaginary parts, respectively. The Stuart-Landau oscillator is of considerable importance in nonlinear hydrodynamic stability theory and has recently been employed as a model of the sub- and supercritical regimes of the circular cylinder wake (Provansal et al 1987). More importantly, the spatial development of nonlinear hydrodynamic stability may be described by a diffusively coupled field of Stuart-Landau oscillators, the Ginzburg-Landau equation (*cf* § 3.2.3).

2.2.1 Harmonic Entrainment

Entrainment behaviour of the λ-ω oscillator is investigated by applying a two-dimensional forcing signal (by symmetry considerations) :

$$\begin{bmatrix} x_t \\ y_t \end{bmatrix} = \begin{bmatrix} \lambda(r) & -\omega(r) \\ \omega(r) & \lambda(r) \end{bmatrix} \begin{bmatrix} x_t \\ y_t \end{bmatrix} + B \begin{bmatrix} \cos(\nu t) \\ \sin(\nu t) \end{bmatrix} \tag{4.10}$$

Again, in polar coordinates the dynamics of entrainment become more apparent :

$$\begin{aligned} r_t &= r\,\lambda(r) + B\cos(\nu t - \theta) \\ \theta_t &= \omega(r) + \frac{B}{r}\sin(\nu t - \theta) \end{aligned} \tag{4.11}$$

When the rotation of θ at, or near, the forcing frequency is eliminated by describing the temporal evolution of the phase difference $\phi = \nu t - \omega(r)$ instead,

$$\begin{aligned} r_t &= r\,\lambda(r) + B\cos\phi \\ \phi_t &= [\nu - \omega(r)] - \frac{B}{r}\sin\phi\ , \end{aligned} \tag{4.12}$$

regions of stable entrainment for the $\lambda-\omega$ oscillator may be determined from the stable equilibrium points of the second-order system (4.12). It is readily verified that equation (4.12) is identical to what is obtained for the van der Pol oscillator by assuming a harmonic solution with slowly varying parameters. Consequently, the solutions obtained to first order for entrainment in the van der Pol oscillator are exact for the $\lambda-\omega$ oscillator with the provision for generalised defining functions $\lambda(r)$ and $\omega(r)$ and linear(!) detuning σ.

For weak forcing compared to the strength of attraction of the limit cycle of the autonomous system, the time scales of r_t and ϕ_t are widely different. On the entrainment-relevant time scale of the phase difference, equation (4.12) becomes effectively one-dimensional, $\phi_t=\phi_t(r_0,\phi(t))$, with r_0 the steady state value. Stable solutions for the reduced system exist for values $|\phi| < \frac{\pi}{2}$. and the boundaries of stable entrainment are defined by $|\nu-\omega(r_0)|=\frac{B}{r_0}$.

Curiously, this region has been mistaken for describing entrainment in the $\lambda-\omega$ oscillator at all forcing amplitudes (Provansal et al 1987), but stable entrainment is obviously found also for values $|\phi| > \frac{\pi}{2}$. This is illustrated in *figure* 4.5 which shows the catchment region of entrainment in the $B-\nu$ plane for the example $\lambda=1-r^2$, $\omega(r)=\omega_0$. The $\vee$-shaped boundary separates the two regions $r_0 > 1$, $|\phi| < \frac{\pi}{2}$, and $r_0 < 1$, $|\phi| > \frac{\pi}{2}$, where r_0 is the entrained oscillation amplitude. The curve $r_0=1/\sqrt{2}$ is the entrainment boundary for larger detuning. The crossing of this boundary is accompanied by a supercritical Hopf bifurcation, whereby a stable focus becomes unstable and is surrounded by a stable limit cycle that represents almost periodic oscillations. Note that the limit cycle can be rather small in size and need not encircle the origin. These smaller limit cycles correspond to quasi-entrainment. The average oscillator frequency, although modulated, is the same as the forcing frequency. Finally, the region surrounding the intersection of the two boundary curves is topologically complex (Holmes and Rand 1983).

2.2.2 Super-/Sub-Harmonic Entrainment and Multi-Frequency Excitation

It has been shown how the van der Pol oscillator reduces to λ-ω form by applying averaging techniques. This connexion between the two systems readily highlights the major limitions of λ-ω oscillators, namely the absence of super-/sub-harmonic entrainment – a property that is averaged out, as it were.

However, by exploiting the fact that higher-harmonic entrainment in the van der Pol oscillator is equivalent to driving the system at the respective higher harmonic[6] instead, one

[6] In contrast to sub-harmonic entrainment, a higher harmonic of the forcing term is generated at the system nonlinear characteristic *via* non-phaseshifting frequency multiplication.

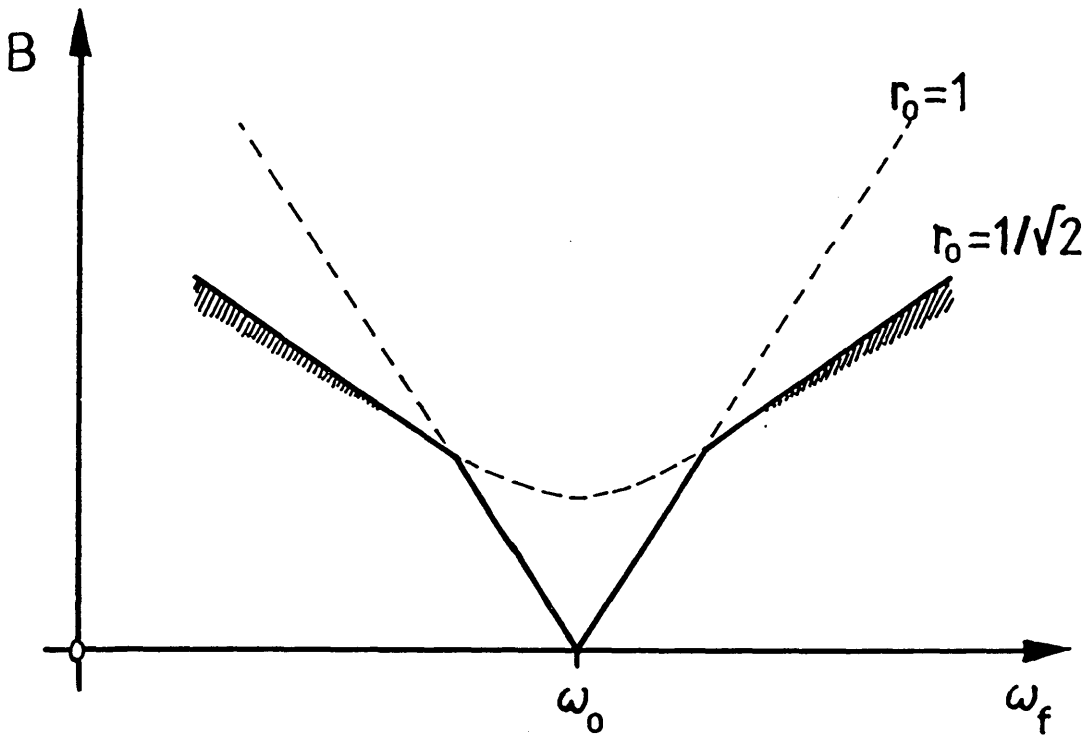

Figure 4.5 Catchment region of harmonic entrainment for a $\lambda-\omega$ oscillator with $\lambda(r)=1-r^2$, $\omega(r)=\omega_0$. The hatched regions indicate quasi-entrainment. On the locus $r_0=1$, with r_0 the entrained oscillation amplitude, $|\phi|=\frac{\pi}{2}$. In the neighbourhood of the intersection of the two curves $r_0=1$ and $r_0=1/\sqrt{2}$ complicated transitions occur.

arrives at the concept of multi-frequency excitation.

The entrainment diagram of the forced λ-ω system

$$\begin{aligned} r_t &= r\,\lambda(r) + \sum_k B_k \cos(k\omega_F t + \theta_{0k} - \theta) \\ \theta_t &= \omega(r) + \tfrac{1}{r}\sum_k B_k \sin(k\omega_F t + \theta_{0k} - \theta) \end{aligned} \tag{4.13}$$

shows regions of stable harmonic, sub- and higher-harmonic entrainment in neighbourhoods $k\omega_F \approx \omega(r_0)$ for values k=1, $\frac{1}{2}$, $\frac{1}{3}$,..., 2, 3,... (*figure* 4.6). Clearly, this method affords a high degree of control over the size of the entrainment regions and the phase difference between oscillator and forcing signal. Importantly, resonance competition will not lead to irregular behaviour as none of the entrainment regions other than the region of harmonic entrainment are an intrinsic part of the oscillator dynamics.

The concept of multi-frequency excitation will prove useful in connexion with the modelling of integer-ratio synchronisation in coupled oscillator systems (*cf* Ch V § 3).

2.3 Phase Description and Perturbation Ideas

It was pointed out in § 2 that trajectory motion in a limit-cycling system is effectively one-dimensional, leading to a corresponding definition of degrees of freedom. However, the notion of phase, marked off along the limit cycle, does not translate to forced systems in a straightforward manner. Intuitively, one may expect the phase concept to carry over to synchronisation in weakly forced systems, as exemplified in § 2.2.1 for the $\lambda-\omega$ oscillator. Below, these ideas are elaborated upon.

A study of phaselocking in the van-der-Pol oscillator led Adler (1946), to the formulation of a phase equation for nonlinear oscillators with memory-less nonlinearities, describing the temporal evolution of the phase difference ϕ between the self-oscillation and the forcing signal as a function of detuning $\Delta\omega$ and forcing amplitude E:

$$\phi_t = \Delta\omega - \frac{E}{E_0}\sin\phi \tag{4.14}$$

With the aid of that equation, the transient process of 'pull-in' as well as a distorted beat note could be described in detail.

Some twenty years later Winfree (1967), in a seminal paper on biological rhythms and populations of coupled oscillators, outlined perturbation ideas to reduce generalised relaxation

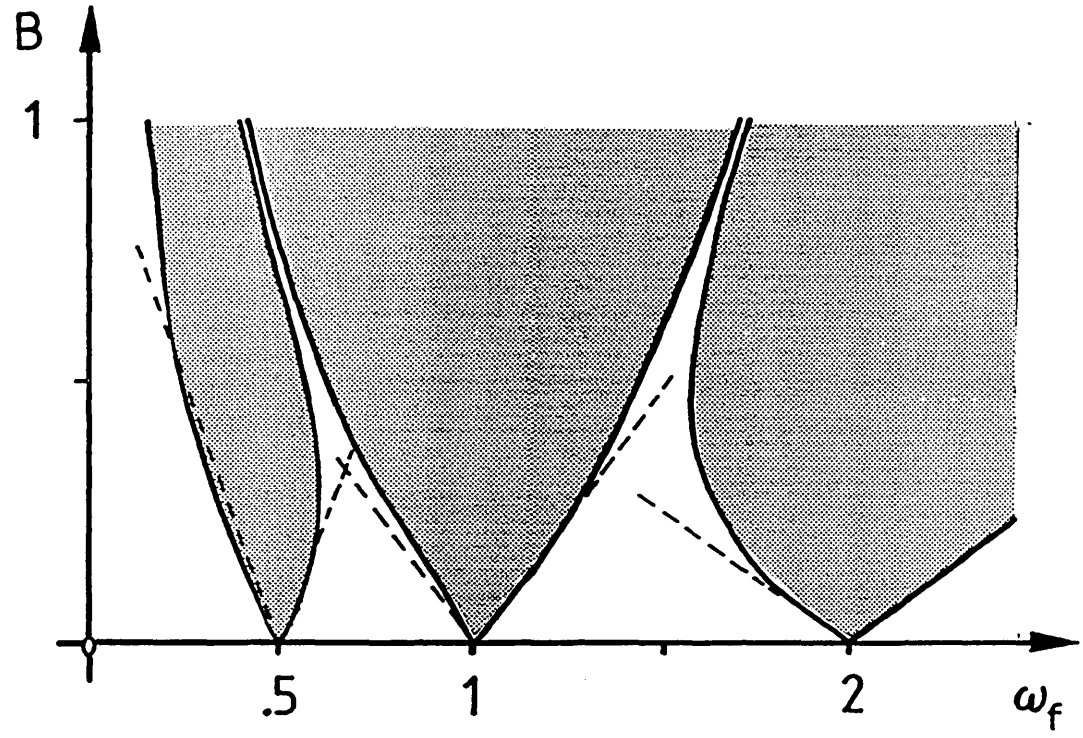

Figure 4.6 Entrainment regions of a $\lambda-\omega$ oscillator ($\lambda(r)=1-r^2$, $\omega(r)=1$), with multi-frequency excitation (ω_f, 2 ω_f and 1/2 ω_f; identical forcing amplitudes), obtained by numerical simulation. The corresponding regions for single-frequency excitation are indicated by the broken lines.

oscillators to oscillator-specific sensitivity functions and a definition of phase, specified on the (high dimensional) limit cycle. More recently, these ideas which Winfree (1980) concedes were introduced with "merely handwaving arguments", were explicated physically (Kuramoto 1981) and put on a mathematical footing using perturbation techniques (Neu 1979*a*, 1979*b*, 1980).

Essentially, the limit cycle of an oscillator is supposed to possess stiffness in orbital shape against weak perturbations. However, although the trajectory will hardly deviate from its natural closed orbit, the phase along the orbit will experience accelerating or decelerating effects. The state of the oscillator is thus effectively specified by its phase value which itself is a function of the perturbation. A further dynamical reduction is made possible by the observation that a weak perturbation produces a long time scale compared to the free oscillator dynamics. The two time scales may be separated by averaging methods. What remains is a phase evolution equation that depends on slow phase variables only *e.g.* the phase difference between the perturbation and the oscillator.

The orbital stiffness idea was demonstrated for the weakly forced $\lambda-\omega$ oscillator (*cf.* § 2.2.1). The extraction of long time scale perturbations, on the other hand, need not be considered in the case of the $\lambda-\omega$ oscillator, but is relevant to the van der Pol oscillator, for example.

The importance of reducing higher dimensional oscillations to a one-dimensional phase description for weak perturbation cannot be overemphasised because it allows the analytical treatment of populations of coupled relaxation oscillators, constituting typical complex dynamical systems.

As might be expected, the dimensional reduction of a weakly forced nonlinear oscillator, using formal methods, leads to phase descriptions very similar to Adler's equation and to the phase evolution of the weakly forced $\lambda-\omega$ oscillator. Given an oscillator with intrinsic frequency ω_0, forcing frequency ω_f, and normalised forcing amplitude ϵ, its phase evolves according to :

$$\theta_t = \omega_0 + \epsilon\, \Gamma(\omega_f t-\theta) + \mathcal{O}(\epsilon^2), \tag{4.15}$$

or, by considering the temporal evolution of the phase difference $\phi=\omega_f t-\theta$,

$$\phi_t = (\omega_f-\omega_0) - \epsilon\, \Gamma(\phi) + \mathcal{O}(\epsilon^2)\,. \tag{4.16}$$

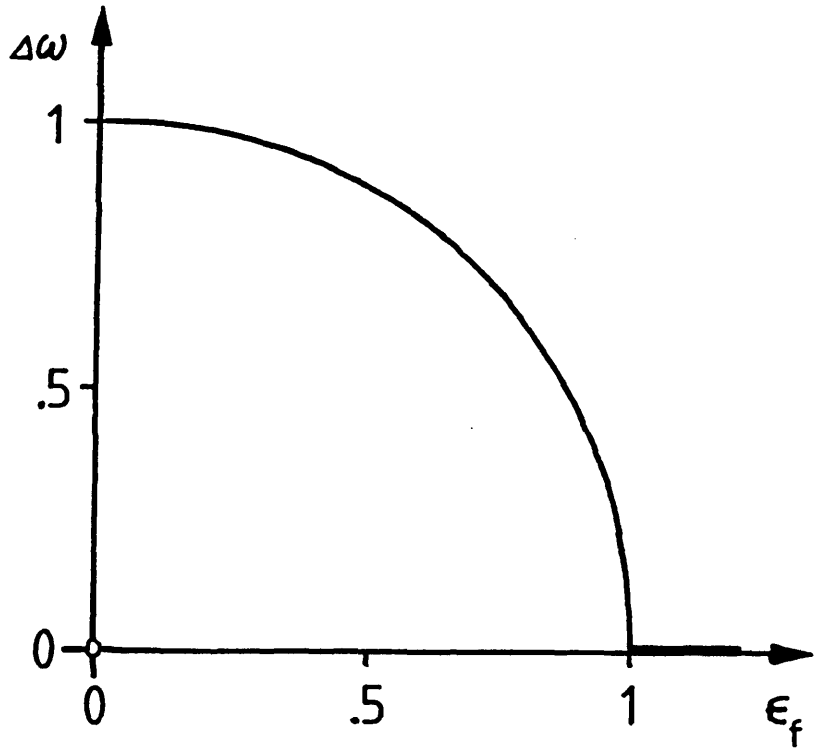

Figure 4.7 Frequency pulling in a weakly forced oscillator. The dynamics are described by the phase-difference evolution equation $\varphi_t=(\omega_f-\omega_0)-\epsilon\ \sin\varphi$. $\Delta\omega$ denotes the time-averaged frequency difference $\overline{\varphi_t}$. Note that for $\Gamma=\sin\varphi$, $\Delta\omega=\sqrt{\epsilon_c{}^2-\epsilon^2}$.

Here, the phase difference function Γ is a general odd 2π-periodic function of its argument, $|\Gamma| \leq 1$.

As pointed out earlier, stable phase-locking exists for $|\phi| < \frac{\pi}{2}$, and for $|\omega_f - \omega| > \epsilon$ the phase locking cannot be maintained. Long time intervals of slow variations in ϕ are punctuated by brief intervals of rapid fluctuations, a behaviour that is occasionally referred to as rhythm splitting (Neu 1979*b*). As the difference between frequency 'detuning' and ϵ is increased, variations in ϕ become less abrupt. An analytical solution for this region outside phase-locking has been derived by Kuramoto and Yamada (1976) :

$$\begin{aligned} \tan(\phi(t)) &= A \tan\Big(\pi F t + \arctan[\tan(\pi\phi(0)/A]\Big) \\ A &= \sqrt{\frac{|(\omega_f-\omega_0)+\epsilon|}{|(\omega_f-\omega_0)-\epsilon|}} \qquad F = \sqrt{|(\omega_f-\omega_0)-\epsilon^2|} \end{aligned} \tag{4.17}$$

Concurrent with changes from rhythm splitting to sinusoidal fluctuations, the frequency pulling diminishes and the time-averaged oscillator frequency $\overline{\theta_t}$ approaches its intrinsic value ω_0. Kuramoto (1984a) gives details of this frequency-pulling process. Near the critical forcing amplitude $\epsilon_c = |\omega_f - \omega|$ the frequency difference $|\overline{\theta_t} - \omega_f|$ behaves like

$$|\overline{\theta_t} - \omega_f| \propto \sqrt{\epsilon_c - \epsilon} \ . \tag{4.18}$$

A numerical simulation illustrates the frequency pulling phenomenon rather well (*figure* 4.7).

2.4 Sampled Phase Description and Chaos

The phase description of a forced nonlinear oscillator is obtained by greatly abstracting from the potentially complex oscillator dynamics, and only the basic properties of harmonic synchronisation are retained in the one-dimensional form (4.16). Interestingly though, higher dimensions of the oscillator dynamics may be recovered, as it were, by considering a discrete-time version of equation (4.16). For example, solving equation (4.16) by Euler's method :

$$\varphi(n+1) = \varphi(n) + T[(\omega_f - \omega_0) - \epsilon\, \Gamma(\varphi(n))] \ , \tag{4.19}$$

where $\varphi(n) = \phi(nT)$. Equation (4.19) has been used as a building block for the numerical study of large populations of weakly interacting nonlinear oscillators (Daido 1986, Sakaguchi and

Kuramoto 1986, Daido 1987), but is more adequately understood in the context of Poincaré return maps where equation (4.19) is known as the circle map. These iterated maps serve to describe dynamical systems (Collet and Eckmann 1980) and have proved very useful in classifying choatic behaviour.

Return maps $x_{i+1}=F(x_i)$, $x_i \in \mathbb{R}^{n-1}$ are a means of studying systems of dimension n with periodic trajectories *e.g.* systems with periodically varying coefficients or periodic forcing terms. The reduction in dimension by one is the result of observing trajectories in the $n-$dimensional phase space through a surface, the Poincaré section, of dimension $(n-1)$, such that the trajectories are everywhere transverse to the surface. The return map then provides a mapping from a point on this surface to its first return point. Further reductions in return-map dimension are possible if the dynamics are sufficiently simple. For example, the qualitative dynamics of one form of the third-order Lorenz equation, the Rössler attractor, are described exhaustively by a one-dimensional uni-modal return map by considering the distance of return points from the origin (Thompson and Stewart 1986).

Circle maps, defined through

$$\theta(n+1) = \theta(n) + \Omega + g(\theta(n)), \qquad g(\theta(n)) = g(\theta(n)+1)\,, \tag{4.20}$$

can be thought of as 'lifts' of mappings from the circle to itself and have been used to describe spontaneously beating chick heart cells (Glass *et al* 1986), general forced nonlinear oscillators (Ding 1986), Josephson junctions in microwave fields and charge-density waves in electric fields (Jensen *et al* 1984, Bohr *et al* 1984). To study phase locking in circle maps, the frequency of the underlying dynamical system is required, described by the winding number

$$W = \lim_{n\to\infty} \frac{\theta(n)-\theta(0)}{n}\,. \tag{4.21}$$

Note that $\theta(n)$ is the $n-$th iteration of the map $\theta(n+1)=f(\theta(n))$ for initial value $\theta(0)$. For the standard sine circle map,

$$\theta(n+1) = \theta(n) + \Omega - \frac{K}{2\pi}\sin 2\pi\theta(n)\,, \tag{4.22}$$

it has been shown that the winding number locks-in at every single rational number P/Q in a non-zero interval $\Delta\Omega$ (Herman 1977). For K close to zero these phase locking intervals are quite small (*figure* 4.8), but with increasing K the widths of all phase locked intervals increase

and the total width of quasi-periodic orbits decreases correspondingly. At $K=1$, where the sine circle map becomes noninvertible, the intervals completely fill up this critical line (Jensen et al, *ibid*). Above $K=1$, the phase-locked intervals, or resonances, start to overlap and chaos occurs. The orbit jumps between resonances in an erratic way and the observed chaos is a 'frustrated' response of the system due to resonance overlap.

This scenario is of course highly reminiscent of the earliest observations of irregular start-up transients in the van der Pol oscillator and has thus taken us from complex dynamical behaviour in a third-order system to dynamically reduced one-dimensional systems and, to complete the circle and recover lost dimensions, return maps.

3. Multiple-Degree-of-Freedom Oscillations

Having discussed basic properties of, and phase description methods for dealing with, single-degree-of-freedom oscillations, this section looks at oscillator systems involving several – and in the continuum limit an infinite number of – degrees of freedom. Interest here is limited to certain qualitative differences produced by the quantitative change. Qualitatively new phenomena include self-organisation (mutual synchronisation) of populations of coupled oscillators, kinematic and trigger waves, and a form of chaos that requires an infinite number of degrees of freedom. Consequently, unidirectionally coupled oscillator systems, such as the system used by van der Pol and van der Mark (1928) to describe abnormal functioning of the vertebrate heart or an oscillator-chain model of the human small intestine (Diamant *et al* 1970), will not be discussed.

Conceptually, self-organisation and kinematic waves on the one hand, and trigger waves and turbulence on the other hand, may be identified with populations of oscillators with intrinsic frequency distribution and populations of identical oscillators, respectively.[7]

3.1 Interactions of Non-Identical Oscillators

Synchronisation in populations of mutually coupled oscillators reflects the phase-space volume contracting property of dissipative systems (Nicolis and Prigogine 1977), and major interest in this phenomenon has come from the study of biological oscillations.

In connexion with the human alpha rythm, Wiener (1958) explored analytically the possibility that myriads of individual oscillatory processes mutually synchronise to produce a common rhythm. Other examples include chick pacemaker nodes comprising spontaneously

[7] This classification is only correct approximately. Self-organisation is also observed in populations of identical oscillators with random noise disturbances.

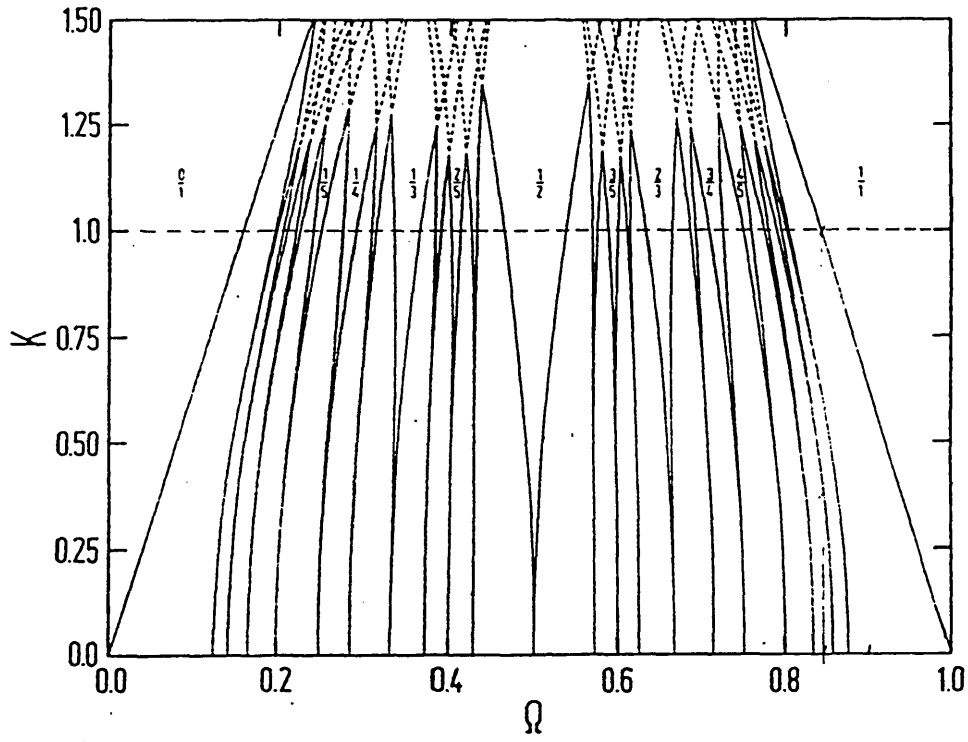

Figure 4.8 Entrainment diagram of the sine circle map $\theta_{n+1}=\theta_n+\Omega-K/2\pi\ \sin(2\pi\theta_n)$. Note the symmetry and periodicity in Ω. At the forcing amplitude $K_c=1$ the entrainment regions fill up the critical line (after Jensen *et al* 1984).

beating cells (Winfree 1967), and the electrical activitiy of the gastro-intestinal system (Nelson and Becker 1968, Sarna *et al* 1971, Robertson-Dunn and Linkens 1974).

3.1.1 A Pair of Oscillators

Pairs of mutually coupled oscillators form the building blocks of larger assemblies of mutually interacting oscillators. Much of the behaviour exhibited by these oscillator populations is present in embryonic form in a two-oscillator system and can be inferred from the two-oscillator dynamics (Linkens 1976). Consider therefore two n-dimensional stably limit-cycling systems with intrinsic frequencies ω_x and ω_y,

$$\underline{x}_t = F(\underline{x}) , \qquad \underline{y}_t = G(\underline{y}) , \qquad \underline{x},\ \underline{y} \in \mathbb{R}^n , \tag{4.23}$$

mutually interacting through weak generalised diffusive coupling,

$$\underline{x}_t = F(\underline{x}) + \epsilon\ \underline{D}\ [\underline{y} - \underline{x}] , \qquad \underline{y}_t = G(\underline{y}) + \epsilon\ \underline{D}\ [\underline{x} - \underline{y}] , \tag{4.24}$$

where $\underline{D} \in \mathbb{R}^n \times \mathbb{R}^n$ is a diffusion matrix with self-diffusivities d_{ii} and cross-diffusivities d_{ij}. The phase equations of the dimensionally reduced coupled oscillator system are

$$\theta_t^{\,x} = \omega_x + \epsilon\ \Gamma(\phi) \quad \text{and} \quad \theta_t^{\,y} = \omega_y + \epsilon\ \Gamma(-\phi) , \ \text{where}\ \ \phi = \theta^y - \theta^x \tag{4.25}$$

Because of the functional dependence on the phase difference only, the two equations reduce to a single phase difference equation :

$$\phi_t = (\omega_y - \omega_x) - \epsilon\ (\Gamma(\phi) - \Gamma(-\phi)) . \tag{4.26}$$

It is noted that equation (4.26) fully describes the phase difference evolution in a two-oscillator system that consists of λ-ω oscillators with identical amplitude dynamics $\lambda(r)$ and amplitude-independent ω. The simplicity of equation (4.26) allows most of the mutual entrainment properties to be studied qualitatively. For instance, if Γ is an even function of the phase difference, $\Gamma(-\phi)=\Gamma(\phi)$, synchronisation is impossible, because the coupling terms cancel. Similarly, if Γ is odd, $\Gamma(-\phi)=-\Gamma(\phi)$, the common frequency of entrainment is the arithmetic mean of the intrinsic frequencies. Generally, if Γ is a non-even function, entrainment at a common frequency above or below the intrinsic frequencies is possible. Stability of a solution

ϕ_0 is guaranteed by $d\phi_t/d\phi<0$ at ϕ_0. For an oscillator pair with near-identical frequencies $\omega_x \approx \omega_y$, so-called in-phase or anti-phase coupling is possible. Phaselocking then implies that the second term on the right hand side of equation (4.26) be identical zero. Because $(\Gamma(\phi)-\Gamma(-\phi))$ is odd and 2π periodic, solutions are either $\phi_0=0$ or $\phi_0=\pi$. From stability analysis it follows that the in-phase solution $\phi_0=0$ is stable for $d\Gamma(\phi)/d\phi > 0$ at ϕ_0. Conversely, the anti-phase solution is stable for $d\Gamma(\phi)/d\phi < 0$ at ϕ_0.

The coupling Γ is a function of the diffusion matrix $\underline{D}$ and has been calculated for particular second-order systems, *viz.* coupled λ-ω oscillators and van der Pol oscillators (Ermentrout and Kopell 1984, Kuramoto 1984*a*). For λ-ω systems with normalised $\lambda(r)$ dependence $\lambda(r)=1-r^2$, Γ has the form :

$$\Gamma(\phi) = \left\{\omega' \frac{d_{11}+d_{22}}{4} + \frac{d_{21}-d_{12}}{2}\right\}\{\cos\phi - 1\} + \left\{\omega' \frac{d_{12}-d_{21}}{4} + \frac{d_{11}+d_{22}}{2}\right\}\sin\phi \tag{4.27}$$

Here ω' denotes the derivative of $\omega(r)$ at the stable limit cycle solution r_0, $\omega'=d\omega(r_0)/dr_0$. This gives an indication of the range of applicability of the phase description method. It is interesting to note that the frequency dependence on amplitude and the nonsymmetry of $\underline{D}$ may cancel each other to produce a function Γ which is odd. For van der Pol oscillators, if the coupling has resistive, capacitive and inductive components, d_r, d_c and d_l, respectively,

$$\Gamma(\phi) = d_r \sin\phi + (d_l-d_c)(\cos\phi-1) \tag{4.28}$$

Note that for either system $\Gamma(0)=0$. This reflects the generalised diffusive type of coupling (Kuramoto 1984*a*). Mutual synchronisation is effected in $\lambda-\omega$ systems, without $\omega(r)$ dependence, by self-diffusive coupling and for van der Pol oscillators by resistive coupling.[8]

3.1.2 Populations of Oscillators and Continuum Limit

Differences in the treatment of assemblies of a finite number of interacting oscillators and the continuum limit of oscillating fields are mostly technical in nature. Whilst on the typical scale of investigation the underlying physical system may safely be taken to be space-

[8] The simplicity of the above analysis for a weakly coupled two-oscillator system is in stark contrast to the efforts involved in treating a pair of strongly coupled van der Pol oscillators (*e.g.* Storti and Rand 1982).

time continuous, analysis is frequently carried out in discrete space in order to avoid phase- or amplitude singularities (Kuramoto 1984*b*) or to employ matrix-algebraic methods (Ermentrout and Kopell 1984). As will be seen shortly (§ 3.1.2.2), however, the continuum limit of discrete space analysis need not be trivial and may entail singular behaviour.

In its most general formulation, a system with local dynamics and linear(!) spatial interactions is described by an integro-differential equation :

$$\underline{x}_t(s,t) = F(\underline{x}(s,t),s) + \epsilon \int_{-\infty}^{\infty} \underline{K}(r-s)\, \underline{x}(r,t)\, \mathrm{d}r \quad s,\, r \in \mathbb{R}^3 \tag{4.29}$$

Here, the kernel $\underline{K}$ introduces the length scale of spatial interaction into the equation. For many physical systems where the spatial interactions are highly localised e.g. hydrodynamic systems, or chemical reaction-diffusion system, a kernel of the form $\underline{K}(r-s)=\delta(r-s)\nabla^2$ is assumed. However, systems with electromagnetic field interactions such as ferromagnetic systems are characterised by distinctly non-local dynamics and have only recently received renewed attention (Elmer 1988).

In the subsequent two sections synchronisation properties of oscillator populations with long-range and diffusive interactions are discussed exemplarily.

3.1.2.1 Long Range Coupling

A particular form of long-range interaction in populations of limit-cycling oscillators is closely related to mean field ideas of thermodynamic phase transitions, as observed *e.g.* in magnetic spin orientation. According to an idealised model called the Husimi-Temperly model, each spin is postulated to interact with all the remaining spins with equal strength. If the magnetic spins are initially randomly orientated, the gradual lowering of ambient temperature will result in a sudden collective organisation. By substituting oscillator for spin the model becomes a community of oscillators with uniform interaction. Analytical results for this type of long-range coupling have been derived by methods analogous to the thermodynamic transition (Kuramoto 1984*a*). In usual phase description,

$$\frac{\mathrm{d}\theta_i}{\mathrm{d}t} = \omega_i + \epsilon \frac{1}{N} \sum_j \Gamma(\theta_j, \theta_i) \quad , \quad i=1,\ldots,N \tag{4.30}$$

The analytical treatment of equation (4.30) requires the coupling to be diffusive, $\Gamma(\theta_j, \theta_i)=\sin(\theta_j-\theta_i)$, and the intrinsic frequencies to be randomly distributed according to some density function $g(w)$, symmetric about ω_0. The analysis proceeds by the *ansatz*

$$\sigma\, e^{j\Omega} = \frac{1}{N} \sum_i e^{j\theta_i} \tag{4.31}$$

which defines a complex order parameter and is assumed to be time-independent, for large N. Equation (4.30) may then be rewritten, using trigonometric identities,

$$\frac{d\theta_i}{dt} = \omega_i + \epsilon\, \sigma \sin(\Omega t + \theta - \theta_i) \tag{4.32}$$

or, expressed in terms of the relative phase $\psi_i = \theta_i - \Omega t - \theta$,

$$\frac{d\psi_i}{dt} = \omega_i - \Omega - \epsilon\, \sigma \sin\psi_i \tag{4.33}$$

This equation is, of course, known from the synchronisation in forced or mutually coupled oscillators and its solution is known. Depending on the frequency difference $|\omega_i - \Omega| \lesseqgtr \epsilon\, \sigma$, oscillator i is either entrained to the oscillating field or not. Equation (4.33) is a self-consistent equation for the complex order parameter and can be treated analytically for simple frequency distributions $g(\omega)$. Let this distribution be a Lorentzian,

$$g(\omega) = \frac{\gamma}{\pi[(\omega - \omega_0)^2 + \gamma^2}} \tag{4.34}$$

It may then be shown that

$$\sigma = \begin{cases} \sqrt{1 - \frac{2\gamma}{\epsilon}} & , \ \epsilon > \epsilon_c \\ 0 & , \ \text{otherwise.} \end{cases} \tag{4.35}$$

By symmetry, $\Omega = \omega_0$ and $\epsilon_c = \frac{2}{\pi g(\omega_0)}$. For subcritical coupling the oscillators are effectively independent as σ is identically zero (equation 4.35). Near but above criticality the order parameter σ is highly sensitive to changes of ϵ, $d\sigma/d\epsilon = \infty$, thus exhibiting typical threshold behaviour. This is demonstrated in *figure* 4.9 for a population of $N = 100$ oscillators with non-random intrinsic frequency distribution.

3.1.2.2 Diffusive Coupling

Short range interactions in oscillator populations with intrinsic frequency distribution have been used to model various physiological systems such as the slow-wave electrical activity

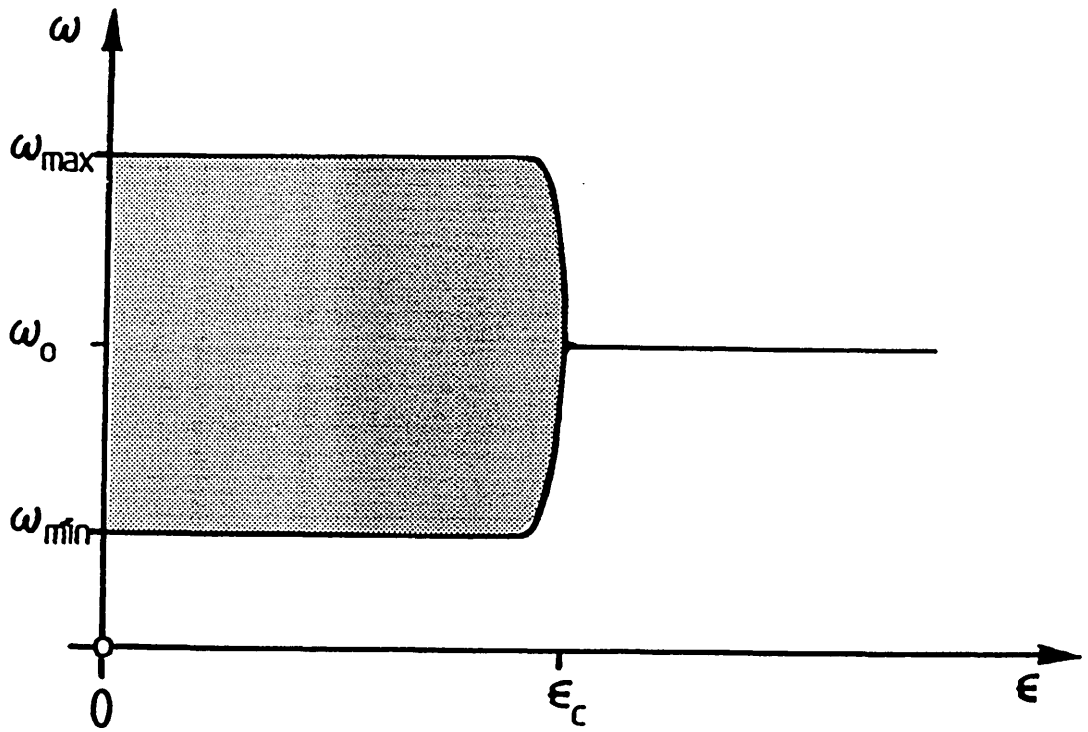

Figure 4.9 Schematic diagram of the phase transition in a population (N=100) of uniformly coupled oscillators (attractive coupling: $\Gamma=\sin\psi$). The intrinsic oscillator frequencies are uniformly, non-randomly distributed in $[\omega_{min}, \omega_{max}]$. The dependence of the average oscillator frequencies on the coupling strength ϵ is shown, determined from numerical simulation.

of the mammalian small intestine (Robertson-Dunn and Linkens 1974), neural control of locomotion (Bay and Hemami 1987), and swimming in fish (Cohen *et al* 1982). Central properties are the formation of locally synchronised clusters and, for spatially organised systems, the presence of so called *kinematic* or *pseudo* waves (Kopell and Howard 1973*a*, Winfree 1972). Exemplary results are discussed for systems of one-dimensional spatial extension, both space-discrete and -continuous.

Ermentrout and Kopell (1984) considered a chain of $N+1$ weakly coupled oscillators. The intrinsic oscillator frequencies form a linear gradient and the mutual coupling is nearest neighbour. Specifically, the coupling is diffusive, isotropic, and weak interactions of magnitude ϵ are assumed. A system of phase difference equations was then derived that allowed the calculation of the critical coupling strength for global synchronisation :

$$\begin{aligned}
&\frac{d\theta_1}{dt} = \omega_1 + \epsilon\, \Gamma(\phi_1) + \mathcal{O}(\epsilon^2) \\
&\frac{d\phi_i}{dt} = \Delta\omega + \epsilon\, [\, \Gamma(\phi_{i+1}) + \Gamma(-\phi_i) - \Gamma(\phi_i) - \Gamma(-\phi_{i-1})] + \mathcal{O}(\epsilon^2)\,, \quad i=1,\ldots N \\
&\Gamma(-\phi_0) = \Gamma(\phi_{n+1}) = 0\,, \quad \Delta\omega = \omega_{i+1} - \omega_i
\end{aligned} \tag{4.36}$$

The coupling functions are those derived for a pair of oscillators in § 3.1.1. For odd Γ there is a unique stable solution above critical coupling. As the coupling strength falls below ϵ_c, a large amplitude stable limit cycle emerges which can be interpreted to correspond to the existence of a pair of frequency plateaus with different frequency. If the coupling is purely resistive, $\Gamma(\phi)=\sin\phi$, then

$$\epsilon_c = \frac{(N+1)^2}{8N}\,(\omega_{max} - \omega_{min}) \tag{4.37}$$

This implies that for a fixed total change in frequency, the larger the N, the harder it is to phase-lock. This contrasts with a non-odd function Γ for which ϵ_c remains finite as $N \to \infty$ (Kopell and Ermentrout 1986). Also, for odd Γ the common frequency is $\bar{\omega}=(\omega_{max}+\omega_{min})/2$, whereas for non-odd Γ the common frequency may lie entirely above or below the intrinsic frequencies. The phase differences ϕ_i are smallest at the ends of the chain and largest at the point where a single frequency plateau divides into two for subcritical coupling. Consequently, kinematic waves are observed along the chain whose phase speed increases toward the break point and decreases behind it.

Some results were also given for anisotropic and non-uniform coupling and for non-odd Γ. For stronger forward coupling than backward coupling, a break in frequency occurs at the lower frequency end. If, on the other hand, the coupling is assumed isotropic but with a gradient in ϵ then, for increasing ϵ with oscillator index i, the break will be in the high-frequency range and for ϵ decreasing the break will be in the low frequency range. Note that the frequency of the phaselocked solution is the same as for uniform isotropic coupling.

The space-continuous equivalent was treated by Ermentrout and Troy (1986). They considered a one-dimensional continuum of $\lambda-\omega$ oscillators in the interval $0 \leq s \leq 1$ with self-diffusive coupling terms only. Functions λ and ω are $\lambda = 1-r^2$ and $\omega = \Omega_0 - \mu s$. Interestingly, if the coupling is of the order of the attraction of the limit cycle, phaselocking is never lost. Rather the amplitude of the oscillations decreases with increasing frequency gradient μ until the origin is re-established. Conversely, for weak coupling frequency plateaus are formed. The upper part of the medium synchronises at a high frequency and the lower part synchronises at a low frequency. The emergence of plateaus is accompanied by singularities. The amplitude at frequency discontinuities must go to zero in order for the phase to remain continuous.

In either of the oscillator systems, the break of the phase locked solution into a pair of frequency plateaus is the scenario near criticality only. Obviously, as the coupling becomes weaker, the two-plateau system will break into more plateaus and clusters of locally synchronised oscillators are observed.[9]

3.2 Interactions of Identical Oscillators

The restriction to oscillator populations with identical intrinsic frequencies has been considered to be rather serious (Winfree 1980), as synchronisation is brought about by infinitesimally small coupling, and studies of the collective temporal phase evolution are few (e.g. Neu 1980). However, this is but one aspect of a variety of phenomena observed in interacting identical oscillators that include multi-modes oscillations, trigger waves and diffusion-induced chaos.

Major developments in this area came in electric circuit theory from the study of distributed multimode oscillations (Scott 1970), but research was also motivated by the observation of multi-mode rhythms in the large intestine (Linkens *et al* 1976). Regular and irregular wave patterns, on the other hand, are exhibited by spatially interacting chemical

[9] Winfree (1980) notes that non-oscillatory, excitable media with a gradient in refractoriness show very much the same behaviour as the coupled oscillator systems with intrinsic frequency gradient.

reactions (Kopell and Howard 1973*a*) and have triggered considerable interest in populations of interacting identical oscillators.

3.2.1 Mode Analysis

Nonlinear mode analysis addresses the existence and stability of simultaneous multi-mode oscillations in distributed arrays of nonlinear oscillatory circuits. The subject was introduced by van der Pol (1922) who noted that nonresonant double-mode oscillations could not occur in a two-degree-of-freedom triode generator with cubic nonlinearity. Double-mode oscillations were treated by Linkens (1976) who found that for a particular form of mutually (nonlinearly!) coupled van der Pol oscillator, an in-phase and anti-phase mode can co-exist stably for some parameter range.

More generally, however, oscillator arrays of several dimensions are considered. Scott (1970), using the equivalent linearisation method of Krylov and Bogoliubov (1947), concluded that two *nonresonant* modes — the ratio of the mode frequencies is an irrational number — can only be excited stably in arrays of minimum dimension two. Other investigators, considering the continuum approximation of oscillator ladder structures, produced essentially the same results (Parmentier 1972, Aumann 1974). Endo and Mori (1976) developed a method for treating arbitrary numbers of van der Pol oscillators mutually coupled by inductances or capacitances in canonical form. First, the possible modes are calculated by analysing the equivalent loss-less circuit. Stability is then ascertained by the equivalent linearisation method. Complications typically arise when mode frequencies are resonant i.e. the ratio of the two mode frequencies is a rational number. Note that the equivalent linearisation method is closely related to the describing function technique (*cf.* § 2.1.2) which loses its appeal of simplicity and becomes unwieldy in the case of commensurate frequencies.

3.2.2 Trigger Waves

Kinematic or pseudo-waves in an oscillatory medium are produced by gradients in oscillation period and can therefore assume infinite apparent phase velocities. In contrast, trigger waves (Zeeman 1972), can be thought of as spreading disturbances that have been introduced at some point in the medium. It is this type of travelling spatial structure that can arise as the result of interaction of diffusion with an oscillating spatially homogeneous chemical reaction. The most widely known example of such a reaction-diffusion system is the Belousov-Zhabotinskii reaction (Tyson 1976), and research into oscillating media was motivated by Marek and Stuchl's experiment (1975) on interacting oscillatory cells in this reaction. This has

led to the introduction of the $\lambda-\omega$ oscillator concept (Kopell and Howard 1973*b*), as a means of analytically studying certain wave patterns in reaction-diffusion systems. The main findings are briefly discussed here. The prototypical reaction-diffusion system

$$\begin{aligned} r_t &= r\,\lambda(r) + \nabla^2 r - r\,|\nabla\theta|^2 \\ \theta_t &= \omega(r) + \tfrac{1}{r^2}\,\nabla\cdot(r^2\nabla\theta) \end{aligned} \tag{4.38}$$

consists of diffusively coupled identical $\lambda-\omega$ oscillators, and the diffusion matrix is assumed not too far from a scalar matrix to simplify the mathematical treatment. The reaction-diffusion system admits plane wave solution and can therefore be formulated in one dimension,

$$\begin{aligned} r_t &= r\,\lambda(r) + r_{xx} - r\,\theta_x{}^2 \\ \theta_t &= \omega(r) + 2\,\tfrac{r_x}{r}\,\theta_x + \theta_{xx} \end{aligned} \tag{4.39}$$

Wave solutions of equation (4.39) are $r=r_0$ and $\theta=\sigma t-\alpha x$ and the frequency and wave number satisfy $\alpha^2=\lambda(r_0)$ and $\sigma=\omega(r_0)$. A necessary condition for stability of plane waves is $\mathrm{d}\lambda(r)/\mathrm{d}r < 0$ at $r=r_0$. For given parameters, waves with sufficiently small wave number are found to be stable.

3.2.3 Diffusion-Induced Chaos

A generalised form of reaction-diffusion equation with nonscalar diffusion matrix is known as the Ginzburg-Landau equation (named after a similar equation in super-conductivity, de Gennes 1966) or Stewartson-Stuart equation,

$$\psi_t = a\,\psi + b\,\psi_{xx} - c\,|\psi|^2\psi \qquad a,\ b,\ c,\ \psi \in \mathbb{C}\,. \tag{4.40}$$

This equation has been shown to result from applying reductive perturbation methods to partial-differential systems in the vicinity of a Hopf bifurcation (Kuramoto 1984*a*). For parameters $b,\ c \in \mathbb{R}$, equation (4.40) reduces to the soliton-producing nonlinear Schrödinger equation. The Ginzburg-Landau equation is not only known in chemical reactions with diffusion (Kuramoto and Tsuzuki 1974) but also in other contexts such as nonlinear hydrodynamic stability theory (Stewartson and Stuart 1971), phase transitions in optical

systems (Graham and Haken 1968), population biology (Lin and Kahn 1982) and neural fields (Ermentrout 1982). Equation (4.40) is readily seen to be the spatially extended version of the Stuart-Landau equation (§ 2.2) and comprises $\lambda-\omega$ oscillators with defining functions $\lambda(r)=a_r-c_r r^2$ and $\omega(r)=a_i-c_i r^2$. The elements of the diffusion matrix are $d_{11}=d_{22}=b_r$ and $d_{12}=-d_{21}=-b_i$. It is these last two terms that introduce considerably more complicated dynamics than the behaviour exhibited by equation (4.38). Some aspects are discussed qualitatively below.

Equation (4.40) clearly possesses plane wave solutions $\psi=A\exp j(kx-\omega t)$ where k and ω are real. Solving for A and ω gives

$$A^2 = \frac{a_r-k^2 b_r}{c_r} \quad \text{and} \quad \omega = k^2 b_i + \frac{c_i}{c_r}(a_r-k^2 b_r) - a_i \tag{4.41}$$

Linear stability analysis shows that all plane wave solutions are unstable for parameters

$$\alpha^2 = 1 + \frac{b_i\, c_i}{b_r\, c_r} < 0\,, \tag{4.42}$$

suggesting that both cross-diffusive coupling terms as well as the amplitude dependence of the frequency $\omega(r)$ are necessary for instability to occur. More insight into the instability mechanism is gained by considering weak spatial interaction (Kuramoto 1984*a*). Equation (4.40) may then be reduced to a phase description that allows the diffusion-induced irregularities to be studied in detail. Suffice it to say at this point that the derivative $d\Gamma(\phi)/d\phi$ at $\phi=0$ is identical to α^2. Consequently the onset of diffusion-induced instability results from the anti-phase coupling of the $\lambda-\omega$ oscillators. Kuramoto (*ibid*) provides further intuitive arguments for this mechanism. Consider an initially uniform oscillation with wave number $k=0$. The effect of the anti-phase coupling is to rotate the phase along the spatial dimension. This leads to changes in oscillator amplitude which in turn affects the frequency. If phase rotation and frequency changes have co-operative effects, then instability occurs.

Routes to chaos in the Ginzburg-Landau equation have been studied in detail. For instance, Kuramoto observes that for weak diffusion the transition may be described by a one-dimensional uni-modal return map which shows typical period-doubling bifurcations to chaos (Lauwerier 1986). Other routes to chaos are known as well (Sirovich and Newton 1987) but further studies are required to arrive at a more complete description of the dynamics of this equation.

Control over successive instabilities in the Ginzburg-Landau equation is most readily afforded by considering finite spatial size. It will be recalled that results were derived for infinite spatial extension. Given the characteristic length scale of equation (4.40), $1/\alpha$, for a system size L of the same order the number of unstable modes may be expected to be of order one. With growing L, more modes become unstable and the behaviour grows in complexity. This scenario is illustrated in *figure* 4.10. The Ginzburg-Landau equation was solved numerically for different system sizes, starting with a value of L of the order of the characteristic length scale. The spatial frequency content grows with increasing system size, indicating the successive appearance of unstable system modes. The finite system size guarantees a finite bandwidth of spatial fluctuations and is important for numerical investigations of spatio-temporal chaos.

4. Concluding Remarks

This chapter concludes with two observations. First, the $\lambda-\omega$ oscillator forms the basis for general systems that bifurcate *via* a Hopf bifurcation. With defining functions $\lambda(r)$ and $\omega(r)$ of the form $a-br^2$, the $\lambda-\omega$ oscillator describes the small-amplitude behaviour of a system of ordinary differential equations or, with added diffusive term, of a sytems of partial differential equations.

Secondly, the behaviour exhibited by populations of interacting oscillators considerably transgresses the simple synchronisation phenomena of forced single-degree-of-freedom oscillators. When distributed systems of non-identical oscillators are considered, spatially localised or global synchronisation is possible. Furthermore, the concept of functionally composite nonlinear oscillations offers a potentially useful modelling tool for nonlinear systems with oscillatory activity in a wide band of frequencies. Such an approach will find application in flow instabilities, as described in the following chapter, but may equally be relevant to biological oscillations.

When distributed systems of identical oscillators are considered, spatial pattern formation, phase singularities and turbulence arise. In these systems the phase relationship between oscillators assumes a central role. An example of such a distributed system, the Ginzburg-Landau equation, will be studied in chapter VI.

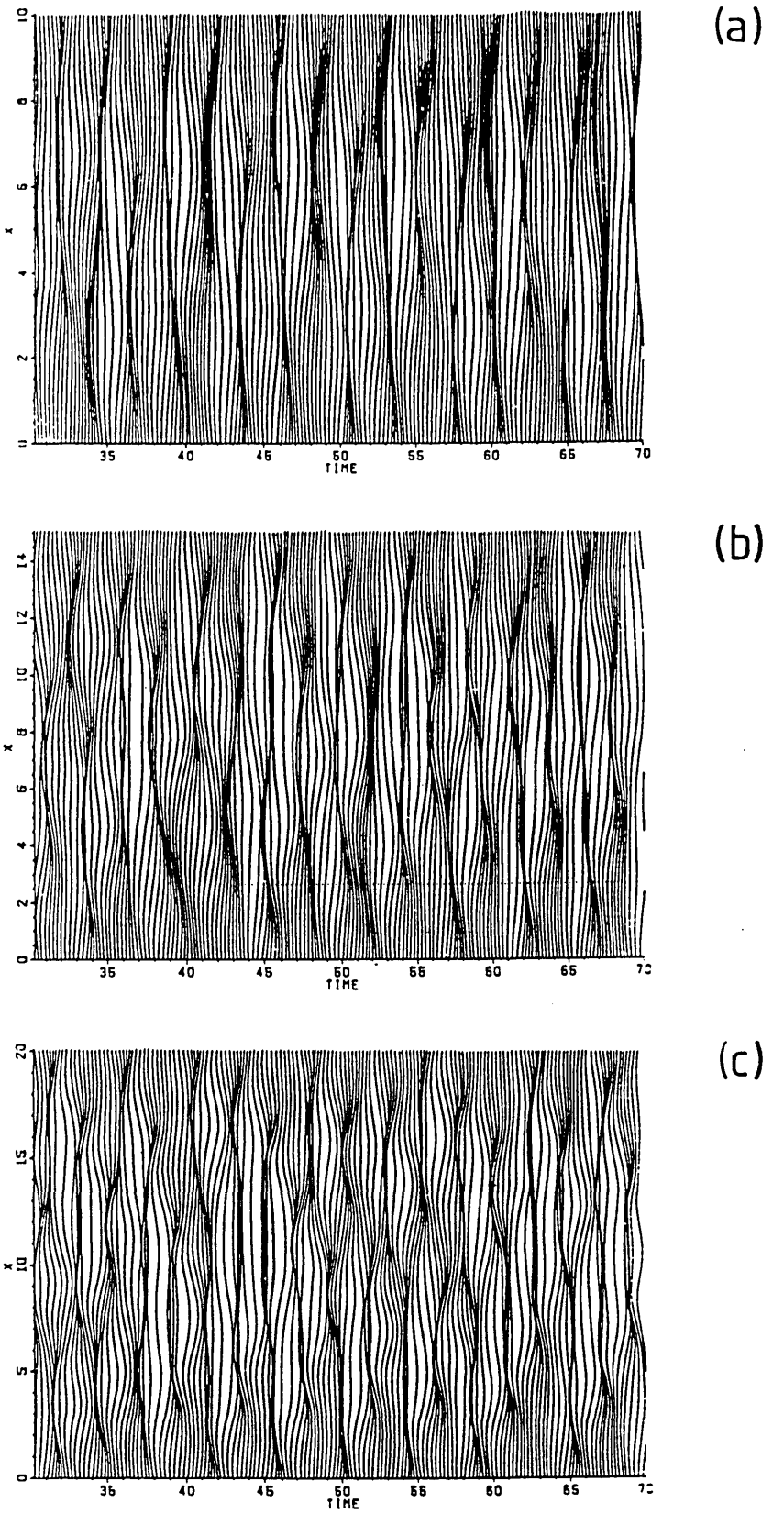

Figure 4.10 Successive instabilities of the finite size Ginzburg-Landau equation with boundary conditions $\psi(0)=\psi(L)=0$. The characteristic length scale is $1/\alpha=10$. (*a*) $L=10$. (*b*) $L=15$. (*c*) $L=20$.

Literature Cited

Adler R (1946). A study of locking phenomena in oscillators. *Proc IRE* 34 pp 351 (reprinted in *Proc IEEE Vol* 61 pp 1380).

Appleton E V (1922). The automatic synchronisation of triode oscillators. *Proc Cambridge Phil Soc London* 21 pp 231.

Atherton D P (1975). *Nonlinear Control Engineering* (London: Van Nostrand Reinhold).

Aumann H M (1974). Standing waves on a multimode ladder oscillator. *IEEE Trans Circuit Theory CT*-21 pp 461.

Bardakjian B L and Sarna S K (1980). A computer model of human colonic electrical control activity. *IEEE Trans Biomed Eng BME*-27 pp 193.

Bay J S and Hemami H (1987). Modelling of a neural pattern generator with coupled nonlinear oscillators. *IEEE Trans Biomed Eng BME*-34 pp 297.

Bearman P W (1984). Vortex shedding from oscillating bluff bodies. *Ann Rev Fluid Mech* 16 pp195.

Berger E, Breitschwerdt K and Kobayashi T (1979). Comparison of oscillator-model theory with experiments on vortex-excited vibrations. *Euro Mech Colloq* 119 (London).

Bishop R E D and Hassan A Y (1964). The lift and drag forces on a circular cylinder oscillating in a flowing fluid. *Proc Roy Soc* A 277 pp 51.

Bohr T, Bak P and Jensen M H (1984). Transition to chaos by interaction of resonances in dissipative systems II. Josephson junctions, charge-density waves, and standard maps. *Phys Rev A* 30 pp 1970.

Cartwright M L (1945). Forced oscillations in nearly sinusoidal systems. *J IEE* 95 pp 88.

Cartwright M L and Littlewood J E (1945). On nonlinear differential equations of the second order. *J London Math Soc* 20 pp 180.

Chua L O and Green D N (1974). Synthesis of nonlinear systems. *IEEE Trans Circ Syst CAS*-21 pp 286.

Cohen A H and Wallen P (1980). The neurone correlate of locomotion in fish. *Exp Brain Res* 41 pp 11.

Cohen A H, Holmes P J and Rand R H (1982). The nature of coupling between sequential oscillators of the lamprey spinal generator. *J Math Biol* 13 pp 345.

Cohen A H and Harris-Warrick R M (1984). Strychnine eliminates alternating motor ouput during fictive locomotion in the lamprey. *Brain Res* 293 pp 164.

Collet P and Eckmann J P (1980). *Iterated Maps on the Interval as Dynamical Systems.* Progress in Physics Vol 1 (Boston: Birkhäuser).

Daido H (1986). Discrete-time population dynamics of interacting self-oscillators. *Progr Theor Phys* 75 pp 1460.

Daido H (1987). Population dynamics of randomly interacting self-oscillator. I. Tractable models without frustration. *Progr Theor Phys* 77 pp 622.

de Gennes P G (1966). *Superconductivity of Metals and Alloys* (New York: Benjamin).

Dewan E M (1972). Harmonic entrainment of van der Pol oscillations: phaselocking and asynchronous quenching. *IEEE Trans Autom Contr AC*-17 pp 655.

Diamant N E, Rose T K and Davison E J (1970). Computer simulation of intestinal slow-wave frequency gradient. *American J Physiol* 219 pp 1684.

Ding E J (1986). Analytic treatment of periodic orbit systematics for a nonlinear driven oscillator. *Phys Rev A* 34 pp 3547.

Elmer F J (1988). Nonlinear and non-local dynamics of spatially extended systems: stationary states, bifurcations and stability. *Physica D* 30 pp 321.

Endo T and Mori S (1976). Mode analysis of a multimode ladder oscillator. *IEEE Trans Circuits Syst CAS*-23 pp 100.

Ermentrout G B (1982). Asymptotic behaviour of statistically homogeneous neural nets. *in: Competition and Cooperation in Neural Nets.* eds S Amari and M A Arbib, Lecture Notes in Biomathematics Vol 45 (Berlin: Springer-Verlag).

Ermentrout G B and Kopell N (1984). Frequency plateaus in a chain of weakly coupled oscillators, I. *SIAM J Math Anal* 15 pp 215.

Ermentrout G B and Troy W C (1986). Phaselocking in a reaction-diffusion system with a linear frequency gradient. *SIAM J Appl Math* 46 pp 359.

Feynman R P, Leigthon R B, Sands M (1964). *Lectures on Physics* (Reading, Mass: Addison-Wesley).

Glansdorff P and Prigogine I (1971). *Thermodynamic Theory of Structure, Stability, and Fluctuations* (London: Wiley).

Glass L, Shrier A and Bélair J (1986). Chaotic cardiac rythms. *in: Chaos.* ed. A V Holden (Manchester: Univ Press).

Graham R and Haken H (1968). Quantum theory of light propagation in a fluctuating laser-active medium. *Z Phys* 213 pp 420.

Guckenheimer J and Holmes P (1983). *Nonlinear Oscillations, Dynamical Systems, and Bifurcations of Vector Fields* (New York: Springer-Verlag).

Hale J K (1969). *Ordinary Differential Equations* (New York: Wiley).

Hartlen R T and Currie I G (1970). Lift-oscillator model for vortex-induced vibration. *Proc ASCE J Eng Mech* 96 pp 577.

Hayashi C (1964). *Nonlinear Oscillations in Physical Systems* (New York: McGraw-Hill).

Herman M R (1977). Mesure de Lebesgue et nombre de rotation. *in*: *Geometry and Topology.* eds J Palis and M deCarmo, Lecture Notes in Mathematics Vol 597 (New York: Springer).

Hirsch M W and Smale S (1974). *Differential Equations, Dynamical Systems and Linear Algebra* (New York: Academic Press).

Holmes P and Rand R H (1983). Bifurcations of the forced van der Pol oscillator. *Quart Appl Math* pp 495.

Iwan W D and Blevis R D (1974). A model for vortex induced oscillations of structures. *J Appl Mech* 41 pp 581.

Jensen M H, Bak P and Bohr T (1984). Transition to chaos by interaction of resonances in dissipative systems I. Circle maps. *Phys Rev A* 30 pp 1960.

Joseph D D (1985). Hydrodynamic stability and bifurcation. *in*: *Hydrodynamic Instabilities and the transition to turbulence.* eds Swinney H L and Gollub J P, Topics in Applied Physics 45 (Berlin: Springer-Verlag).

Kennedy M P and Chua L O (1986). Van der Pol and Chaos. *IEEE Trans Circuits Syst CAS-*33 pp 974.

Kitney R I (1975). An analysis of the nonlinear behaviour of the human thermal vasomotor control system. *J Theor Biol* 52 pp 231.

Kopell N and Howard L N (1973*a*). Horizontal bands in the Belousov reaction. *Science* 180 pp 1171.

Kopell N and Howard L N (1973*b*). Plane wave solutions to reaction-diffusion systems. *Stud Appl Math* 52 pp 291.

Kopell N and Ermentrout G B (1986). Symmetry and phase-locking in chains of weakly coupled oscillators. *Comm Pure Appl Math* 39 pp 623.

Krylov N M and Bogoliubov N N (1947). *Introduction to Nonlinear Mechanics* (New Jersey: Princeton Univ Press).

Kuramoto Y(1981). Rhythms and turbulence in populations of chemical oscillators. *Physica A* 106 pp 128.

Kuramoto Y (1984*a*). *Chemical Oscillations, Waves, and Turbulence* (Berlin: Springer-Verlag).

Kuramoto Y (1984*b*). Cooperative dynamics of oscillator community. *Progr Theor Phys Suppl* 79 pp 223.

Kuramoto Y and Tsuzuki T (1974). Reductive perturbation approach to chemical instabilities. *Progr Theor Phys* 52 pp 1399.

Kuramoto Y and Yamada T (1976). Pattern formation in oscillatory chemical reactions. *Progr Theor Phys* 56 pp 724.

Landau L D (1944). К проблеме турбулентности. ДокладыАкадемииНаук СССР 44 (On the problem of turbulence. *C R Dokl Akad Sci USSR* 44 pp 311).

Lauwerier H A (1986). One-dimensional iterative maps. *in*: *Chaos.* ed. Holden A V. (Manchester: Manchester Univ Press).

Levi M (1981). Qualitative analysis of the periodically forced relaxation oscillations. *Mem Amer Math Soc* 32 pp 244.

Levinson N (1949). A second order differential equation with singular solutions. *Ann Math* 50 pp 127.

Lichtenberg A J and Lieberman M A (1983). *Regular and Chaotic Motion* (New York: Springer-Verlag).

Lin J and Kahn P B (1982). Phase and amplitude instability in delay-diffusion population models. *J Math Biol* 13 pp 383.

Linkens D A (1976). Stability of entrainment conditions for a particular form of mutually coupled van der Pol oscillators. *IEEE Trans Circuits Syst CAS*-23 pp 113.

Linkens D A, Taylor I and Duthie H L (1976). Mathematical modelling of the colorectal myoelectrical activity in humans. *Trans IEEE BME*—23 pp 101.

Linkens D A and Kitney R I (1983). Integer-ratio entrainment in mutually-coupled nonlinear oscillators. *J Theor Biol* 100 pp

Mandelstam L and Papalexi N (1932). Über Resonanzerscheinungen bei Frequenzteilung. *Z Phys* 73 pp 223.

Marek M and Stuchl I (1975). Synchronisation in two interacting oscillatory systems. *Biophys Chem* 4 pp 241.

Mees A I (1981). *Dynamics of Feedback Systems* (Chichester: Wiley).

Mees A I and Chua L O (1979). The Hopf bifurcation and its applications to nonlinear oscillations in circuits and systems. *IEEE Trans Circuits Syst CAS*-26 pp 235.

Nelson T S and Becker J C (1968). Simulation of the electrical and mechanical gradient of the small intestine. *Amer J Physiol* 214 pp 749.

Neu J C (1979*a*). Chemical waves and the diffusive coupling of limit cycle oscillators. *SIAM J Appl Math* 36 pp 509.

Neu J C (1979*b*). Coupled chemical oscillators. *SIAM J Appl Math* 37 pp 307.

Neu J C (1980). Large populations of coupled chemical oscillators. *SIAM J Appl Math* 38 pp 305.

Nicolis G and Prigogine I (1977). *Self-Organisation in Nonequilibrium Systems — From Dissipative Structures to Order through Fluctuations* (New York: Wiley).

Ogburn W F and Thomas D S (1922). Are inventions inevitable? A note on social evolution. *Political Science Quarterly* 37 pp 83.

Parker T S and Chua L O (1983). A computer-assisted study of forced relaxation oscillations. *IEEE Trans Circuits Syst CAS*-30 pp 518.

Parker T S and Chua L O (1987). Chaos: A tutorial for engineers. *Proc IEEE* 75 pp 982.

Parkinson G V and Smith J D (1964). The square prism as an aeroelastic nonlinear oscillator. *Quart J Mech Appl Math* 17 pp 225.

Parmentier R D (1972). Lumped multimode oscillations in the continuum approximation. *IEEE Trans Circuit Theory CT*-19 pp 142.

Provansal M, Mathis C and Boyer L (1987). Bénard-von Kármán instability : transient and forced regimes. *J Fluid Mech* 182 pp 1.

Rayleigh J W S (1894). *The Theory of Sound* (London: Macmillan).

Robertson-Dunn B and Linkens D A (1974). A mathematical model of the slow-wave electrical activity of the human small intestine. *Med Biol Eng* 12 pp 750.

Sakaguchi H and Kuramoto Y (1986). A soluble active rotator model showing phase transitions via mutual entrainment. *Progr Theor Phys* 76 pp 576.

Sarna S K, Daniel E E and Kingma Y J (1971). Simulation of slow-wave eletrical activity of small intestine. *Amer J Physiol* 221 pp 166.

Scott Ac (1970). Distributed multimode oscillations of one and two spatial dimensions. *IEEE Trans Circuit Theory CT*-17 pp 55.

Sirovich L and Newton P K (1987). Ginzburg-Landau equation: stability and bifurcations. *in: Stability of Time-Dependent and Spatially Varying Flows.* eds D L Dwoyer and M Y Hussaini (New York: Springer-Verlag).

Smale S (1967). Differentiable dynamical systems. *Bull Amer Math Soc* pp 747.

Stoker J J (1950). *Nonlinear Vibrations* (New York: Wiley).

Storti D W and Rand R H (1982). Dynamics of two strongly coupled van der Pol oscillators. *Int J Nonlin Mech* 17 pp 143.

Stewarston K and Stuart J T (1971). A nonlinear instability theory for a wave system in plane Poiseuille flow. *J Fluid Mech* 48 pp 529.

Stuart J T (1960). On the nonlinear mechanics of wave disturbances in stable and unstable parallel flows. *J Fluid Mech* 9 pp 353.

Stuart J T and Di Prima R C (1978). The Eckhaus and Benjamin-Feir resonance mechanism. *Proc Roy Soc A* 362 pp 27.

Tang Y S, Mees A I and Chua L O (1983). Synchronisation and chaos. *IEEE Trans Circuits Syst CAS*-30 pp 620.

Thompson J M T and Stewart H B (1986). *Nonlinear Dynamics and Chaos.* (Chichester: Wiley).

Tomita K (1986). Periodically forced nonlinear oscillators. *in*: *Chaos*, ed. A V Holden (Manchester: Manchester University Press.

Tyson J J (1976). *The Belousov-Zhabotinskii Reaction.* Lecture Notes in Biomathematics Vol 10, ed. Levin S (Berlin: Springer-Verlag).

van der Pol B (1922). An oscillation hysteresis in a triode generator with two degrees of freedom. *Phil Mag* 43 pp 700.

van der Pol B and van der Mark J (1927). Frequency demultiplication. *Nature* 120 pp 363.

van der Pol B and van der Mark J (1928).The heart beat considered as a relaxation oscillation, and an electrical model of the heart. *Phil Mag* (*7th ser*) 6 pp 763.

Wiener N (1958). *Nonlinear Problems in Random Theory.* (New York: Wiley).

Winfree A T (1967). Biological rythms and the behaviour of populations of coupled oscillators. *J Theoret Biol* 16 pp 15.

Winfree A T (1972). Spiral waves of chemical activity. *Science* 175 pp 634.

Winfree A T (1980). *The Geometry of Biological Time* (New York: Springer-Verlag).

Wolf A (1986). Quantifying chaos with Lyapunov exponents. *in*: *Chaos*, ed. A V Holden (Manchester: Manchester Univ Press).

Zeeman E C (1972). Differential equations for the heartbeat and nerve impulse. *in*: *Towards a Theoretical Biology* 4 ed. C H Waddington (Chicago: Aldine).

CHAPTER V

CO-OPERATIVE DYNAMICS OF A COUPLED-OSCILLATOR SYSTEM AND THE FORCED FREE SHEAR LAYER

Summary

A phenomenological model of nonlinear mode competition between instability waves in the forced free shear layer is proposed. The model comprises mutually interacting nonlinear oscillators with distribution in intrinsic frequencies and exhibits 'locking-on' behaviour, reduction in broadband fluctuations under forcing and induced subharmonic oscillations.

The nonlinear oscillator concept is motivated in § 1 and the functionally composite oscillator model is introduced, discussed and compared to the free shear layer, in the remainder of this chapter.

1. Introduction

Brief mention was made in chapter IV of the modelling of (forced) cylinder wake flows by nonlinear oscillators. Although not rigorously justifiable on the basis of fluid dynamic principles, the nonlinear oscillator concept is certainly supported by linear flow stability considerations and experimental evidence. Wake flows contain regions of absolute instability, making these flows relatively insensitive to disturbances (Huerre and Monkewitz 1985). Importantly, absolute instability supports the view that the cylinder wake can be treated as a Hopf bifurcated flow (Provansal *et al* 1987, Chomaz *et al* 1988) with flow oscillations building up temporally. Furthermore, the flow velocity fluctuations are characterised by a fairly discrete spectral component. This suggests that the pertinent dynamics may be sufficiently described by single-degree-of-freedom oscillators.

In contrast, free shear layers behave significantly differently. As evidenced by the extreme sensitivity to low-level forcing, these flows are typically convectively unstable.[1] Flow instabilities therefore cannot build up temporally, but grow spatially. In addition, velocity fluctuations are spread over a broad band of frequencies. The free shear layer in its early stages of development may therefore be regarded as a narrowband amplifier of upstream low-level noise (Kibens 1980).

[1] There are exceptions. If the velocity ratio $R=\Delta U/2\bar{U}$ of a mixing layer (*cf* Ch II § 3.1) is greater than $R_c=1.315$ instabilities develop temporally. Jets become absolutely unstable if sufficiently hot.

Nonetheless, observations in forced free shear layers have repeatedly been linked to synchronisation phenomena of self-sustained oscillations. As reported by Oster and Wygnanski (1982), "*with increasing amplitude of the surging one may note a marked increase in energy at the forcing frequency and a relative reduction at high frequencies, so that the integral of all spectral components of* u *remains approximately constant*". The suppression of broadband fluctuations in the free shear layer under forcing is referred to as "phase locking" (Kibens *ibid*) or "locking on" (Acton 1980, Crighton 1981) and has been associated with self-sustained oscillations in a free shear layer impinging on an edge (Rockwell and Naudascher 1979). Forced mixing layer phenomena (Ho and Huang 1982) have been likened to frequency locking in nonlinear oscillators (Aref 1983). The observations made by Oster and Wygnanski (*ibid*) were identified recently as a form of asynchronous quenching, with the proviso that multiple-degree-of-freedom oscillators be considered (Staubli 1985).

Furthermore, the flow organisation in the presence of forcing has been hypothesised to reflect latent order or structure (Crow and Champagne 1971) or, in the words of Kibens (*ibid*), "*an underlying degree of organisation intensified by the phase locking of the excitation process*".

It is proposed here to combine the 'phase locking' and 'latent order' concepts in a phenomenological model of the forced free shear layer that comprises a population of uniformly interacting oscillators with intrinsic frequency distribution. On the classical view of hydrodynamic stability theory that the unsteady mixing layer is conceptualised as the superposition of (nonlinearly) interacting instability waves that propagate in the downstream direction, the assembly of interacting oscillators is identified with a collection of single-frequency instability waves. The oscillator population is therefore not primarily associated with a spatially distributed system. Only insofar as characteristic frequencies of the free shear layer change with downstream distance, do spatial concepts enter into the model.

The proposed phenomenological model is largely qualitative in nature, but a quantitative formulation is introduced here as well to explicate certain characteristic properties.

2. The Basic Coupled Oscillator Model

Consider a population of N relaxation oscillators with essentially quadratic nonlinearities and a uniform distribution of intrinsic frequencies over some interval. Let the oscillators interact uniformly and assume the mutual coupling to be attractive. Furthermore, forcing is incorporated in the form of an external field that uniformly acts on the population.

Such models were studied in embryonic form by Ohsuga *et al* (1985) who considered a

two-oscillator system with external forcing, and more recently by Sakaguchi (1988) for large numbers of interacting oscillators. Models with external fields are extensions of the earlier discussed phase transition models (*cf.* Ch IV § 3.1.2.1) and additional properties include the competing influences of the external field and the oscillator mean field.

2.1 Latent Order and Self-Synchronisation

In the absence of an external field, the well known threshold behaviour is observed. For subcritical coupling strength the oscillators exhibit fluctuations in instantaneous frequencies but are effectively independent with regard to time averaged behaviour *i.e.* no frequency pulling is observed. Above the threshold of global synchronisation well defined phase relationships exist among the oscillators. Now, it will be recalled that the complex order parameter σ, defined as the sum over oscillator representative phasors $\exp\theta_i$, is a measure of the self-organisation of the population. If the physically meaningful quantity $Re\{\sigma\}$ which represents the sum over oscillator 'outputs' $\cos\theta_i$, is measured instead, what is observed spectrally is a threshold transition from broadband fluctuations to a single discrete frequency component whereby the total spectral power remains approximately constant.

To adopt the forced free shear layer viewpoint for a moment, the oscillator population possesses a latent degree of order or structure which is artificially intensified by increasing the mutual interaction. Importantly, latent order may also be intensified by an external field. This property is discussed below.

2.2 Locking On and Forced Synchronisation

The control of autonomous periodic activity by external stimuli is – not surprisingly – well known in biological systems. Myocardial cells with autonomous rhythms are entrained by the electrical pulse of the pacemaker (Yamaguchi *et al* 1980). Evoked EEG potentials are thought to be generated by stimulated populations of auto-rythmic neurones (Wiener 1958). Oshuga *et al* (1985) introduced the term *holonic system* to describe the two hierarchical levels of self-synchronisation and forced synchronisation. In their two-oscillator model, both co-operative and competitive effects of the external forcing field were observed. When the two oscillators were not mutually entrained, an external field of frequency close to the frequency of mutual entrainment produced synchronisation at low forcing amplitudes. When, on the other hand, the two oscillators were mutually entrained, considerably larger amplitudes were required to synchronise the oscillators with the external forcing.

These ideas were generalised to large numbers of interacting oscillators by Sakaguchi

(1988) who studied a simple phase description model analytically as well as numerically. For a fixed intrinsic frequency distribution and subcritical coupling strength, an increasing number of oscillators became entrained to the external field as the forcing amplitude was increased. Importantly, the external field strength required to achieve forced synchronisation in the presence of mutual (subcritical) coupling, could be significantly lower than without mutual coupling. This applied in particular to cases where the forcing frequency and the frequency of global self-synchronisation were not too far apart and self- and forced synchronisation co-operated.

2.3 Numerical Results

Numerical results for forced entrainment of a population of N oscillators with intrinsic frequency distribution have been obtained for the following coupled circle-map lattice:

$$\theta_i(n+1) = \theta_i(n) + \omega_i + \epsilon \sum_j \Gamma\{\theta_j(n),\theta_i(n)\} \qquad i=1, ..., N;\ \omega_{i+1} < \omega_i \qquad (5.1)$$

This discrete-time version of the phase description of a system of weakly coupled nonlinear oscillators is increasingly being adopted as a convenient means of studying large numbers of oscillators with long-range interactions (Daido 1986, Sakaguchi and Kuramoto 1986, Daido 1987). Note that for disturbances to a sine circle map of order $1/2\pi$ or larger, the response is potentially chaotic (Ch IV § 2.4). Similar results were obtained for coupled circle map lattices (Kaneko 1986).

In the basic coupled oscillator model, the coupling function Γ is assumed to have the form $\Gamma=\sin(\theta_j-\theta_i)$, but a more complicated variant will be employed in § 3. For trigonometric coupling functions the summation over all coupling terms in equation (5.1) is greatly simplified as it becomes independent of oscillator index i :

$$\theta_i(n+1) = \theta_i(n) + \omega_i + \epsilon\,[\,\sigma_s \cos\theta_i - \sigma_c \sin\theta_i\,]$$

$$\sigma_s = \sum_j \sin\theta_j \qquad \sigma_c = \sum_j \cos\theta_j \qquad j=1,...,N \qquad (5.2)$$

Results for a population of $N=100$ uniformly coupled oscillators under external forcing are shown in *figure* 5.1. The coupling is subcritical and the displayed waveform (*figure* 5.1*a*) is a weighted average of individual oscillator outputs $\cos\theta_i$, modelling a spatial-average type measurement process with emphasis on a narrow band of frequencies. This implies a scenario

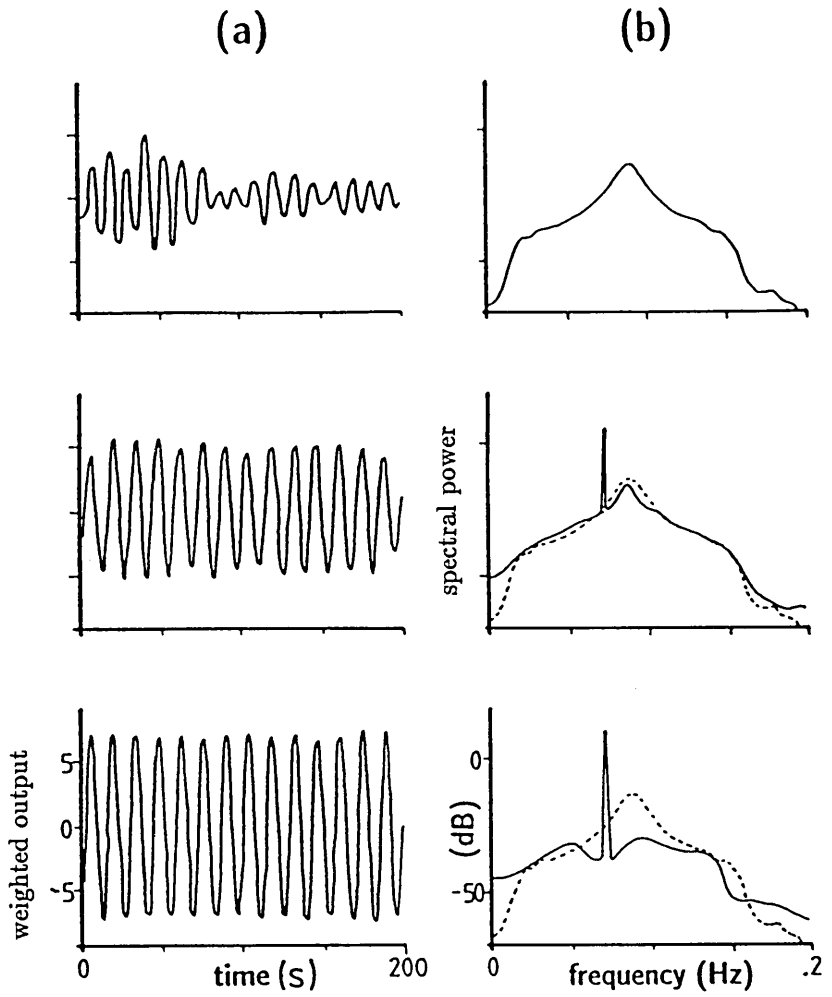

Figure 5.1 Forced synchronisation in the basic coupled-oscillator model (N=100; $\omega_i \in$ [1.0,0.1], (uniform, non-random distribution); ϵ=0.005 (sub-threshold); ω_f=0.45; ϵ_f=0.0, 0.03, 0.06). (*a*) Weighted oscillator field $\sum_i w_i \cos\theta_i$. (*b*) Corresponding averaged power spectrum estimate.

where intrinsic oscillator frequencies are associated with spatial coordinates, as suggested with reference to the free shear layer (*cf* § 4.2). *Figure* 5.1*b* shows the corresponding power spectral estimate and the concentration of energy at the forcing frequency is clearly visible.

Not surprisingly, the depression in the immediate neighbourhood of the forcing frequency is very similar to the characteristic sharp population drop in the number density near the frequency of synchronisation (Kuramoto 1984, Sakaguchi 1988). This reflects the effective spectral range of forced synchronisation.

3. The Extended Coupled Oscillator Model

In this section the importance of higher- and subharmonic frequency entrainment is stressed. As outlined in § 2 the oscillator nonlinearity is assumed quadratic, emphasising the existence of regions of even integer ratio of entrainment. The following form of coupling is assumed to represent these additional features :

$$\Gamma\{\theta_j(n),\theta_i(n)\} = \begin{cases} \sum_k a_k \sin(\theta_j(n) - k\,\theta_i(n)) & j < i \\ \sum_k a_k \sin(k\,\theta_j(n) - \theta_i(n)) & j > i \end{cases} \qquad k=1,2,4,... \tag{5.3}$$

Equation (5.3) is an extension of the multi-frequency concept introduced in Ch IV § 2.2.1 and allows for mutual coupling at integer frequency ratios. The weights a_k determine the respective size of harmonic and super-/subharmonic catchment regions of entrainment, and the particular choice of k reflects the quadratic nonlinearity property of the oscillators. Assumptions regarding physically meaningful types of super-/subharmonic entrainment between oscillators of different frequencies and the requirement for mutually consistent phase combinations — kth-harmonic ($1/k$th-harmonic) coupling from oscillator j to i (i to j) — are expressed in the anisotropic form of coupling.

A cautionary note is necessary at this point. Formulation (5.3) clearly does not describe integer-ratio synchronisation of mutually coupled relaxation oscillators (*e.g.* Linkens and Kitney 1983). As the two mechanisms of super- and subharmonic frequency entrainment in relaxation oscillators are fundamentally different, integer-ratio entrainment is strongly dependent on the type of coupling and is typically observed for a narrow range of parameters only. Contrast this with the multi-harmonic coupling of the extended model which suggests that the physical *pendant* of equation (5.3) involves nonlinear interaction between the oscillators. After all, super- and subharmonics of a given fundamental frequency are *generated* by the coupling mechanism (5.3). This type of mutual coupling must consequently be regarded

as a greatly simplified form of a frequency demultiplication or subharmonic generation mechanism. This approach will find application again in chapter VI in the context of subharmonic waves.

3.1 Latent Order and Integer-Ratio Self-Synchronisation

Extrapolating from self-synchronisation in harmonically coupled oscillators, similar behaviour is expected in the case of combined harmonic and super-/subharmonic coupling. In fact, if the intrinsic frequencies ω_i span several octaves, global synchronisation implies the formation of locally synchronised oscillator clusters, with the cluster frequencies interrelated by integer ratios 2,4 etc. Obviously, the self-synchronisation process is not as distinct as for harmonic coupling. 'Spurious' super- and subharmonics — forcing terms at those frequencies other than the entrained oscillator frequency — are a source of noise interfering with the synchronisation process. This phenomenon was investigated by Sakaguchi (1988). He noted that self-synchronisation in a population of oscillators with external independent random noise does not change qualitatively with respect to phase transitions. Macroscopic oscillations emerge beyond the critical coupling strength, but there are no oscillators perfectly entrained to it.

Equation (5.1) with the generalised coupling function (5.2) has been solved numerically and results are presented in *figure* 5.2. The number of oscillators is $N=20$ and the intrinsic frequencies span an interval somewhat larger than two octaves[2]. Consequently, only three entrainment regions are considered ($a_k=1$, $k=1,2$ and 4). Referring to the figure, the intrinsic oscillator frequencies (solid line) are ordered on the abscissa to form a linear frequency gradient. For subcritical coupling strength the averaged oscillator frequencies, or winding numbers (Ch IV § 2.4),

$$\overline{\omega_i} = \lim_{m\to\infty} \frac{\theta(n+m)-\theta(n)}{m-n} \tag{5.4}$$

lie close to their intrinsic values (broken line). Slightly above the critical coupling, three clusters have emerged with frequency ratios 2 (or $\frac{1}{2}$). A few oscillators in the transition region between the frequency plateaus are not entrained at either cluster frequency but come to lie in between. If the coupling is well above the critical value, all oscillators will form part of the clusters.

[2]The number of oscillators may seem rather small. However, as validated by test runs for $N=100$, no qualitatively new behaviour is observed for large numbers of oscillators. Secondly, the computational load is considerably larger for model (equation 5.3). Note that the simplifications of equation (5.2) do not apply here.

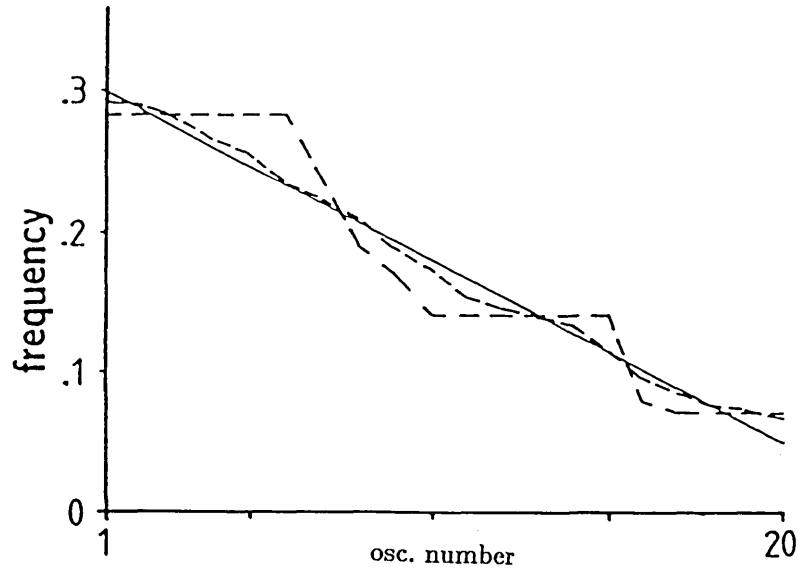

Figure 5.2 Self-synchronisation in the extended coupled-oscillator model (N=20, $\omega_i \in$ [0.3,0.05]). The intrinsic frequency distribution is shown by the solid line. The effect of subcritical (ϵ=0.004) and supercritical (ϵ=0.005) coupling strength on the average oscillator frequencies is illustrated by the dashed lines.

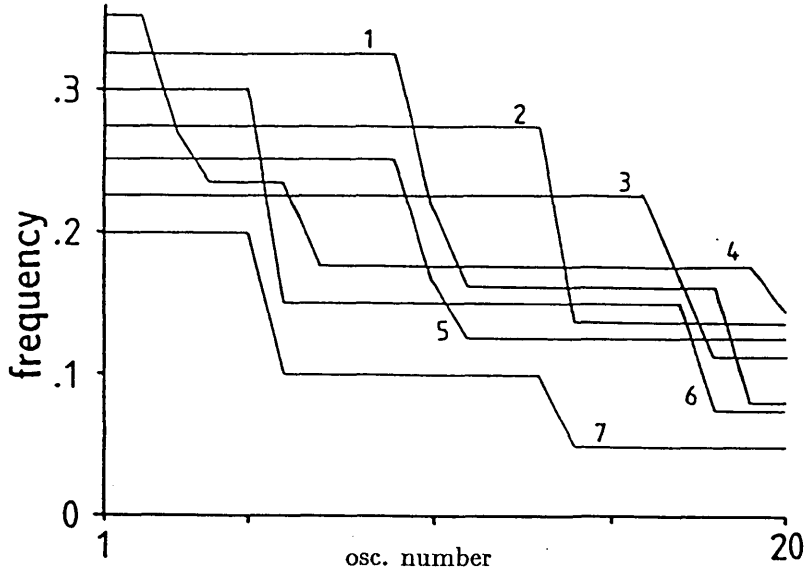

Figure 5.3 Response of the extended oscillator model to an external field (fundamental ω_f and higher harmonics $2\omega_f$, $4\omega_f$ and $8\omega_f$; identical forcing strengths), at different forcing frequencies (N=20, $\omega_i \in$ [0.3,0.05], ϵ=0.004; cases 1–7: (1) ω_f=0.325, (2) 0.275, (3) 0.225, (4) 0.175, (5) 0.125, (6) 0.075, (7) 0.025; ϵ_f=0.06). The different modes of forced synchronisation are: mode I ($\overline{\omega_1}=\omega_f$): (1), (2) and (3); mode II ($\overline{\omega_1}=2\omega_f$): (4) and (5); mode IV ($\overline{\omega_1}=4\omega_f$): (6); mode VIII ($\overline{\omega_1}=8\omega_f$): (7).

Again, the frequency plateau formation above some critical coupling strength may be interpreted as an underlying degree of organisation in the oscillator population. And as before, this organisation is raised above the critical value, as it were, by the co-operative effect of an external field.

3.2 Locking On and Integer-Ratio Forced Synchronisation

The external forcing field is assumed to be a general periodic function of fundamental period $2\pi/\omega_f$ and forcing strength ϵ_f :

$$\theta_i(n+1) = \theta_i(n) + \omega_i + \epsilon \sum_j \Gamma\{\theta_j(n), \theta_i(n)\} + \epsilon_f \sum_{\substack{k \\ k=1,2,4,...}} b_k \sin(k\,\omega_f\, n - \theta_i(n)) \; ; \qquad (5.5)$$

The weights b_k determine the relative amplitude of higher harmonics of the forcing function. The synchronisation behaviour of the extended model under forcing is obviously much richer than that of the basic model. Different harmonics of the external field will entrain different oscillators of the population and plateau boundaries will move with forcing frequency. To gain some insight into the mechanism of forced synchronisation, equation (5.5) was solved for a number of values of ω_f and ϵ_f. Specifically, in one set of runs the forcing frequency was varied over the range of intrinsic oscillator frequencies, with ϵ_f as paramter. In a second run the field strength was varied, with ω_f as independent paramter. The results of the first set of experiments are summarised in *figure* 5.3. The strength of the mutual coupling ϵ is identical to the value in *figure* 5.2 for subcritical coupling. Referring to *figure* 5.3, the response frequency graphs labelled 1 through 7 may be classified according to the ratio of the response frequency at the high frequency end to the forcing frequency. Cases (1), (2) and (3) comprise mode I synchronisation. Here the high frequency end is entrained by the fundamental forcing frequency and the corresponding ratio is one. Furthermore, in the low-frequency region a synchronised plateau at half the forcing frequency is observed. As ω_f decreases, the response switches discontinuously from mode I to mode II or second-harmonic entrainment, as exemplified by cases (4) and (5). Interestingly, a stable intermediate plateau of frequency ratio 4/3 exists in case (4), connecting the second-harmonic and the harmonic plateau. For forcing frequencies in the bottom range of intrinsic frequencies, mode IV (case (6)) and even mode VIII (case (7)), entrainment are observed. Note that the frequency-halving positions for a particular mode move to the right with decreasing forcing frequency.

In the second set of experiments ϵ_f was varied, keeping ω_f fixed at different values

(mode I, mode II and mode IV). *Figure* 5.4*a* shows results for mode I synchronisation and variations of the field strength by a factor of three. As ϵ_f is increased the fundamental plateau grows in size displacing the half-harmonic plateau. In contrast, mode II (*figure* 5.4*b*) and mode IV (*figure* 5.4*c*) synchronisation are much less sensitive to changes in forcing field strength. The transition regions between the frequency plateaus change by one, or at most two, oscillator positions.

Finally, in *figure* 5.5 the 'spatio-temporal' dynamics of the oscillator population are visualised for mode I synchronisation. Traces of the oscillator outputs $\cos\theta_i$ are plotted at consecutive times, vertically displaced[3]. Without external field, the overall appearance is rather irregular and little structure is discernible (*figure* 5.5*a*). Occasionally several 'fronts' merge and travel in 'downstream' direction. This picture changes dramatically in the presence of an external field (*figure* 5.5*b*). Very regular structures are observed that undergo a pairing process at position 8. This process is completed around position 12 or 13 and near the low-frequency end another pairing process sets in. Thus, although the frequency plateau diagrams (*figure* 5.3, 5.4) suggest an abrupt, highly localised frequency-halving, the merging process effectively takes place over some non-zero distance.

Important aspects of the above findings are discussed in the next two sections.

3.2.1 Induced Subharmonic Synchronisation

As was briefly referred to when introducing mode I entrainment, clusters or plateaus of oscillators entrained at half the fundamental forcing frequency merit closer inspection because they are produced not by the external field. Instead, an induction mechanism is operative. By virtue of the coupling (equation 5.3), the oscillator cluster entrained by the fundamental forcing frequency generates an organised field of frequency one half the fundamental. This in turn acts on oscillators whose intrinsic frequencies are too low for synchronisation at the fundamental, but more susceptible to the suhbarmonic. It is these induced frequency plateaus that are observed in *figure* 5.5*b*. As can be seen from the figure and also from *figure* 5.4 the induction process is not confined to the first subharmonic. The induced plateau at half the fundamental forcing frequency acts itself on oscillators of lower intrinsic frequency, inducing a synchronised cluster at a quarter of the fundamental forcing frequency.

---

[3] A few explanatory words are necessary at this point regarding the term 'spatio-temporal'. The labelling of the abscissa of *figure* 5.5 as (discrete) 'space' is admittedly somewhat premature although the correlation between the streamwise coordinate of the free shear layer and the oscillator intrinsic frequencies was briefly alluded to in § 1. Further details of this analogy are deferred to § 4.2.1.1.

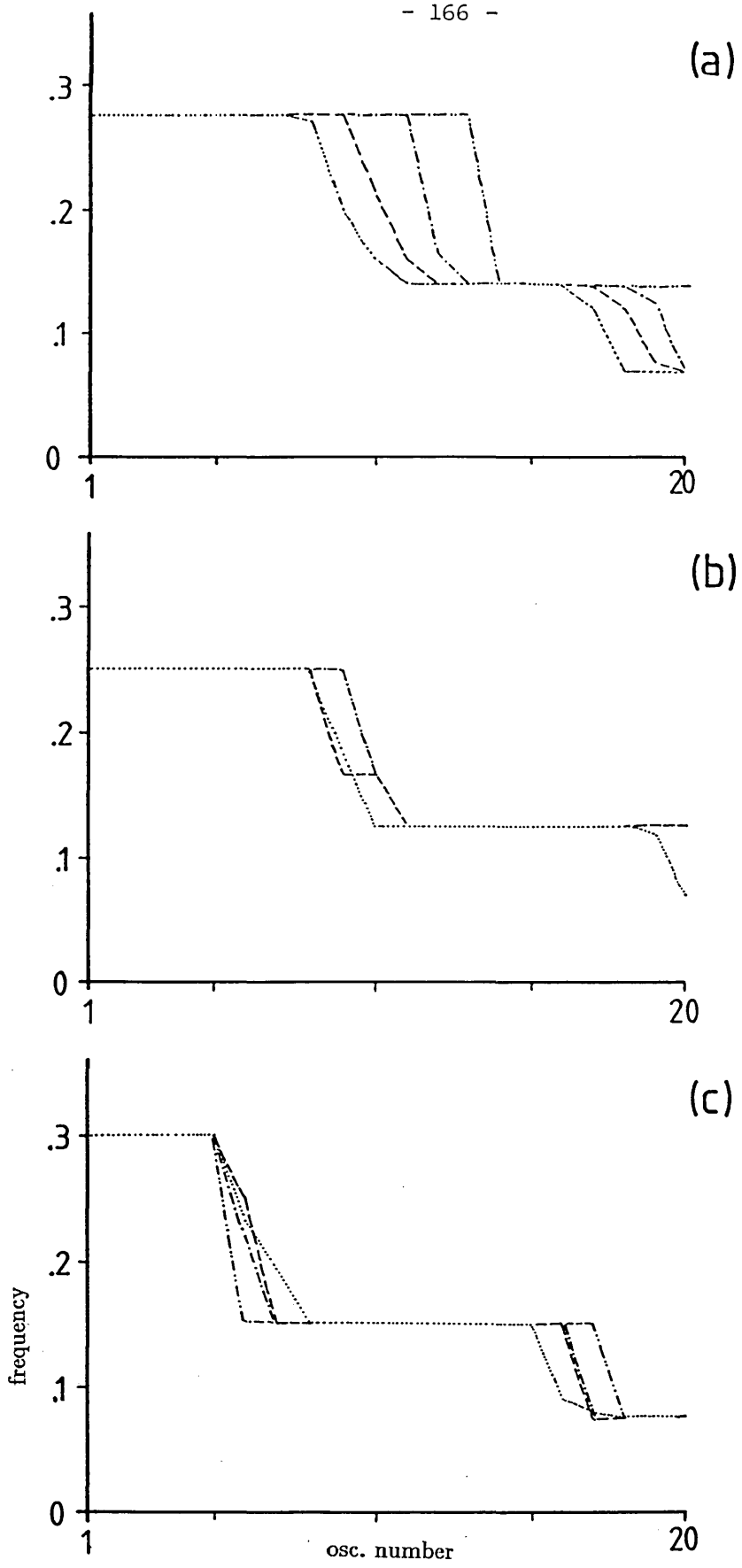

Figure 5.4 Susceptibility of plateau formation to variations in forcing strength (N=20, ϵ=0.004; ϵ_f=0.03 (····), 0.05 (----), 0.07 (-·--), 0.09 (-···). (*a*) Mode I forcing, ω_f=0.275. (*b*) Mode II forcing, ω_f=0.125. (*c*) Mode IV forcing, ω_f=0.075.

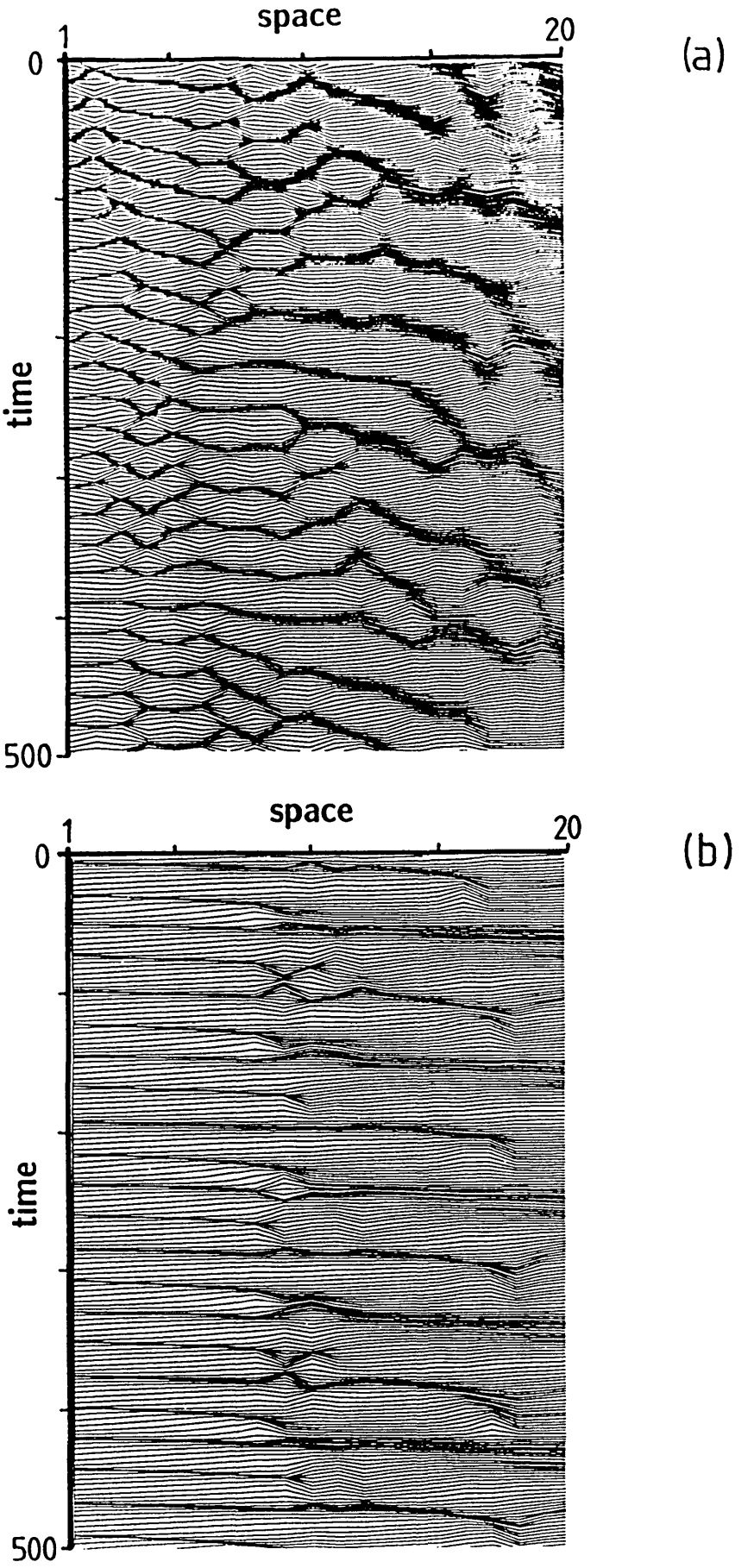

Figure 5.5 Visualisation of the 'spatio-temporal' dynamics of the extended oscillator model ($\epsilon=0.004$) for mode I forcing ($\omega_f=0.275$). Traces of the system output $\cos\theta_i(n)$, $i=1,..,20$ are shown at consecutive times n. (a) $\epsilon=0$. (b) $\epsilon_f=0.03$).

In summary, the organisation of oscillators in the high frequency region induces organisation throughout the population. Obviously, this regularisation process can be initiated in any portion of the population because the oscillator interaction in the model is isotropic and uniform. The importance of this mechanism for the understanding of the dependence of the plateau frequency, size and position on ω_f and ϵ_f is discussed in the following section.

3.2.2 Resonance Competition

The main findings of the numerical study of the influence of ω_f and ϵ_f on plateau formation in the extended coupled-oscillator model are : (1) the discontinuous switching of the response frequency; (2) the sensitivity of the harmonic plateau size on field strength under mode I forcing; (3) conversely, the relative insensitivity to the field strength under higher mode forcing. These observations are explained here on the basis of single-oscillator entrainment and the induced subharmonic synchronisation concept.

The discontinuous switching of the response frequency is not peculiar to our long-range coupled oscillator model. Any nonlinear system near a supercritical Hopf bifurcation with super-/subharmonic resonance properties exhibits frequency jumps as the excitation frequency is varied continuously whilst keeping the excitation amplitude fixed. Examples of this are given in chapter IV for the multi-frequency excited $\lambda-\omega$ oscillator (Ch IV *figure* 4.6). For large enough forcing the transition between different response modes is abrupt. Compare the entrainment diagram of the multi-frequency excited $\lambda-\omega$ oscillator to single-frequency excitation (Ch IV *figure* 4.5). In the latter system the entrained region grows with increasing forcing whereas in the former system entrainment boundaries are much less variable as neighbouring resonance regions compete for the dominant system response. Note that in example (Ch IV *figure* 4.6) the amplitudes of all harmonics are identical and changes in the balance of resonance competition are readily effected by unequal amplitudes.

The differences between mode I and higher mode synchronisation are readily explained now. The absence of resonance competition in mode I forcing makes the response sensitive to variations in forcing field strength. With increasing ϵ_f, more oscillators are entrained by the external field, and the induced subharmonic clusters move to the low frequency region correspondingly. In contrast, resonance competition is effective in higher mode synchronisation, and boundaries between clusters, entrained by the fundamental and higher harmonics of the external field, are relatively insensitive to changes in field strength. The identification of induced subharmonic plateaus or clusters is therefore important in explaining sensitivity brought about by resonance competition.

3.2.3 Miscellaneous Aspects of Forced Synchronisation

Two further aspects that are not as readily classified as the previous two, deserve mention here. First, the existence of a 4/3 plateau in one of the mode II forcing experiments. This kind of super-harmonic synchronisation was also observed by Sakaguchi (1988), and appears to be peculiar to populations of one-dimensional oscillators. Sakaguchi offered no detailed explanation for this phenomenon but noted that the self- and external field interact to produce a stable response at commensurate frequencies. Secondly, the consistent observation that the frequency-halving positions in the oscillator model under subharmonic forcing move to the low-frequency region when the forcing frequency is decreased. Mention is made of this phenomenon because the same observation will be made again in the context of the forced free shear layer. As in § 3.2.2, this observation is explained by resorting to the resonance mechanism. The intrinsic frequencies form a negative frequency gradient and therefore the boundary regions of entrainment move to the lower frequency region when the forcing frequency is decreased.

4. A Phenomenological Model

It is the purpose of this section to relate the coupled oscillator model to the free shear layer as outlined in § 1. To this end the pertinent shear layer dynamics are reviewed below, unless discussed already in chapter II.

4.1 Some Free Shear Layer Phenomenology

There is considerable experimental evidence of forced flow regularisation in free shear layers. Also, detailed studies have shown the suppression of broadband velocity fluctuations in the presence of forcing in both plane mixing layers and axisymmetric jets. Induced subharmonics are most clearly observed in axisymmetric jets but the mechanism has also been utilised to study subharmonic evolution in the plane mixing layer. Furthermore, a systematic study exists on higher mode forcing in the mixing layer that provides much qualitative information. Representative studies for each of these aspects of the forced free shear layer are discussed below.

4.1.1 Suppression of Broadband Fluctuations

As mentioned above, increased regularity is observed in both mixing layers and axisymmetric jets. The physical mechanism underlying this flow organisation is the same for both flow types yet the interest in the latter flow is rather more practical in nature. The

suppression of broadband fluctuations in jet flows is closely related to the technical problem of jet engine exhaust noise suppression. Studies of the forced mixing layer, on the other hand, are guided by a more fundamental interest in flow instability and transition. The view taken there is that by exerting some control over the flow by means of forcing, investigations of flow instability and transition are greatly facilitated, whilst at the same time preserving the basic flow structure.

Miksad (1972) gave results of hot-wire measurements of streamwise velocity fluctuations in the mixing layer between two parallel air streams (velocity ratio R=0.72, R=0.69), excited by sound (*figure* 5.6). He commented on the much more organised appearance of the disturbance field in terms of discrete frequency components. Unfortunately, his results for the unforced and forced mixing layer are comparable on a purely qualitative level only as the spectral energy measurements are rendered quantitatively meaningless by "arbitrary units" scaling.

The more recent study by Oster and Wygnanski (1982) was quoted in § 1 to support the nonlinear-oscillator approach. As in Miksad's experiments, hot-wire anemometry was used to investigate the flow evolution of the forced mixing layer, formed by the merging of two parallel air streams (velocity ratio R=0.25). Forcing was introduced at the initiation of the mixing layer by a thin flap mounted at the trailing edge of the splitter plate. Energy spectra of streamwise velocity fluctuations at some downstream position in the mixing layer are shown in *figure* 5.7 for various forcing amplitudes. These measurements do indeed support the view that energy is exchanged between the natural instability and the fundamental forcing frequency. This, and the large difference between forcing frequency, and the frequency of the natural instability explain Staubli's (1985) asynchronous quenching hypothesis.

A particularly interesting study is that of Crow and Champagne (1971) because it relates rather more to the experimental findings of this study. Crow and Champagne considered an air jet at Re=10^5 forced at St=0.30 near the natural frequency of vortex shedding. The jet boundary layer was tripped to destroy short interfacial waves immediately downstream of the nozzle and to achieve a measure of jet exit speed independence. The acoustic forcing was approximately 2% of the mean exit speed. The measurements (*figure* 5.8), clearly show the reduction in broadband levels of axial velocity fluctuation.

Yet another, again more recent study of the forced free shear layer was by Kibens (1980). Specifically interested in jet engine exhaust noise he concentrated on sound pressure measurements in the near- and far field of a jet at Re=50,000. The forcing was introduced

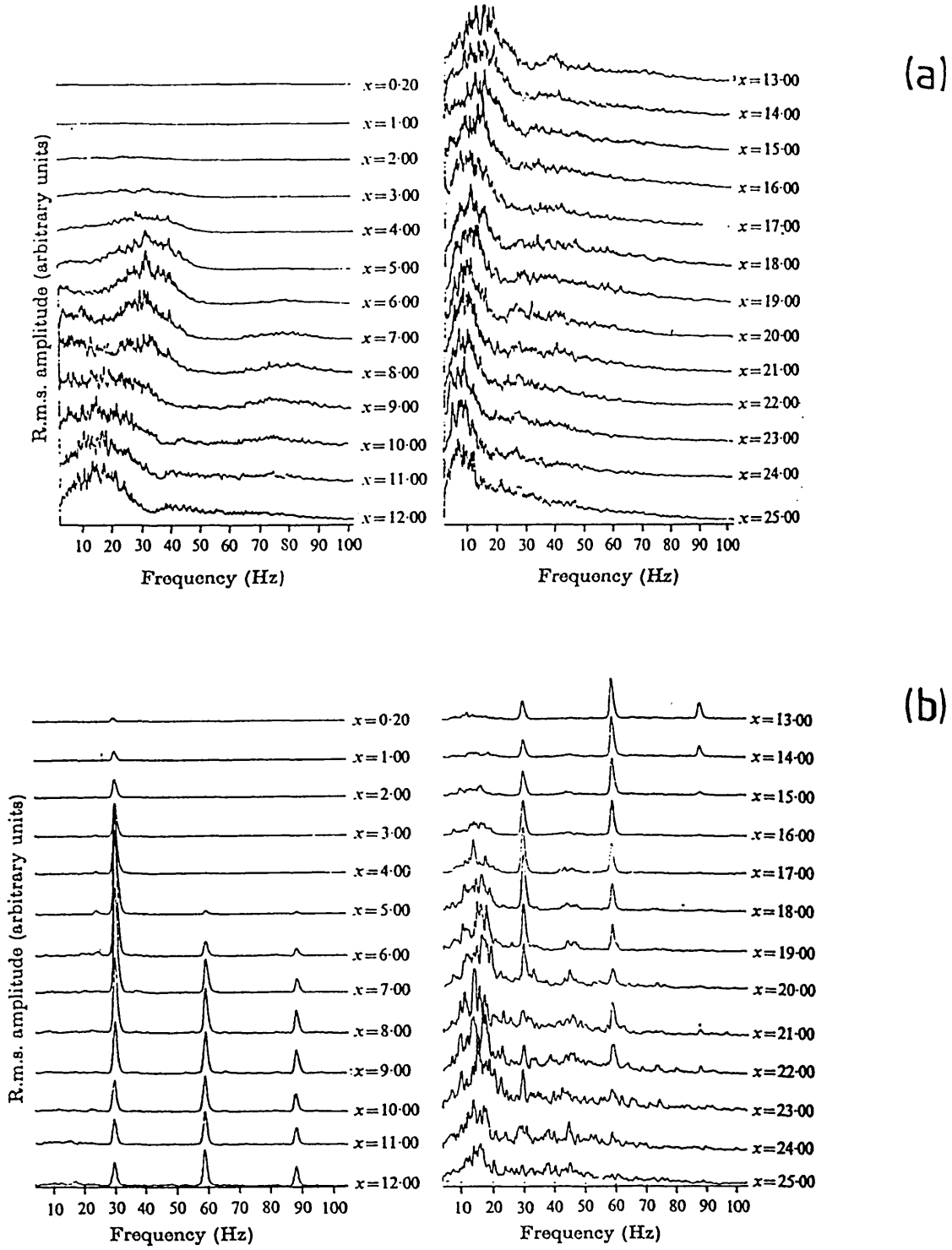

Figure 5.6 Energy spectra of streamwise flow velocity fluctuations in a plane mixing layer at consecutive downstream positions x (after Miksad 1972). (*a*) Natural instability. (*b*) Sinusoidal sound excitation at $f=29.5$ Hz.

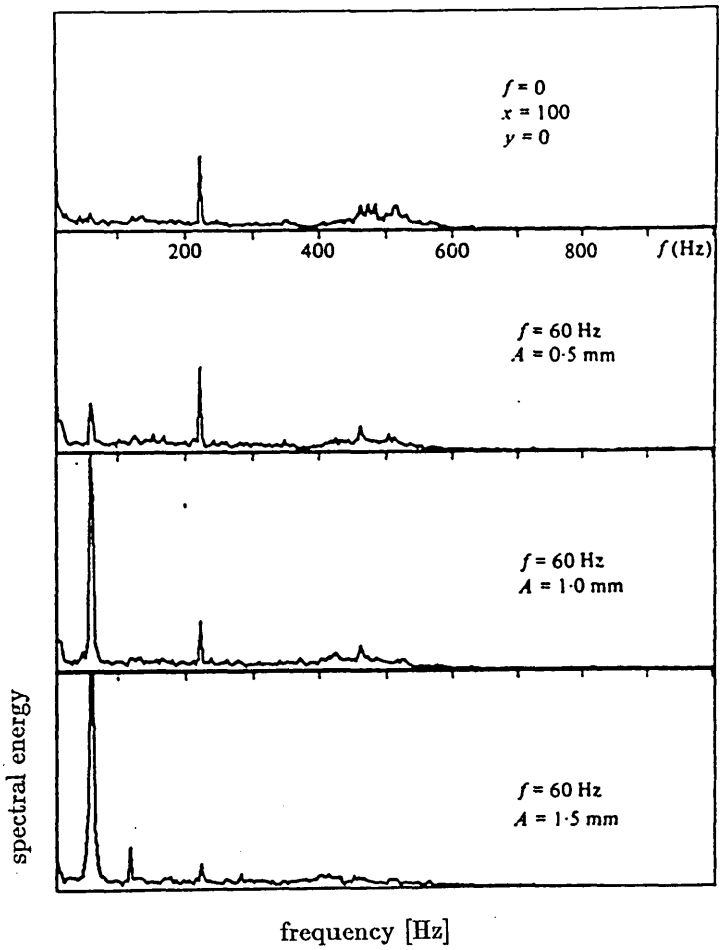

Figure 5.7 Energy spectra of streamwise velocity fluctuations in a forced mixing layer (after Oster and Wygnanski 1982). Natural broadband fluctuations are observed in the interval 400−600 Hz. The frequency component at 230 Hz is thought to be a subharmonic of the vortex shedding. Excitation is by means of a thin flap at the trailing edge of the splitter plate at f=60 Hz. The forcing amplitude is indicated by the amplitude of oscillation A of the flap.

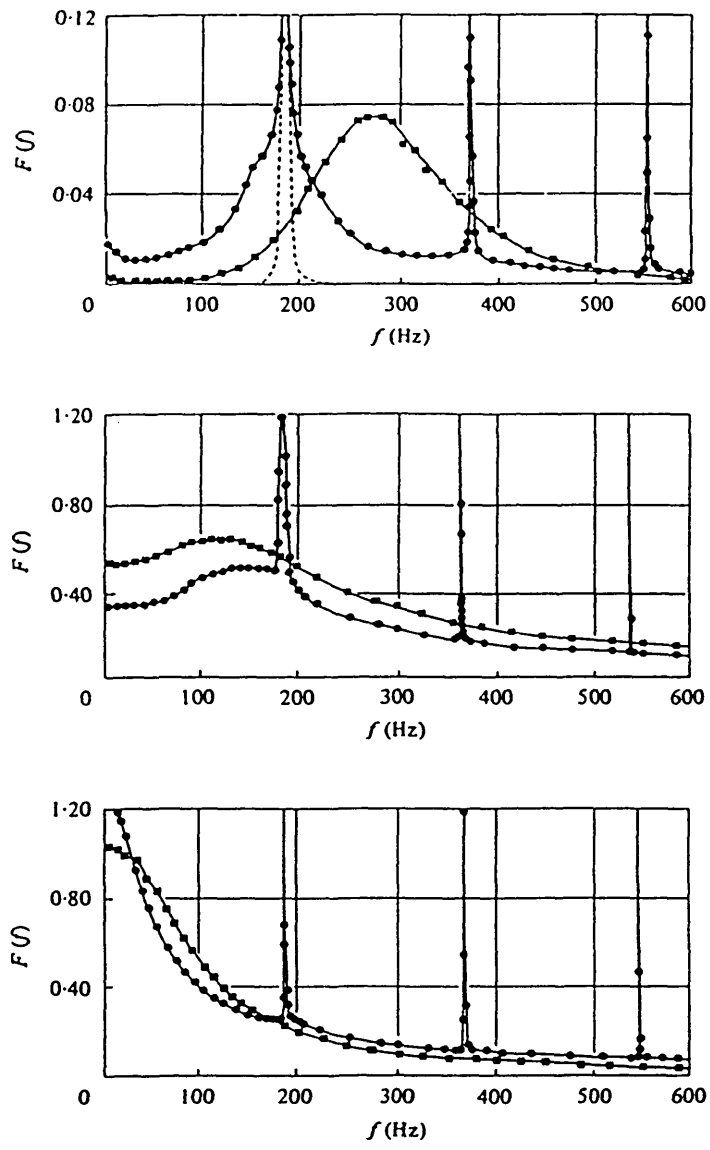

Figure 5.8 Flow velocity spectra in a forced axisymmetric jet (Re=1.06 x 10^5) at downstream position x/D=4 and radial position (*a*) r/D=0, (*b*) r/D=0.5, (*c*) r/D=0.75 (after Crow and Champagne 1971). Also given are the spectra of the unforced jet. The excitation frequency is f=185 Hz (St_D=0.30) and the forcing amplitude is 2% of the mean jet exit speed.

locally through the nozzle exit as an azimuthally coherent perturbation and the excitation level was below the measurement noise level. Unlike Crow and Champagne's experiments, the jet boundary layer was not tripped. Instead the forcing was near the shear layer mode instability (St=3.54, based on jet diameter) and interaction with the jet column mode instability was observed. Centreline hot-wire measurements showed that with excitation as much as 90% of the total turbulent energy was contained in coherent structures as opposed to about 60% without excitation. Nearfield sound pressure measurements clearly showed the suppression of noise levels (*figure* 5.9*a*,*b*). A further aspect of this study is discussed below.

4.1.2 Induced Subharmonic Regularisation

Kibens observed that the shear layer constitutes a narrow band amplifier. When the departure of excitation frequency f_e from the shear layer instability f_s was more than 10%, the flow essentially reverted to unforced conditions. However, when f_e was near the shear layer instability, flow regulation could extend well into the region of the jet column instability. Downstream of the region of coherent structures phase locked by the fundamental a vortex pairing cascade $f_e/2$, $f_e/4$ and $f_e/8$ was observed (*figure* 5.9*c*). The vortex pairing was most pronounced when the cascade frequency $f_e/8$ (St=0.44) was near the jet column instability f_j. This implies that the interaction between the two jet instabilites is strongest if $f_j \simeq f_s/8$, a condition which is controlled by the thickness of the initial jet boundary layer. When these conditions were not properly met the coherent structures decayed soon after the first or at most second pairing.

Flow regularisation of the first vortex pairing was also reported by Acton (1980) in a numerical modelling of an axisymmetric jet. She considered the inviscid limit $Re=\infty$, arguing that large eddy motion is essentially inviscid. The harmonic excitation was applied in the Strouhal number range St=0.1 – 2.0 and the excitation level varied from 0.5% to 10% of the mean jet exit speed. Apart from the facility with which system parameters and boundary conditions are changed, the numerical modelling has the added advantage that complete spatio-temporal descriptions of, amongst other quantities, the velocity fluctuations are obtained which allows for comprehensive visualisation[4] (*figure* 5.10). This figure shows the temporal evolution of radial velocity traces over the first few diameters, taken in the jet shear layer. Results are given for both the unforced and the forced (St=1.5, 10% forcing amplitude) jet. The choice of the recording position and the radial velocity component ensures a visualisation most representative of the vortical structures in the jet. Referring to *figure* 5.10*a*, the formation and evolution of eddies is fairly irregular, in particular merging locations are not

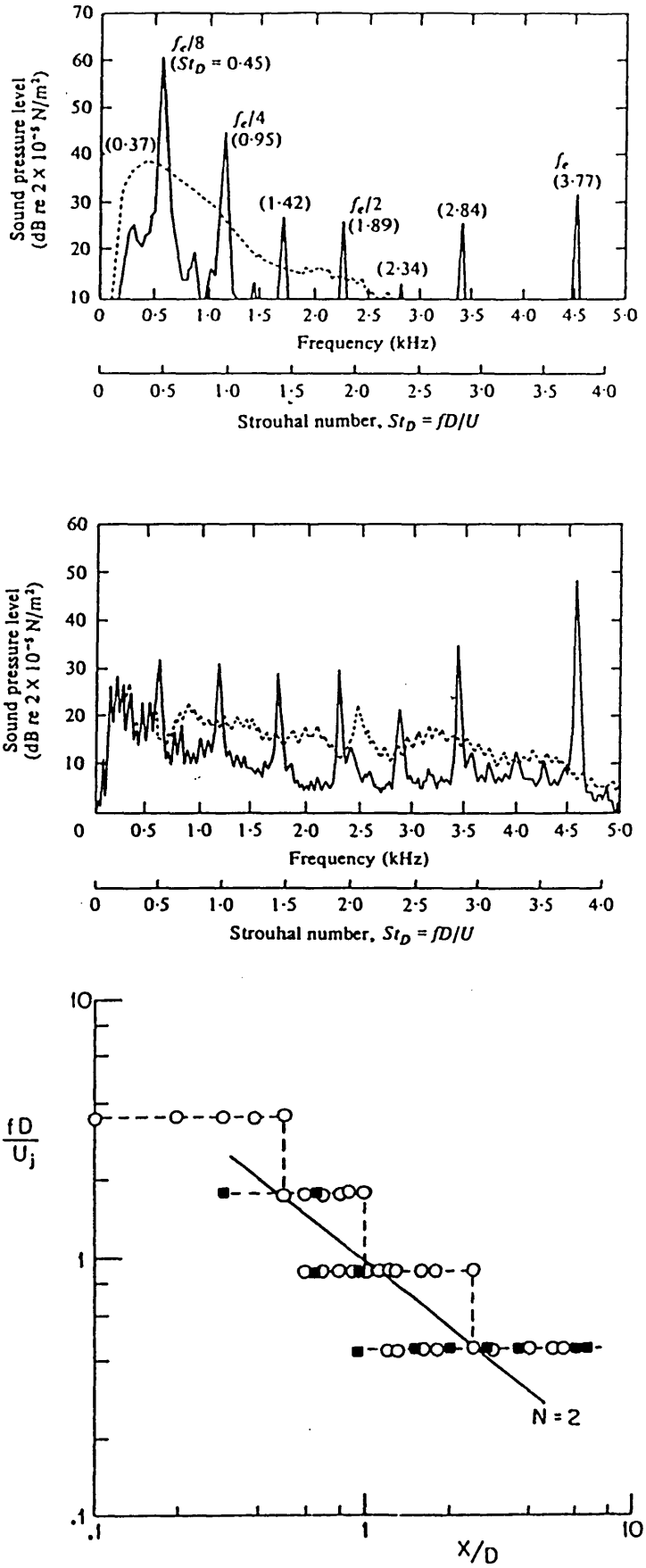

Figure 5.9 Sound pressure spectrum of an acoustically excited axisymmetric jet (Re=5 x 10^4) at downstream position (*a*) x/D=1.0, radial position r/D=1.0 and (*b*) x/D=50, r/D=50 (after Kibens 1980). The spectrum of the non-excited jet is given by the broken line. The excitation frequency is St_D=3.77. The excitation level is below the measurement noise level. (*c*) Evolution of vortex passage frequency in the excited jet. Frequency measurements are taken in the jet shear layer (o) and at the jet centre line (□). The solid line denotes the predictions by the feedback equation (Laufer and Monkewitz 1980).

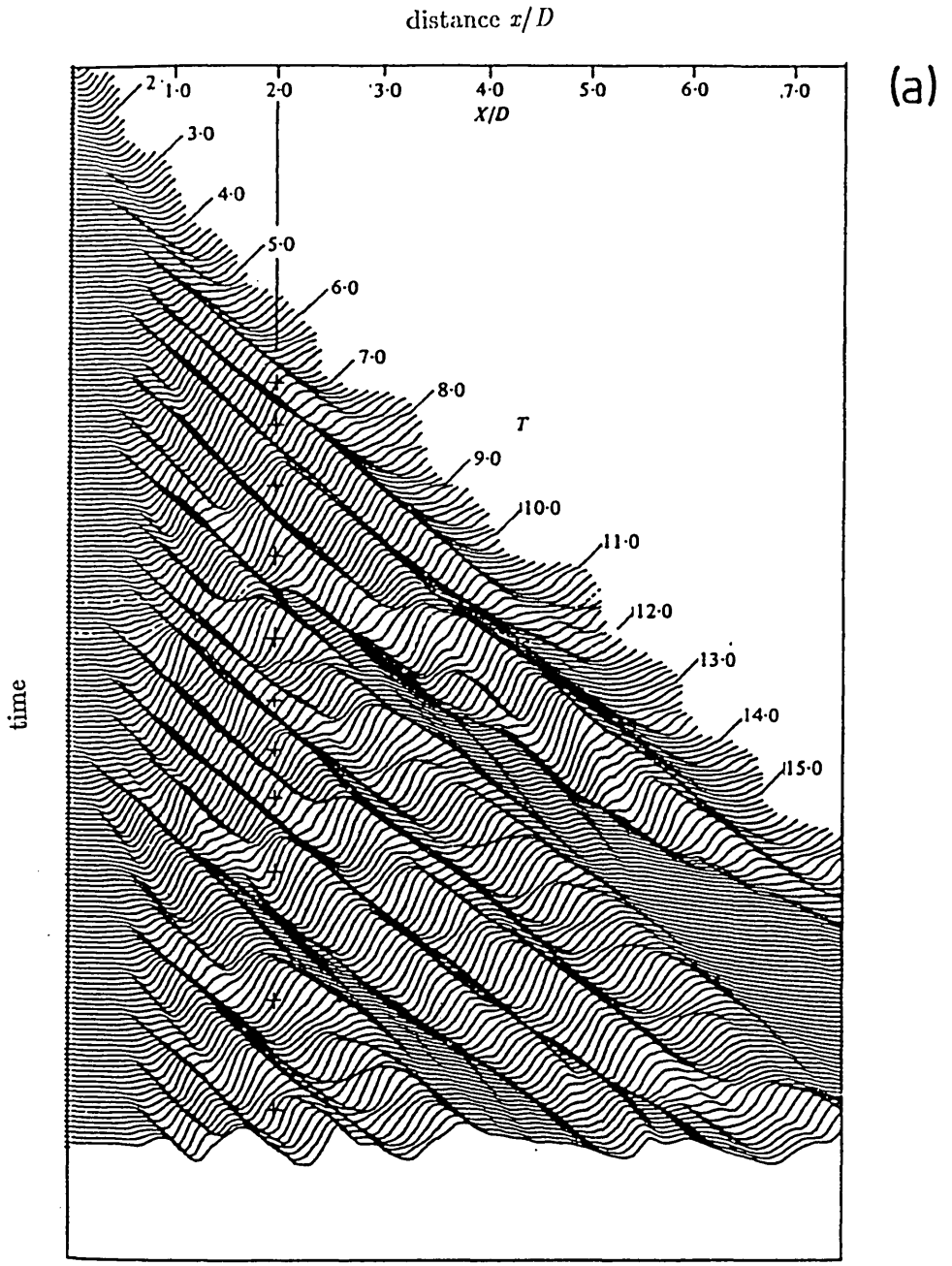

Figure 5.10 (*a*) The axial distribution of radial velocity at equal time intervals in an unforced axisymmetric jet (after Acton 1980). (*b*) Flow excitation at $St_D=1.5$ and excitation level $A=2\%$.

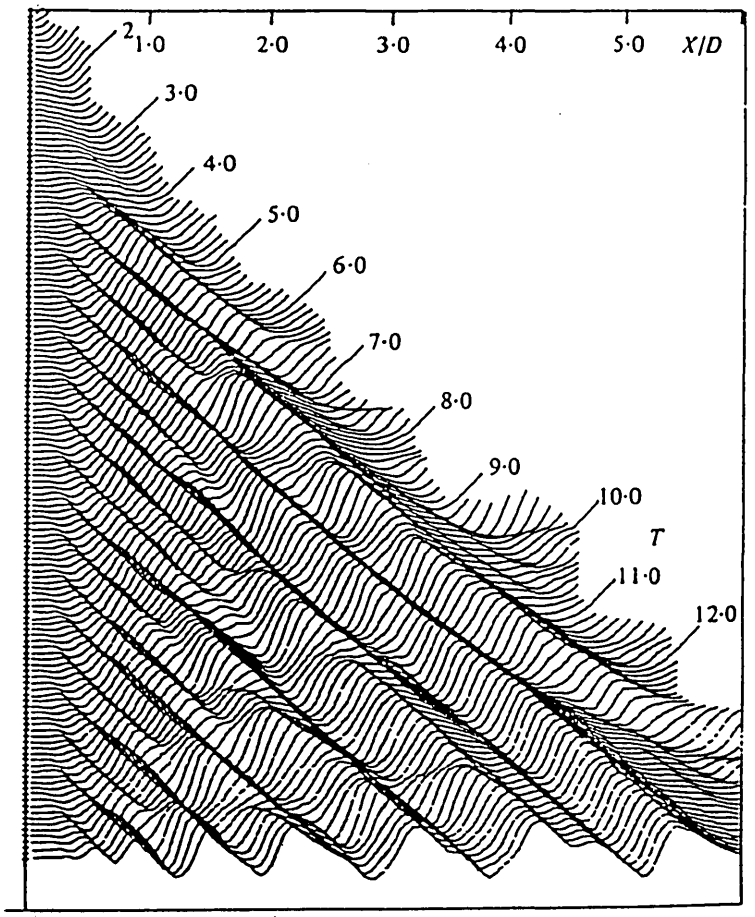

(b)

well defined. When the jet is forced by planar surging at a frequency near the initial eddy formation frequency (shear layer mode), this process is greatly regularised (*figure* 5.10*b*). Eddies form very regularly and the first pairing, indicated by the merging of crests, becomes highly localised. The organised structure is maintained somewhat beyond the pairing point but further downstream control over the flow is lost.

4.1.3 Subharmonic Forcing

The study by Ho and Huang (1982) provides a systematic account of the forced mixing layer response to variations in forcing frequency and amplitude. In their experiment the mixing layer was formed by the merging of two parallel water streams of velocities U_1=5.0 cm s^{-1} and U_2=9.5 cm s^{-1} (velocity ratio R=0.31). Forcing was introduced by perturbing the flow rates of both streams by means of butterfly valves in the supply section. A hot-film anemometer placed in the mixing layer provided the information for the spread of the mixing layer and the vortex passage frequency.

Findings of this study that are relevant to our coupled oscillator model are summarised in *figures* 5.11*a* and 5.11*b*. The second figure has been adapted from Ho and Huang (*ibid*) because the emphasis of their investigation was placed on the spreading rate of the forced mixing layer. To begin with, the response frequency of the forced mixing layer *i.e.* the frequency of vortex formation, switches discontinuously and with noticeable hysteresis between modes which are defined by the ratio of the response frequency to the forcing frequency (*figure* 5.11*a*). As the mode diagram shows, except for mode I forcing the response frequency stays below f_m which is the most probable frequency of vortex formation in the unforced mixing layer. With respect to this phenomenon, Ho and Huang (*ibid*) noted that, although no plausible explanation is available at present, the response frequencies are always dispersive, or at most equal to the most probable frequency.

Details of the spatial development of the vortex passage frequency in the forced mixing layer are given in *figure* 5.11*b*. Without forcing, vortices are formed on average at f_m=5.06 Hz

[4] On the other hand, the disadvantages of numerical modelling schemes potentially outweigh the advantages and are not dispensed with easily. Crucial points include the excessive computational load, let alone the computing costs, and the problems when large parameter spaces need to be scanned quickly to arrive at a qualitative understanding of a complex dynamical system. It is for these reasons that the study of interacting oscillator populations has often resorted to 'old-fashioned' electronic circuit implementation (Winfree, Linkens and co-workers). In fact, there is a certain paradigmatic dimension to the issue of hardware *vs.* software implemenation. Robert Shaw (*The dripping faucet as a model chaotic system.* Aerial Press: Santa Cruz CA 1984) reported on repeatedly rejected grant applications for the investigation of his model chaotic system, a numerical modelling of which would have been prohibitively time- and cost consuming.

and the vortex passage frequency is constant before merging. When the merging, which is not well defined spatially in the unforced mixing layer, begins the vortex passage frequency decreases linearly. In mode I forcing the vortex merging can be delayed considerably, but behind the merging point the flow essentially reverts to the unforced conditions. When the forcing frequency is lowered below some threshold value the response switches to mode II forcing. Now two frequency plateaus are observed and the first vortex merging process becomes highly localised[5]. The response frequency is twice the forcing frequency and the merging process is strictly one of pairing so that after the merging a plateau of constant vortex passage frequency at the forcing frequency exists. Within the mode II, if the forcing frequency is lowered the merging points are shifted downstream. No similarly detailed information was given on mode III forcing although it was noted that this usually involved the merging of two vortices first and the merging of the new vortex with a third one further downstream. Finally, the mode IV forced mixing layer is characterised by two localised pairings with three plateaus of constant vortex passage frequency.

So far the discussion has been about mixing layers under low forcing levels. At high levels of forcing ($\simeq$ 2% of the mean flow velocity), however, the forced mixing layer behaves entirely differently and a phenomenon called *collective interaction* is observed (Ho and Nosseir 1981). Eddies initially are formed within a wide band near the most probable frequency f_m and then undergo a collective merging process, bypassing the higher modes of the response frequency. This results in the formation of large scale coherent structures at the forcing frequency itself. The two phenomena associated with collective interaction are the high spreading rate and the large drop in the vortex passage frequency.

The general dependence of the merging locations in the forced mixing layer on variations in forcing amplitudes is not well documented. From the flow visualisation in Ho and Huang (*ibid*) it can be inferred that with increasing – low – levels of forcing, the merging locations tend to be moved upstream. However, as Ho and Huerre (1984) noted, adjustments in forcing level do not provide an efficient way to shift merging locations. An example of a jet, forced at $f_f = f_m/2$, is given where the forcing amplitude needs to be increased by a factor of 37 (!) to shift merging locations upstream by one wavelength.

[5] Localisation must be understood relative to the wavelength of the response frequency. The distance over which localised merging occurs typically spans one wavelength. This rule has guided in deriving the vortex passage frequency diagram (*figure* 5.11*b*).

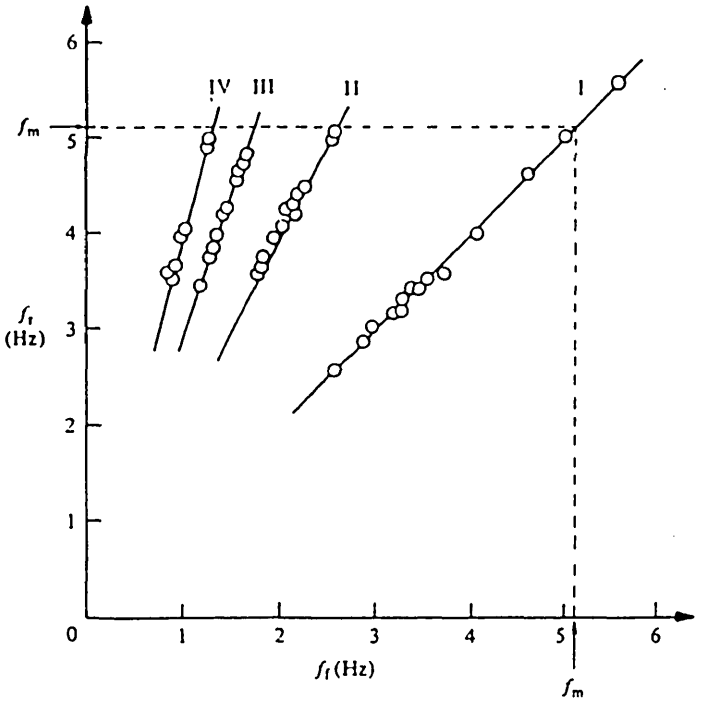

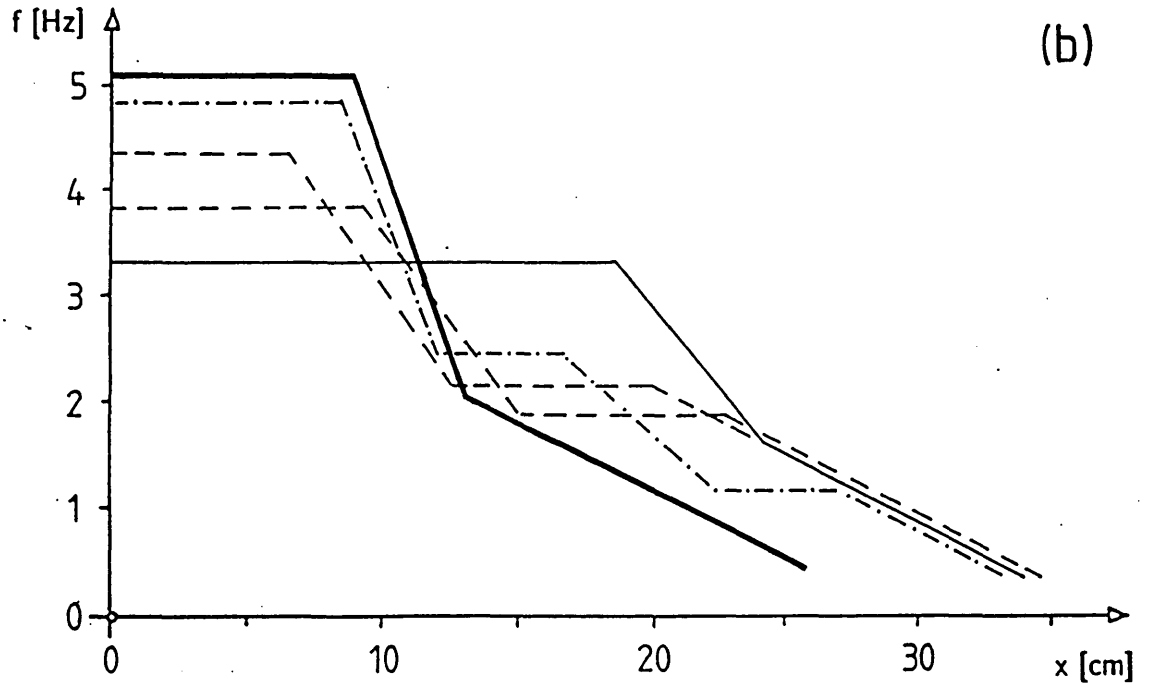

Figure 5.11 (*a*) Shear layer response frequency *vs.* forcing frequency in a forced plane mixing layer (after Ho and Huang 1982). The natural vortex shedding frequency is f_m=5.06 Hz. The forcing level is about 0.1%. (*b*) The vortex passage frequency in the unforced (—) mixing layer (adapted from Ho and Huang). Mode I forcing at 3.29 Hz (—). Mode II forcing at 1.92 Hz and 2.18 Hz (---). Mode IV forcing at 1.21 Hz (-·--).

4.2 Enumerating Analogies

Having discussed properties and concepts of both the coupled oscillator model and the forced free shear layer, we are now in a position to substantiate and qualify the nonlinear oscillator analogy of the forced free shear layer.

4.2.1 The Basic Oscillator Model

Here we elaborate on the parallels between a collection of single-frequency instability waves and coupled nonlinear oscillators.

4.2.1.1 Without Forcing

In classic hydrodynamic stability theory, the downstream development of coherent structures is viewed as the continuing nonlinear mode competition, taking place in Fourier space between a finite number of waves. For example, the emergence of a subharmonic component at half the frequency of the fundamental wave is accounted for by considering the parametric-resonance form of interaction between a fundamental and subharmonic wave (Kelly 1967).

It is now proposed to relate a population of linearly interacting nonlinear oscillators with uniform coupling, to nonlinearly competing instability waves in the free shear layer. The spatially distributed character enters into the coupled oscillator model through the downstream change of the free shear layer length scale. In the unforced mixing layer, the vortex merging process is random in time and space and the spreading rate of the mixing layer is linear. Equally, the average vortex passage frequency decreases linearly (*cf figure* 5.11). The relationship is qualitatively similar for the forced mixing layer. A global feedback model (Laufer and Monkewitz 1980) predicts the dominant frequency of the forced mixing layer to follow an inverse-distance rule $f \propto 1/x$. Translated to the coupled oscillator model, a distribution in intrinsic frequencies correlates with a streamwise spatial distribution. This, however, identifies the uniform coupling as a particular form of long range interaction. It will be recalled that uniform coupling is necessary if global as opposed to local synchronisation is to be observed in an oscillator population.

Returning to the global feedback model, long range interactions are considered an important aspect of free shear layer dynamics. Dimotakis and Brown (1976) argued that the free shear layer must be viewed globally because the $1/x$ decrease of induced velocity expected from the Biot-Savart law is exactly compensated by a corresponding linear increase in the circulation of vortices. Laufer and Monkewitz (*ibid*) observed that in a free jet the flow oscillations near the nozzle exit were amplitude modulated by the large scale structures of the

preferred mode of the jet at the end of the potential core. Finally, the study of Ho and Nosseir (1981) on an impinging jet suggested that a global feedback loop mechanism is operative, linking downstream conditions to the initial shear layer.

The analogy between the latent order concept of the free shear layer and phase transition in a coupled oscillator population has been described in detail (*cf* § 2.1, § 3.1).

4.2.1.2 With External Field

The nonlinear oscillator analogy of the forced free shear layer has its root in the observation that mode competition between an artificially generated single-frequency wave and natural broadband background noise leads to the suppression of the broadband component and a very organised train of vortex structures. Needless to say, there is therefore close agreement between the experimental findings of this study (Ch III § 5) and the experiments described in § 4.1 on the one hand, and the behaviour of the coupled oscillator model in the presence of an external field, on the other hand. The external field represents those instability waves that are induced to grow and attain high amplitudes, thence interacting unidirectionally with the other waves.

It is worth recalling the parallels drawn by Rockwell and Naudascher (1979) between the free shear layer impinging on an edge and the forced free shear layer. In either flow the free shear layer contains a discrete frequency component which Ho and Huang (1982) considered an essential characteristic of self-sustained flow oscillations. In the forced free shear layer, flow regularisation is brought about by the high amplitude instability wave artificially generated by the forcing. In the former flow the mechanism responsible for the selection of a particular frequency is one of resonance of a feedback loop (*cf.* § 4.2.1.1). In this context Laufer (1981) noted that both the resonance of the impinging shear layer and the global feedback in the free shear layer are described by the same feedback equation.

The similarities between these two flows and self- and forced synchronisation in the basic oscillator model are intriguing. The feedback of pressure perturbations provided by an impingement edge may be thought of as intensifying the long-range coupling present in the free shear layer. This in turn results in global organisation. In the forced free shear layer, on the other hand, latent order is raised above the background noise level by the co-operative effects of the self-field and the external field.

4.2.2 The Extended Oscillator Model

The distributed character of the coupled oscillator model *i.e.* its long range coupling, becomes particularly important for the extended version with combined harmonic and super-/sub-harmonic coupling. In the extended oscillator model, latent order and forced synchronisation involve interactions over several octaves of intrinsic frequency.

4.2.2.1 Without Forcing

In model (5.5), the formation of integer-ratio clusters of synchronised oscillators was seen to be the result of combined mutual harmonic and super-/sub-harmonic coupling. Adopting the viewpoint of the oscillator population as a spatially organised system again, a length scale of interaction of the order of the distance spanned by a cascade of frequency-halving plateaus is necessary to ensure this kind of self-synchronisation or underlying organisation. This mechanism of 'vortex pairing' is certainly supported by Kibens' (1980) experiment. Indeed, his findings suggest that long range interactions in the jet shear layer are of the order of several diameters connecting the two jet instability modes, the initial shear layer mode and the jet column mode at the end of the potential core. Importantly, the results are in close agreement with what is predicted by the global feedback model (*figure* 5.9*c*).

4.2.2.2 With External Field

Resonance competition and induced subharmonic regularity are the two mechanisms underlying the observations of the extended oscillator model with external field. Against the background of the forced free shear layer phenomena reported in § 4.1, these mechanisms can shed further light on the nonlinear oscillator analogy.

In the forced flow experiments of Miksad (1971), Kibens (1980) and Acton (1980), the shear layer response frequency as defined in (Ho and Huang 1982) was the same as the forcing frequency and downstream flow organisation involved induced subharmonic structures. The same mechanism, albeit less distinct, was operative in the mode I forced mixing layer (Ho and Huang *ibid*), and explains the relatively high sensitivity to forcing amplitude.

The comprehensive subharmonic forcing experiments by the same authors provide further clues regarding subharmonic induction and resonance competition. The collective interaction observed at high forcing levels suggests that the forcing is dominantly harmonic, causing entrainment of a large number of oscillators whose intrinsic frequencies are near the forcing frequency. The high frequency end, however, is unaffected and not discernibly organised. At low forcing levels, the type of forcing must be decided on the basis of the

sensitivity of the free shear layer response to variations in forcing amplitude. For example, if the sensitivity of merging locations is taken to be fairly low then this may be explained by the competition between the fundamental forcing frequency and higher harmonics thereof[6]. If, on the other hand, merging locations tend to be susceptible to forcing levels then the higher harmonic response of the forced free shear layer may be the result of induced higher harmonics.

The overall picture, if somewhat tentative, is that a clear distinction must be made between externally imposed and internally generated spectral components. The importance of this distinction lies in its verification by susceptibility analysis.

The above discussion allows a substantiated and qualified interpretation of the particular interaction between the forcing field and the self-field (equation 5.5). The external field comprises spectral components at the fundamental forcing frequency and possibly higher harmonics, but not subharmonics, at least not of comparable amplitude. Instead, subharmonics are generated internally by the combined action of oscillators entrained by the forcing field. This is in close agreement with the generation of subharmonics in the free shear layer, as described by Miksad (1971), and summarised in a phenomenological model (Ho 1982). The external field may therefore be thought of as a collection of high-amplitude single-frequency instability waves at the fundamental forcing frequency and its higher harmonics. These synchronise instability waves in a wide band around the forcing frequency. It is worth restating that the subharmonic generation mechanism is independent of the external field action. What is important for subharmonic generation is the synchrony of oscillators at the fundamental, not the amplitude of instability waves at the forcing frequency.

5. Discussion

An equally appropriate heading for this section might have been "Enumerating Limitations" to emphasise shortcomings of the nonlinear oscillator analogy. Before identifying these limitations, let us briefly summarise the analogies.

The nonlinear mode competition between instability waves is compared here to the linear interaction between nonlinear oscillators[7]. Secondly, regarding the global feedback model of the free shear layer, Laufer (1981) remarked that free shear layer dynamics cannot be expressed in terms of a "local gradient diffusion model" but only by a long range force field.

---

[6] Again the problem with many forced flow experiments is that the spectral content of the forcing function is poorly documented. For instance, one can only speculate as to the monochromatic character of the excitation employed in the experiments of Ho and Huang. In our experiments where flow perturbations are introduced by periodically shutting a valve the forcing is rich in harmonics and the shear layer response is due to multi-harmonic excitation.

This is of course the view taken in the oscillator model with uniform coupling. Thirdly, what is referred to as self-sustained flow oscillations in the impinging shear layer and locking on in the forced shear layer, has its analogy in self- and forced synchronisation of the oscillator population. Finally, the generation of subharmonics in the free shear layer has its counterpart in the subharmonic coupling mechanism of the extended oscillator model.

The major limitation of our phenomenological model is readily highlighted by comparison to nonlinear mode competition between instability waves. Based on temporal records of point velocity measurements, the oscillator model provides an Eulerian description of temporally evolving flow instabilities. In contrast, instability waves in the free shear layer are usually considered to be spatially developing. In this respect it should be recalled that, whatever spatial distribution is assigned to an oscillator population such as this model, the phase difference, conveying information on spatial organisation, will always be a contingent quantity. Thus, shear layer aspects relating to the spatial growth of instability waves or the transfer of energy between waves are unaccounted for. For instance, it is commonly accepted that there is a subharmonic feedback in a free jet (Laufer 1981). However, this does not explain how a subharmonic wave is amplified and how it extracts energy from a fundamental wave.

Returning to the significance of the phase difference in coupled oscillator systems, it is expected that an assembly of identical oscillators is more relevant to spatially developing waves. This naturally takes us to the Ginzburg-Landau equation which constitutes the simplest field of nonlinear oscillators. This equation is analysed in the following chapter in respect to its possible relevance to the free shear layer.

[7] Too strong an emphasis must not be placed on the difference between linear and nonlinear interaction. The two approaches are conceptually different and therefore comparable on a phenomenological level only. What is described as nonlinear interaction between waves is integral part of oscillator dynamics by definition.

Literature Cited

Acton E (1980). A modelling of large eddies in an axisymmetric jet. *J Fluid Mech* 98 pp 1.

Aref H (1983). Integrable, chaotic, and turbulent vortex motion in two-dimensional flows. *Ann Rev Fluid Mech* 15 pp 345.

Chomaz J M, Huerre P and Redekopp L G (1988). Bifurcations to local and global modes in spatially developing flows. *Phys Rev Let* 60 pp 25.

Crighton D G (1981). Acoustics as a branch of fluid mechanics. *J Fluid Mech* 106 pp 261.

Crow S C and Champagne F H (1971). Orderly structure in jet turbulence. *J Fluid Mech* 48 pp 547.

Daido H (1986). Discrete-time population dynamics of interacting self-oscillators. *Progr Theor Phys* 75 pp 1460.

Daido H (1987). Population dynamics of randomly interacting self-oscillators. *Progr Theor Phys* 77 pp 622.

Dimotakis P E and Brown G L (1976). The mixing layer at high Reynolds numbers: large scale structure dynamics and entrainment. *J Fluid Mech* 78 pp 535.

Ho C-M (1982). Local and global dynamics of free shear layers. *in*: *Numerical and Physical Aspects of Aerodynamic Flows.* ed. T Cebeci. Springer-Verlag: New York.

Ho C-M and Huang L-S (1982). Subharmonics and vortex merging in mixing layers. *J Fluid Mech* 119 pp 443.

Ho C-M and Huerre P (1984). Perturbed free shear layers. *Ann Rev Fluid Mech* 16 pp 365.

Ho C-M and Nosseir N S (1981). Dynamics of an impinging jet. Part 1. The feedback phenomenon. *J Fluid Mech* 105 pp 119.

Huerre P and Monkewitz P A (1985). Absolute and convective instabilities in free shear layers. *J Fluid Mech* 159 pp 151.

Kaneko (1986). *Collapse of Tori and Genesis of Chaos in Dissipative Systems* (Singapore: World Scientific).

Kelly R E (1967). On the stability of an inviscid shear layer which is periodic in space and time. *J Fluid Mech* 27 pp 657.

Kibens V (1980). Discrete noise spectrum generated by an acoustically excited jet. *AIAA J* 18 pp 434.

Kuramoto Y (1984). *Chemical Oscillations, Waves, and Turbulence* (Berlin: Springer Verlag).

Laufer J (1981). Instability and turbulence in jets. *in: Transition and Turbulence.* ed. R E Meyer Academic Press: New York.

Laufer J and Monkewitz P A (1980). On turbulent jet flow in a new perspective. *AIAA Paper No* 80–0962.

Linkens D A and Kitney R I (1983). Integer-ratio entrainment of mutually-coupled nonlinear oscillators. *J Theor Biol* 100 pp .

Miksad R E (1971). Experiments on the nonlinear stages of free shear layer transition. *J Fluid Mech* 56 pp 695.

Ohsuga M, Yamaguchi Y and Shimizu H (1985). Entrainment of two coupled van der Pol oscillators by an external oscillation. *Biol Cybern* 51 pp 325.

Oster D and Wygnanski I (1982). The forced mixing layer between parallel streams. *J Fluid Mech* 123 pp 91.

Provansal M, Mathis C and Boyer L (1987). Bénard-von Karmán instability: transient and forced regimes. *J Fluid Mech* 182 pp 1.

Rockwell D and Naudascher E (1979). Self-sustained oscillations of impinging free shear layers. *Ann Rev Fluid Mech* 11 pp 67.

Sakaguchi H (1988). Cooperative phenomena in coupled oscillator systems under external fields. *Progr Theor Phys* 79 pp 39.

Sakaguchi H and Kuramoto Y (1986). A soluble active rotor model showing phase transitions *via* mutual entrainment. *Progr Theor Phys* 76 pp 576.

Staubli T (1985). Entrainment of self-sustained oscillations: phase locking or asynchronous quenching? *ASME 10th Biennial Conf on Mech Vibr and Noise, Fluid Struct Interaction.* Cincinnati, Ohio.

Wiener N (1958). *Nonlinear Problems in Random Theory* (New York: Wiley).

Yamaguchi Y, Kometani K and Shimizu H (1980). A theoretical study of synchronisation of two myocardial cells. *J Theor Biol* 82 pp 231.

CHAPTER VI

EVOLUTION OF SUBHARMONICS IN A MODIFIED GINZBURG–LANDAU EQUATION

Summary

The time dependent generalised Ginzburg-Landau equation with convective term describes certain open flow systems. A modified, spatially discrete form of this equation that allows for the inclusion of subharmonics of a driven fundamental wave structure is found to give rise to a subharmonic cascade, typically associated with free shear layer growth.

In § 1 and 2, the hydrodynamic context of the Ginzburg-Landau equation is established and typical open flow dynamics are discussed. The remainder of the chapter concerns the modified Ginzburg-Landau equation and its subharmonic cascade process.

1. Introduction

Debatable though the relevance of the Ginzburg-Landau equation to hydrodynamic stability may be — for instance, the cubic term $|\psi|^2\psi$ was introduced on purely heuristic grounds, to account for weak nonlinearity — this equation has received considerable attention as a model open flow system. This includes steady and transient shear flows (Deissler 1987*a*, Deissler 1987*b*, Landman 1987), such as boundary layer flows over a flat plate or plane Poiseuille flow, as well as wakes and inhomogeneous jets (Chomaz *et al* 1988). The two mechanisms that constitute the relevant open flow behaviour are absolute/convective instability and the Benjamin-Feir mechanism of side-band, or modulational, instability. For 'boundary layer' and 'Poiseuille' flow, the side-band and convective instability combine to produce a spatial transition to turbulence *via* turbulent bursts. For 'wake' flows or 'inhomogeneous' jets, the mechanism of interest is the absolute/convective instability, and the Ginzburg-Landau equation is considered linearly stable with respect to modulational disturbances. By introducing spatially varying system parameters, regions of absolute and convective instability are generated. Near the wake flow origin, the system behaves locally absolutely unstable and is thus relatively insensitive to disturbances. Further downstream, the character of the instability changes from locally absolute to locally convective instability.

In this chapter, with regard to separated shear flows, global convective instability will be assumed and, as for the wake or hot jet, stability to modulational disturbances. In addition, a form of subharmonic resonance will have to be incorporated to account for the wave pairing. This forms the theme of the present chapter. Below, the Ginzburg-Landau equation in the

context of open flow systems is reviewed briefly.

2. The Ginzburg-Landau Equation as a Model Open Flow System

Let us recall that in hydrodynamic stability the generalised Ginzburg-Landau equation

$$\psi_t = a\,\psi + b\,\psi_{xx} - c\,|\psi|^2\psi - v_G\psi_x \tag{6.1}$$

is a generic amplitude equation for fluid problems where a continuum of wavenumbers becomes unstable as the control parameter is increased above a finite threshold. The control parameter may be, for example, the Reynolds number, the Taylor number or the Rayleigh number. For plane Poiseuille flow the control parameter is related to parameter a by

$$a_r \propto \quad Re - Re_c\,. \tag{6.2}$$

More specifically, the Ginzburg-Landau equation describes the development of weakly nonlinear flow disturbances in space as well as time near a Hopf bifurcation. Bifurcations are supercritical if $c_r > 0$, and subcritical if $c_r < 0$.

The first-order spatial-derivative term ψ_x in equation (6.1) is readily seen to be related to the type of reference frame in which the spatio-temporal evolution of ψ is observed. If equation (6.1) is transformed to a reference frame moving at speed v_G this term vanishes and is thus identifed as a 'mean flow' generating convective term[1].

Fluid systems that have been reduced to a simplified form of equation (6.1) without convective term include the Rayleigh-Bénard convection (Segel 1969, Newell and Whitehead 1969), Taylor-Couette flow (Kogelman and Di Prima 1970), plane Poiseuille flow (Stewartson and Stuart 1971) and wind-induced water waves (Blennerhassett 1980). Numerical studies of the simplified G-L equation have shown that it gives rise to instability, bifurcation, motion on low-dimensional tori and chaos (Stuart and Di Prima 1978, Moon, Huerre and Redekopp 1983, Nozaki and Bekki 1983, Bretherton and Spiegel 1983, Keefe 1985).

2.1 Convective Instability

Additional phenomena that are otherwise lost as mere transients can be observed in a stationary frame of reference and have been studied under conditions when equation (6.1) is

[1]Obviously, the convective term cannot be removed by a Galilean transformation when boundary conditions at fixed spatial positions are imposed.

convectively unstable (Deissler 1985, Deissler 1987*a*). Given an initial perturbation $\psi(x,t_0)$, convective instability in the Ginzburg-Landau equation is defined by

$$\lim_{t\to\infty} |\psi(x,t)| \to 0 \quad \text{and} \quad \lim_{t\to\infty} |\psi(x+v_G t,t)| \to \infty \tag{6.3}$$

That is, in a stationary frame of reference perturbations will decay whereas in a co-moving frame they will grow. Following Deissler (1985), convective instability in a system (with nonperiodic boundary conditions) is ascertained by first calculating the eigenvalues of the system with the given set of boundary conditions and by then calculating the system eigenvalues with periodic boundaries imposed instead. If the latter system is unstable and the original system is stable then the system under study is convectively unstable. The Ginzburg-Landau equation is convectively unstable if the following conditions are met :

$$a_r > 0 \quad \text{and} \quad a_r - \frac{{v_G}^2 b_r}{4\,|b|^2} < 0 \tag{6.4}$$

which simply says that perturbations must be convected downstream faster than they would spread in the co-moving frame due to the absolute instability condition $a_r > 0$ and the diffusion effects.

Under conditions of convective instability the G-L equation models an open flow system with distinct spatial regions. Low-level external noise, applied at the upstream boundary, results in spatially growing waves that are subject to a selective amplification mechanism — a scenario similar to what is observed in the early stages of boundary layer and free shear layer instability. Beyond the linear region the exponential growth of waves decreases as nonlinear effects come into play. Wave structures may break up in the transition region due to modulational instability, causing intermittent high frequency fluctuations to occur and eventually the nonlinear dynamics dominate the flow in the fully developed region.

Analytical and qualitative results for both the linear and nonlinear region of the convectively unstable Ginzburg-Landau equation are summarised below.

2.2 Spatial Amplification of Boundary Noise

By definition, perturbations play an important part in the dynamics of the convectively unstable Ginzburg-Landau equation. A single local perturbations produces a temporary structure whereas continuous perturbations will result in a permanent structure referred to as *noise sustained structure* (Deissler 1985).

As outlined above, the Ginzburg-Landau equation acts as an amplifier for the upstream boundary condition $\psi(x_0,t)$ in the linear region where nonlinear effects are negligible. Analytical results for this noise amplification region are obtained by considering

$$\psi_t = a\,\psi + b\,\psi_{xx} - v_G\,\psi_x \tag{6.5}$$

A solution of this equation is

$$\psi(x,t) = \sum_{k=-\infty}^{\infty} A_k\, e^{\beta_k x}\, e^{-j\omega_k t} \tag{6.6}$$

where $-j\omega_k = a - \beta_k v_G + \beta_k{}^2 b$. Solving for β_k gives

$$\beta_k = \frac{1}{2b}\left[\, v_G - \sqrt{v_G{}^2 - 4b(a+j\omega_k)}\,\right], \tag{6.7}$$

from which the growth factor $\beta_r(\omega) = \mathrm{Re}\{\beta_k\}$, the wave number $\beta_i(\omega) = \mathrm{Im}\{\beta_k\}$ and the phase speed $c_r(\omega) = \frac{\omega}{\beta_i(\omega)}$ of the spatially growing waves are calculated (*figure* 6.1). Referring to the figure, the spatial waves are seen to be amplified selectively. Waves of frequency ω_k are amplified if $\beta_r(\omega_k) > 0$ and attenuated if $\beta_r(\omega_k) < 0$. Maximum amplification occurs for the frequency

$$\omega_{k,m} = -a_i + \beta_{i,m} v_G - (\beta_{r,m}{}^2 - \beta_{i,m}{}^2)\, b_i - 2\,\beta_{r,m}\beta_{i,m} b_r \tag{6.8}$$

where

$$\beta_{r,m} = \frac{b_r}{2|b|^2}\left(v_G - \sqrt{v_G - 4a_r\frac{|b|^2}{b_r}}\right)$$

$$\beta_{i,m} = -\frac{b_i}{2|b|^2}\left(v_G - \sqrt{v_G{}^2 - 4a_r\frac{|b|^2}{b_r}}\right)$$

Furthermore, apart from a discontinuity at $\beta_i = 0$, the wave speed c_r is approximately constant above $\omega_{k,m}$ *i.e.* spatially growing waves are dispersive below the most amplified frequency and non-dispersive above.

The selective amplification of spatially growing waves in the linear region is further quantified by considering upstream boundary white noise. An estimate for the spatially evolving power spectrum is (Deissler 1987*a*),

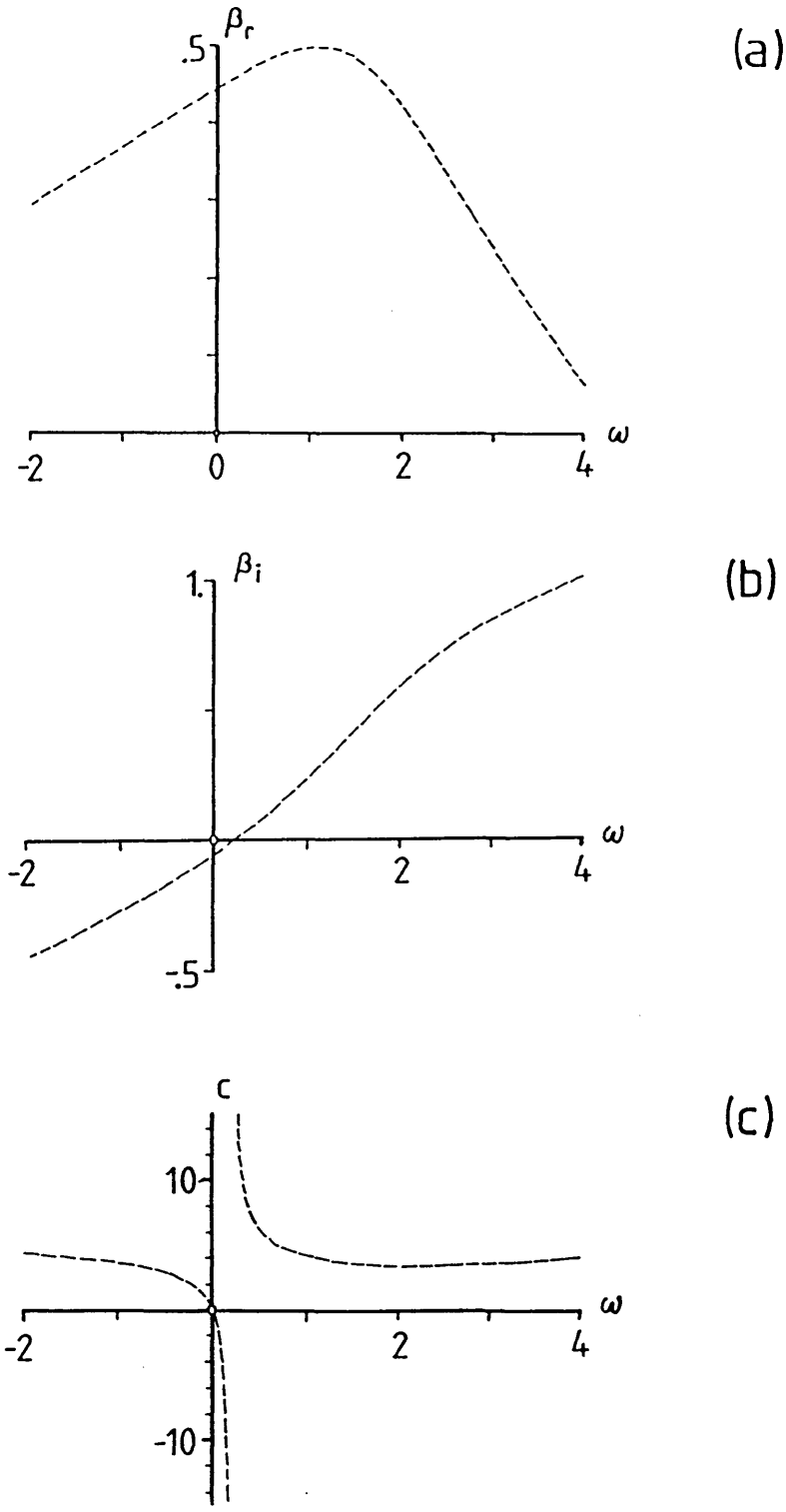

Figure 6.1 Wave solution of the convectively unstable Ginzburg-Landau equation in the linear region (a=(2,0), b=(2,0), c=(0.5,0.1) and v_G=5.0). (a) Spatial growth factor. (b) Wave number. (c) Phase speed.

$$S(\omega,x) = S_0\,\sigma^2\,\mathrm{e}^{2\beta_r(\omega)x} \tag{6.9}$$

where σ^2 is the variance of the upstream boundary noise. Expression (6.9) shows that the linear region may be regarded as the continuum limit of a cascade of narrowband amplifiers with gain characteristic $\beta_r(\omega)$. Interestingly, the cascade analogy also serves to describe – at least qualitatively – phenomena observed in the nonlinear region of a modified Ginzburg-Landau equation (*cf.* § 3.3).

2.3 Intermittency and Convective Chaos

Beyond the linear region the exponential growth of waves decreases as nonlinear effects come into play. The full nonlinear equation (6.1) admits an exact solution – the Stokes solution – of the form

$$\psi(x,t) = A\,\mathrm{e}^{j(kx-\omega t)} \tag{6.10}$$

where k and ω are real and are related by $\omega = ja+kv_G-jk^2b-jc|A|^2$. Solving for k and $|A|$ gives

$$k = \frac{v_G \pm [v_G{}^2-4(b_rc_i/c_r-b_i)(a_i-c_ia_r/c_r+\omega)]^{1/2}}{2(b_rc_i/c_r-b_i)} \tag{6.11}$$

and

$$|A| = \sqrt{\frac{a_r-k^2b_r}{c_r}}\ . \tag{6.12}$$

Again, the wavenumber is a function of frequency. As to the sign in equation (6.11) that gives the correct solution, Deissler (1987*a*) noted that there is no conclusive answer to this ambiguity except that what is observed in numerical simulations is the wave with smaller k. This observation is consistent with stability investigations for waves in the Ginzburg-Landau equation (Ch IV § 3.2.2). Modulational stability analysis showed that small wavenumber solutions are the ones destabilised last.

Note that in general the transition from linear to nonlinear region is characterised by a change in wavenumber, as the values obtained from equations (6.7) and (6.11) are usually different and can even have different signs. This has the rather curious effect that waves are travelling in opposite directions in the linear and nonlinear region, a peculiarity that imposes

restrictions on physically meaningful system parameters, but finds no mention in (Deissler 1985, Deissler 1987*a*).

Returning to the stability of wave solutions in the nonlinear region, the stability investigation of equation (6.1) is equivalent to the corresponding problem for equation (6.1) without convective term and periodic boundary conditions. Waves of any wavenumber are unstable if (*cf.* Ch IV § 3.2.3)

$$1 + \frac{b_i\, c_i}{b_r\, c_r} < 0 \,. \tag{6.13}$$

Consider now the generalised Ginzburg-Lanau equation with low-level noise applied at the upstream boundary, under conditions of convective instability and modulational instability. The noise will be amplified spatially and become increasingly narrowband with downstream distance. As the nonlinear dynamics become significant these spatially growing waves will saturate and break up. Importantly, if the Ginzburg-Landau equation is driven by a single frequency the evolving waves will not break up as there are no sideband perturbations to initiate the instability[2]. The break up is characterised by intermittent high frequency fluctuations generated by the nonlinear term $|\psi|^2\psi$. These high frequency bursts occur randomly in space and time and are correlated with the fluctuations of the wave structure in the linear region.

Beyond the transition region, the nonlinear dynamics dominate and no correlation exists between the dynamics of the fully developed region and the linear region. The irregular behaviour observed in the fully developed region of the convectively unstable Ginzburg-Landau equation suggests the possibility of chaos (not associated with a strange attractor!). However, the application of Lyapunov exponents as a measure of chaos (*cf.* Ch IV § 2.1.3) will lead to problems in convectively unstable systems such as the Ginzburg-Landau equation. Two nearby trajectories may exponentially converge on the average in a stationary frame of reference, but they may diverge on the average in some moving reference frame. Deissler and Kaneko (1987) have developed formalisms to decide whether chaos exists in some co-moving reference frame. This form of chaos is called *convective chaos* and has been found to be observed in the Ginzburg-Landau equation. Chaos is ascertained in direct analogy to the determination of the convective instability property of a (linearised) system. If the largest Lyapunov exponent is

[2]As Deissler (1987*a*) pointed out this characteristic is of little consequence as the addition of another small nonlinear term to equation (6.1) will immediately cause the regular structure to break up. In fact, the Ginzburg-Landau equation with added quintic term $|\psi|^4\psi$ has been studied in a more recent paper (Deissler 1987*b*).

negative for the given (fully nonlinear) system, but is positive for periodic boundary conditions imposed instead, then the fully developed region of the flow is convectively chaotic.

2.4 Open Flow Systems

Having outlined the properties of the convectively unstable Ginzburg-Landau equation, it is appropriate to inquire into the similarities with open flow systems such as boundary layer flow over a flat plate or free shear layer flow — as opposed to closed flow systems *e.g.* Rayleigh-Bénard convection or Taylor-Couette flow.

The behaviour seen in the linear region of the Ginzburg-Landau equation is qualitatively similar to what is observed in both boundary layers and free shear layers. In the former flow, as predicted by the Orr-Sommerfeld equation, Tollmien-Schlichting waves form as a result of a spatial and selective amplification of random background fluctuations. Similarly, preferred modes emerge in the free shear layer although waves are not selectively attenuated there[3]. Furthermore, in the free shear layer waves are dispersive below the most amplified frequency and non-dispersive above (Ho and Huerre 1984).

Secondary flow instabilities, however, are fundamentally different for boundary layers and free shear layers, and this is where the similarities between what is observed in the transition region of the Ginzburg-Landau equation and the free shear layer end. Intermittent turbulent bursts are characteristic of the final stage of breakdown into turbulence in boundary layers but have not yet been observed in free shear layers. Instead, a subharmonic at half the frequency of the linearly most unstable wave makes its appearance. This secondary flow instability initiates the streamwise growth of the free shear layer thickness and has been attributed to the parametric resonance mechanism of a basic periodic flow (Kelly 1967). Ultimately, three-dimensional flow instabilities develop in both shear flows, a scenario the Ginzburg-Landau equation clearly is not capable of modelling.

2.5. Transition from Laminar to Periodic Flow

The discussion so far has been about the dynamics of the Ginzburg-Landau equation in a stationary frame of reference because of the interest in phenomena that are transients in a co-moving frame. By analogy, transients in a stationary reference frame become steady states in the co-moving frame and can have similar physical significance. Consider, for example, front-like solutions (*figure* 6.2*a*) to the Ginzburg-Landau equation without convective term, that

[3]The difference is that spatial attenuation results in better suppression of broadband levels *i.e.* more regular wave structures.

connect the zero-amplitude and the constant amplitude plane wave states, or hole-like solutions (*figure* 6.2*b*) that connect two different plane wave states. These solutions are hypothesised to have relevance to describing shear flow transition from laminar to bifurcated periodic flow (Landman 1987).

The front-like solutions are of particular interest here because they bear a certain similarity to what is observed in separated flows started from rest. Below some of the results of Landman's investigation of solutions of the Ginzburg-Landau equation of interest in shear flow transition are discussed briefly.

2.5.1 Front-Like Solutions

Landman (*ibid*) considered the Ginzburg-Landau equation without convective term as a description of plane Poiseuille flow near criticality *i.e.* near a subcritical bifurcation. Quasisteady solutions were assumed to have the simple time dependence

$$\psi(x,t) = e^{-j\Omega t}\,\phi(x-ct) \tag{6.14}$$

Inserting equation (6.14) into equation (6.1), with $v_G=0$, the function ϕ was found to satisfy a second order complex Duffing equation. Landman gave a number of analytical results for function ϕ, placing emphasis on zero-amplitude solutions for laminar flow and constant amplitude plane wave solutions for space-time periodic flow. The complex Duffing equation was then investigated numerically in order to find solitary wave solutions that connect the laminar and plane wave states. Front-like solutions were shown to be structurally stable in that they are persistent under perturbations in both Ω and c. Furthermore, these solutions exist for nonzero c implying that fronts will travel faster or slower than waves at the group velocity v_G.

An example of a front solution is shown in *figure* 6.3. This solution connects the steady laminar state at the left boundary to the finite amplitude plane wave state at the right boundary. Importantly, the transition between the two regimes need not be monotonic but can exhibit peaking, as sketched in *figure* 6.2*a*. In Landman's study peaking was observed for subcritical Reynolds numbers, $a_r < 0$, and smooth transitions for supercritical Reynolds numbers, $a_r > 0$.

2.6 Concluding Remarks

The Ginzburg-Landau equation describes general systems of partial differential equations near a Hopf bifurcation and has consequently found application in a large variety of

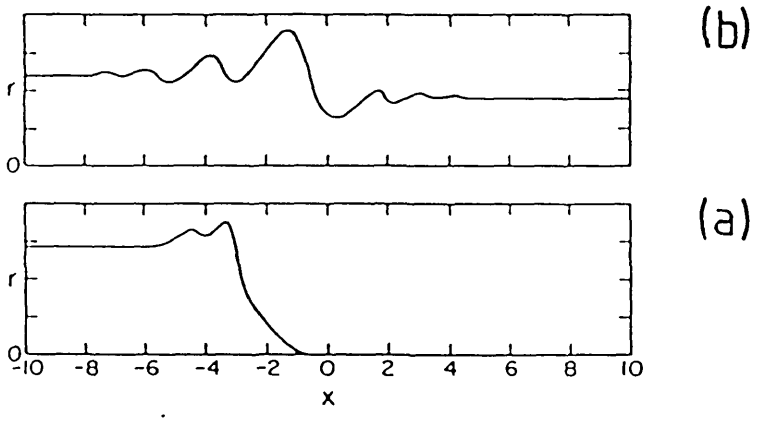

Figure 6.2 Solitary-wave type solutions of the Ginzburg-Landau equation (after Landman 1987). The modulus $r=|\psi|$ is given. (*a*) Front solution. (*b*) Hole solution.

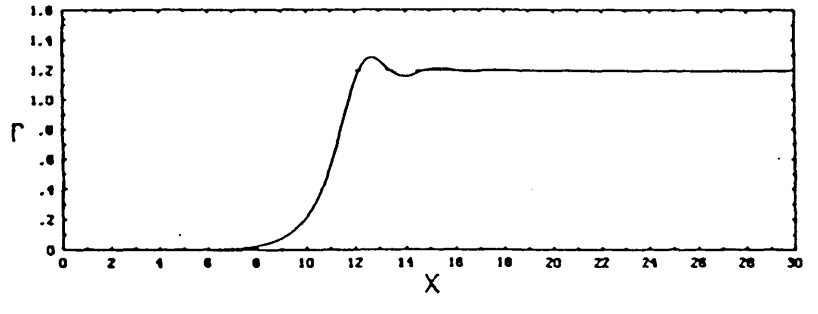

Figure 6.3 Structurally stable front solution to the Ginzburg-Landau equation for subcritical Reynolds number, $a_r < 0$, and subcritical bifurcation $c_r < 0$ (after Landman 1987). The modulus $r=|\psi|$ is given.

contexts ranging from hydrodynamics to population biology and neural networks. Despite its simple structure the Ginzburg-Landau equation is exceedingly rich in dynamic behaviour, and has been suggested to be of relevance to parallel shear flow instabilities and transition. It must be borne in mind, however, that in the fluid dynamic context the Ginzburg-Landau equation is a truncation of the Navier-Stokes equations. How much of the behaviour of the Ginzburg-Landau equation carries over to the full fluid dynamic problem remains to be assessed yet, and the connection is largely speculative.

But there are other viewpoints to this question. A chapter in Drazin and Reid's (1981) monograph on hydrodynamic stability is headed by the following epigram : "*It is in the nature of Applied Mathematics that one should be concerned not only with the application of existing mathematical theories and methods, but also with the stimulation of new mathematical problems, through the study of interesting problems in science, and the attempts to solve these problems*" (C C Lin 1964). It is largely in this context that the study of the Ginzburg-Landau equation must be understood.

3. Subharmonic Evolution in a Modified Ginzburg-Landau Equation

In the following sections the possibility is investigated of free shear layer type secondary flow instabilities in a modified form of the convectively unstable (but modulationally stable!) Ginzburg-Landau equation. No attempts are made at implementing a parametric resonance mechanism for the generation of subharmonics. Rather, in an *ad hoc* approach to studying the spatial evolution of successive subharmonic waves, subharmonics of a driven fundamental wave structure are generated locally. The spatial evolution of subharmonic waves is studied numerically and a possible mechanism for the subharmonic cascade in the modified Ginzburg-Landau equation is suggested. Finally, the results are compared to the behaviour seen in the vortex pairing region of the free shear layer.

3.1 Subharmonic Generation and Discrete Space

In its simplest formulation, the emergence of subharmonics of a fundamental mode in the free shear layer is explained by appealing to the instability of an array of point vortices (Lamb 1932). More realistic approaches consider the stability of a bifurcated space-time periodic shear flow (Kelly 1967).

Here, a *post facto* approach is taken that circumvents the subharmonic resonance problem. Subharmonics of a given fundamental wavefrom are generally synthesised by nonlinear resonance in sub- or supercritical nonlinear oscillators or, if specified combinations of

super-/sub-harmonics of the fundamental are required, by nonlinear synthesis systems of minimum order three (Chua and Green 1974). In this study a simple phase scaling method has proved expedient instead. Subharmonics at half the frequency of a driven fundamental wave structure in the Ginzburg-Landau equation are synthesised locally by rescaling the phase of $\psi = r\, e^{j\theta}$:

$$\psi_{1/2} = \epsilon\, r\, e^{j[\frac{1}{2}\theta - \theta_0]} \tag{6.15}$$

Here, the phase difference between fundamental and half-harmonic is defined by θ_0 and ϵ determines the relative magnitude of the subharmonic. Note that equation (6.15) is the direct extension to complex waveforms of the multi-frequency concept employed in chapter V.

With regard to the coupling of the half-harmonic term $\psi_{1/2}$ to a fundamental propagating wave structure in the Ginzburg-Landau equation, the use of an explicitly space-discrete formulation of equation (6.1) — as opposed to an implicitly space-discrete numerical scheme — is necessary for two reasons. Firstly, if the subharmonic is to form the fundamental itself in some downstream region the implied frequency halving discontinuity will lead to phase singularities. As pointed out in chapter IV in the context of the emergence of frequency plateaus in a field of mutually interacting $\lambda-\omega$ oscillators, the amplitude $|\psi|$ must go to zero at the plateau boundaries in order for the phase to remain continuous. Such singularity problems are avoided in discrete-space formulations. Secondly, the spatial growth of the subharmonic becomes finite only if equation (6.1) is treated as a chain of mutually coupled $\lambda-\omega$ oscillators. More specifically, consider the coupling of $\psi_{1/2}$ terms to neighbouring oscillators[4] in a spatially discrete version of equation (6.1). For that purpose, equation (6.1) is rewritten in polar coordinates,

$$\begin{aligned} r_t &= r\,\lambda(r) + b_r(r_{xx} - r\,\theta_x^2) - b_i(2\,r_x\theta_x + r\,\theta_{xx}) - v_G r_x \\ \theta_t &= \omega(r) + b_r(2\,\tfrac{r_x}{r}\theta_x + \theta_{xx}) + b_i(\tfrac{r_{xx}}{r} - \theta_x^2) - v_G\theta_x \end{aligned} \tag{6.16}$$

where $\lambda(r) = a_r - c_r r^2$ and $\omega(r) = a_i - c_i r^2$. Assuming a central difference scheme of spatial

[4] It has been suggested (referee of *Physics Letters A*) to incorporate the subharmonic term (6.15) by solving the Ginzburg-Landau equation for the modified field $\bar{\psi} = \psi + \psi_{1/2}$. The deficiency of such an approach is that the two waves are not decoupled properly. Consequently the waves will not amplify independently and no pairing is observed. However, such a decoupling is provided by the mechanism (6.17).

differentiation and adding locally synthesised subharmonic terms, equation (6.16) becomes

$$\begin{aligned}\frac{dr_k}{dt} &= r_k\,\lambda(r_k) + (\tilde{b}_r-\tfrac{1}{2}\tilde{v}_G)\,R_{C,k-1} + (\tilde{b}_r+\tfrac{1}{2}\tilde{v}_G)\,R_{C,k+1} - \\ &\qquad \tilde{b}_i(R_{S,k-1} + R_{S,k+1}) - 2\,\tilde{b}_r\,r_k \\ \frac{d\theta_k}{dt} &= \omega(r_k) + \frac{1}{r_k}\Big((\tilde{b}_r-\tfrac{1}{2}\tilde{v}_G)\,R_{S,k-1} + (\tilde{b}_r+\tfrac{1}{2}\tilde{v}_G)\,R_{S,k+1} + \\ &\qquad \tilde{b}_i\,(R_{C,k-1} + R_{C,k+1}) - 2\,\tilde{b}_i\,r_k\Big)\end{aligned} \tag{6.17}$$

where $r_k = r(k\Delta,t)$, $\theta_k = \theta(k\Delta,t)$, $\tilde{b} = \frac{b}{\Delta^2}$, $\tilde{v}_G = \frac{v_G}{\Delta}$ and

$$\begin{aligned}R_{C,k+1} &= r_{k+1}\,[\,\cos(\theta_{k+1}-\theta_k) + \epsilon\cos(\theta_{k+1}-\tfrac{1}{2}\theta_k)\,] \\ R_{C,k-1} &= r_{k-1}\,[\,\cos(\theta_{k-1}-\theta_k) + \epsilon\cos(\tfrac{1}{2}\theta_{k-1}-\theta_k)\,] \\ R_{S,k+1} &= r_{k+1}\,[\,\sin(\theta_{k+1}-\theta_k) + \epsilon\sin(\theta_{k+1}-\tfrac{1}{2}\theta_k)\,] \\ R_{S,k-1} &= r_{k-1}\,[\,\sin(\theta_{k-1}-\theta_k) + \epsilon\sin(\tfrac{1}{2}\theta_{k-1}-\theta_k)\,]\end{aligned}$$

Now, it will be recalled that convective instability in the Ginzburg-Landau equation is the result of the competing influences of convection and diffusion. It is readily appreciated that no such mechanism is operative in the case of the subharmonic. Its spatial growth rate is governed by an effective gain between neighbouring oscillators and becomes infinite in the continuum limit $\Delta \to 0$ of equation (6.17).

3.2 Numerical Study

This section summarises the results of a numerical investigation of subharmonic evolution in the convectively unstable Ginzburg-Landau equation.

3.2.1 Parameters and Numerical Scheme

The starting point for the numerical analysis is the Ginzburg-Landau equation as a nonlinear amplifier of upstream boundary perturbations and as a nonlinear wave guide *i.e.* in convectively unstable form. Furthermore, stability to modulational perturbations is stipulated in order to avoid boundary layer type secondary instabilities. System parameters that guarantee these conditions are $a=(2,0)$, $b=(2,0)$, $c=(0.5,0.1)$ and $v_G=5.0$. Modulational stability is readily seen to result from letting $\mathrm{Im}\{b\}=0$ (equation 6.13). The system size is $L=200$ and the Ginzburg-Landau equation is driven by a single frequency input at the upstream boundary, $\psi(0,t)=A_0\exp(-j\omega_0 t)$ with frequency $\omega_0=1.0$ and amplitude $A_0=0.1$.

This rather high amplitude level ensures a short linear region, and the system is dominated by nonlinear effects. The downstream boundary condition is $\psi(L,t)=0$ and has little effect on the evolving wave structure. The spatial discretisation parameter $\Delta=1.0$ is determined from comparison of numerical and analytically predicted results for the nonlinear region and, to lower accuracy, for the linear region. This is a compromise between keeping the number of spatial points in the spatially discretised formulation (6.17) reasonably small and a linear region short compared to the system size.

The numerical scheme itself is a fourth-order Runge-Kutta method (Hall and Watt 1976) with fixed step size to allow for easy calculation of power spectrum estimates. Initial experimentation with various integration schemes had shown that for oscillator-field problems in polar coordinate formulation a Gear's method with variable step size and interpolated output readings is generally preferrable in terms of computational speed to a Runge-Kutta scheme. However, the working space required for Gear's method is considerably larger than for Runge-Kutta methods[5].

3.2.2 Results

Results are presented in *figures* 6.4 and 6.5. Note that the system size extends beyond the displayed region. Hence downstream boundary effects are not visible. Referring to *figure* 6.4, in the absence of locally synthesised subharmonics an exponentially growing wave structure is observed in the linear region $x<12$. This structure saturates further downstream at an amplitude level $|\psi|=1.92$, and propagates at constant speed $k=-0.274$ after a small change in wavenumber.

In contrast, if a half-harmonic is generated locally ($\epsilon=0.1$, $\theta_0=0$) this picture changes dramatically. The effect is best illustrated in *figure* 6.5. Here the spatio-temporal wave dynamics are visualised by plotting traces of $\mathrm{Re}\{\psi(x,t)\}$ at consecutive times. The driven wave structure is seen to undergo a series of very regular pairings whereby a leading wave crest is systematically retarded near the point of coalescence. Further details of the wave pairing and spectral evolution process are given in *figure* 6.4. Near the upstream boundary the wave structure evolves as for $\epsilon=0$. However, the energy of the fundamental mode very soon saturates at a low level and decays at the expense of its rapidly growing half-harmonic which, upon saturation, becomes itself the fundamental. The change from harmonic to subharmonic

[5] To give an idea of the computational load involved in solving equation (6.17), a run for a single set of parameters can take up to one hour of CPU time on a CDC Cyber mainframe. Convert this to actual processing time and typical times will be up to ten hours — the charges for such a job are around £ 100.

mode is accompanied by the evolution of a second subharmonic mode and the exchange of energy between modes is repeated further downstream. What is observed therefore is a cascade of frequency halving steps with the discontinuities occurring in the saturation region of the respective half-harmonic mode. With increasing distance from the upstream boundary this scenario becomes less well defined. Fundamental modes tend to amplify again irregularly in the region downstream of the coalescence point and spurious subharmonics (not displayed) and a zero frequency component emerge. Consequently the frequency halving locations no longer coincide with the subharmonic saturation point and the distance between successive coalescence points shows some variability.

The wave merging process shows a certain, although not consistent, dependence on the phase difference θ_0. For the present parameters the results are identical for $\theta_0=0$ and $\theta_0=\pi/2$, but for $\theta_0=\pi$ the first pairing occurs further downstream with wavenumber and amplitude left unchanged, relative to the merging positions. For other parameters the dependence on θ_0 is more pronounced and in some cases an overall decrease in amplitude and spectral level is observed for nonzero θ_0.

3.2.3 Comparison with Analytical Results

Both the wavenumber and the amplitude change with downstream distance, but are not directly related to individual mode evolution because they represent the mode averaged behaviour. However, the changes in wavenumber agree qualitatively with what is predicted by the Stokes solution for a single frequency wave of the respective frequency plateau frequency (*figure* 6.4*c*). This suggests that in each frequency plateau region the mode of the respective frequency is dominant.

The evolution of the amplitude is not as easily explained. The depressions around merging locations are most probably related to large phase variations near frequency discontinuities. Indeed, these amplitude depressions become more pronounced for greater spatial resolution as expected from the discussion of § 3.1. The single frequency wave solution for our particular parameter set and a four octave change in frequency predicts a corresponding increase in amplitude by 3.6%. An increase in amplitude is certainly observed in the numerical findings, however, the overall changes are much greater indicating that spectral components other than the fundamental contribute to the overall wave.

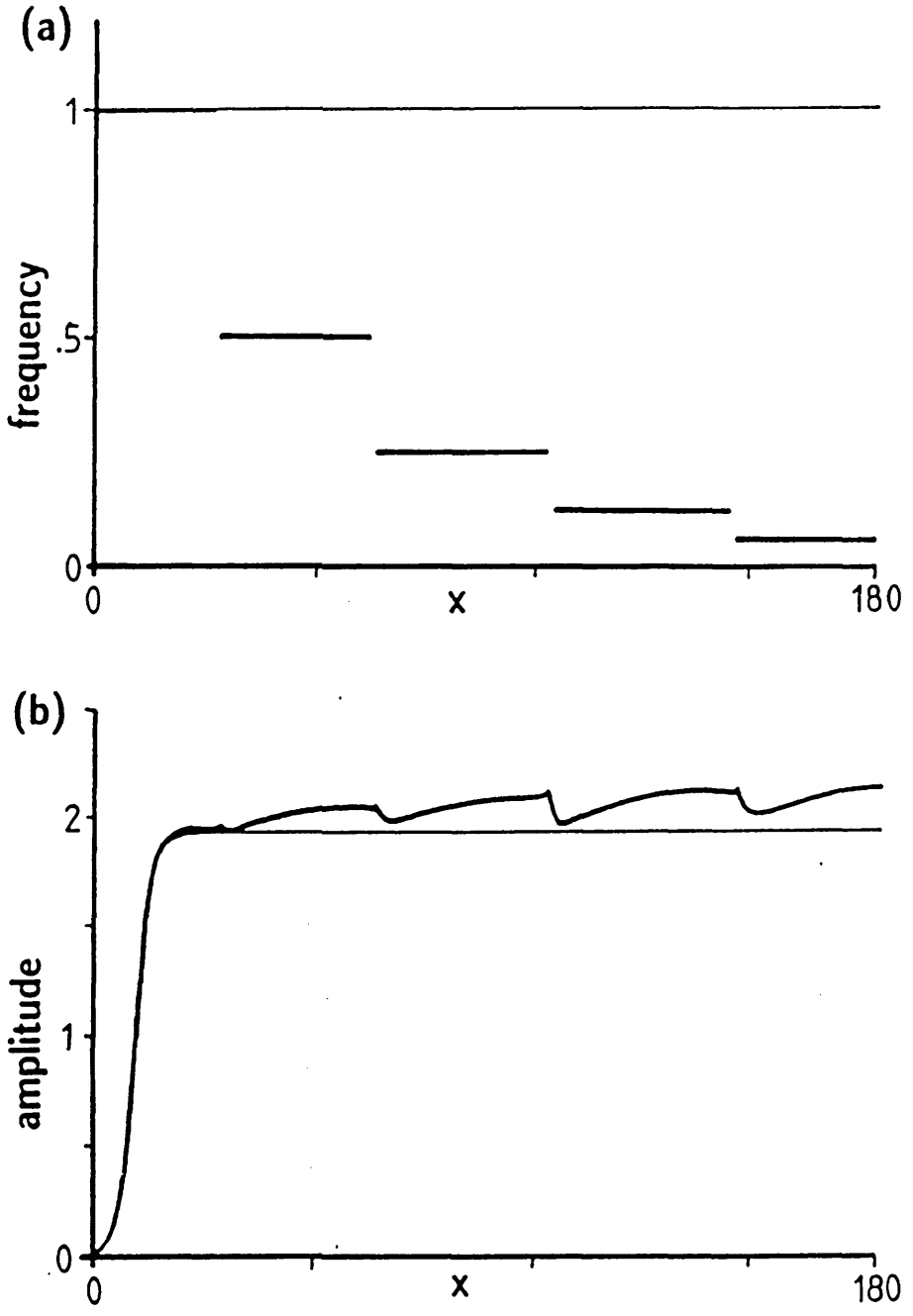

Figure 6.4 Evolution of subharmonics in the modified Ginzburg-Landau equation for $\theta_0=0$, and $\epsilon=0$ (—), $\epsilon=0.1$ (▬). (a=(2,0), b=(2,0), c=(0.5,0.1) and $v_G=5.0$). (a) Average local frequency $\overline{\theta_t(x,t)}$. (b) Corresponding average amplitude $\overline{r(x,t)}$. (c) Local wave number. (d). Spectral evolution of the wave structure in space. The dotted line shows the evolution of the dc-component.

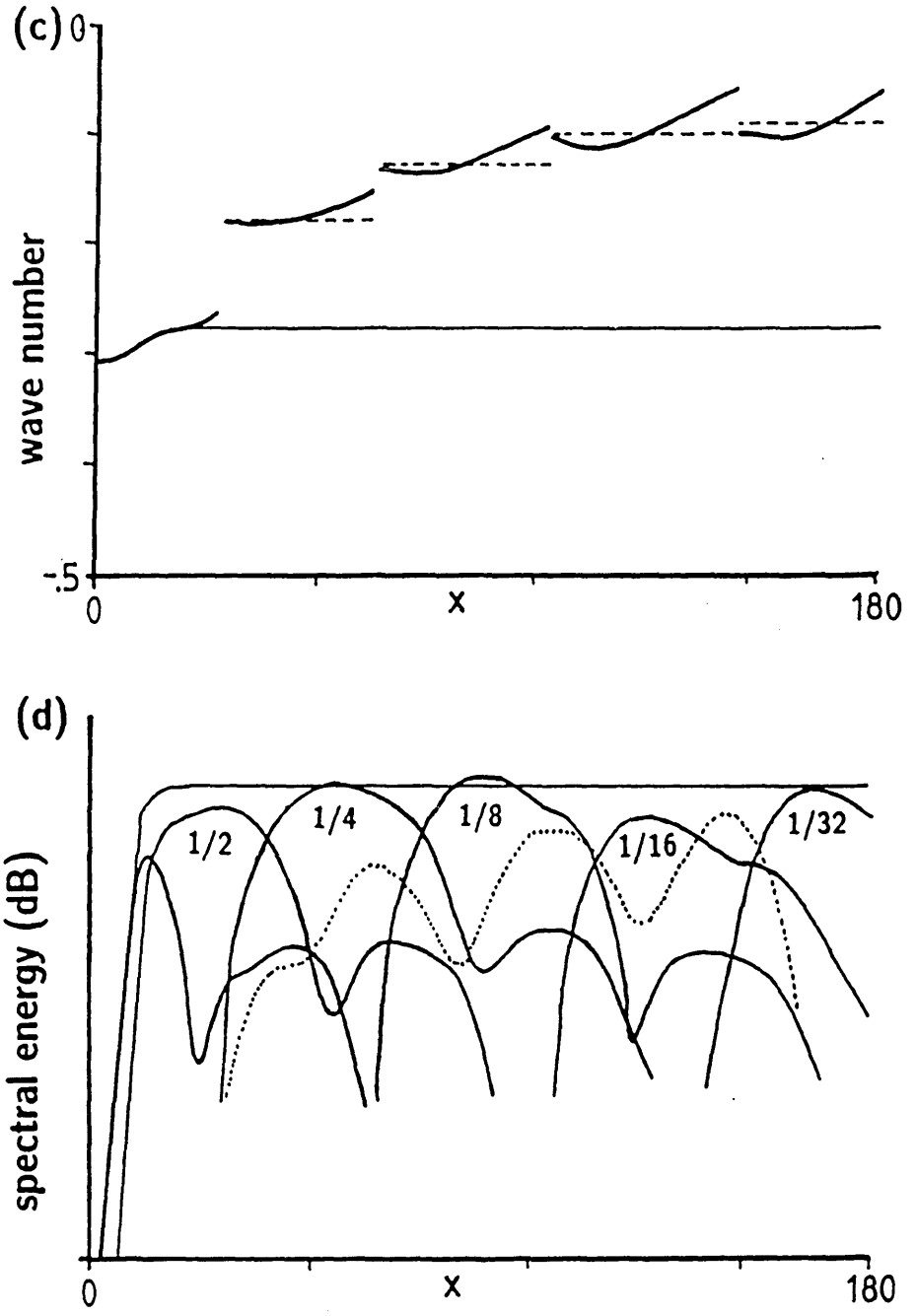
(c)
0
wave number
-.5
0
x
180
(d)
spectral energy (dB)
1/2
1/4
1/8
1/16
1/32
0
x
180

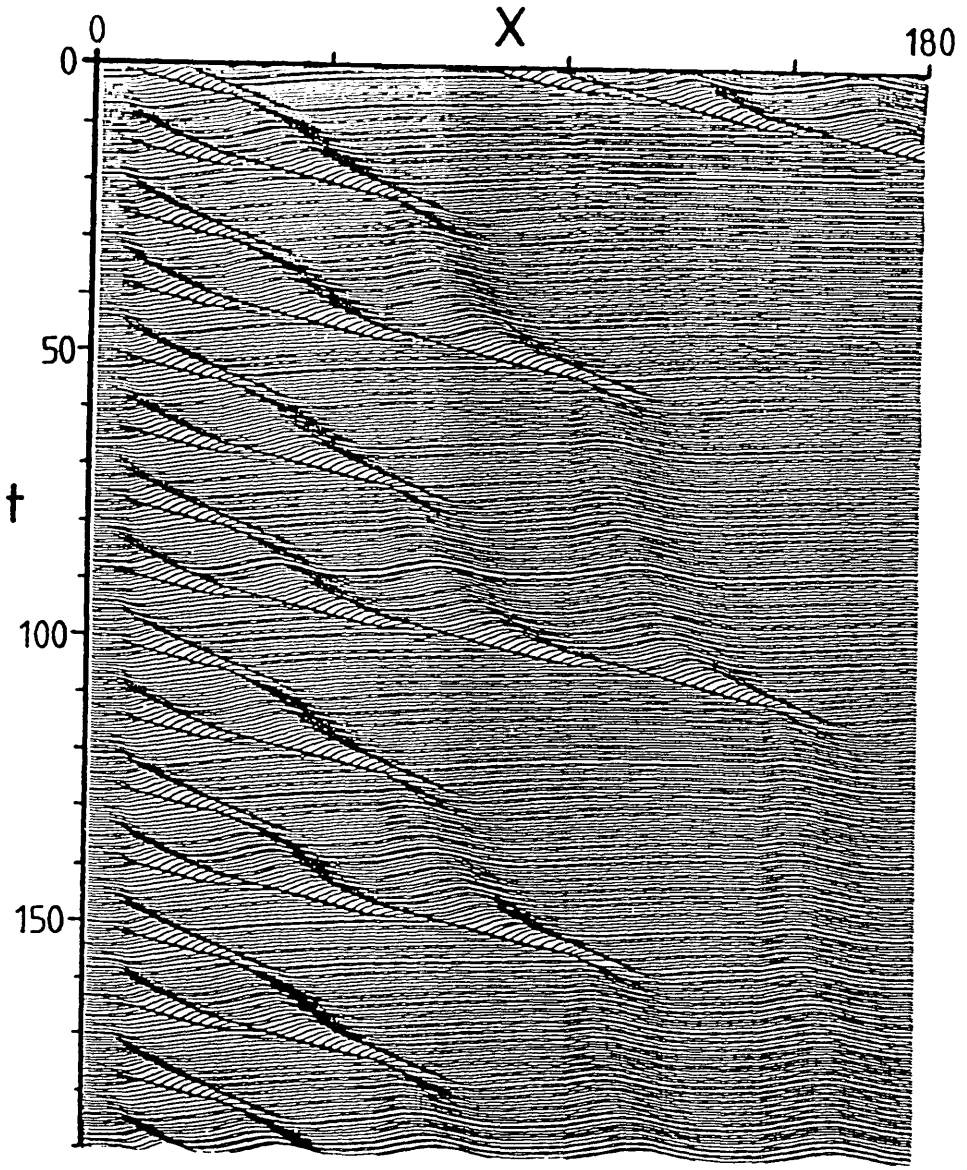

Figure 6.5 Visualisation of the spatio-temporal dynamics of the subharmonic evolution process. The profile $\mathrm{Re}\{\psi(x,t_i)\}$ is plotted at consecutive times $t_i=iT$, $T=0.5$.

3.3 Mode Energy Transfer — A Possible Mechanism

The central behaviour of the modified Ginzburg-Landau equation under single-frequency excitation is summarised in the spectral evolution diagram (*figure* 6.4*d*), and all other quantities such as the average wave frequency may be deduced qualitatively from that behaviour.

The transfer of energy from a fundamental to successive subharmonic modes is not immediately apparent, let alone fully understood. Certainly, considering a single frequency wave structure ($\epsilon=0$), the effect of small nonzero ϵ will be one of spatial amplification of a co-travelling structure at half the fundamental frequency. Due to the convective term the coupling is mostly forward (equation 6.17), and the coupling strength ϵ determines the spatial growth rate of the half-harmonic which, incidentally, can be much greater than that of the original single frequency wave structure. These differences are noticeable in *figure* 6.4*d* from the different gradients in the linear region.

As for the intermittent high frequency bursts, the nonlinear term $|\psi|^2\psi$ is central to the instability mechanism and determines the extraction of energy from the fundamental.

3.3.1 Two-Frequency Excitation of a Subcritical Oscillator

It will be recalled that in the linear region the convectively unstable Ginzburg-Landau equation behaves like a cascade of narrowband amplifiers *i.e.* a chain of forward coupled subcritical nonlinear oscillators with positive gain. The convective instability mechanism suggests that — qualitatively — the same analogy may apply to the nonlinear region. Given a finite-time perturbation at the upstream boundary of equation (6.1), the response of the $\lambda-\omega$ oscillators along the space dimension will eventually return to zero again. Consequently the convective instability mechanism may be thought of as an effective load that acts on each oscillator, producing passive resonator like subcritical behaviour. As regards nonlinear effects the modified Ginzburg-Landau equation may therefore be conceptualised as a chain of unidirectionally (forward) coupled subcritical $\lambda-\omega$ oscillators. What is lost in this model is primarily the wave guide behaviour. The wave speed becomes infinite as it were.

Now, a unidirectionally coupled chain may be analysed by successively applying the output of an element of the chain to its 'downstream' neighbour. This has been done numerically for a $\lambda-\omega$ oscillator, $\lambda(r)=\mu-r^2$, $\mu < 0$, driven by a two-frequency excitation at ω_{f_2} and ω_{f_2}. The two frequencies need not be related harmonically, of course. The (complex) oscillator output is Fourier analysed to obtain estimates of the oscillator response at the respective excitation frequency. Keeping the amplitude A_1 of the 'fundamental' frequency fixed,

the 'subharmonic' amplitude A_2 is increased stepwise. The qualitative behaviour of the subcritical oscillator with subharmonic amplitude as parameter is sketched in *figure* 6.6. For low amplitude levels A_2, the energy level at ω_{f_2} is correspondingly low and, apart from low level combination frequencies, the dominant response is at the fundamental ω_{f_1}. Expectedly, increasing A_2 leads to an increase in output energy level at ω_{f_2}, but at the same time a decrease in the energy at the fundamental. At a certain forcing level A_2, the oscillator response switches discontinuously to ω_{f_2}, but the qualitative dependence of the output energy levels on parameter A_2 remains unchanged.

Although for this two-frequency excitation model the overall change in output energy level is of the order of a few decibels only, this result is important from a qualitative viewpoint. The frequency switching phenomenon itself is a subsidiary phenomenon observed also in linear systems. Importantly, however, in a linear system there is no interaction between the various spectral components of the multi-frequency excitation. For the subcritical $\lambda-\omega$ oscillator the nonlinear interaction is very pronounced.

3.3.1.1 Describing Function Analysis

Interestingly, the form of interaction in oscillators with multi-frequency excitation described above has received little attention. Most investigations centre around the problem of combination resonances (*e.g.* Nayfeh and Mook 1979).

The mode energy transfer is in fact readily explained by the describing function method (Atherton 1975). As pointed out in an earlier chapter, this method is closely related to the method of harmonic balance and produces reasonably accurate results for nonlinear systems where spurious super-/sub-harmonics are insignificant or have an appropriate phase relationship (Treiber 1985).

The observed mode competition is qualitatively similar to the quenching of self-sustained nonlinear oscillations by a large amplitude external stimulus. The describing function analysis for such a system requires the nonlinear oscillator in feedback loop formulation. Now consider a subcritical nonlinear oscillator with a dominant excitation at the fundamental frequency. In contrast to self-sustained oscillations in a supercritical oscillator, here the insufficient phase shift around the loop is compensated by the excitation. The describing function for a two sinusoidal input shows that an additional input at an incommensurate frequency (or commensurate frequency, but irrelevant frequency ratio with respect to the system nonlinearity) will increase the nonlinear gain of the fundamental. Consequently, the oscillator output at the fundamental drops.

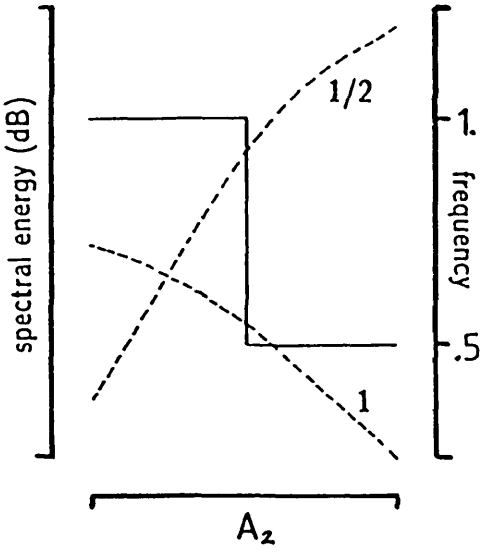

Figure 6.6 Mode competition in a subcritical $\lambda-\omega$ oscillator ($\lambda(r)=-0.5-r^2$, $\omega(r)=1$) with two-frequency excitation (A_1,ω_1) and (A_2,ω_2). The amplitude A_2 ($\omega_2=0.5$) is varied while keeping A_1 ($\omega_1=1.0$) constant. The broken lines indicate the variation of the output energy at ω_1 and ω_2. The oscillator frequency (—) jumps discontinuously from ω_1 to ω_2 at a critical amplitude A_2.

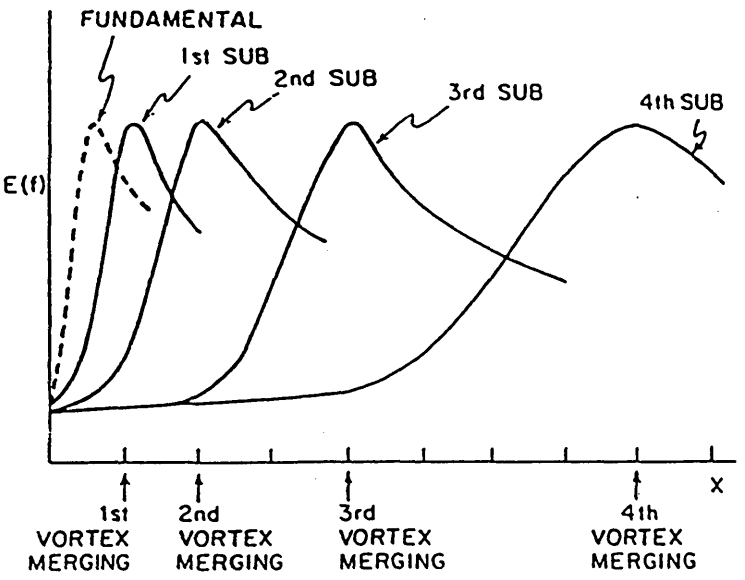

Figure 6.7 The subharmonic evolution model (after Ho 1982). $E(f)$ denotes the streamwise energy content, scaled by the shear layer thickness.

3.3.2 Discussion

The two-frequency excitation model can help explain the energy transfer in the modified Ginzburg-Landau equation. From the coupling (6.17) it is clear that the input to an element of the $\lambda-\omega$ oscillator chain comprises a local fundamental and its subharmonic. As outlined before, the coupling also provides the successive amplification of the local subharmonic along the chain. Consequently, in a first approximation, *diagram* (6.6) may be used to describe the spatial evolution of a fundamental wave and its subharmonic in the modified Ginzburg-Landau equation. This is done by replacing parameter A_2 by the spatial coordinate. The approximation becomes better if the subharmonic generation mechanism is accounted for properly. Note that as soon as the average frequency switches to the local subharmonic, another subharmonic is generated. This new subharmonic is amplified spatially and interacts with its fundamental thereby limiting and eventually reversing the growth of its fundamental.

In summary, the half-harmonic of *figure* 6.6 will saturate around the frequency discontinuity, completing the description of the subharmonic evolution mechanism of the modified Ginzburg-Landau equation.

4. Comparison with Free Shear Layer Evolution

While it is true that the modified Ginzburg-Landau equation describes a nonlinear wave guide with interaction between a fundamental and subharmonic mode, it provides no clues as to the type of instability that leads to the emergence of this subharmonic. This forms part of the *a priori* knowledge about the pairing of coherent structures in the free shear layer that has been incorporated phenomenologically in the Ginzburg-Landau equation. Nonetheless, it may be worth comparing in somewhat greater detail the results of § 3 with the spectral evolution, thought to underlie the free shear layer growth.

4.1 A Subharmonic Evolution Model

Experimental findings on the spatial development of subharmonics in a forced free shear layer (*e.g.* Miksad 1972, Ho and Huang 1982) have been generalised in a phenomenological subharmonic evolution model (Ho 1982) (*figure* 6.7), that combines both the local instability process and the global feedback mechanism to arrive at a description of the free shear layer growth.

Near the shear layer origin vortical structures develop from the initial instability wave at the local fundamental frequency. A subharmonic wave is selected by parametric resonance (Kelly 1967) and amplifies. The location where the first subharmonic saturates serves as a

reference location for vortex merging. Importantly, the shear layer thickness doubles around the vortex pairing location. This changes the local length scale and initiates another cycle of subharmonic evolution. The first subharmonic evolves to the local fundamental and a new subharmonic wave is selected.

The merging locations are determined by the global feedback mechanism. This mechanism requires the distance to the first merging event to be the same as the distance between the first and second merging, merging distances being doubled thereafter.

4.2 Discussion

A comparison of the findings of § 3 and Ho's phenomenological model is instrumental in outlining the limitations of the modified Ginzburg-Landau equation in the context of free shear layer evolution. Qualitatively, the spectral evolution observed in the Ginzburg-Landau equation (*figure* 6.4*d*) and the subharmonic evolution model (*figure* 6.7) agree in a number of points. Both are characterised by a cascade process of substitution of a local subharmonic for its fundamental. The vortex merging positions, defined by the saturation region of the local subharmonic, agree with the frequency halving transitions of the modified Ginzburg-Landau equation. In either description, the generation of subharmonics is considered from a phenomenological viewpoint. As pointed out by Ho and Huang (1982), subharmonics must be viewed as the catalyst of merging, not as its outcome.

Equally important, fundamental differences exist. These regard the distinctly non-local dynamics and the change of length scale in the free shear layer on the one hand, and the diffusion-type dynamics and space-invariant parameters of the Ginzburg-Landau equation on the other hand. Laufer (1981) concluded his discussion of jet transition and turbulence with the remark that "*the turbulent transport process is actuated by a long range force field, the induced pressure field, and therefore cannot be expressed in terms of a local gradient diffusion model*". The global feedback model is the only one that correctly predicts the merging locations in the free shear layer. Not surprisingly, therefore, the merging distances in the modified Ginzburg-Landau equation bear no physical resemblance. Concurrent with the vortex pairing a doubling in shear layer thickness occurs, transforming the local subharmonic into the local fundamental. As evidenced by the changes in wavenumber (*figure* 6.4*c*) such a length scale change is not found in formulation 6.17. Instead, a new cycle of subharmonic evolution is initiated by the change in local frequency. Finally, regarding the phase difference θ_0 between the fundamental wave and its subharmonic, from Kelly's (1967) analysis of the subharmonic resonance mechanism in free shear layers it is expected that the larger the phase difference the

smaller the subharmonic peak. This behaviour is not systematically observed in our investigation and the influence of θ_0 on the subharmonic evolution process clearly needs further detailed investigation.

5. Conclusions

The modified Ginzburg-Landau equation exhibits behaviour that is reminiscent of the evolution of subharmonics in the free shear layer. Central to the subharmonic cascade process are the co-existence of a local fundamental and its subharmonic and the nonlinear interaction between the two waves. The former is brought about by the local synthesis of a subharmonic whilst the latter results from the local dynamics of the Ginzburg-Landau equation. However, the mode energy transfer mechanism is not bound by the particular $\lambda-\omega$ dynamics of the Ginzburg-Landau equation and may be expected to be observed in any field of nonlinear oscillators that is convectively unstable to perturbations. This suggests that the subharmonic cascade is structurally stable in the sense that small changes in the local dynamics of the oscillator field will not dramatically alter the subharmonic evolution process.

Obviously, the modified Ginzburg-Landau equation provides subharmonic evolution in a very rudimentary form. Subharmonics are synthesised locally and new cycles of subharmonic growth are initiated by the discontinuous change in local frequency. Yet what appears most interesting is the nonlinear interaction between the local fundamental and its subharmonic. More work will be required to fully understand this mechanism.

Literature Cited

Atherton D P (1975). *Nonlinear Control Engineering* (London: Van Nostrand Reinhold).

Blennerhassett P J (1980). On the generation of waves by wind. *Phil Trans Roy Soc London* 298A pp 451.

Bretherton C S and Spiegel E A (1983). Intermittency through modulational instability. *Phys Let* 96A pp 152.

Chomaz J M, Huerre P and Redekopp L G (1988). Bifurcations to local and global modes in spatially developing flows. *Phys Rev Let* 60 pp 25.

Chua L O and Green D N (1974). Synthesis of nonlinear systems. *IEEE Trans Circ Syst CAS-*21 pp 286.

Deissler R J (1985) Noise-sustained structure, intermittency and the Ginzburg-Landau equation. *J Stat Phys* 40 pp 371.

Deissler R J (1987a) Spatially growing waves, intermittency, and convective chaos in an open-flow system. *Physica* 25D pp 233.

Deissler R J (1987*b*). Turbulent bursts, spots and slugs in a generalised Ginzburg-Landau equation. *Phys Let A* 120 pp 334.

Deissler R J and Kaneko K (1987). Velocity dependent Lyapunov exponents as a measure of chaos for open flow systems. *Phys Let A* pp.

Drazin P G and Reid W H (1981). *Hydrodynamic Stability* (Cambridge Univ Press).

Hall G and Watt J M (1976). *Modern Numerical Methods for Ordinary Differential Equations* (Oxford: Clarendon Press).

Ho C-M (1982). Local and global dynamics of free shear layers. *in: Numerical and Physical Aspects of Aerodynamic Flows.* ed Cebeci T (New York: Springer-Verlag).

Ho C-M and Huang L-S (1982). Subharmonics and vortex merging in mixing layers. *J Flid Mech* 119 pp 443.

Ho C-M and Huerre P (1984). Perturbed free shear layers. *Ann Rev Fluid Mech* 16 pp 365.

Keefe L (1985) Dynamics of perturbed wavetrain solutions of the Ginzburg-Landau equation. *Stud Appl Math* 78 pp 91.

Kelly R E (1967). On the stability of an inviscid shear layer which is periodic in space and time. *J Fluid Mech* 27 pp 657.

Kogelman S and Di Prima R C (1970). Stability of spatially periodic supercritical flows in hydrodynamics. *Phys Fluids* 13 pp 1.

Lamb H (1932). *Hydrodynamics* (Cambridge Univ Press).

Landman M J (1987). Solutions of the Ginzburg-Landau equation of interest in shear flow transition. *Stud Appl Math* 76 pp 187.

Laufer J (1981). Instability and turbulence in jets. *in: Transition and Turbulence.* ed Meyer R E (New York: Academic Press).

Miksad R E (1972). Experiments on the nonlinear stages of free shear layer transition. *J Fluid Mech* 56 pp 695.

Moon H, Huerre P and Redekopp L G (1983) Transition to chaos in the Ginzburg-Landau equation. *Physica* 7D pp 135.

Nayfeh A H and Mook T (1979). *Nonlinear Oscillations* (New York: Wiley).

Newell A C and Whitehead J A (1969) Finite bandwidth finite amplitude convection. *J Fluid Mech* 38 pp 279.

Nozaki K and Bekki N (1983). Pattern selection and spatiotemporal transition to chaos in the Ginzburg-Landau equation. *Phys Rev Let* 51 pp 2171.

Segel L A (1969). Distant side walls cause slow amplitude modulation of cellular convection. *J Fluid Mech* 38 pp 203.

Stewartson K and Stuart J T (1971) A nonlinear instability theory for a wave system in plane Poiseuille flow. *J Fluid Mech* 48 pp 529.

Stuart J T and Di Prima R C (1978) The Eckhaus and Benjamin-Feir resonance mechanisms. *Proc Roy Soc London* 362A pp 27.

Treiber J (1985). Theoretical analysis of a nonlinear model of arterial pressure control. MSc thesis, Technische Universität Berlin.

CHAPTER VII

CONCLUSIONS

This chapter concludes the investigation of poststenotic flow instabilities with a recapitulation of the reported work and a discussion of implications and future work.

1. Laser Doppler Velocimetry

The inherent limitations of laser Doppler velocimetry — as the result of the random distribution of scatterers in the flow and the finite size of the measuring volume — are generally acknowledged in LDV studies and have been treated theoretically (George and Lumley 1973, Durrani and Greated 1977). In contrast, the demodulation of the Doppler signal by *e.g.* frequency tracking is often tacitly assumed to be free of error (*e.g.* Deshpande and Giddens 1980). In fact, intermittent loss of tracking is an integral part of any form of frequency demodulation of the Doppler signal. The infinite variance of the transit-time noise implies that the Doppler signal invariably falls below arbitrarily small noise levels occasionally. Though a number of sources contribute to the noise *viz.* optical, photodetection and electronic system noise, it is usually the optical noise that dominates.

Our analysis of the dropout process in LDV frequency tracking systems showed that it is not only low to intermediate tracking rates that cause a degradation of the instantaneous velocity signal by tracking noise, but equally the average frequency of dropouts. When the unlock frequency is of the order of the bandwidth of the velocity signal, the incurred measurement error can be significant.

The tracking performance is improved by minimising the optical noise. This involves carefully matching the power requirements of the coherent light source, the measuring volume size and the scattering properties of the flow seeding material. However, a typical LDV set-up for small flow geometries — 5mW He-Ne laser and about 120mm lens focal length, as used in our experiments or by Deshpande and Giddens (*ibid*) — is prone to optical noise problems and requires an assessment of the influence of tracking noise on flow velocity measurements. It is recommended therefore that, particularly when measuring turbulent flow, estimates of the average frequency of dropout be obtained. This will give a first approximation of the measurement error to be expected from tracking imperfections.

2. Stenotic Flow Experiments

These experiments aimed at assessing the structural stability of oscillatory flow disturbances in poststenotic flows in the presence of ambient noise. With arterial wall vibrations a possible source of noise, the approach taken was to decouple the fluid mechanic from the solid (wall) mechanic problem. This method is an important prerequisite for the understanding of complex flow problems and has been adopted, for example, for the investigation of self-excited oscillations in flow through collapsible tubes (Pedley and Stephanoff 1985), or in the study of vortex-induced oscillations (Bearman 1984). Because the determinants of the ambient noise are largely unknown, well defined perturbations were generated artificially. This has the advantage that the number of configurational parameters is kept to a minimum and possible resonant interactions between the flow and the distensible wall are categorically excluded.

The oscillatory flow disturbances in pulsatile flow were found to be significantly less susceptible to perturbations than what was expected from quasisteady analysis, making these flow disturbances fairly structurally stable in the sense that they are expected to persist under moderate flow perturbations. Possible explanations for this reduced susceptibility were sought in the transient behaviour of impulsively started orifice flows.

This brings us to the discussion of future investigations of this phenomenon. Still further simplifications of the flow problem will be required *i.e.* the removal of the downstream bounding walls. This allows the separation of the poststenotic separated shear layer instability from the retarding effects of the downstream walls. For example, Khalifa and Giddens (1981) compared free and confined jet-like flows downstream of a contoured stenosis, and Lieber and Giddens (1988) considered flow through a 90% contoured stenosis, thus effectively excluding bounding wall effects.

The study of laminar jet flow instabilities under time-varying flow conditions is expected to further elucidate the dynamics of the free shear layer instability. From a dynamical system viewpoint the importance of a transient analysis is readily appreciated. Whereas steady flow experiments are instrumental in gaining an understanding of the selective noise amplification mechanism and of the nonlinear mode competition in the (forced) free shear layer, additional dynamical properties will be deduced from starting and stopping flows or from pulsatile flow rate variations. For instance, it is conceivable that temporal variations in flow rate provide a phase reference for the otherwise irregular formation of vortices. This will

lead to a much more organised flow field, increasing the amplitude of oscillatory flow disturbances.

Future experiments should also investigate starting and stopping flows using more realistic model stenoses with streamwise extent. The orifice flow had already given some clues for the interpretation of the start-up and stopping features of poststenotic flow disturbances. Starting flow through the contoured stenosis models is expected to produce weaker start-up vortices due to the lower shear and the proximity to the walls.

Finally, we note that the resonant behaviour of the forced separated shear layer aids in interpreting flow disturbances downstream of more complicated stenosis geometries. The resonance phenomenon proved very useful in a preliminary study of flow past a plasticine protusion with ill-defined geometry. The optimal measuring position for detecting coherent flow disturbances could best be determined under forced flow conditions.

3. The Free Shear Layer and Co-operative Phenomena

Co-operative phenomena come readily to mind when investigating the forced free shear layer. The very concept that the free shear layer possesses an underlying degree of organisation that is intensified by applying an artificially introduced phase reference is suggestive of self- and forced synchronisation in a population of non-identical oscillators with external field. The analogy is further supported by the striking similarities between the effects an impingement edge and flow excitation have on a mixing layer (Rockwell and Naudascher 1979). The former provides an hydroacoustic feedback of energy — analogous to increased coupling, possibly with additional phase shift — and the latter generates a strong instability wave — corresponding to an external field.

The characteristics of the oscillator population are derived from the physics of the free shear layer. The most amplified frequency in the free shear layer scales with the local momentum thickness which grows linearly beyond the first vortex merging, and the vortex-induced velocity field has long-range effects. This suggests that the oscillators be non-identical and that the interaction between them be non-local.

It was demonstrated that such an oscillator population, with appropriate coupling, can serve as a simple model of the 'locking-on' phenomena in the forced free shear layer. Without external field, the population exhibits no discernible self-organisation due to the weak mutual coupling. That there is latent order in this population, however, is shown by increasing the coupling strength. The population then clusters into self-synchronised subsets which, when arranged spatially, from a frequency-halving cascade. When an external field is applied, the

underlying order is intensified and typical forced synchronisation phenomena are observed, concomitant with a concentration of oscillator energy at the forcing frequency. Furthermore, the synchronisation is global to the population, with oscillators of lower intrinsic frequency forming synchronised clusters at the subharmonics of the fundamental forcing frequency. The cluster formation is more sensitive to variations in forcing frequency than forcing amplitude, as expected from the intrinsic frequency distribution.

The oscillator population can thus be viewed as a model system of flow synchronisation. This is not to suggest, however, that the free shear layer be conceptualised as an oscillator continuum with streamwise intrinsic frequency gradient. The oscillator model provides an Eulerian description of flow synchronisation phenomena in the forced free shear layer and the contingent character of kinematic waves in such oscillator fields must be emphasised. To complicate matters, Eulerian concepts of flow synchronisation are difficult to reconcile with the Lagrangian concept of the spatially evolving free shear layer. However, it is not the purpose here to enter into a discussion of flow synchronisation in terms of spatial theory. Our approach to flow organisation in the forced free shear layer is phenomenological and consequently the proposed model is greatly removed from fundamental physical principles. What makes the oscillator model interesting, in our view, is the extension of nonlinear oscillator concepts to extrinsic flows, previously applied to intrinsic flows such as wake flows.

Returning to the transition in the forced free shear layer from irregular spatio-temporal dynamics to a very organised state, co-operative effects are observed in a variety of contexts including biological oscillations (brain waves, heartbeat), and equilibrium (magnetic spin, superconductivity) and non-equilibrium statistical mechanics (lasers), and are associated with functionally composite systems. Removed from the particular physical context such systems are regarded as synergetic systems (Haken 1978). Central to the synergetic approach is the slaving principle which claims the possibility of eliminating a large number of rapidly decaying degrees of freedom in nonlinear dissipative systems.

Is it quite possible that an order parameter may be derived from an appropriately truncated form of the Navier-Stokes equations, that describes these co-operative phenomena?

4. The Modified Ginzburg-Landau Equation

Although itself an oscillator field, the Ginzburg-Landau equation is conceptually different from the phenomenological model of flow synchronisation. Derived in the nonlinear theory of hydrodynamic stability, the Ginzburg-Landau equation describes the evolution in space as well as time of weakly nonlinear instability waves and is considered a model open flow

system. Only recently has a Ginzburg-Landau equation with space-dependent control parameter a_r (*cf.* Ch VI § 1) been proposed as a model of both the absolutely and convectively unstable regions of wakes behind bluff bodies (Chomaz *et al* 1988).

In this study the possibility of a subharmonic cascade of instability waves was explored. Without attempting to incorporate a subharmonic resonance mechanism — the Ginzburg-Landau equation after all has only the minimum complexity for supporting nonlinear waves — artificially generated subharmonic components of a fundamental wave were introduced and found to result in a cascade of energy transfer from a local fundamental instability wave to its subharmonic. It was suggested that the energy transfer mechanism is qualitatively similar to the quenching of self-sustained oscillations by an external excitation. Clearly, more work needs to be directed at the evolution of subharmonics in the modified Ginzburg-Landau equation in order to arrive at a more complete understanding of the underlying mechanism. This will include perturbing the (unmodified!) Ginzburg-Landau equation with propagating wave solution by a single-frequency disturbance, injected locally in the nonlinear region. It is expected that, with increasing amplitude of the perturbation the travelling wave amplitude decreases until at a certain critical point the average wave frequency switches to the perturbation frequency. This would support the view that indeed an independently amplifying subharmonic quenches its fundamental, thus initiating the wave pairing.

Let us compare this tentative scenario of subharmonic evolution in the modified Ginzburg-Landau equation with Ho's (1982) model of the free shear layer that unifies the present knowledge of free shear layer evolution. On the presupposition that subharmonics are generated by Kelly's nonlinear subharmonic resonance mechanism, Ho's model concentrates on the doubling of the shear layer thickness around vortex pairing locations. As a result of this doubling of length scale the locally most amplified frequency becomes the subharmonic and another cycle of vortex pairing is started. This explains the paradox that linear stability theory is able to describe a highly nonlinear flow. In the modified Ginzburg-Landau equation, on the other hand, it is the change in local frequency around wave pairing positions that initiates new pairing cycles. The change from fundamental to subharmonic is a purely nonlinear mechanism because the dispersion relation remains unchanged. This defines the limitations of the Ginzburg-Landau equation in respect to the free shear layer.

The Ginzburg-Landau equation *per se*, however, has been receiving ever increasing attention over the past few years, both as a model open flow system and because of its complex transition sequences to chaos. The recent discovery that the Ginzburg-Landau equation can

combine absolutely and convectively unstable regions which is in qualitative agreement with the behaviour of spatially developing flows such as wakes or inhomogeneous jets, is an exciting example illustrating the potential of this equation.

Literature Cited

Bearman P W (1984). Vortex shedding from oscillating bluff bodies. *Ann Rev Fluid Mech* 16 pp 195.

Chomaz J M, Huerre P and Redekopp L G (1988). Bifurcations to local and global modes in spatially developing flows. *Phys Rev Let* 60 pp 25.

Deshpande M D and Giddens D P (1980). Turbulence measurements in a constricted tube. *J Fluid Mech* 97 pp 65.

Durrani T S and Greated C A (1977). *Laser Systems in Flow Measurement* (New York: Plenum).

George W K and Lumley J L (1973). The laser Doppler velocimeter and its application to the measurement of turbulence. *J Fluid Mech* 60 pp 321.

Haken H (1978). *Synergetics – An Introduction* (Berlin: Springer-Verlag).

Ho C-M (1982). Local and global dynamics of free shear layers. *in: Numerical and Physical Aspects of Aerodynamic Flows.* ed T Cebeci (New York: Springer-Verlag).

Khalifa A M A and Giddens D P (1981). Characterisation and evolution of poststenotic flow disturbances. *J Biomech* 14 pp 279.

Lieber B B and Giddens D P (1988). Apparent stresses in disturbed pulsatile flows. *J Biomech* 21 pp 287.

Pedley T J and Stephanoff K D (1985). Flow along a channel with a time-dependent indentation in one wall: the generation of vorticity waves. *J Fluid Mech* 160 pp 337.

Rockwell D and Naudascher E (1979). Self-sustained oscillations of impinging free shear layers. *Ann Rev Fluid Mech* 11 pp 67.